

Transformer and Inductor Design Handbook

FOURTH EDITION

Transformer and Inductor Design Handbook

FOURTH EDITION

Colonel Wm. T. McLyman



CRC Press

Taylor & Francis Group

Boca Raton London New York

CRC Press is an imprint of the
Taylor & Francis Group, an **informa** business

CRC Press
Taylor & Francis Group
6000 Broken Sound Parkway NW, Suite 300
Boca Raton, FL 33487-2742

© 2011 by Taylor and Francis Group, LLC
CRC Press is an imprint of Taylor & Francis Group, an Informa business

No claim to original U.S. Government works

Printed in the United States of America on acid-free paper
10 9 8 7 6 5 4 3 2 1

International Standard Book Number-13: 978-1-4398-3688-0 (Ebook-PDF)

This book contains information obtained from authentic and highly regarded sources. Reasonable efforts have been made to publish reliable data and information, but the author and publisher cannot assume responsibility for the validity of all materials or the consequences of their use. The authors and publishers have attempted to trace the copyright holders of all material reproduced in this publication and apologize to copyright holders if permission to publish in this form has not been obtained. If any copyright material has not been acknowledged please write and let us know so we may rectify in any future reprint.

Except as permitted under U.S. Copyright Law, no part of this book may be reprinted, reproduced, transmitted, or utilized in any form by any electronic, mechanical, or other means, now known or hereafter invented, including photocopying, microfilming, and recording, or in any information storage or retrieval system, without written permission from the publishers.

For permission to photocopy or use material electronically from this work, please access www.copyright.com (<http://www.copyright.com/>) or contact the Copyright Clearance Center, Inc. (CCC), 222 Rosewood Drive, Danvers, MA 01923, 978-750-8400. CCC is a not-for-profit organization that provides licenses and registration for a variety of users. For organizations that have been granted a photocopy license by the CCC, a separate system of payment has been arranged.

Trademark Notice: Product or corporate names may be trademarks or registered trademarks, and are used only for identification and explanation without intent to infringe.

Visit the Taylor & Francis Web site at
<http://www.taylorandfrancis.com>

and the CRC Press Web site at
<http://www.crcpress.com>

To My Wife, Bonnie

Contents

Foreword ix

Preface xi

Acknowledgements xiii

About the Author xv

Symbols xvii

Chapter 1

Fundamentals of Magnetics	1-1
---------------------------------	-----

Chapter 2

Magnetic Materials and Their Characteristics	2-1
--	-----

Chapter 3

Magnetic Cores	3-1
----------------------	-----

Chapter 4

Window Utilization, Magnet Wire, and Insulation	4-1
---	-----

Chapter 5

Transformer Design Trade-Offs	5-1
-------------------------------------	-----

Chapter 6

Transformer-Inductor Efficiency, Regulation, and Temperature Rise	6-1
---	-----

Chapter 7

Power Transformer Design	7-1
--------------------------------	-----

Chapter 8

DC Inductor Design, Using Gapped Cores.....	8-1
---	-----

Chapter 9

DC Inductor Design, Using Powder Cores	9-1
--	-----

Chapter 10

AC Inductor Design	10-1
--------------------------	------

Chapter 11

Constant Voltage Transformer (CVT)	11-1
--	------

Chapter 12

Three-Phase Transformer Design.....	12-1
-------------------------------------	------

Chapter 13	
Flyback Converters, Transformer Design	13-1
Chapter 14	
Forward Converter, Transformer Design, and Output Inductor Design	14-1
Chapter 15	
Input Filter Design	15-1
Chapter 16	
Current Transformer Design.....	16-1
Chapter 17	
Winding Capacitance and Leakage Inductance	17-1
Chapter 18	
Quiet Converter Design	18-1
Chapter 19	
Rotary Transformer Design	19-1
Chapter 20	
Planar Transformers and Inductors.....	20-1
Chapter 21	
Derivations for the Design Equations	21-1
Chapter 22	
Autotransformer Design.....	22-1
Chapter 23	
Common-Mode Inductor Design	23-1
Chapter 24	
Series Saturable Reactor Design.....	24-1
Chapter 25	
Self-Saturating, Magnetic Amplifiers	25-1
Chapter 26	
Designing Inductors for a Given Resistance.....	26-1

Foreword

Colonel McLyman is a well-known author, lecturer and magnetic circuit designer. His previous books on transformer and inductor design, magnetic core characteristics and design methods for converter circuits have been widely used by magnetics circuit designers.

In his 4th edition, Colonel McLyman has combined and updated the information found in his previous books. He has also added five new subjects such as autotransformer design, common-mode inductor design, series saturable reactor design, self-saturating magnetic amplifier and designing inductors for a given resistance. The author covers magnetic design theory with all of the relevant formulas. He has complete information on all of the magnetic materials and core characteristics along with the real world, step-by-step design examples.

This book is a must for engineers doing magnetic design. Whether you are working on high “rel” state of the art design or high volume, or low cost production, this book will help you. Thanks Colonel for a well-done, useful book.

*Robert G. Noah
Application Engineering Manager (Retired)
Magnetics, Division of Spang and Company
Pittsburgh, Pennsylvania*

Preface

I have had many requests to update my book *Transformer and Inductor Design Handbook*, because of the way power electronics has changed in the past few years. I have been requested to add and expand on the present Chapters. There are now twenty-six Chapters. The new Chapters are autotransformer design, common-mode inductor design, series saturable reactor design, self-saturating magnetic amplifier and designing inductors for a given resistance, all with step-by-step design examples.

This book offers a practical approach with design examples for design engineers and system engineers in the electronics industry, as well as the aerospace industry. While there are other books available on electronic transformers, none of them seem to have been written with the user's viewpoint in mind. The material in this book is organized so that the design engineer, student engineer or technician, starting at the beginning of the book and continuing through the end, will gain a comprehensive knowledge of the state of the art in transformer and inductor design. The more experienced engineers and system engineers will find this book a useful tool when designing or evaluating transformers and inductors.

Transformers are to be found in virtually all electronic circuits. This book can easily be used to design light-weight, high-frequency aerospace transformers or low-frequency commercial transformers. It is, therefore, a design manual.

The conversion process in power electronics requires the use of transformers, components that frequently are the heaviest and bulkiest item in the conversion circuit. Transformer components also have a significant effect on the overall performance and efficiency of the system. Accordingly, the design of such transformers has an important influence on overall system weight, power conversion efficiency, and cost. Because of the interdependence and interaction of these parameters, judicious trade-offs are necessary to achieve design optimization.

Manufacturers have for years assigned numeric codes to their cores to indicate their power-handling ability. This method assigns to each core a number called the area product, A_p , that is the product of its window area, W_a , and core cross-section area, A_c . These numbers are used by core suppliers to summarize dimensional and electrical properties in their catalogs. The product of the window area, W_a , and the core area, A_c , gives the area product, A_p , a dimension to the fourth power. I have developed a new equation for the power-handling ability of the core, the core geometry, K_g . The core geometry, K_g , has a dimension to the fifth power. This new equation gives engineers faster and tighter control of their design. The core geometry coefficient, K_g , is a relatively new concept, and magnetic core manufacturers are now beginning to put it in their catalogs.

Because of their significance, the area product, A_p , and the core geometry, K_g , are treated extensively in this handbook. A great deal of other information is also presented for the convenience of the designer. Much of the material is in tabular form to assist the designer in making the trade-offs best suited for the particular application in a minimum amount of time.

Designers have used various approaches in arriving at suitable transformer and inductor designs. For example, in many cases a rule of thumb used for dealing with current density is that a good working level is 1000 circular mils per ampere. This is satisfactory in many instances; however, the wire size used to meet this requirement may produce a heavier and bulkier inductor than desired or required. The information presented here will make it possible to avoid the use of this and other rules of thumb, and to develop a more economical and better design.

The author or the publisher assumes no responsibility for any infringement of patent or other rights of third parties that may result from the use of circuits, systems, or processes described or referred to in this handbook.

I wish to thank the manufacturers represented in this book for their assistance in supplying technical data.

Colonel Wm. T. McLyman

Acknowledgements

In gathering the material for this book, I have been fortunate in having the assistance and cooperation of several companies and many colleagues. As the author, I wish to express my gratitude to all of them. The list is too long to mention them all. However, there are some individuals and companies whose contributions have been significant. Colleagues that have retired from Magnetics include Robert Noah and Harry Savisky who helped so greatly with the editing of the final draft. Other contributions were given by my colleagues at Magnetics, Lowell Bosley and his staff with the sending of up-to-date catalogs and sample cores. I would like to thank colleagues at Micrometals Corp., Jim Cox and Dale Nicol, and George Orenchak of TSC International. I would like to give a special thanks to Richard (Oz) Ozenbaugh of Linear Magnetics Corp. for his assistance in the detailed derivations of many of the equations and his efforts in checking all the design examples. I would also like to give special thanks to Steve Freeman of Rodon Products, Inc. and Charles Barnett of Leightner Electronics, Inc. for building and testing all of the magnetic components used in the design examples.

There are individuals I would like to thank: Dr. Vatche Vorperian of Jet Propulsion Laboratory (JPL) for his help in generating and clarifying equations for the Quiet Converter; Jerry Fridenberg of Fridenberg Research, Inc. for modeling circuits on his SPICE program; Dr. Gene Wester of (JPL) for his inputs and Kit Sum for his assistance in the energy storage equations. I also want to thank the late Robert Yahiro for his help and encouragement over the years.

About The Author

Colonel Wm. T. McLyman has retired as a senior member of the Avionics Equipment Section of the Jet Propulsion Laboratory (JPL) affiliated with the California Institute of Technology in Pasadena, California. He has fifty-four years of experience in the field of Magnetics and holds fourteen United States Patents on magnetics-related concepts. Through his thirty years at JPL, he has written over seventy JPL technical memorandums, new technology reports, and tech-briefs on the subject of magnetics and circuit designs for power conversion. He has worked on projects for NASA including the Pathfinder Mission to Mars, Cassini, Galileo, Magellan, Viking, Voyager, MVM, Hubble Space Telescope, and many others.

He has been on the lecture circuit for over twenty-nine years speaking in the United States, Canada, Mexico, and Europe on the design and fabrication of magnetic components. He is known as a recognized authority in magnetic design. He is the president of his company called Kg Magnetics, Inc., which specializes in power magnetics design.

He has also written a book entitled *Design and Fabrication of High Reliability Magnetic Devices*. This book is based on fabricating and testing Hi-Rel magnetic devices. He also markets through Kg Magnetics, Inc. a magnetics design and analysis software computer program called “Titan” for transformers and inductors, see Figure 1. This program operates on Windows 95, 98, 2000, and NT.

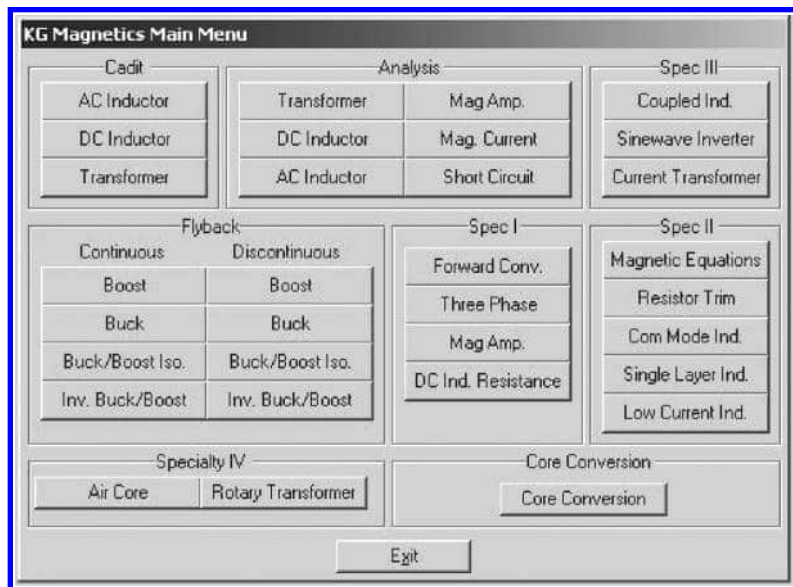


Figure 1. Computer Design Program Main Menu.

Kg Magnetics, Inc.

Colonel Wm. T. McLyman, (President)

www.kgmagnetics.com

colonel@kgmagnetics.com

Idyllwild, CA 92549

Symbols

α	regulation, %
A_c	effective cross section of the core, cm^2
A_p	area product, cm^4
A_t	surface area of the transformer, cm^2
A_w	wire area, cm^2
$A_{w(B)}$	bare wire area, cm^2
$A_{w(I)}$	insulated wire area, cm^2
A_{wp}	primary wire area, cm^2
A_{ws}	secondary wire area, cm^2
A-T	amp turn
AWG	American wire gage
B	flux, teslas
B_{ac}	alternating current flux density, teslas
ΔB	change in flux, teslas
B_{dc}	direct current flux density, teslas
B_m	flux density, teslas
B_{\max}	maximum flux density, teslas
B_o	operating peak flux density, teslas
B_{pk}	peak flux density, teslas
B_r	residual flux density, teslas
B_s	saturation flux density, teslas
C	capacitance
C_n	new capacitance
C_p	lumped capacitance
C_s	stray capacitance
CM	circular mils
CM	common mode
D_{AWG}	wire diameter, cm
$D_{(\min)}$	minimum duty ratio
$D_{(\max)}$	maximum duty ratio
D_w	dwell time duty ratio
DM	differential mode
E	voltage
E_{Line}	line-to-line voltage
E_{Phase}	Line to neutral voltage
Energy	energy, watt-second
ESR	equivalent series resistance

η	efficiency
f	frequency, Hz
F	fringing flux factor
F_m	magneto-motive force, mmf
F.L.	full load
G	winding length, cm
γ	density, in grams-per-cm ²
ϵ	skin depth, cm
H	magnetizing force, oersteds
H	magnetizing force, amp-turns
H_c	magnetizing force required to return flux to zero, oersteds
ΔH	delta magnetizing force, oersteds
H_o	operating peak magnetizing force
H_s	magnetizing force at saturation, oersteds
I	current, amps
I_c	charge current, amps
I_c	control current, amps
ΔI	delta current, amps
I_{dc}	dc current, amps
I_g	gate current, amps
I_{in}	input current, amps
I_{Line}	input line current, amps
I_m	magnetizing current, amps
I_o	load current, amps
$I_{o(max)}$	maximum load current, amps
$I_{o(min)}$	minimum load current, amps
I_p	primary current, amps
I_{Phase}	input phase current, amps
I_s	secondary current, amps
$I_{s(Phase)}$	secondary phase current, amps
$I_{s(Line)}$	secondary line current, amps
J	current density, amps per cm ²
K_c	copper loss constant
K_c	quasi-voltage waveform factor
K_e	electrical coefficient
K_{ew}	control winding coefficient
K_f	waveform coefficient

K_g	core geometry coefficient, cm ⁵
K_j	constant related to current density
K_s	constant related to surface area
K_u	window utilization factor
K_{up}	primary window utilization factor
K_{us}	secondary window utilization factor
K_{vol}	constant related to volume
K_w	constant related to weight
L	inductance, henry
l	is a linear dimension
λ	density, grams per cm ³
L_c	open circuit inductance, henrys
L_c	control winding inductance, henrys
$L_{(crt)}$	critical inductance
l_g	gap, cm
l_m	magnetic path length, cm
L_p	primary inductance, henrys
l_t	total path length, cm
MA	magnetic amplifier
mks	meters-kilogram-seconds
MLT	mean length turn, cm
mmf	magnetomotive force, F_m
MPL	magnetic path length, cm
mW/g	milliwatts-per-gram
μ	permeability
μ_e	effective permeability
μ_i	initial permeability
μ_Δ	incremental permeability
μ_m	core material permeability
μ_o	permeability of air
μ_r	relative permeability
n	turns ratio
N	turns
N_c	control turns
N_g	gate turns
N_L	inductor turns
N_n	new turns

N_p	primary turns
N_s	secondary turns
N.L.	no load
P	watts
P_c	control power loss, watts
P_{cu}	copper loss, watts
P_{fe}	core loss, watts
P_g	gap loss, watts
P_{gain}	power gain, factor
ϕ	magnetic flux
P_{in}	input power, watts
P_L	inductor copper loss, watts
P_o	output power, watts
P_p	primary copper loss, watts
P_s	secondary copper loss, watts
P_Σ	total loss (core and copper), watts
P_t	total apparent power, watts
P_{tin}	autotransformer input power, volt-amps
P_{to}	autotransformer output power, volt-amps
P_{VA}	primary, volt-amps
R	resistance, ohms
R_{ac}	ac resistance, ohms
R_c	control resistance, ohms
R_{cu}	copper resistance, ohms
R_{dc}	dc resistance, ohms
R_e	equivalent core loss (shunt) resistance, ohms
R_g	reluctance of the gap
$R_{in(equiv)}$	reflected load resistance, ohms
R_L	load resistance, ohms
R_m	reluctance
R_{mt}	total reluctance
R_o	load resistance, ohms
$R_{o(R)}$	reflected load resistance, ohms
R_p	primary resistance, ohms
R_R	ac/dc resistance ratio
R_s	secondary resistance, ohms
R_t	total resistance, ohms

ρ	resistivity, ohm-cm
S_1	conductor area/wire area
S_2	wound area/usable window
S_3	usable window area/window area
S_4	usable window area/usable window area + insulation area
S_{np}	number of primary strands
S_{ns}	number of secondary strands
S_{VA}	secondary volt-amps
SR	saturable reactor
T	total period, seconds
t_{off}	off time, seconds
t_{on}	on time, seconds
t_r	time constant, seconds
T_r	temperature rise, degrees C
t_w	dwell time, seconds
U	multiplication factor
V_{ac}	applied voltage, volts
V_c	control voltage, volts
$V_{c(pk)}$	peak voltage, volts
V_d	diode voltage drop, volts
V_{in}	input voltage, volts
$V_{in(max)}$	maximum input voltage, volts
$V_{in(min)}$	minimum input voltage, volts
V_n	new voltage, volts
V_o	output voltage, volts
V_p	primary voltage, volts
$V_{p(rms)}$	primary rms voltage, volts
$V_{r(pk)}$	peak ripple voltage
$V_{s(LL)}$	secondary line-to-line voltage, volts
$V_{s(LN)}$	secondary line to neutral voltage, volts
V_s	secondary voltage, volts
ΔV_{CC}	capacitor voltage, volts
ΔV_{CR}	capacitor ESR voltage, volts
ΔV_p	delta primary voltage, volts
ΔV_s	delta secondary voltage, volts
VA	volt-amps
W	watts

W/kg	watts-per-kilogram
WK	watts-per-kilogram
W _a	window area, cm ²
W _{ac}	control window area, cm ²
W _{a(eff)}	effective window area, cm ²
W _{ag}	gate window area, cm ²
W _{ap}	primary window area, cm ²
W _{as}	secondary window area, cm ²
W _t	weight, grams
W _{tcu}	copper weight, grams
W _{tf}	iron weight, grams
w-s	watt-seconds
X _L	inductive reactance, ohms

Chapter 1

Fundamentals of Magnetics

Table of Contents

1. Introduction.....	1-3
2. Magnetic Properties in Free Space	1-3
3. Intensifying the Magnetic Field	1-4
4. Simple Transformer	1-7
5. Magnetic Core.....	1-8
6. Fundamental Characteristics of a Magnetic Core	1-9
7. Hysteresis Loop (B-H Loop)	1-11
8. Permeability	1-12
9. Magnetomotive Force (mmf) and Magnetizing Force (H).....	1-15
10. Reluctance	1-16
11. Air Gap	1-18
12. Controlling the dc Flux with an Air Gap	1-20
13. Types of Air Gaps	1-21
14. Fringing Flux	1-22
15. Material Permeability, (μ_m).....	1-23
16. Air Gaps.....	1-23
17. Fringing Flux, F	1-24
18. Gapped, dc Inductor Design.....	1-25
19. Fringing Flux and Coil Proximity	1-26
20. Fringing Flux, Crowding	1-27
21. Fringing Flux and Powder Cores.....	1-28

Introduction

Considerable difficulty is encountered in mastering the field of magnetics because of the use of so many different systems of units – the centimeter-gram-second (cgs) system, the meter-kilogram-second (mks) system, and the mixed English units system. Magnetics can be treated in a simple way by using the cgs system. There always seems to be one exception to every rule and that is permeability.

Magnetic Properties in Free Space

A long wire with a dc current, I , flowing through it, produces a circulatory magnetizing force, H , and a magnetic field, B , around the conductor, as shown in Figure 1-1, where the relationship is:

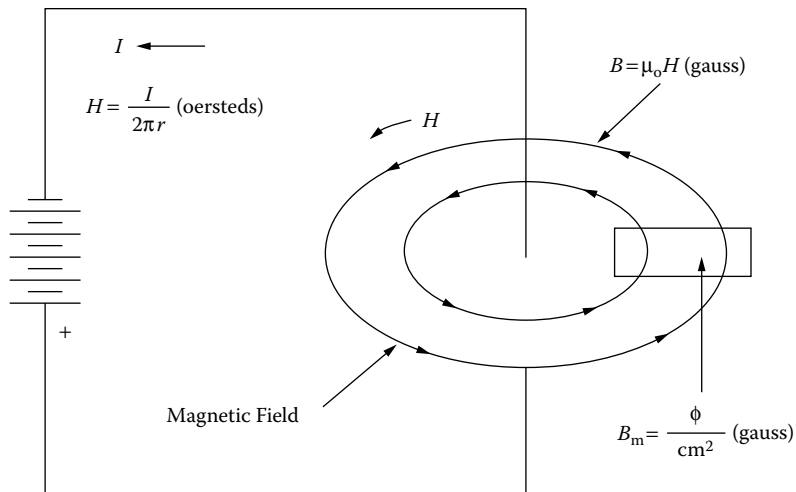


Figure 1-1. A Magnetic Field Generated by a Current Carrying Conductor.

The direction of the line of flux around a straight conductor may be determined by using the “right hand rule” as follows: When the conductor is grasped with the right hand, so that the thumb points in the direction of the current flow, the fingers point in the direction of the magnetic lines of force. This is based on so-called conventional current flow, not the electron flow.

When a current is passed through the wire in one direction, as shown in Figure 1-2(A), the needle in the compass will point in one direction. When the current in the wire is reversed, as in Figure 1-2(B), the needle will also reverse direction. This shows that the magnetic field has polarity and that, when the current I , is reversed, the magnetizing force, H , will follow the current reversals.

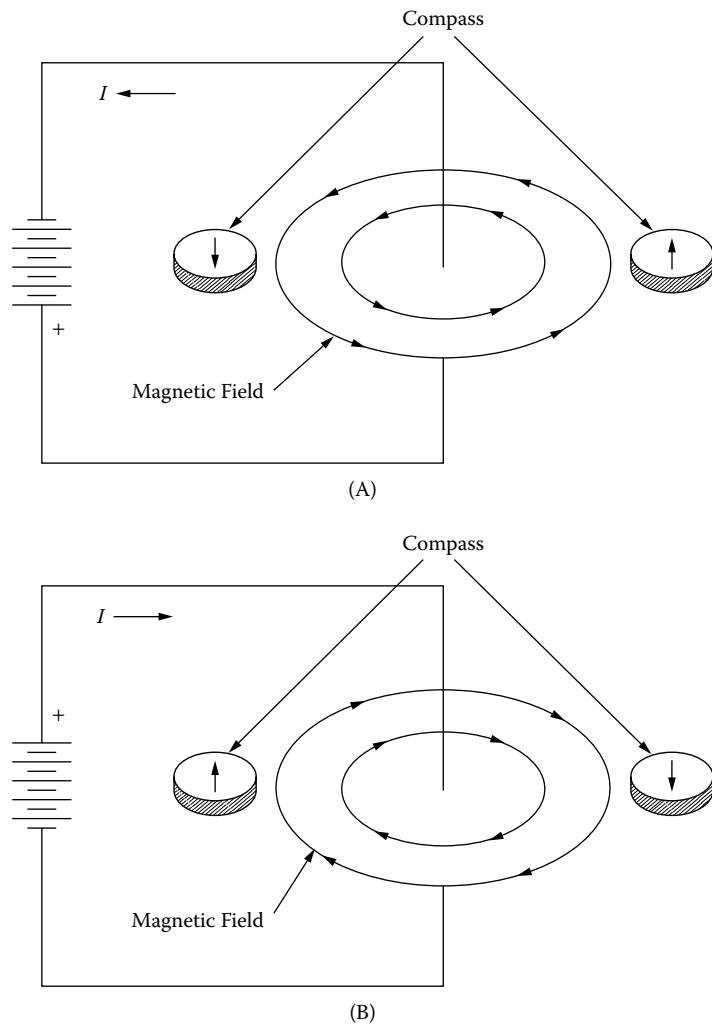


Figure 1-2. The Compass Illustrates How the Magnetic Field Changes Polarity.

Intensifying the Magnetic Field

When a current passes through a wire, a magnetic field is set up around the wire. If the conductors, as shown in [Figure 1-3](#), carrying current in the same direction are separated by a relatively large distance, the magnetic fields generated will not influence each other. If the same two conductors are placed close to each other, as shown in [Figure 1-4](#), the magnetic fields add, and the field intensity doubles.

$$\gamma = \frac{B^2}{8\pi\mu}, \quad [\text{energy density}] \quad [1-1]$$

If the wire is wound on a dowel, its magnetic field is greatly intensified. The coil, in fact, exhibits a magnetic field exactly like that of a bar magnet, as shown in [Figure 1-5](#). Like the bar magnet, the coil has a north pole and a neutral center region. Moreover, the polarity can be reversed by reversing the current, I , through the coil. Again, this demonstrates the dependence of the magnetic field on the current direction.

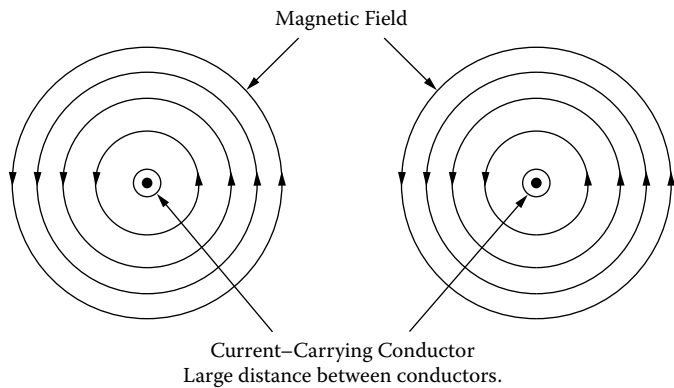


Figure 1-3. Magnetic Fields Produced Around Spaced Conductors.

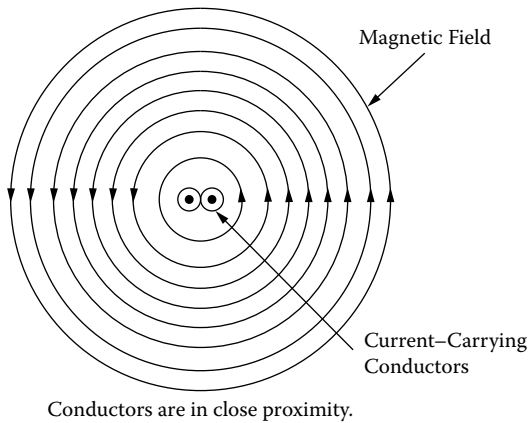


Figure 1-4. Magnetic Fields Produced Around Adjacent Conductors.

The magnetic circuit is the space in which the flux travels around the coil. The magnitude of the flux is determined by the product of the current, I , and the number of turns, N , in the coil. The force, NI , required to create the flux is magnetomotive force (mmf). The relationship between flux density, B , and magnetizing force, H , for an air-core coil is shown in [Figure 1-6](#). The ratio of B to H is called the permeability, μ , and for this air-core coil the ratio is unity in the cgs system, where it is expressed in units of gauss per oersteds, (gauss/oersteds).

$$\begin{aligned}\mu_o &= 1 \\ B &= \mu_o H\end{aligned}\quad [1-2]$$

If the battery, in [Figure 1-5](#), were replaced with an ac source, as shown in [Figure 1-7](#), the relationship between B and H would have the characteristics shown in [Figure 1-8](#). The linearity of the relationship between B and H represents the main advantage of air-core coils. Since the relationship is linear, increasing H increases B , and therefore the flux in the coil, and, in this way, very large fields can be produced with large currents. There is obviously a practical limit to this, which depends on the maximum allowable current in the conductor and the resulting rise.

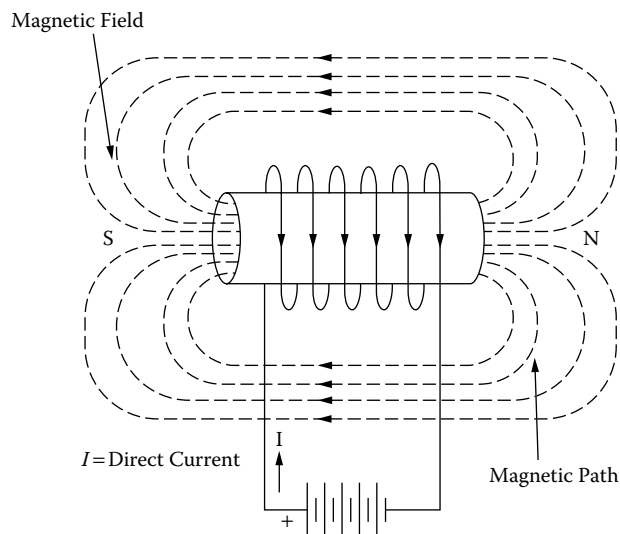


Figure 1-5. Air-Core Coil with dc Excitation.

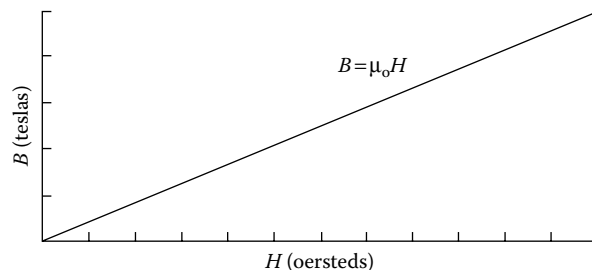


Figure 1-6. Relationship between B and H with dc Excitation.

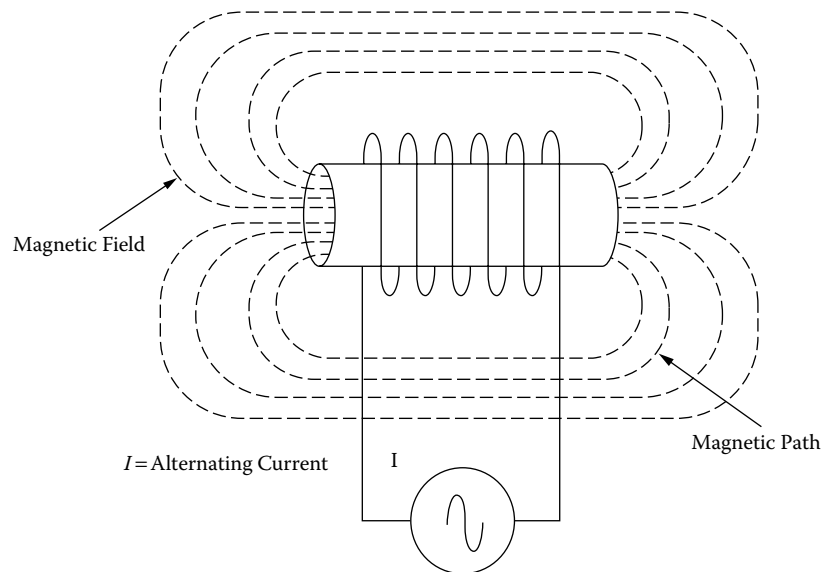


Figure 1-7. Air-Core Coil Driven from an ac Source.

Fields of the order of 0.1 tesla are feasible for a 40°C temperature rise above room ambient temperature. With super cooled coils, fields of 10 tesla have been obtained.

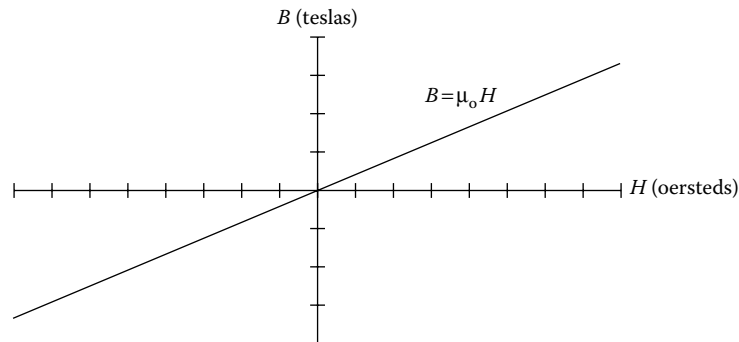


Figure 1-8. Relationship between B and H with ac Excitation.

Simple Transformer

A transformer in its simplest form is shown in Figure 1-9. This transformer has two air coils that share a common flux. The flux diverges from the ends of the primary coil in all directions. It is not concentrated or confined. The primary is connected to the source and carries the current that establishes a magnetic field. The other coil is open-circuited. Notice that the flux lines are not common to both coils. The difference between the two is the leakage flux; that is, leakage flux is the portion of the flux that does not link both coils.

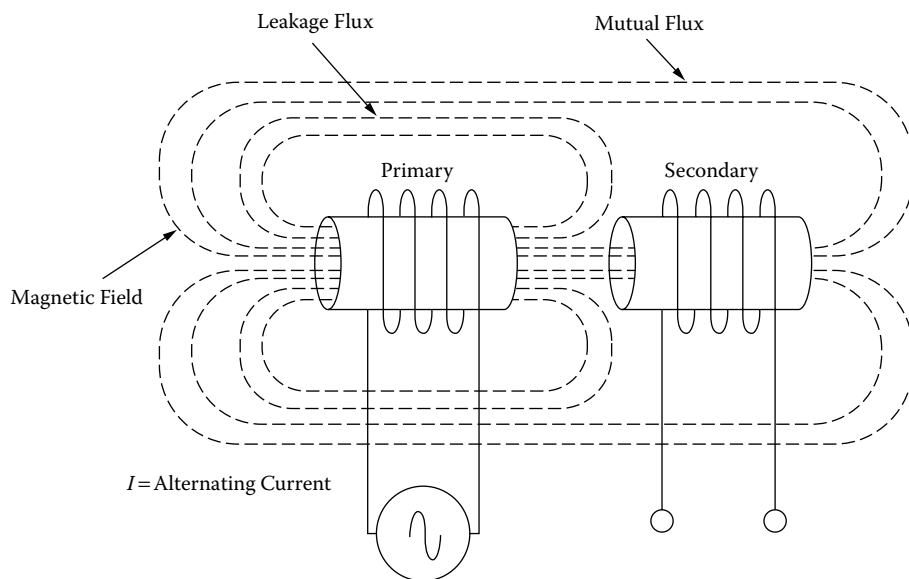


Figure 1-9. The Simplest Type of Transformer.

Magnetic Core

Most materials are poor conductors of magnetic flux; they have low permeability. A vacuum has a permeability of 1.0, and nonmagnetic materials, such as air, paper, and copper have permeabilities of the same order. There are a few materials, such as iron, nickel, cobalt, and their alloys that have high permeability, sometimes ranging into the hundreds of thousands. To achieve an improvement over the air-coil, as shown in Figure 1-10, a magnetic core can be introduced, as shown in Figure 1-11. In addition to its high permeability, the advantages of the magnetic core over the air-core are that the Magnetic Path Length (MPL) is well-defined, and the flux is essentially confined to the core, except in the immediate vicinity of the winding. There is a limit as to how much magnetic flux can be generated in a magnetic material before the magnetic core goes into saturation, and the coil reverts back to an air-core, as shown in Figure 1-12.

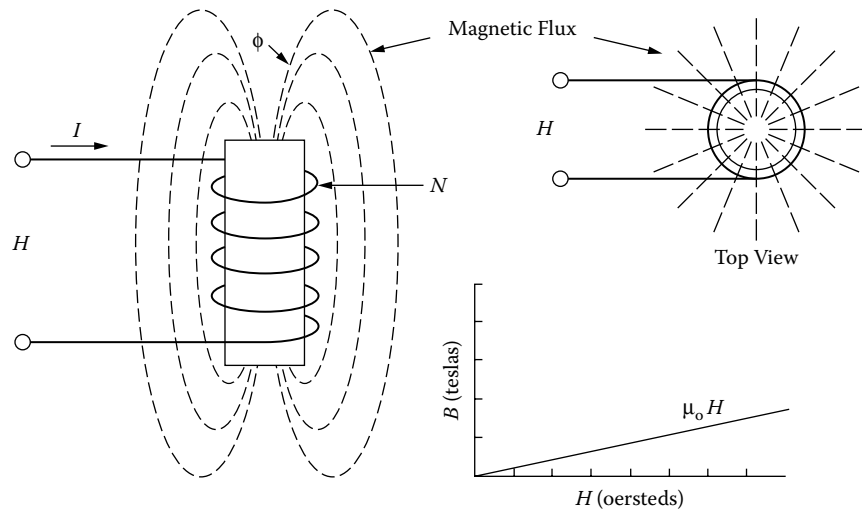


Figure 1-10. Air-Core Coil Emitting Magnetic Flux when Excited.

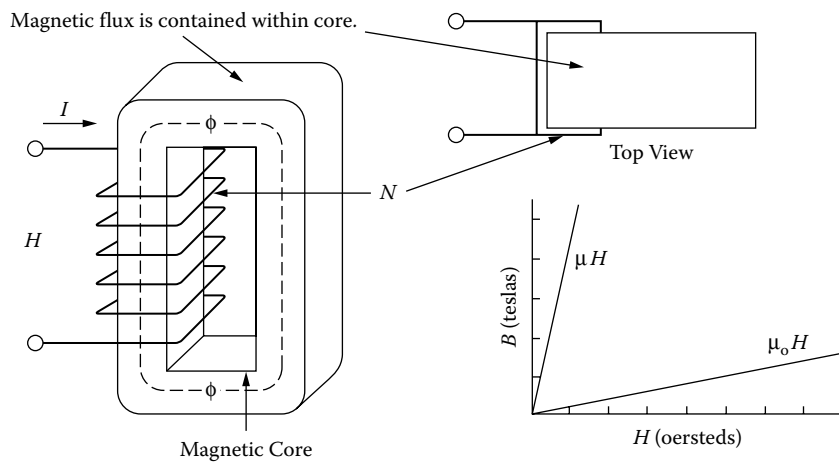


Figure 1-11. Introduction of a Magnetic Core.

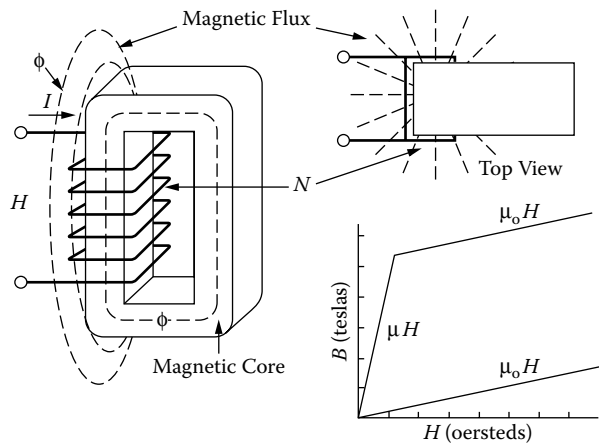


Figure 1-12. Excited Magnetic Core Driven into Saturation.

Fundamental Characteristics of a Magnetic Core

The effect of exciting a completely demagnetized, ferromagnetic material, with an external magnetizing force, H , and increasing it slowly, from zero, is shown in Figure 1-13, where the resulting flux density is plotted as a function of the magnetizing force, H . Note that, at first, the flux density increases very slowly up to point A, then, increases very rapidly up to point B, and then, almost stops increasing. Point B is called the knee of the curve. At point C, the magnetic core material has saturated. From this point on, the slope of the curve is shown in Equation [1-3].

$$\frac{B}{H} = 1, \quad [\text{gauss/oersteds}] \quad [1-3]$$

The coil is now behaving as if it had an air-core. When the magnetic core is in hard saturation, the coil has the same permeability as air, or unity. Following the magnetization curve in [Figure 1-14](#), [Figures 1-15](#) through [Figures 1-16](#) show how the flux in the core is generated from the inside of the core to the outside until the core saturates.

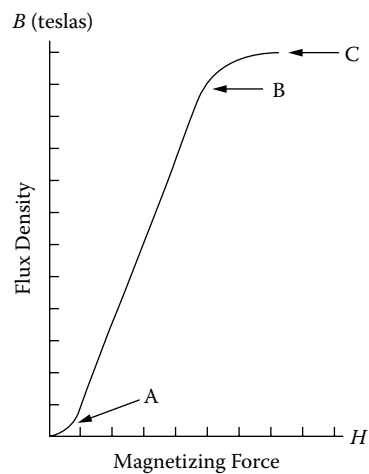


Figure 1-13. Typical Magnetization Curve.

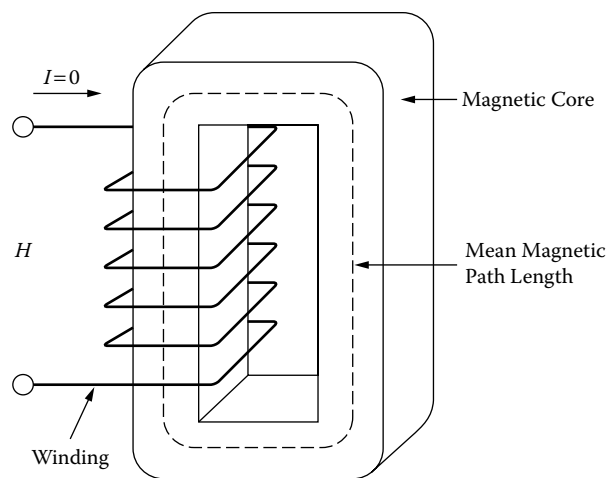


Figure 1-14. Magnetic Core with Zero Excitation.

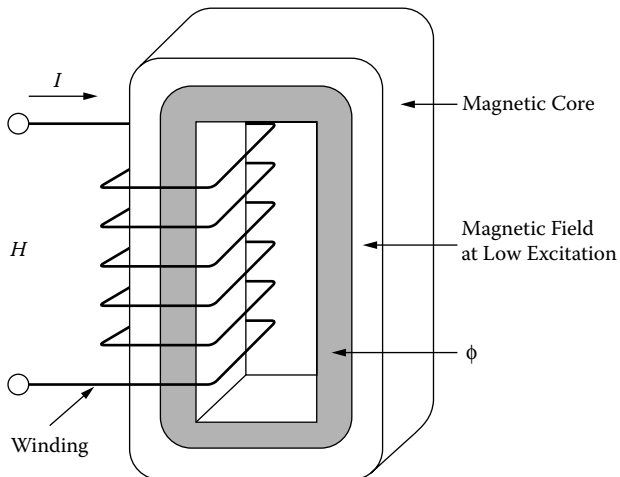


Figure 1-15. Magnetic Core with Low Excitation.

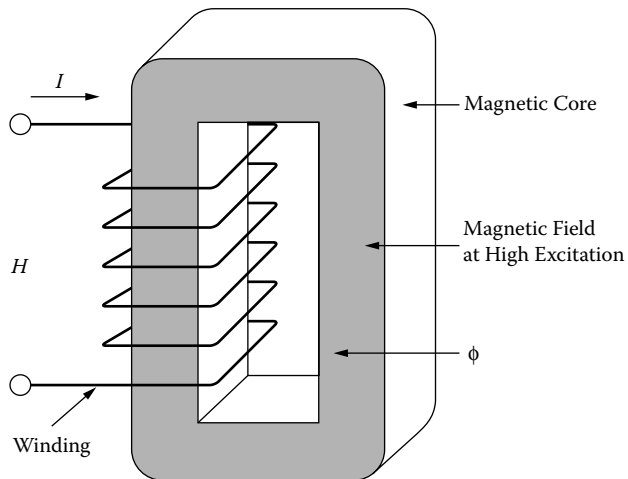


Figure 1-16. Magnetic Core with High Excitation.

Hysteresis Loop (B-H Loop)

An engineer can take a good look at the hysteresis loop and get a first order evaluation of the magnetic material. When the magnetic material is taken through a complete cycle of magnetization and demagnetization, the results are as shown in Figure 1-17. It starts with a neutral magnetic material, traversing the B-H loop at the origin X. As H is increased, the flux density B increases along the dashed line to the saturation point, B_s . When H is now decreased and B is plotted, B-H loop transverses a path to B_r , where H is zero and the core is still magnetized. The flux at this point is called remanent flux, and has a flux density, B_r .

The magnetizing force, H, is now reversed in polarity to give a negative value. The magnetizing force required to reduce the flux B_r to zero is called the coercive force, H_c . When the core is forced into saturation, the retentivity, B_{rs} , is the remaining flux after saturation, and coercivity, H_{cs} , is the magnetizing force required to reset to zero. Along the initial magnetization curve at point X, the dashed line in Figure 1-17, B increases from the origin nonlinearly with H, until the material saturates. In practice, the magnetization of a core in an excited transformer never follows this curve, because the core is never in the totally demagnetized state, when the magnetizing force is first applied.

The hysteresis loop represents energy lost in the core. The best way to display the hysteresis loop is to use a dc current, because the intensity of the magnetizing force must be so slowly changed so that no eddy currents are generated in the material. Only under this condition is the area inside the closed B-H loop indicative of the hysteresis. The enclosed area is a measure of energy lost in the core material during that cycle. In ac applications, this process is repeated continuously and the total hysteresis loss is dependent upon the frequency.

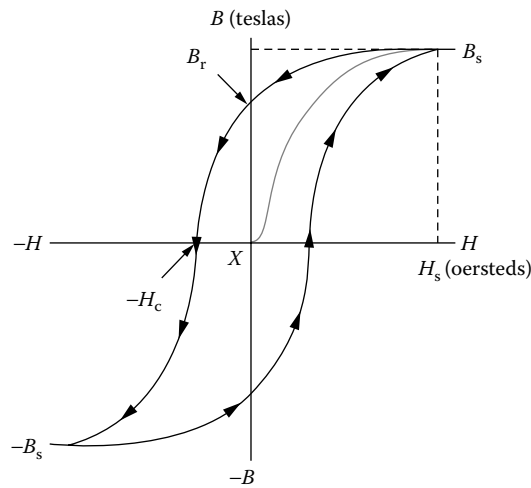


Figure 1-17. Typical Hysteresis Loop.

Permeability

In magnetics, permeability is the ability of a material to conduct flux. The magnitude of the permeability at a given induction is the measure of the ease with which a core material can be magnetized to that induction. It is defined as the ratio of the flux density, B , to the magnetizing force, H . Manufacturers specify permeability in units of gauss per oersteds, as shown in Equation [1-4].

$$\text{Permeability} = \frac{B}{H}, \quad \left[\frac{\text{gauss}}{\text{oersteds}} \right] \quad [1-4]$$

The absolute permeability, μ_0 in cgs units is unity 1 (gauss per oersteds) in a vacuum, as shown in Equation [1-5].

$$\begin{aligned} \text{cgs: } \mu_0 &= 1, \quad \left[\frac{\text{gauss}}{\text{oersteds}} \right] = \left[\frac{\text{teslas}}{\text{oersteds}} (10^4) \right] \\ \text{mks: } \mu_0 &= 0.4\pi(10^{-8}), \quad \left[\frac{\text{henrys}}{\text{meter}} \right] \end{aligned} \quad [1-5]$$

When B is plotted against H , as in [Figure 1-18](#), the resulting curve is called the magnetization curve. These curves are idealized. The magnetic material is totally demagnetized and is then subjected to gradually increasing magnetizing force, while the flux density is plotted. The slope of this curve at any given point gives the permeability at that point. Permeability can be plotted against a typical B-H curve, as shown in [Figure 1-19](#). Permeability is not constant; therefore, its value can be stated only at a given value of B or H .

There are many different kinds of permeability, and each is designated by a different subscript on the symbol μ .

- μ_0 1. Absolute permeability, defined as the permeability in a vacuum.
- μ_i 2. Initial permeability is the slope of the initial magnetization curve at the origin. It is measured at very small induction, as shown in [Figure 1-20](#).
- μ_Δ 3. Incremental permeability is the slope of the magnetization curve for finite values of peak-to-peak flux density with superimposed dc magnetization, as shown in [Figure 1-21](#).
- μ_e 4. Effective permeability. If a magnetic circuit is not homogeneous (i.e., contains an air gap), the effective permeability is the permeability of hypothetical homogeneous (ungapped) structure of the same shape, dimensions, and reluctance that would give the inductance equivalent to the gapped structure.
- μ_r 5. Relative permeability is the permeability of a material relative to that of free space.
- μ_n 6. Normal permeability is the ratio of B/H at any point of the curve, as shown in [Figure 1-22](#).
- μ_{\max} 7. Maximum permeability is the slope of a straight line drawn from the origin tangent to the curve at its knee, as shown in [Figure 1-23](#).
- μ_p 8. Pulse permeability is the ratio of peak B to peak H for unipolar excitation.
- μ_m 9. Material permeability is the slope of the magnetization curve measured at less than 50 gauss, as shown in [Figure 1-24](#).

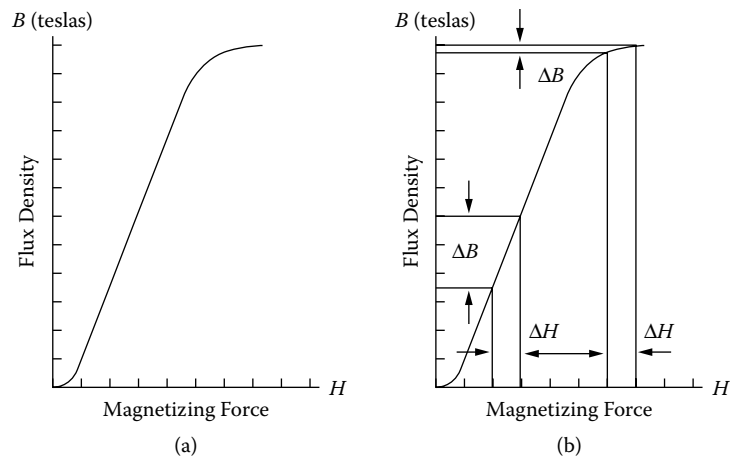


Figure 1-18. Magnetizing Curve.

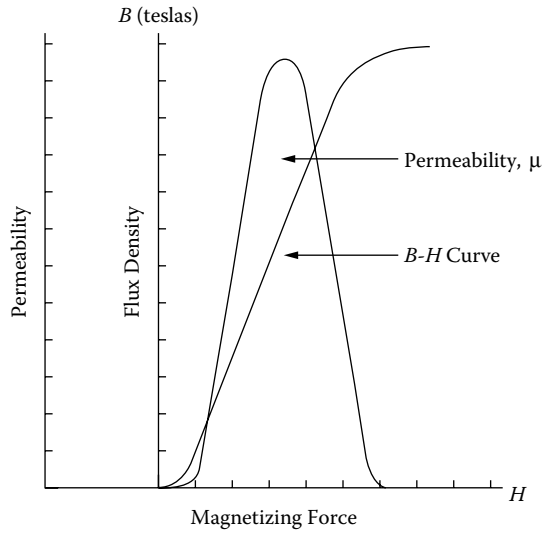


Figure 1-19. Variation of Permeability μ along the Magnetizing Curve.

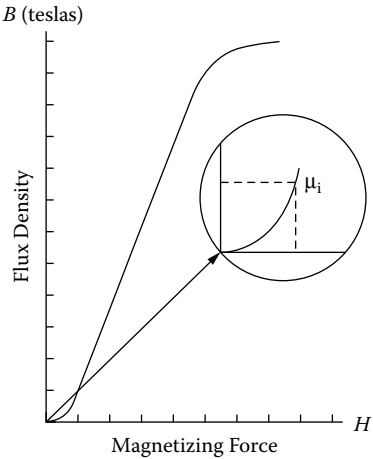


Figure 1-20. Initial Permeability.

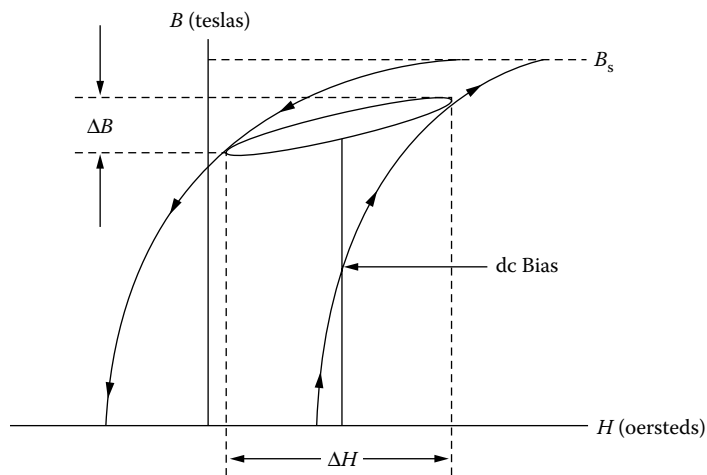


Figure 1-21. Incremental Permeability.

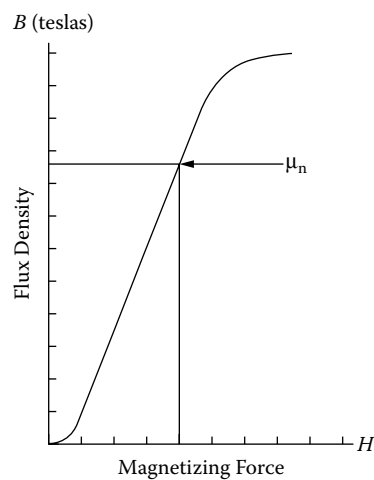


Figure 1-22. Normal Permeability.

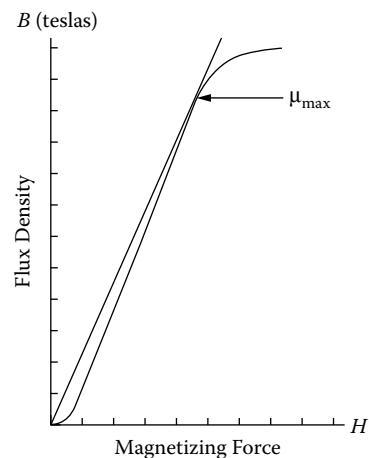


Figure 1-23. Maximum Permeability.

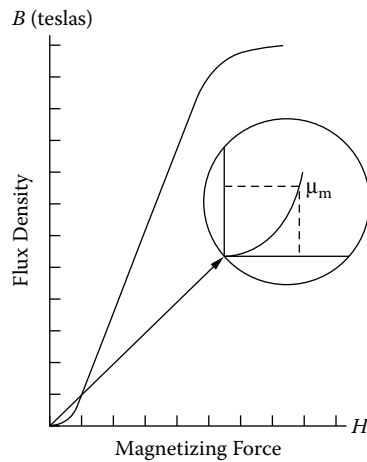


Figure 1-24. Material Permeability.

Magnetomotive Force (mmf) and Magnetizing Force (H)

There are two force functions commonly encountered in magnetics: magnetomotive force, mmf, and magnetizing force, H. Magnetomotive force should not be confused with magnetizing force; the two are related as cause and effect. Magnetomotive force is given by the Equation [1-6].

$$\text{mmf} = 0.4\pi NI, \quad [\text{gilberts}] \quad [1-6]$$

N is the number of turns and I is the current in amperes. Whereas mmf is the force, H is a force field, or force per unit length, as shown in Equation [1-7].

$$H = \frac{\text{mmf}}{\text{MPL}}, \quad \left[\frac{\text{gilberts}}{\text{cm}} = \text{oersteds} \right] \quad [1-7]$$

Substituting,

$$H = \frac{0.4\pi NI}{\text{MPL}}, \quad [\text{oersteds}] \quad [1-8]$$

MPL = Magnetic Path Length in cm.

If the flux is divided by the core area, A_c , we get flux density, B, in lines per unit area, as shown in Equation [1-9].

$$B = \frac{\phi}{A_c}, \quad [\text{gauss}] \quad [1-9]$$

The flux density, B, in a magnetic medium, due to the existence of a magnetizing force H, depends on the permeability of the medium and the intensity of the magnetic field, as shown in Equation [1-10].

$$B = \mu H, \quad [\text{gauss}] \quad [1-10]$$

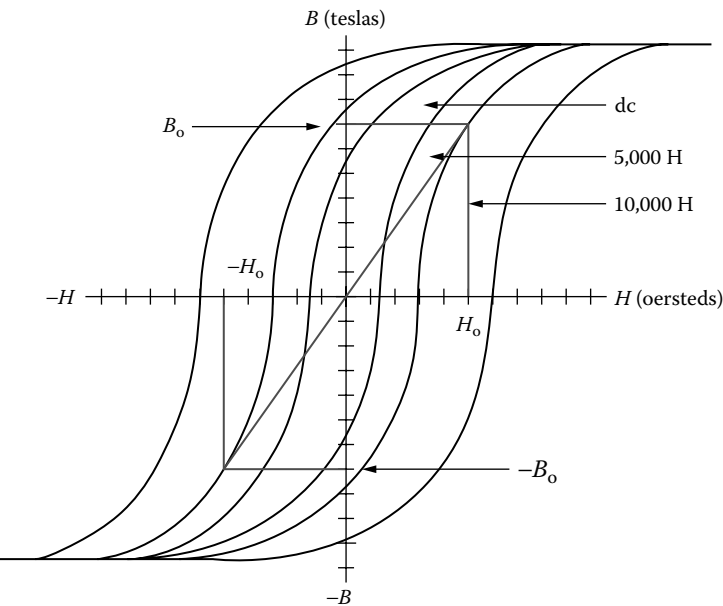


Figure 1-25. Typical B-H Loops Operating at Various Frequencies.

The peak magnetizing current, I_m , for a wound core can be calculated from the following Equation [1-11].

$$I_m = \frac{H_o(MPL)}{0.4\pi N}, \quad [\text{amps}] \quad [1-11]$$

H_o is the field intensity at the peak operating point. To determine the magnetizing force, H_o , use the manufacturer's core loss curves at the appropriate frequency and operating flux density, B_o , as shown in Figure 1-25.

Reluctance

The flux produced in a given material by magnetomotive force (mmf) depends on the material's resistance to flux, which is called reluctance, R_m . The reluctance of a core depends on the composition of the material and its physical dimension and is similar in concept to electrical resistance. The relationship between mmf, flux, and magnetic reluctance is analogous to the relationship between emf, current, and resistance, as shown in Figure 1-26.

$$\begin{aligned} \text{emf } (E) &= IR = \text{Current} \times \text{Resistance} \\ \text{mmf } (F_m) &= \Phi R_m = \text{Flux} \times \text{Reluctance} \end{aligned} \quad [1-12]$$

A poor conductor of flux has a high magnetic resistance, R_m . The greater the reluctance, the higher the magnetomotive force that is required to obtain a given magnetic field.

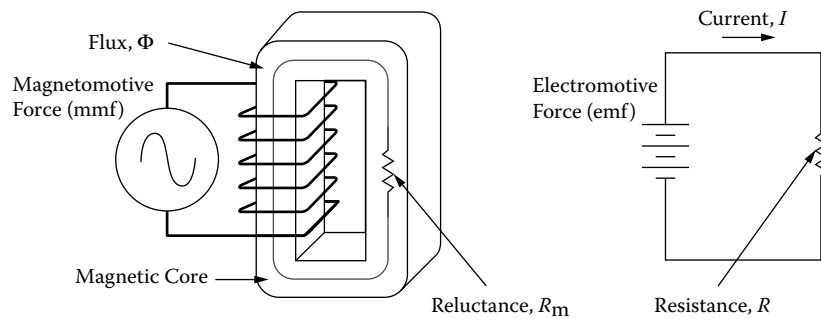


Figure 1-26. Comparing Magnetic Reluctance and Electrical Resistance.

The electrical resistance of a conductor is related to its length l , cross-sectional area A_w , and specific resistance ρ , which is the resistance per unit length. To find the resistance of a copper wire of any size or length, we merely multiply the resistivity by the length, and divide by the cross-sectional area, as shown in Equation [1-13].

$$R = \frac{\rho l}{A_w}, \quad [\text{ohms}] \quad [1-13]$$

In the case of magnetics, $1/\mu$ is analogous to ρ and is called reluctivity. The reluctance, R_m , of a magnetic circuit, is shown in Equation [1-14].

$$R_m = \frac{\text{MPL}}{\mu_r \mu_o A_c} \quad [1-14]$$

Where MPL, is the magnetic path length, cm.

A_c is the cross-section of the core, cm^2 .

μ_r is the permeability of the magnetic material.

μ_o is the permeability of air.

A typical magnetic core is shown in Figure 1-27, illustrating the Magnetic Path Length (MPL) and the cross-sectional area, A_c , of a C core.

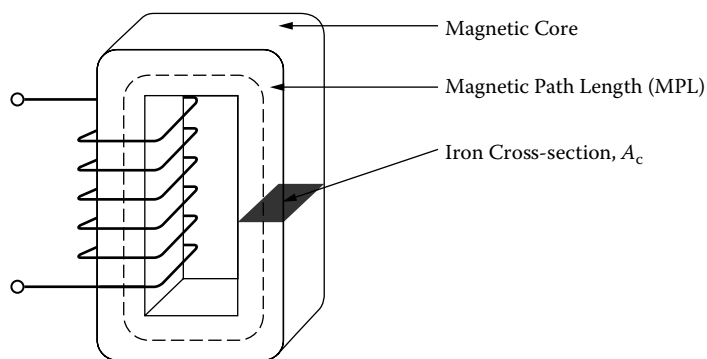


Figure 1-27. Magnetic Core Showing the Magnetic Path Length (MPL) and Iron Cross-section, A_c .

Air Gap

A high permeability material is one that has a low reluctance for a given magnetic path length (MPL) and iron cross-section, A_c . If an air gap is included in a magnetic circuit, as shown in Figure 1-28, which is otherwise composed of low reluctivity material like iron, almost all of the reluctance in the circuit will be at the gap. The reason for this is because the reluctivity of air is much greater than that of a magnetic material. For all practical purposes, controlling the size of the air gap controls the reluctance.

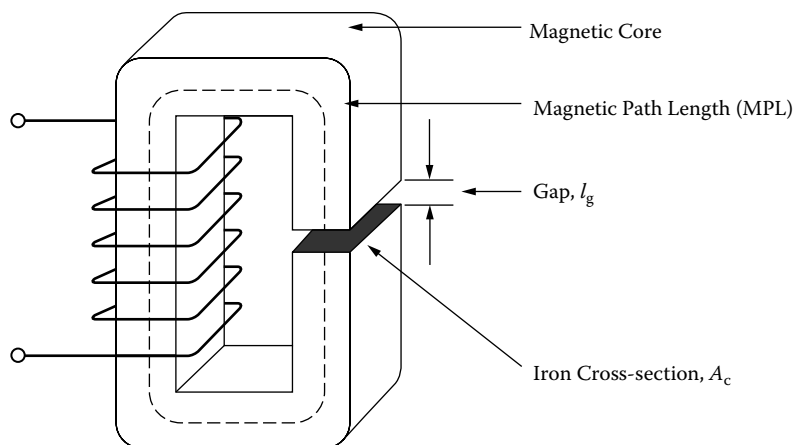


Figure 1-28. A Typical Magnetic Core with an Air Gap.

An example can best show this procedure. The total reluctance of the core is the sum of the iron reluctance and the air gap reluctance, in the same way that two series resistors are added in an electrical circuit. The equation for calculating the air gap reluctance, R_g , is basically the same as the equation for calculating the reluctance of the magnetic material, R_m . The difference is that the permeability of air is 1 and the gap length, l_g , is used in place of the Magnetic Path Length (MPL). The equation is shown in Equation [1-15].

$$R_g = \left(\frac{1}{\mu_o} \right) \left(\frac{l_g}{A_c} \right) \quad [1-15]$$

But, since $\mu_o = 1$, the Equation simplifies to:

$$R_g = \frac{l_g}{A_c} \quad [1-16]$$

Where:

l_g = the gap length, cm.

A_c = the cross-section of the core, cm^2 .

μ_o = the permeability of air.

The total reluctance, R_{mt} , for the core shown in Figure 1-28 is therefore:

$$R_{mt} = R_m + R_g$$

$$R_{mt} = \frac{MPL}{\mu_r \mu_o A_c} + \frac{l_g}{\mu_o A_c} \quad [1-17]$$

Where μ_r is the relative permeability, which is used exclusively with magnetic materials.

$$\mu_r = \frac{\mu}{\mu_o} = \frac{B}{\mu_o H}, \quad \left[\begin{array}{l} \text{gauss} \\ \text{oersteds} \end{array} \right] \quad [1-18]$$

The magnetic material permeability, μ_m , is given by:

$$\mu_m = \mu_r \mu_o \quad [1-19]$$

The reluctance of the gap is higher than that of the iron even when the gap is small. The reason is because the magnetic material has a relatively high permeability, as shown in Table 1-1. So the total reluctance of the circuit depends more on the gap than on the iron.

Table 1-1. Material Permeability

Material Permeability, μ_m	
Material Name	Permeability
Iron Alloys	0.8K to 25K
Ferrites	0.8K to 20K
Amorphous	0.8K to 80K

After the total reluctance, R_t , has been calculated, the effective permeability, μ_e , can be calculated.

$$R_{mt} = \frac{l_t}{\mu_e A_c}, \quad l_t = l_g + MPL \quad [1-20]$$

Where l_t is the total path length and μ_e is the effective permeability.

$$R_{mt} = \frac{l_t}{\mu_e A_c} = \frac{l_g}{\mu_o A_c} + \frac{MPL}{\mu_o \mu_r A_c} \quad [1-21]$$

Simplifying yields:

$$\frac{l_t}{\mu_e} = \frac{l_g}{\mu_o} + \frac{MPL}{\mu_o \mu_r} \quad [1-22]$$

Then:

$$\mu_e = \frac{l_t}{\frac{l_g}{\mu_o} + \frac{MPL}{\mu_o \mu_r}} \quad [1-23]$$

$$\mu_e = \frac{l_g + MPL}{\frac{l_g}{\mu_o} + \frac{MPL}{\mu_o \mu_r}}$$

If $l_g \ll MPL$, multiply both sides of the equation by $(\mu_r \mu_o MPL) / (\mu_r \mu_o MPL)$.

$$\mu_e = \frac{\mu_o \mu_r}{1 + \mu_r \left(\frac{l_g}{MPL} \right)} \quad [1-24]$$

The classic equation is:

$$\mu_e = \frac{\mu_m}{1 + \mu_m \left(\frac{l_g}{MPL} \right)} \quad [1-25]$$

Introducing an air gap, l_g , to the core cannot correct for the dc flux, but can sustain the dc flux. As the gap is increased, so is the reluctance. For a given magnetomotive force, the flux density is controlled by the gap.

Controlling the dc Flux with an Air Gap

There are two similar equations used to calculate the dc flux. The first equation is used with powder cores. Powder cores are manufactured from very fine particles of magnetic materials. This powder is coated with an inert insulation to minimize eddy currents losses and to introduce a distributed air gap into the core structure.

$$\begin{aligned} \mu_r &= \mu_e \\ B_{dc} &= (\mu_r) \left(\frac{0.4\pi NI}{MPL} \right), \quad [\text{gauss}] \\ \mu_r &= \frac{\mu_m}{1 + \mu_m \left(\frac{l_g}{MPL} \right)} \end{aligned} \quad [1-26]$$

The second equation is used, when the design calls for a gap to be placed in series with the Magnetic Path Length (MPL), such as a ferrite cut core, a C core, or butt-stacked laminations.

$$\begin{aligned} \mu_r &= \mu_e \\ B_{dc} &= (\mu_r) \left(\frac{0.4\pi NI}{MPL} \right), \quad [\text{gauss}] \end{aligned} \quad [1-27]$$

Substitute $(MPL\mu_m) / (MPL\mu_m)$ for 1:

$$\mu_r = \frac{\mu_m}{1 + \mu_m \left(\frac{l_g}{MPL} \right)} = \frac{\mu_m}{\frac{MPL\mu_m}{MPL\mu_m} + \mu_m \left(\frac{l_g}{MPL} \right)} \quad [1-28]$$

Then, simplify:

$$\mu_r = \frac{\text{MPL}}{\frac{\text{MPL}}{\mu_m} + l_g} \quad [1-29]$$

$$B_{dc} = \left(\frac{\text{MPL}}{\frac{\text{MPL}}{\mu_m} + l_g} \right) \left(\frac{0.4\pi NI}{\text{MPL}} \right), \quad [\text{gauss}] \quad [1-30]$$

Then, simplify:

$$B_{dc} = \frac{0.4\pi NI}{l_g + \frac{\text{MPL}}{\mu_m}}, \quad [\text{gauss}] \quad [1-31]$$

Types of Air Gaps

Basically, there are two types of gaps used in the design of magnetic components: bulk and distributed. Bulk gaps are maintained with materials, such as paper, Mylar, or even glass. The gapping materials are designed to be inserted in series with the magnetic path to increase the reluctance, R, as shown in Figure 1-29.

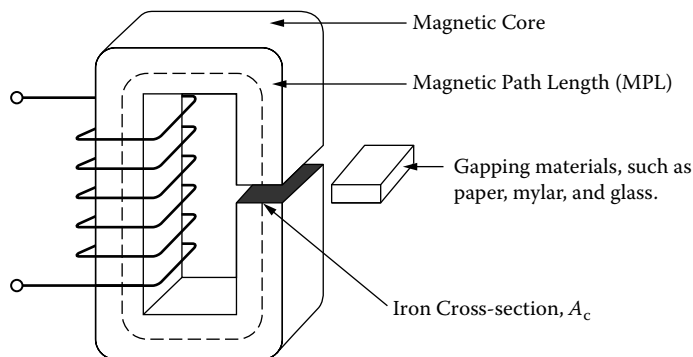


Figure 1-29. Placement of the Gapping Materials.

Placement of the gapping material is critical in keeping the core structurally balanced. If the gap is not proportioned in each leg, then the core will become unbalanced and create even more than the required gap. There are designs where it is important to place the gap in an area to minimize the noise that is caused by the fringing flux at the gap. The gap placement for different core configurations is shown in Figure 1-30. The standard gap placement is shown in Figure 1-30A, C, and D. The EE or EC cores shown in Figure 1-30B, are best-suited, when the gap has to be isolated within the magnetic assembly to minimize fringing flux noise. When the gap is used as shown in Figure 1-30A, C, and D, then, only half the thickness of the calculated gap dimension is used in each leg of the core.

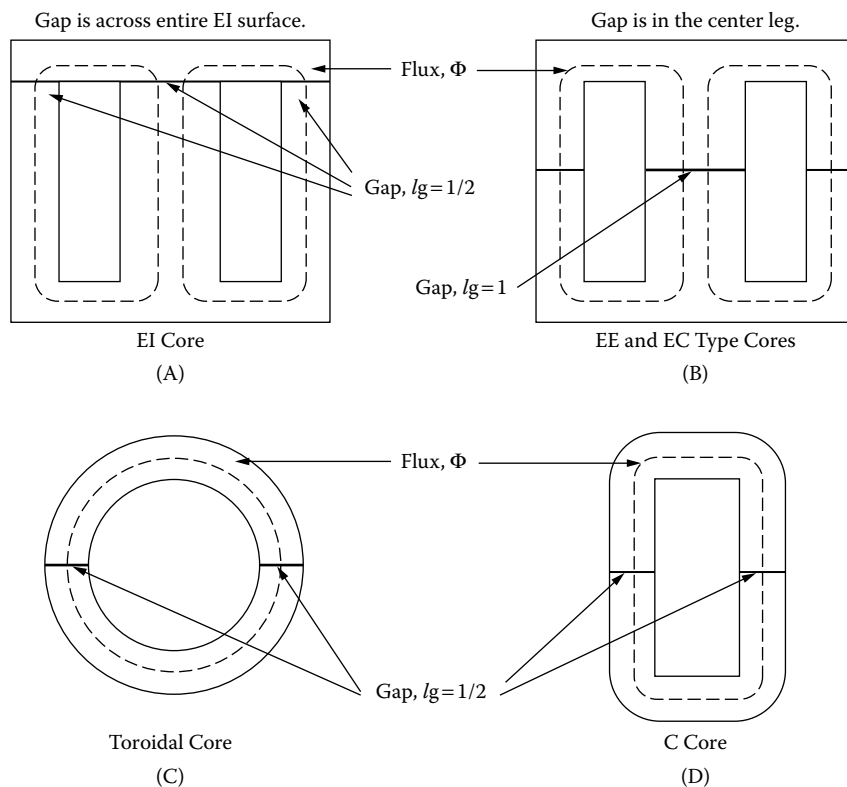


Figure 1-30. Gap Placement using Different Core Configurations.

Fringing Flux

Introduction

Fringing flux has been around since time began for the power conversion engineer. Designing power conversion magnetics that produce a minimum of fringing flux has always been a problem. Engineers have learned to design around fringing flux, and minimize its effects. It seems that when engineers do have a problem, it is usually at the time when the design is finished and ready to go. It is then that the engineer will observe something that was not recognized before. This happens during the final test when the unit becomes unstable, the inductor current is nonlinear, or the engineer just located a hot spot during testing. Fringing flux can cause a multitude of problems. Fringing flux can reduce the overall efficiency of the converter, by generating eddy currents that cause localized heating in the windings and/or the brackets. When designing inductors, fringing flux must be taken into consideration. If the fringing flux is not handled correctly, there will be premature core saturation. More and more magnetic components are now designed to operate in the sub-megahertz region. High frequency has really brought out the fringing flux and its parasitic eddy currents. Operating at high frequency has made the engineer very much aware of what fringing flux can do to hamper a design.

Material Permeability, (μ_m)

The B-H loops that are normally seen in the manufacturers' catalogs are usually taken from a toroidal sample of the magnetic material. The toroidal core, without a gap, is the ideal shape to view the B-H loop of a given material. The material permeability, μ_m , will be seen at its highest in the toroidal shape, as shown in Figure 1-31.

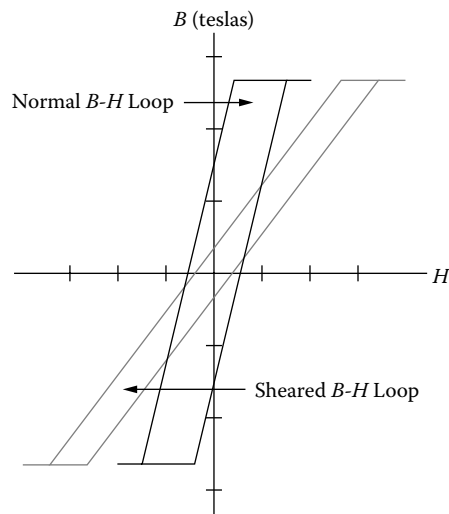


Figure 1-31. The Shearing of an Idealized B-H Loop due to an Air Gap.

A small amount of air gap, less than 25 microns, has a powerful effect by shearing over the B-H loop. This shearing over of the B-H loop reduces the permeability. High permeability ferrites that are cut, like E cores, have only about 80 percent of the permeability, than that of a toroid of the same material. This is because of the induced gap, even though the mating surfaces are highly polished. In general, magnetic materials with high-permeability, are sensitive to temperature, pressure, exciting voltage, and frequency. The inductance change is directly proportional to the permeability change. This change in inductance will have an effect on the exciting current. It is very easy to see, that inductors that are designed into an LC, tuned circuit, must have a stable permeability, μ_e .

$$L = \frac{0.4\pi N^2 A_c \Delta\mu (10^{-8})}{MPL}, \quad [\text{henrys}] \quad [1-32]$$

Air Gaps

Air gaps are introduced into magnetic cores for a variety of reasons. In a transformer design a small air gap, l_g , inserted into the magnetic path, will lower and stabilize the effective permeability, μ_e .

$$\mu_e = \frac{\mu_m}{1 + \mu_m \left(\frac{l_g}{MPL} \right)} \quad [1-33]$$

This will result in a tighter control of the permeability change with temperature, and exciting voltage. Inductor designs will normally require a large air gap, l_g , to handle the dc flux.

$$l_g = \frac{0.4\pi NI_{dc} (10^{-4})}{B_{dc}}, \quad [\text{cm}] \quad [1-34]$$

Whenever an air gap is inserted into the magnetic path, as shown in Figure 1-32, there is an induced, fringing flux at the gap.

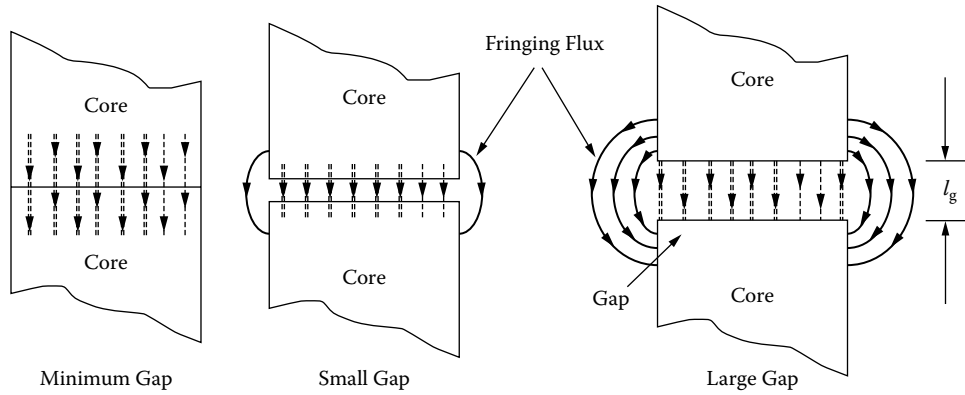


Figure 1-32. Fringing Flux at the Gap.

The fringing flux effect is a function of gap dimension, the shape of the pole faces, and the shape, size, and location of the winding. Its net effect is to shorten the air gap. Fringing flux decreases the total reluctance of the magnetic path and, therefore, increases the inductance by a factor, F , to a value greater than the one calculated.

Fringing Flux, F

Fringing flux is completely around the gap and re-enters the core in a direction of high loss, as shown in [Figure 1-33](#). Accurate prediction of gap loss, P_g , created by fringing flux is very difficult to calculate.

This area around the gap is very sensitive to metal objects, such as clamps, brackets and banding materials. The sensitivity is dependent on the intensity of the magnetomotive force, gap dimensions and the operating frequency. If a metal bracket or banding material is used to secure the core, and it passes over the gap, two things can happen: (1) If the material ferromagnetic is placed over the gap, or is in close proximity so it conducts the magnetic field, this is called "shorting the gap." Shorting the gap is the same as reducing the gap

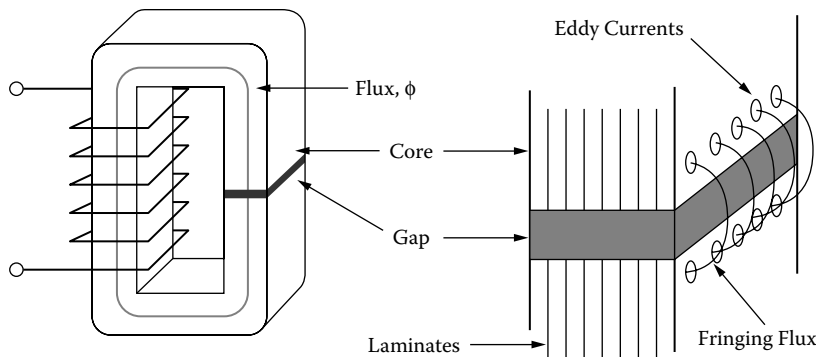


Figure 1-33. Fringing Flux, with High Loss Eddy Currents.

dimension, thereby producing a higher inductance, than designed, and could drive the core into saturation. (2) If the material is metallic, (such as copper, or phosphor bronze), but not ferromagnetic, it will not short the gap or change the inductance. In both cases, if the fringing flux is strong enough, it will induce eddy currents that will cause localized heating. This is the same principle used in induction heating.

Gapped, dc Inductor Design

The fringing flux factor, F , has an impact on the basic inductor design equations. When the engineer starts a design, he or she must determine the maximum values for B_{dc} and for B_{ac} , which will not produce magnetic saturation. The magnetic material that has been selected will dictate the saturation flux density. The basic equation for maximum flux density is:

$$B_{\max} = \frac{0.4\pi N \left(I_{dc} + \frac{\Delta I}{2} \right) (10^{-4})}{l_g + \frac{MPL}{\mu_m}}, \quad [\text{teslas}] \quad [1-35]$$

The inductance of an iron-core inductor, carrying dc and having an air gap, may be expressed as:

$$L = \frac{0.4\pi N^2 A_c (10^{-8})}{l_g + \frac{MPL}{\mu_m}}, \quad [\text{henrys}] \quad [1-36]$$

The inductance is dependent on the effective length of the magnetic path, which is the sum of the air gap length, l_g , and the ratio of the core magnetic path length to the material permeability, (MPL/μ_m). The final determination of the air gap size requires consideration of the fringing flux effect which is a function of the gap dimension, the shape of the pole faces, and the shape, size, and location of the winding. The winding length, or the G dimension of the core, has a big influence on the fringing flux. See, [Figure 1-34](#) and Equation 1-37.

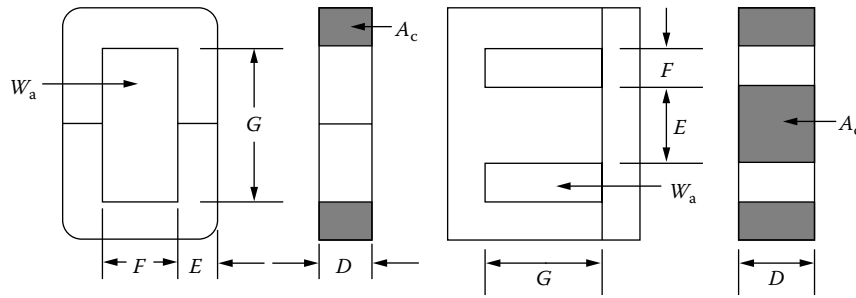


Figure 1-34. Dimensional Call Out for C and E Cores.

The fringing flux decreases the total reluctance of the Magnetic Path Length and, therefore, increases the inductance by a factor of F to a value greater than that calculated. The fringing flux factor is:

$$F = \left(1 + \frac{l_g}{\sqrt{A_c}} \ln \frac{2G}{l_g} \right) \quad [1-37]$$

After the inductance has been calculated using Equation 1-36, the fringing flux factor has to be incorporated into Equation 1-36. Equation 1-36 can now be rewritten to include the fringing flux factor, as shown in Equation 1-38

$$L = F \left(\frac{0.4\pi N^2 A_c (10^{-8})}{l_g + \frac{\text{MPL}}{\mu_m}} \right), \quad [\text{henrys}] \quad [1-38]$$

The fringing flux factor, F , can now be included into Equation 1-35. This will check for premature, core saturation.

$$B_{\max} = F \left(\frac{0.4\pi N \left(I_{dc} + \frac{\Delta I}{2} \right) (10^{-4})}{l_g + \frac{\text{MPL}}{\mu_m}} \right), \quad [\text{teslas}] \quad [1-39]$$

Now that the fringing flux factor, F , is known and inserted into Equation 1-38. Equation 1-38 can be rewritten to solve for the required turns so that premature core saturation will not happen, as shown in Equation 1-40.

$$N = \sqrt{\frac{L \left(l_g + \frac{\text{MPL}}{\mu_m} \right)}{0.4\pi A_c F (10^{-8})}}, \quad [\text{turns}] \quad [1-40]$$

Fringing Flux and Coil Proximity

As the air gap increases, the fringing flux will increase. Fringing flux will fringe out away from the gap by the distance of the gap. If a coil was wound tightly around the core and encompasses the gap, the flux generated

around the magnet wire will force the fringing flux back into the core. The end result will not produce any fringing flux at all, as shown in Figure 1-35. As the coil distance moves away from the core, the fringing flux will increase until the coil distance from the core is equal to the gap dimension.

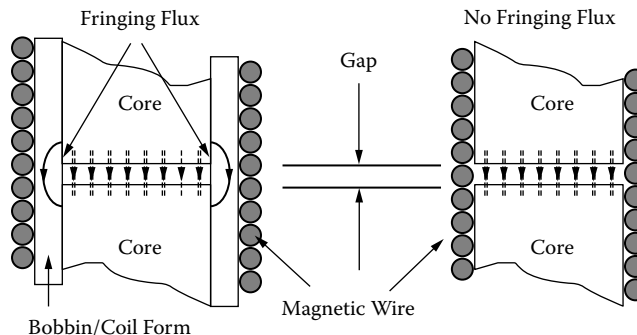


Figure 1-35. Comparing a Tightly-Wound Coil, and a Coil Wound on a Coil Form.

Fringing Flux, Crowding

Flux will always take the path of highest permeability. This can best be seen in transformers with interleaved laminations. The flux will traverse along the lamination until it meets its mating, I or E. At this point, the flux will jump to the adjacent lamination and bypass the mating point, as shown in Figure 1-36.

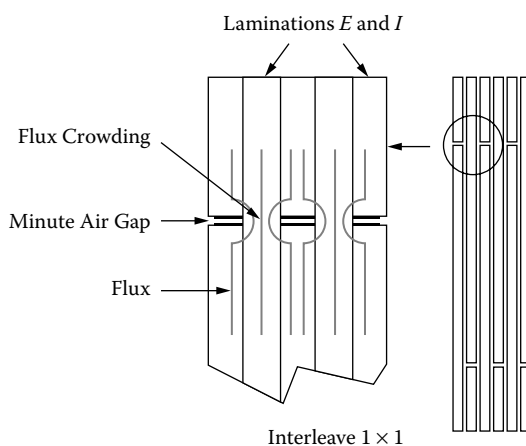


Figure 1-36. Flux Crowding in Adjacent Laminations.

This phenomena can best be seen by observing the exciting current at low, medium and high flux levels, as shown in [Figure 1-37](#). At low levels of excitation, the exciting current is almost square, due to the flux taking the high permeability path, by jumping to the adjacent lamination, as shown in Figure 1-36. As the excitation is increased, the adjoining lamination will start to saturate, and the exciting current will increase and become nonlinear. When the adjacent lamination approaches saturation, the permeability drops. It is then that the flux will go in a straight line and cross the minute air gap, as shown in Figure 1-36.

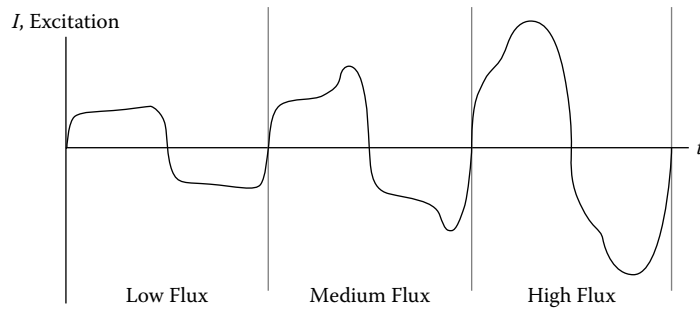


Figure 1-37. Exciting Current, at Different Levels of Flux Density, B.

Fringing Flux and Powder Cores

Designing high frequency converters, using low permeability powder cores, will usually require very few turns. Low perm power cores (less than 60), exhibit fringing flux. Powder cores with a distributed gap will have fringing flux that shorts the gap and gives the impression of a core with a higher permeability. Because of the fringing flux and a few turns, it is very important to wind uniformly and in a consistent manner. This winding is done to control the fringing flux and get inductance repeatability from one core to another, as shown in Figures 1-38 and 1-39.

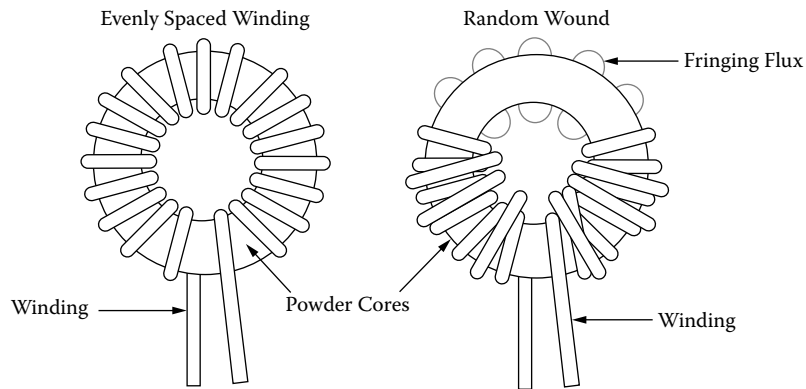


Figure 1-38. Comparing Toroidal, Winding Methods.

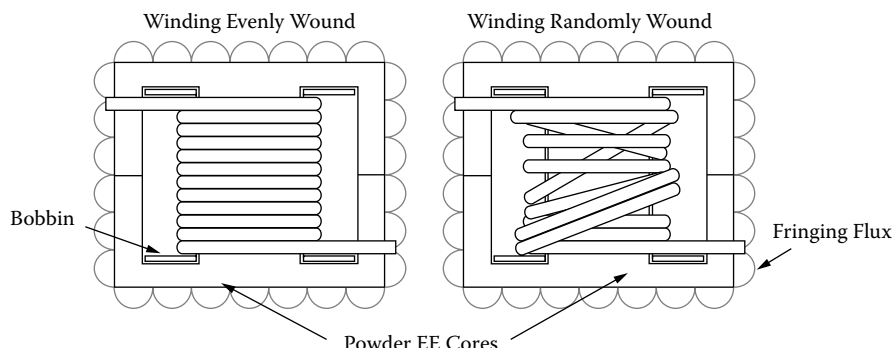


Figure 1-39. Comparing EE Cores, Winding Methods.

Chapter 2

Magnetic Materials and Their Characteristics

Table of Contents

1. Introduction.....	2-3
2. Saturation	2-3
3. Remanence Flux, B_r , and Coercivity H_c	2-4
4. Permeability, μ	2-4
5. Hysteresis Loss, Resistivity, ρ , (core loss)	2-4
6. Introduction to Silicon Steel	2-5
7. Introduction to Thin Tape Nickel Alloys.....	2-5
8. Introduction to Metallic Glass.....	2-9
9. Introduction to Soft Ferrites.....	2-12
10. Manganese-Zinc Ferrites	2-13
11. Nickel-Zinc Ferrites	2-13
12. Ferrite Cross Reference.....	2-16
13. Introduction to Molypermalloy Powder Cores	2-17
14. Introduction to Iron Powder Cores.....	2-17
15. Core Loss	2-24
16. Core Loss Equations.....	2-25
17. Selection of Magnetic Materials.....	2-29
18. Typical Operation	2-29
19. Material Characteristics	2-30
20. Magnetic Material Saturation Defined	2-33
21. Test Conditions	2-36
22. Magnetic Material Saturation Theory.....	2-41
23. Air Gap Effect.....	2-42
24. Effect of Gapping.....	2-42
25. Composite Core Configuration	2-50
26. Summary	2-53

Introduction

The magnetic material is the paramount player in the design of magnetic components. The magnetics design engineer has three standard words when making the normal design trade-off study: cost, size, and performance. He will be happy to stuff any two into the bag. The magnetics engineer is now designing magnetic components that operate from below the audio range to the megahertz range. He is normally asked to design for maximum performance, with the minimum of his parasitic friends' capacitance and leakage inductance. Today, the magnetic materials the engineer has to work with are silicon steel, nickel iron (permalloy), cobalt iron (permendur), amorphous metallic alloys, and ferrites. These also have spin-off material variants, such as moly-permalloy powder, sendust powder, and iron powder cores. From this group of magnetic materials, the engineer will make trade-offs with the magnetic properties for his design. These properties are: saturation, B_s , permeability, μ , resistivity, ρ (core loss), remanence, B_r , and coercivity, H_c .

Saturation

A typical hysteresis loop of a soft magnetic material is shown in Figure 2-1. When a high magnetizing force is encountered, a point is reached where further increase in, H , does not cause useful increase in, B . This point is known as the saturation point of that material. The saturation flux density, B_s , and the required magnetizing force, H_s , to saturate the core are shown with dashed lines.

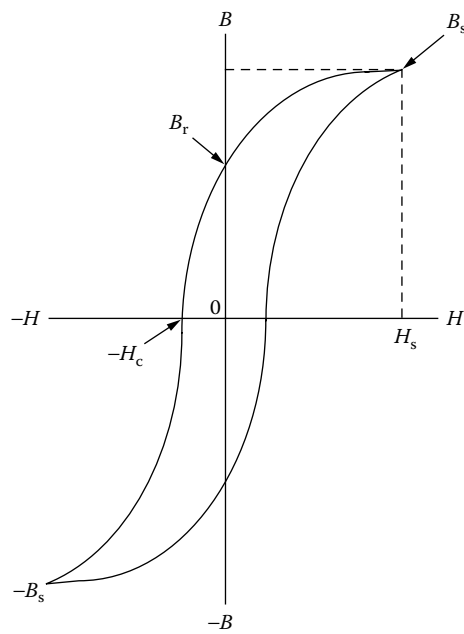


Figure 2-1. Typical B-H or Hysteresis Loop of a Soft Magnetic Material.

Remanence Flux, B_r , and Coercivity H_c

In [Figure 2-1](#) the hysteresis loop clearly shows the remanence flux density, B_r . The remanence flux is the polarized flux remaining in the core after the excitation has been removed. The magnetizing force, $-H_c$, is called coercivity. It is the amount of magnetizing force required to bring the remanence flux density back to zero.

Permeability, μ

The permeability of a magnetic material is a measure of the ease in magnetizing the material. Permeability, μ , is the ratio of the flux density, B , to the magnetizing force, H , as shown in Equation [2-1].

$$\mu = \frac{B}{H}, \quad [\text{permeability}] \quad [2-1]$$

The relationship between B and H is not linear, as shown in the hysteresis loop in [Figure 2-1](#). Then, it is evident that the ratio, B/H , (permeability), also varies. The variation of permeability with flux density, B , is shown in [Figure 2-2](#). Also, it shows the flux density at which the permeability is at a maximum.

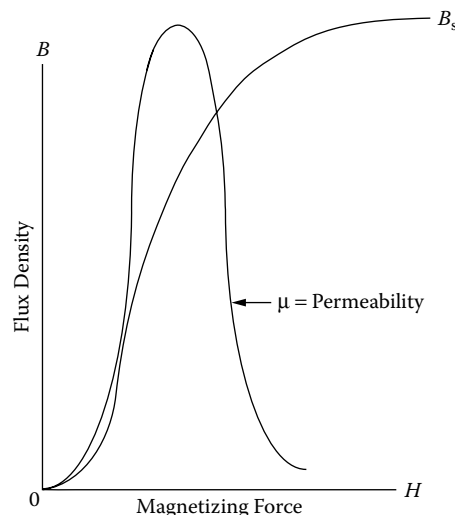


Figure 2-2. Variation in Permeability μ with B and H .

Hysteresis Loss, Resistivity, ρ , (core loss)

The enclosed area within the hysteresis, shown in [Figure 2-1](#), is a measure of the energy lost in the core material during that cycle. This loss is made up in two components: (1) the hysteresis loss and (2) eddy current loss. The hysteresis loss is the energy loss when the magnetic material is going through a cycling state. The

eddy current loss is caused when the lines of flux pass through the core, inducing electrical currents in it. These currents are called eddy currents and produce heat in the core. If the electrical resistance of the core is high, the current will be low; therefore, a feature of low-loss material is high electrical resistance. In the norm, when designing magnetic components, the core loss is a major design factor. Core loss can be controlled by selecting the right material and thickness. Selecting the correct material, and operating within its limits, will prevent overheating that could result in damage to the wire insulation and/or the potting compound.

Introduction to Silicon Steel

Silicon steel was one of the first alloys to be used in transformers and inductors. It has been greatly improved over the years and is probably, pound for pound, the most widely used magnetic material. One of the drawbacks in using steel in the early years was, as the material became older, the losses would increase. With the addition of silicon to the steel, the advantages were twofold: it increased the electrical resistivity, therefore reducing the eddy current losses, and it also improved the material's stability with age.

Silicon steel offers high saturation flux density, a relatively good permeability at high flux density, and a moderate loss at audio frequency. One of the important improvements made to the silicon steel was in the process called cold-rolled, grain-oriented, AISI type M6. This M6 grain-oriented steel has exceptionally low losses and high permeability. It is used in applications requiring high performance and the losses will be at a minimum.

Introduction to Thin Tape Nickel Alloys

High permeability metal alloys are based primarily on the nickel-iron system. Although Hopkinson investigated nickel-iron alloys as early as 1889, it was not until the studies by Elmen, starting in about 1913, on properties in weak magnetic fields and effects of heat-treatments, that the importance of the Ni-Fe alloys was realized. Elmen called his Ni-Fe alloys, "Permalloys," and his first patent was filed in 1916. His preferred composition was the 78Ni-Fe alloy. Shortly after Elmen, Yensen started an independent investigation that resulted in the 50Ni-50Fe alloy, "Hipernik," which has lower permeability and resistivity but higher saturation than the 78-Permalloy, (1.5 teslas compared to 0.75 teslas), making it more useful in power equipment.

Improvements in the Ni-Fe alloys were achieved by high temperature anneals in hydrogen atmosphere, as first reported by Yensen. The next improvement was done by using grain-oriented material and annealing it, in a magnetic field, which was also in a hydrogen atmosphere. Kelsall and Bozorth did this work. Using these two methods, a new material, called Supermalloy, was achieved. It has a higher permeability, a lower coercive force, and about the same flux density as 78-Permalloy. Perhaps the most important of these factors is the

magnetic anneal, which, not only increases permeability, but also provides a “square” magnetization curve, important in high frequency power conversion equipment.

In order to obtain high resistance, and therefore lower core losses for high frequency applications, two approaches have been followed: (1) modification of the shape of metallic alloys and (2) development of magnetic oxides. The result was the development of thin tapes and powdered alloys in the 1920's, and thin films in the 1950's. The development of thin film has been spurred by the requirements of aerospace, power conversion electronics from the mid 1960's to the present.

The Ni-Fe alloys are available in thicknesses of 2 mil, 1 mil, 0.5 mil, 0.25 and 0.125 mil. The material comes with a round or square B-H loop. This gives the engineer a wide range of sizes and configurations from which to select for a design. The iron alloy properties for some of the most popular materials are shown in Table 2-1. Also, given in Table 2-1, is the Figure number for the B-H loop of each of the magnetic materials.

Table 2-1. Magnetic Properties for Selected Iron Alloys Materials

Iron Alloy Material Properties								
Material Name	Composition	Initial Permeability μ_i	Flux Density Teslas B_s	Curie Temp. °C	dc, Coercive Force, H_c Oersteds	Density grams/cm ³ δ	Weight Factor x	Typical B-H Loop Figures
Silicon	3% Si 97% Fe	1.5 K	1.5-1.8	750	0.4-0.6	7.63	1.000	(2-3)
Supermendur*	49% Co 49% Fe 2% V	0.8 K	1.9-2.2	940	0.15-0.35	8.15	1.068	(2-4)
Orthonol	50% Ni 50% Fe	2 K	1.42-1.58	500	0.1-0.2	8.24	1.080	(2-5)
Permalloy	79% Ni 17% Fe 4% Mo	12 K-100 K	0.66-0.82	460	0.02-0.04	8.73	1.144	(2-6)
Supermalloy	78% Ni 17% Fe 5% Mo	10 K-50 K	0.65-0.82	460	0.003-0.008	8.76	1.148	(2-7)

* Field Anneal.
x Silicon has unity weight factor.

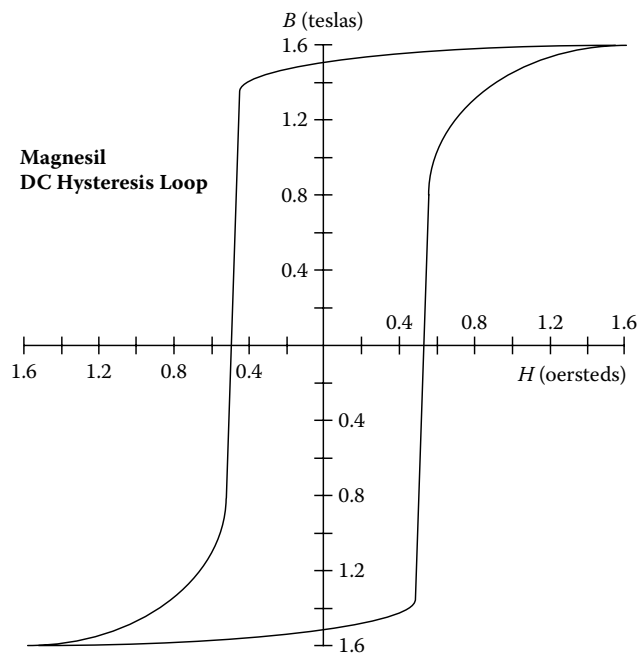


Figure 2-3. Silicon B-H Loop: 97% Fe 3% Si.

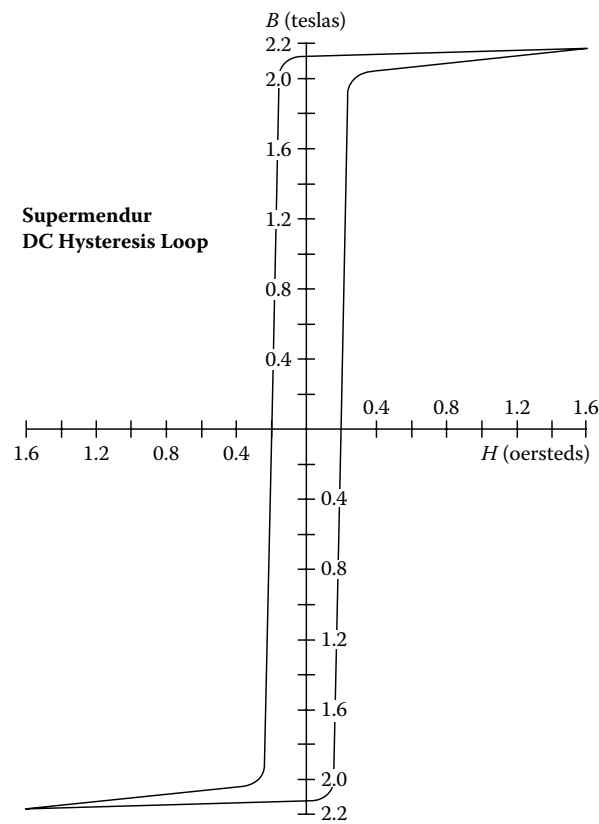


Figure 2-4. Supermendur B-H Loop: 49% Fe 49% Co 2% V.

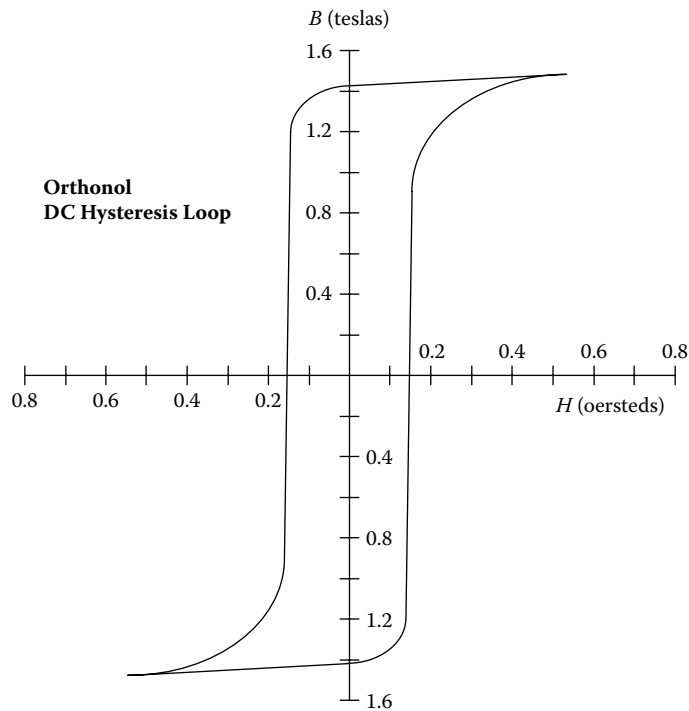


Figure 2-5. Orthonol B-H Loop: 50% Fe 50% Ni.

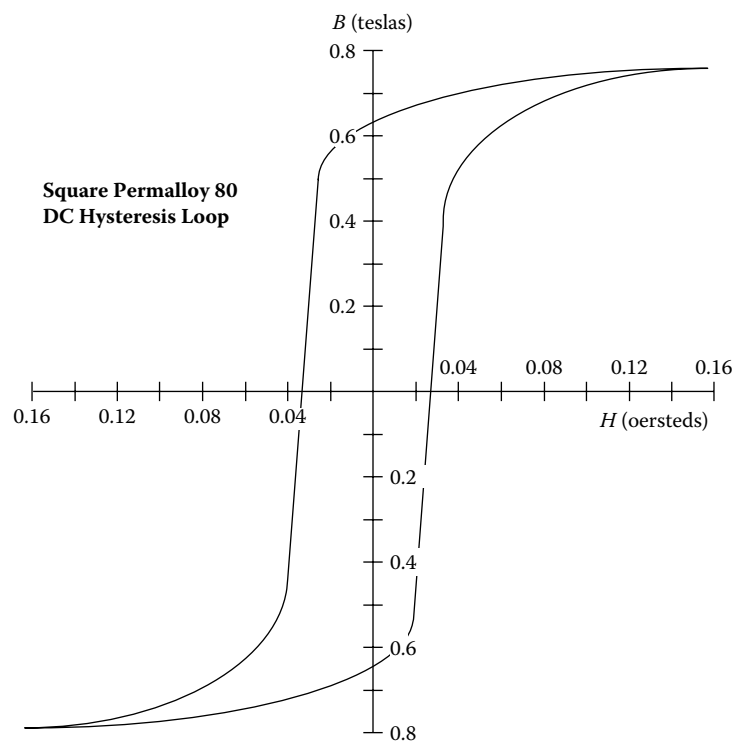


Figure 2-6. Square Permalloy 80 B-H Loop: 79% Ni 17% Fe 4% Mo.

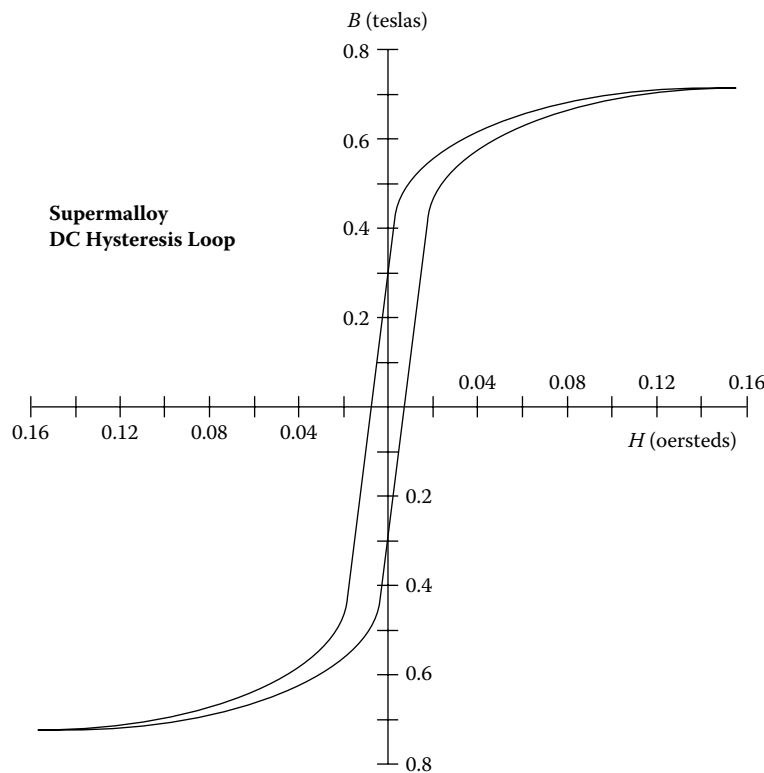


Figure 2-7. Supermalloy B-H Loop: 78% Ni 17% Fe 5% Mo.

Introduction to Metallic Glass

The first synthesis of a metallic glass drawing wide attention among material scientists, occurred in 1960. Klement, Willens and Duwez reported that a liquid, AuSi alloy, when rapidly quenched to liquid nitrogen temperature, would form an amorphous solid. It was twelve years later that Chen and Polk produced ferrous-based metallic glasses in useful shapes with significant ductility. Metallic glasses have since survived the transition from laboratory curiosities to useful products, and currently are the focus of intensive technological and fundamental studies.

Metallic glasses are generally produced, by liquid quenching, in which a molten metal alloy is rapidly cooled, at rates on the order of 10^5 degrees/sec., through the temperature at which crystallization normally occurs. The basic difference between crystalline (standard magnetic material) and glassy metals is in their atomic structures. Crystalline metals are composed of regular, three-dimensional arrays of atoms, which exhibit long-range order. Metallic glasses do not have long-range structural order. Despite their structural differences, crystalline and glassy metals of the same compositions exhibit nearly the same densities.

The electrical resistivities of metallic glasses are much larger, (up to three times higher), than those of crystalline metals of similar compositions. The magnitude of the electrical resistivities and their temperature coefficients in the glassy and liquid states are almost identical.

Metallic glasses are quite soft magnetically. The term, "soft," refers to a large response of the magnetization to a small-applied field. A large magnetic response is desirable in such applications as transformers and inductors. The obvious advantages of these new materials are in high frequency applications with their high induction, high permeability, and low core loss.

There are four amorphous materials that have been used in high frequency applications: 2605SC, 2714A, 2714AF and Vitroperm 500F. Material 2605SC offers a unique combination of high resistivity, high saturation induction, and low core loss, making it suitable for designing high frequency dc inductors. Material 2714A is a cobalt material that offers a unique combination of high resistivity, high squareness ratio B_r/B_s , and very low core loss, making it suitable for designing high frequency aerospace transformers and mag-amps. The Vitroperm 500F is an iron based material with a saturation of 1.2 teslas and is well-suited for high frequency transformers and gapped inductors. The high frequency core loss for the nanocrystalline 500F is lower than some ferrite, even operating at a high flux density. The amorphous properties for some of the most popular materials are shown in Table 2-2. Also, given in Table 2-2, is the Figure number for the B-H loop of each of the magnetic materials.

Table 2-2. Magnetic Properties for Selected Amorphous Materials

Amorphous Material Properties								
Material Name	Major Composition	Initial Permeability μ_i	Flux Density Telsas B_s	Curie Temperature °C	dc, Coercive Force, H_c Oersteds	Density grams/cm ³ δ	Weight Factor x	Typical B-H Loop Figures
2605SC	81% Fe 13.5% B 3.5% Si	1.5K	1.5-1.6	370	0.4-0.6	7.32	0.957	(2-8)
2714A	66% Co 15% Si 4% Fe	0.8K	0.5-0.65	205	0.15-0.35	7.59	0.995	(2-9)
2714AF	66% Co 15% Si 4% Fe	2K	0.5-0.65	205	0.1-0.2	7.59	0.995	(2-10)
Nanocrystal Vitroperm 500F*	73.5% Fe 1% Cu 15.5% Si	30K-80K	1.0-1.2	460	0.02-0.04	7.73	1.013	(2.11)

* Vitroperm is the trademark of Vacuumschmelze.
x Silicon has a unity weight factor. See [Table 2.1](#).

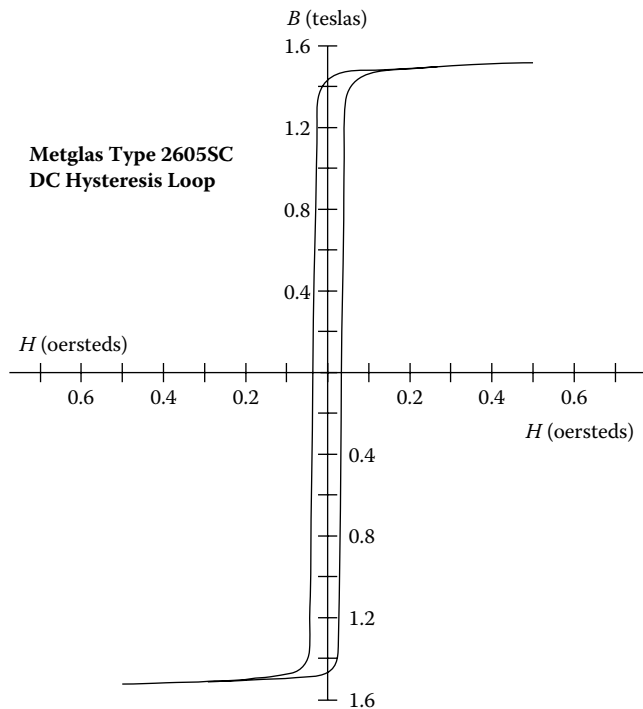


Figure 2-8. Amorphous 2605SC B-H Loop: 81% Fe 13.5% B 3.5% Si.

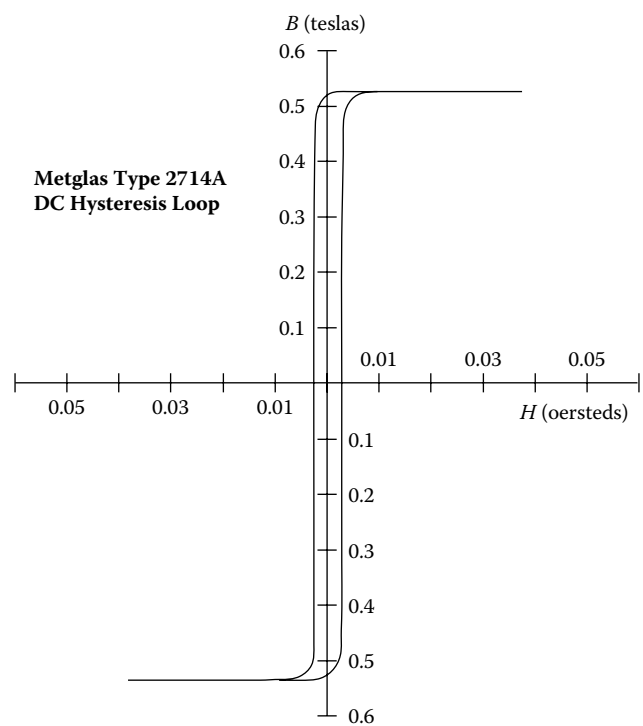


Figure 2-9. Amorphous 2714A B-H Loop: 66% Co 15% Si 4% Fe.

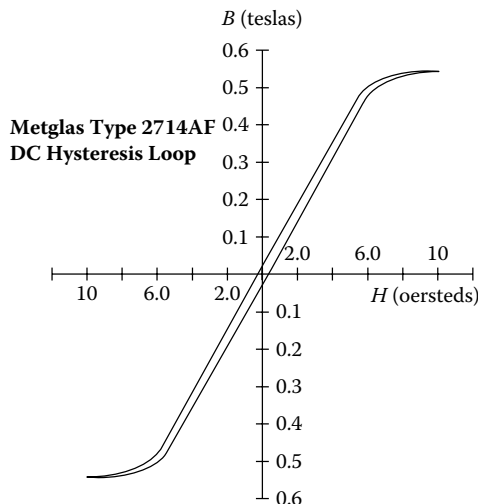


Figure 2-10. Amorphous 2714AF B-H Loop: 66% Co 15% Si 4% Fe.

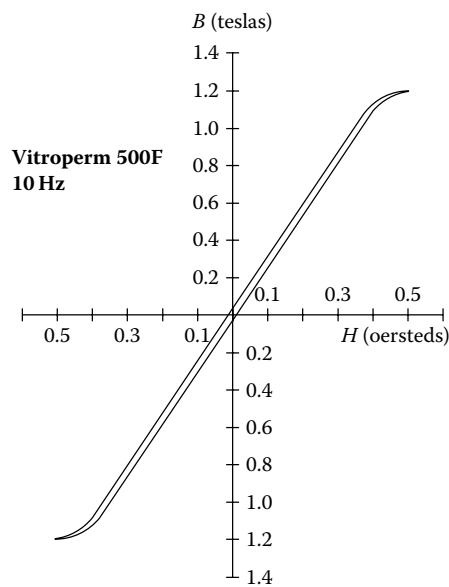


Figure 2-11. Vitroperm 500F B-H Loop: 73.5% Fe 15.5% Si 1% Cu.

Introduction to Soft Ferrites

In the early days of electrical industry, the need for the indispensable magnetic material was served by iron and its magnetic alloys. However, with the advent of higher frequencies, the standard techniques of reducing eddy current losses, (using laminations or iron powder cores), was no longer efficient or cost effective.

This realization stimulated a renewed interest in “magnetic insulators,” as first reported by S. Hilpert in Germany, in 1909. It was readily understood that, if the high electrical resistivity of oxides could be combined with desired magnetic characteristics, a magnetic material that was particularly well-suited for high frequency operation would result.

Research to develop such a material was being performed by scientists in various laboratories all over the world, such as V. Kato, T. Takei, and N. Kawai in the 1930's in Japan, and by J. Snoek of the Philips' Research Laboratories in the period 1935-1945 in The Netherlands. By 1945, Snoek had laid down the basic fundamentals of the physics and technology of practical ferrite materials. In 1948, the Neel Theory of ferromagnetism provided the theoretical understanding of this type of magnetic material.

Ferrites are ceramic, homogeneous materials composed of oxides; iron oxide is their main constituent. Soft ferrites can be divided into two major categories; manganese-zinc and nickel-zinc. In each of these categories, changing the chemical composition, or manufacturing technology, can manufacture many different Mn-Zn and Ni-Zn material grades. The two families of Mn-Zn and Ni-Zn ferrite materials complement each other, and allow the use of soft ferrites from audio frequencies to several hundred megahertz. Manufacturers do not like to handle manganese-zinc in the same area, or building with nickel-zinc, because one contaminates the other, which leads to poor performance yields. The basic difference between manganese-zinc and nickel-zinc is shown in Table 2-3. The biggest difference is manganese-zinc has a higher permeability and nickel-zinc has a higher resistivity. Shown in [Table 2-4](#) are some of the most popular and new ferrite materials. Also, given in Table 2-4, is the Figure number for the B-H loop of each of the materials.

Table 2-3. Comparing Manganese-Zinc and Nickel-Zinc Basic Properties

Basic Ferrite Material Properties					
Materials	Initial Permeability μ_i	Flux Density B_{max} Teslas	Curie Temperature, °C	dc, Coercive Force, H_c Oersteds	Resistivity Ω - cm
Manganese Zinc	750-15 K	0.3-0.5	100-300	0.04-0.25	10-100
Nickel Zinc	15-1500	0.3-0.5	150-450	0.3-0.5	10^6

Manganese-Zinc Ferrites

This type of soft ferrite is the most common, and is used in many more applications than the nickel-zinc ferrites. Within the Mn-Zn category, a large variety of materials are possible. Manganese-zinc ferrites are primarily used at frequencies less than 2 MHz.

Nickel-Zinc Ferrites

This class of soft ferrite is characterized by its high material resistivity, several orders of magnitude higher than Mn-Zn ferrites. Because of its high resistivity, Ni-Zn ferrite is the material of choice for operating from 1-2 MHz to several hundred megahertz.

The material permeability, μ_m , has little influence on the effective permeability, μ_e , when the gap dimension is relatively large, as shown in [Table 2-5](#).

Table 2-4. Magnetic Properties for Selected Ferrite Materials

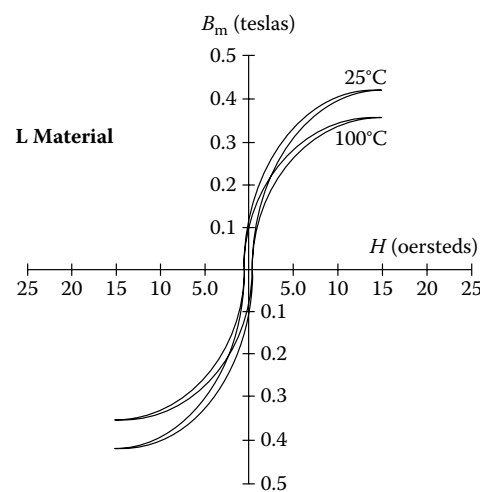
Ferrites Material Properties							
*Magnetics Material Name	Initial Permeability μ_i	Flux Density Teslas $B_s @ 15 \text{ Oe}$	Residual Flux Teslas B_r	Curie Temperature $^{\circ}\text{C}$	dc, Coercive Force, Hc Oersteds	Density grams/cm ³ δ	Typical B-H Loop Figures
L	900	0.42 T	0.15 T	>300	0.94	4.8	(2-12)
R	2300	0.50 T	0.12 T	>230	0.18	4.8	(2-13)
P	2500	0.50 T	0.12 T	>230	0.18	4.8	(2-13)
T	2300	0.47 T	0.16 T	>215	0.25	4.8	NA
F	5000	0.49 T	0.10 T	>250	0.2	4.8	(2-14)
W	10,000	0.43 T	0.07 T	>125	0.15	4.8	(2-15)

* Magnetics, a Division of Spang & Company.

Table 2-5. Permeability, and Its Effect on Gapped Inductors

Comparing Material Permeabilities					
*Material	μ_m	Gap, inch	Gap, cm	**MPL, cm	μ_e
L	900	0.04	0.101	10.4	92
R	2300	0.04	0.101	10.4	98
P	2500	0.04	0.101	10.4	99
F	3000	0.04	0.101	10.4	100

* The materials are from Magnetics, a Division of Spang & Company.
** Core, ETD44.

**Figure 2-12.** Ferrite B-H Loop, L Material at 25 and 100°C.

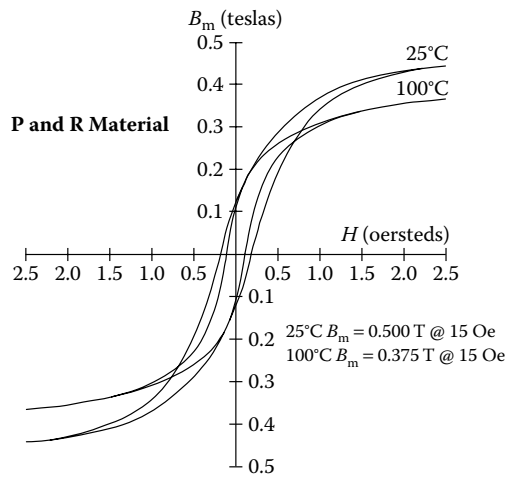


Figure 2-13. Ferrite B-H Loop, P & R Material at 25 and 100°C.

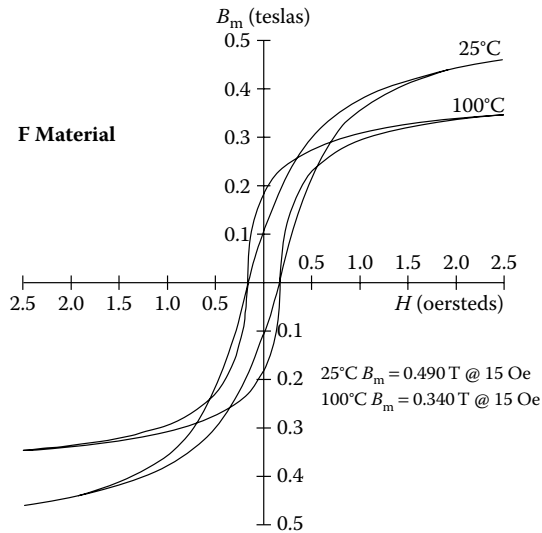


Figure 2-14. Ferrite B-H Loop, F Material at 25 and 100°C.

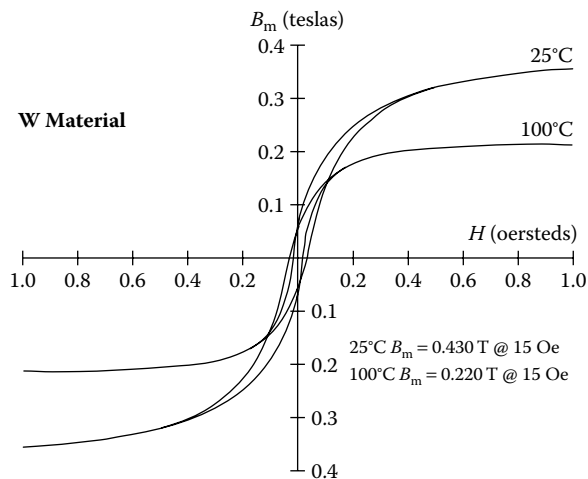


Figure 2-15. Ferrite B-H Loop, W & H Material at 25 and 100°C.

Ferrite Cross Reference

A similar ferrite cross-reference has been made in Table 2-6. This table has been put together using some of the leading ferrite manufacturers. The ferrite materials in Table 2-6 have been organized for materials best suited for power transformers, power inductors and common-mode filters.

Table 2-6. Similar Ferrite Materials Best Suited for Power and Filters

Similar Ferrite Materials Used for Power and Filters							
Application	Power	Power	Power	Power	Filter	Filter	Filter
Manufacturers	Material Designation						
Magnetics	1* L	2* R	3* P	F	J	W	
Permeability, μ_i	900	2300	2500	3000	5000	10000	
Ferroxcube	3F45	3F3	3C94	3C91	3E27	3E5	3E7
Permeability, μ_i	900	2000	2300	3000	6000	10000	15000
Fair-Rite		77	78		75	76	
Permeability, μ_i		2000	2300		5000	10000	
EPCOS		N97	N72	T41	T65	T38	T46
Permeability, μ_i		2300	2500	2800	5200	10000	15000
TDK Corp.		PC40	PC44	H5A	HP5	H5C2	H5C3
Permeability, μ_i		2300	2400	3300	5000	10000	15000
MMG		F44	F45	F5A	F-10	FTA	FTF
Permeability, μ_i		1800	2000	2300	6000	10000	15000
Ceramic Mag			MN80C	MN8CX	MN60	MN100	
Permeability, μ_i			2050	3100	6500	9000	
TSC Ferrite Int.		TSF-7099	TSF-7070	TSF-8040	TSF-5000	TSF-010K	
Permeability, μ_i		2000	2200	3100	5000	10000	

1. High Frequency power material 500 kHz & up.
 2. Lowest loss at 80°C-100°C, 25kHz to 250 kHz.
 3. Lowest loss at 60°C-80°C.

Introduction to Molypermalloy Powder Cores

The nickel-iron (Ni-Fe) high permeability magnetic alloys (permalloy) were discovered in 1923 and 1927. Permalloy alloys were successfully used in powder cores, greatly contributing to the carrier wave communications of the time.

In the early 1940's, the Bell Telephone Laboratory and the Western Electric Company developed a new material, trademarked Molybdenum Permalloy Powder (MPP), into cores. This new material was developed for loading coils, filtering coils, and transformers at audio and carrier frequencies in the telephone facility. The use of such cores has been extended to many industrial and military circuits. The stability of permeability and core losses with time, temperature, and flux level, are particularly important to engineers designing tuned circuits and timing circuits. This new material has given reliable and superior performance over all past powder core materials.

Molybdenum permalloy powder, [2 Molybdenum (Mo)-82 Nickel (Ni)-16 Iron (Fe)], is made by grinding hot-rolled and embrittled cast ingots; then, the alloy is insulated and screened to a fineness of 120 mesh for use in audio frequency applications, and 400 mesh for use at high frequencies.

In the power conversion field, the MPP core has made its greatest impact in switching power supplies. The use of MPP cores and power MOSFET transistors has permitted increased frequency, resulting in greater compactness and weight reduction in computer systems. The power supply is the heart of the system. When the power supply is designed correctly, using a moderate temperature rise, the system will last until it becomes obsolete. In these power systems there are switching inductors, smoothing choke coils, common mode filters, input filters, output filters, power transformers, current transformers and pulse transformers. They cannot all be optimally designed using MPP cores. But, in some cases, MPP cores are the only ones that will perform in the available space with the proper temperature rise.

Introduction to Iron Powder Cores

The development of compressed iron powder cores as a magnetic material for inductance coils, stemmed from efforts of Bell Telephone Laboratory engineers to find a substitute for fine iron-wire cores. The use of iron powder cores was suggested by Heaviside in 1887, and again, by Dolezalek in 1900.

The first iron powder cores of commercially valuable properties were described by Buckner Speed, in U.S. Patent No. 1274952, issued in 1918. Buckner Speed and G.W. Elman published a paper in the A.I.E.E.

Transactions, "Magnetic Properties of Compressed Powdered Iron," in 1921. This paper describes a magnetic material, which is well suited to the construction of cores in small inductance coils and transformers, such as those used in a telephone system. These iron powder cores were made from 80 Mesh Electrolytic Iron Powder. The material was annealed, then, insulated by oxidizing the surface of the individual particles. In this way, a very thin and tough insulation of grains of iron was obtained; this did not break down when the cores were compressed. A shellac solution was applied to the insulated powder as a further insulator and binder. This was how Western Electric Company manufactured toroidal iron powder cores until about 1929. Today's iron powder cores are manufactured in much the same way, using highly pure iron powder and a more exotic insulator and binder. The prepared powder is compressed under extremely high pressures to produce a solid-looking core. This process creates a magnetic structure with a distributed air-gap. The inherent high saturation flux density of iron, combined with the distributed air-gap, produces a core material with initial permeability of less than 100, and with high-energy storage capabilities.

The dc current does not generate core loss, but an ac or ripple current does generate core loss. Iron powder material has higher core loss than some other, more expensive, core materials. Most dc-biased inductors have a relatively small percentage of ripple current and, thus, core loss will be minimal. However, core loss will sometimes become a limiting factor in applications with a relatively high percentage of ripple current at very high frequency. Iron powder is not recommended for inductors with discontinuous current or transformers with large ac flux swings.

In today's market low cost, iron powder cores are typically used in low and high frequency power switching conversion applications for differential-mode, input and output power inductors. Because iron powder cores have such low permeability, a relatively large number of turns are required for the proper inductance, thus keeping the ac flux at a minimum. The penalty for using iron powder cores is usually found in the size and efficiency of the magnetic component.

There are four standard powder materials available for power magnetic devices: Molypermalloy (MPP) Powder Cores with a family of curves, as shown in [Figure 2-20](#); High flux (HF) Powder Cores with a family of curves, as shown in [Figure 2-21](#); Sendust Powder Cores, *(Kool μ), with a family of curves, as shown in [Figure 2-22](#); and Iron Powder Cores, with a family of curves, as shown in [Figure 2-23](#). The powder cores come in a variety of permeabilities. This gives the engineer a wide range in which to optimize the design. The powder core properties for the most popular materials are shown in [Table 2-7](#). Also, given in Table 2-7, is the Figure number for the B-H loop of each of the powder core materials. In [Table 2-8](#) is a listing of the most popular permeabilities for each of the powder core materials.

* Trademark of Magnetics Division, Spang and Company.

Table 2-7. Powder Core Material Properties

Powder Core Material Properties							
Material Name	Composition	Initial Permeability μ_i	Flux Density Teslas B_s	Curie Temperature °C	dc, Coercive Force, Hc Oersteds	Density grams/cm ³ δ	Typical B-H Loop Figures
MPP	80% Ni 20% Fe	14-550	0.7	460	0.3	8	(2-16)
High flux	50% Ni 50% Fe	14-160	1.5	500	1	7.6	(2-17)
Sendust (Kool M μ)	85% Fe 9% Si 6% Al	26-125	1	500	0.5	5.5	(2-18)
Iron Powder	100% Fe	4.0-125	0.5-1.4	770	5.0-9.0	3.3-7.2	(2-19)

Table 2-8. Standard Powder Core Permeabilities

Standard Powder Core Permeabilities				
Powder Material	MPP	High Flux	Sendust (Kool M μ)	Iron Powder
Initial Permeability μ_i				
10				X
14	X	X		X
26	X	X	X	
35				X
40			X	
55				X
60	X	X	X	X
75			X	X
90			X	
100				X
125	X	X	X	X
147	X	X		
160	X	X		
173	X			
200	X			
300	X			
550	X			

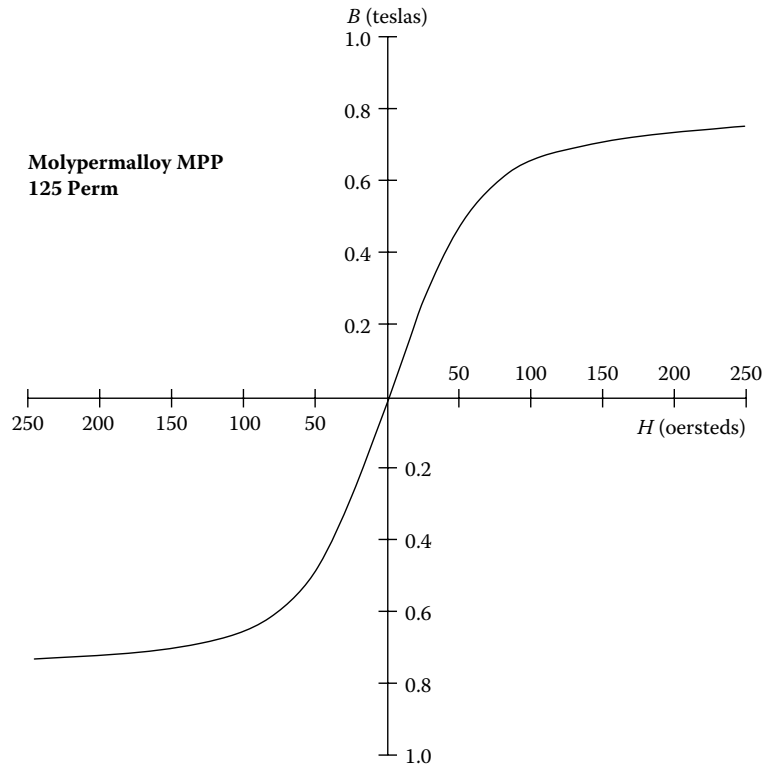


Figure 2-16. Molypermalloy Powder Core, 125 Perm.

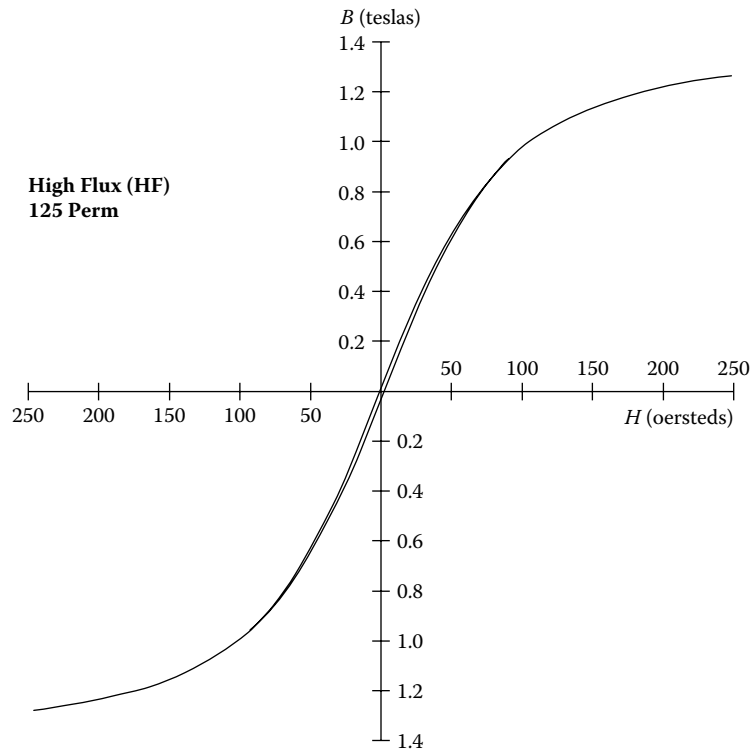


Figure 2-17. High Flux Powder Core, 125 Perm.

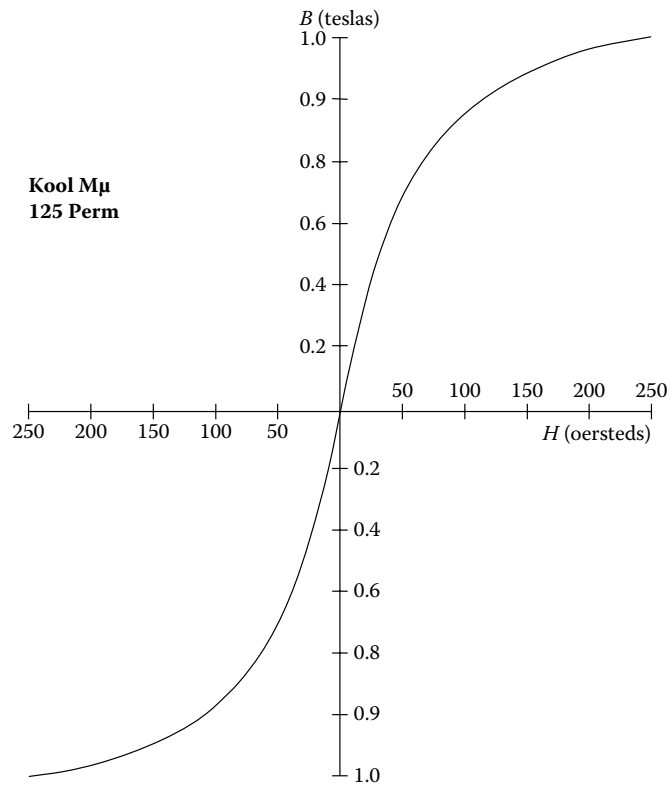


Figure 2-18. Sendust (Kool $M\mu$) Powder Core, 125 Perm.

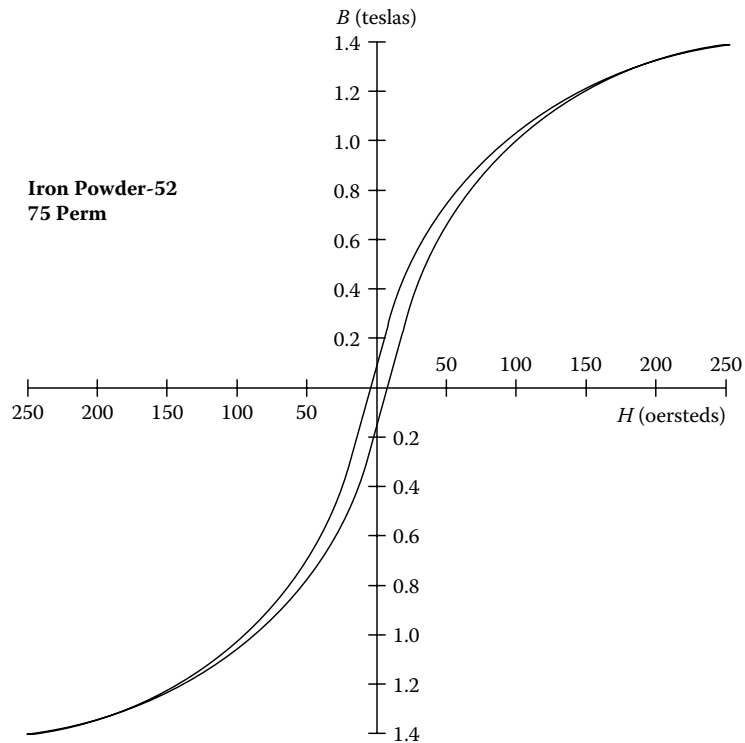


Figure 2-19. Iron Powder (-52) Core, 75 Perm.

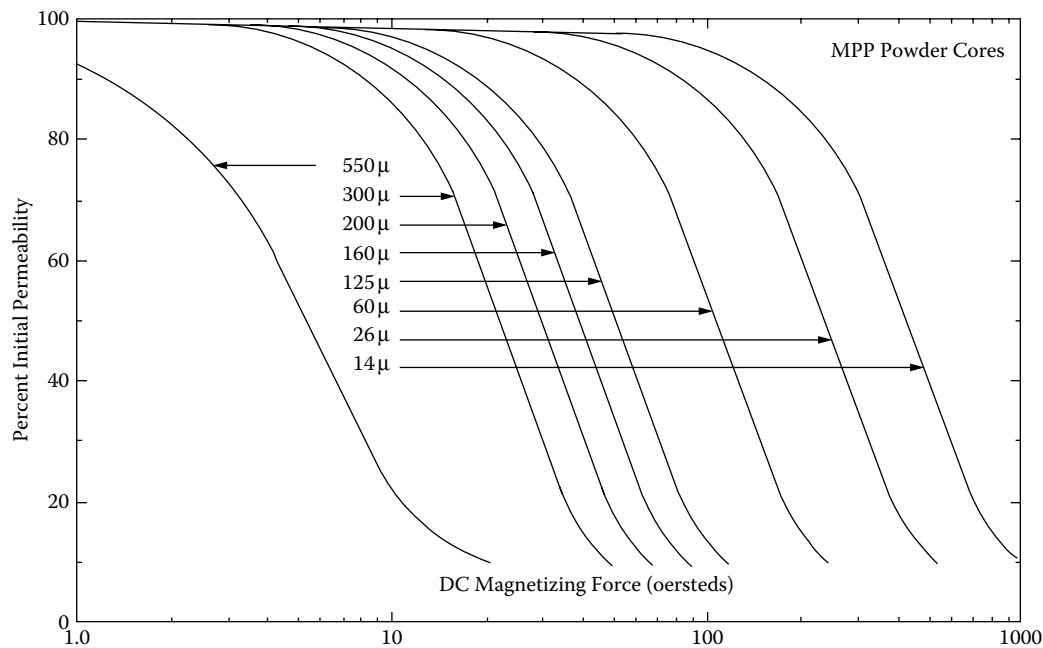


Figure 2-20. Permeability Versus dc Bias for Molypermalloy Powder Cores.

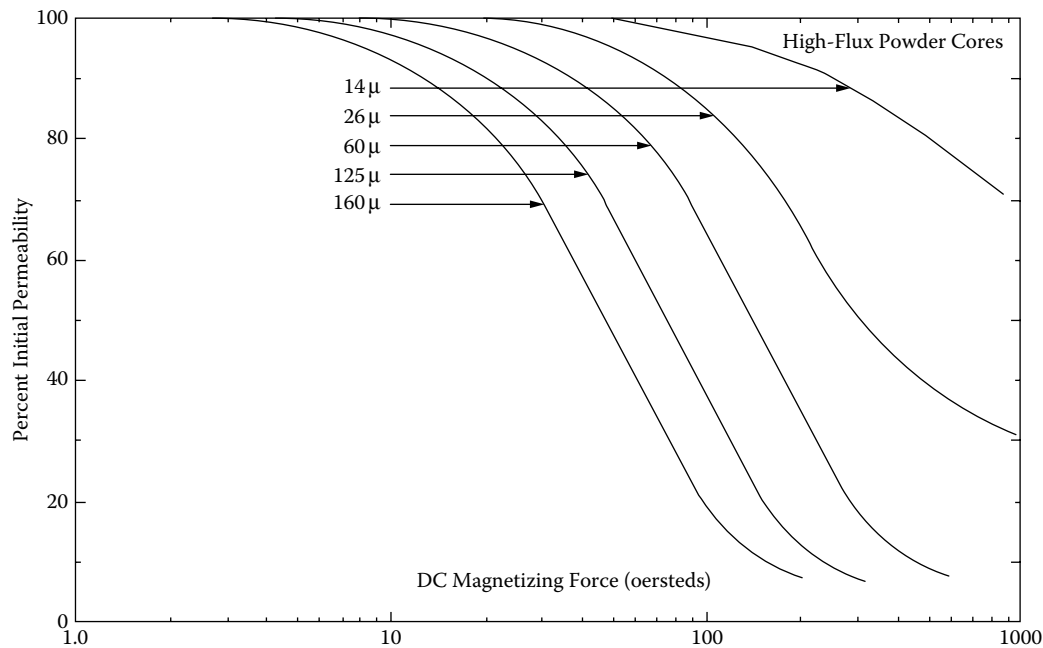


Figure 2-21. Permeability Versus dc Bias for High Flux Powder Cores.

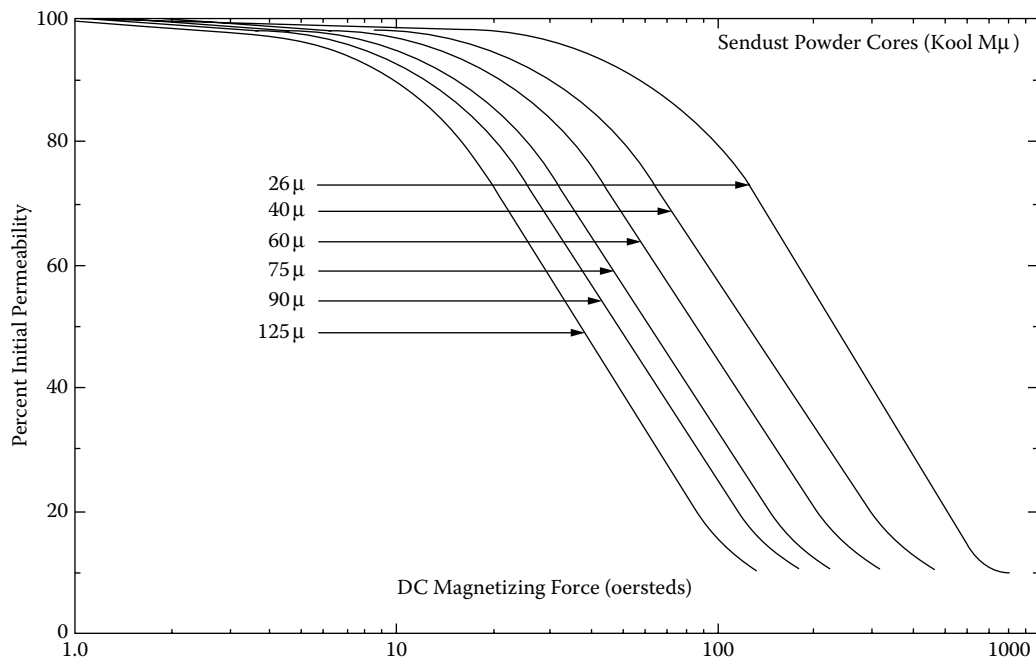


Figure 2-22. Permeability Versus dc Bias for Sendust Powder Cores.

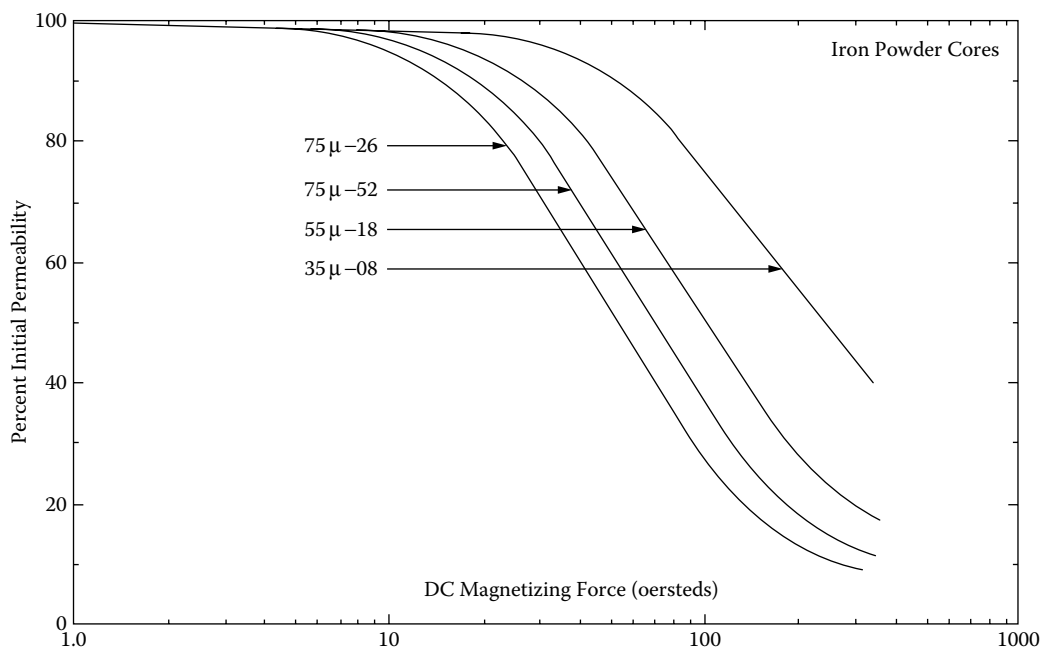


Figure 2-23. Permeability Versus dc Bias for Iron Powder Cores.

Core Loss

The designer of power magnetic components, such as transformers and inductors, requires specific knowledge about the electrical and magnetic properties of the magnetic materials used in these components. There are two magnetic properties that are of interest, the dc and the ac. The dc B-H hysteresis loop is a very useful guide for comparing the different types of magnetic materials. It is the ac magnetic properties that are of interest to the design engineer. One of the most important ac properties is the core loss. The ac core loss is a function of the magnetic material, magnetic material thickness, magnetic flux density, B_{ac} , frequency, f , and operating temperature. Thus, the choice of the magnetic material is based upon achieving the best characteristic using the standard trade-off, such as cost, size, and performance.

All manufacturers do not use the same units when describing their core loss. The user should be aware of the different core loss units when comparing different magnetic materials. A typical core loss graph is shown in Figure 2-24. The vertical scale is core loss, and the horizontal scale is flux density. The core loss data is plotted at different frequencies, as shown in Figure 2-24.

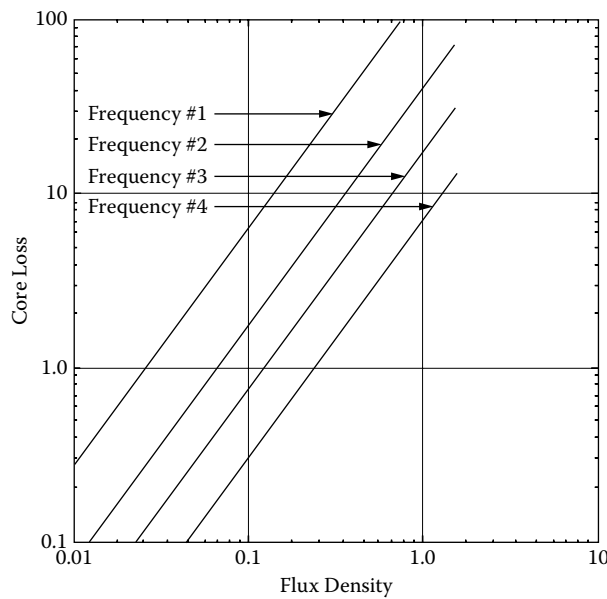


Figure 2-24. Typical Graph for Plotting Core Loss at Different Frequencies.

Vertical Scale

Here is a list of core loss units used by manufacturers:

1. watts per pound
2. watts per kilogram
3. milliwatts per gram
4. milliwatts per cubic centimeter (cm^3)

Horizontal Scale

Here is a list of flux density units used by manufacturers:

1. gauss
2. kilogauss
3. teslas
4. millitesla

The data can be plotted or presented in either hertz or kilohertz.

Core Loss Equations

Manufacturers are now presenting the core loss in the form as shown in Equation [2-2].

$$\text{watts / kilogram} = k f^{(m)} B^{(n)} \quad [2-2]$$

Here, again, the units will change from one manufacturer to another. In the following tables the manufacturer's core loss data has been organized with the same units for all core losses. The data was modified to put the data in metric units, gauss to teslas, and watts per pound to watts per kilogram. The coefficients for Magnetics Inc. molypermalloy powder cores, (MPP), using Equation [2-2] are shown in Table 2-9. The coefficients for Magnetics Inc. High Flux powder cores, (HF), using Equation [2-2] are shown in [Table 2-10](#). The coefficients for Magnetics Inc. Sendust powder cores, (Kool-M μ), using Equation [2-2] are shown in [Table 2-11](#). The coefficients for iron alloy materials using Equation [2-2] are shown in [Table 2-12](#).

Table 2-9. Core Loss Coefficients for MPP Powder Cores

Core Loss Equation Factors				
Magnetics MPP Powder Cores				
Material	Permeability μ	Coefficient k	Coefficient (m)	Coefficient (n)
MPP	14	0.005980	1.320	2.210
MPP	26	0.001190	1.410	2.180
MPP	60	0.000788	1.410	2.240
MPP	125	0.001780	1.400	2.310
MPP	147-160-173	0.000489	1.500	2.250
MPP	200-300	0.000250	1.640	2.270
MPP	550	0.001320	1.590	2.360

Table 2-10. Core Loss Coefficients for High Flux Powder Cores

Core Loss Equation Factors				
Magnetics HF Powder Cores				
Material	Permeability μ	Coefficient k	Coefficient (m)	Coefficient (n)
High Flux	14	0.04280	1.26	2.52
High Flux	26	0.04180	1.25	2.55
High Flux	60	0.04140	1.23	2.56
High Flux	125	0.01300	1.32	2.59
High Flux	147	0.00940	1.41	2.56
High Flux	160	0.00940	1.41	2.56

Table 2-11. Core Loss Coefficients for Sendust Powder Cores

Core Loss Equation Factors				
Magnetics Kool-M μ Powder Cores				
Material	Permeability μ	Coefficient k	Coefficient (m)	Coefficient (n)
Sendust	26	0.000693	1.460	2.000
	40	0.000693		
	60	0.000634		
	75	0.000620		
	90	0.000614		
	125	0.000596		

The coefficients for amorphous materials, using Equation [2-2] are shown in [Table 2-13](#). The coefficients for Magnetics ferrite materials, using Equation [2-2] are shown in [Table 2-14](#). The coefficients for Micrometals iron powder materials, using Equation [2-3] are shown in [Table 2-15](#).

$$\text{watts/kilogram} = \left(\frac{f B_{ac}^3}{(a) + (b) B_{ac}^{0.7} + (c) B_{ac}^{1.35}} \right) + (d) f^2 B_{ac}^2 \quad [2-3]$$

Table 2-12. Core Loss Coefficients for Iron Alloy Cores

Core Loss Equation Factors					
Iron Alloy					
Material	Thickness mil's	Frequency Range	Coefficient k	Coefficient (m)	Coefficient (n)
50/50 Ni-Fe	1.00		0.0028100	1.210	1.380
	2.00		0.0005590	1.410	1.270
	4.00		0.0006180	1.480	1.440
Supermendur	2.00		0.0236000	1.050	1.300
	4.00	400 Hz	0.0056400	1.270	1.360
Permalloy 80	1.00		0.0000774	1.500	1.800
	2.00		0.0001650	1.410	1.770
	4.00		0.0002410	1.540	1.990
Supermalloy	1.00		0.0002460	1.350	1.910
	2.00		0.0001790	1.480	2.150
	4.00		0.0000936	1.660	2.060
Silicon	1.00		0.0593000	0.993	1.740
	2.00		0.0059700	1.260	1.730
	4.00		0.0035700	1.320	1.710
	12.00		0.0014900	1.550	1.870
	14.00		0.0005570	1.680	1.860
	24 M27 non-or	50-60 Hz	0.0386000	1.000	2.092

Table 2-13. Core Loss Coefficients for Amorphous Materials

Core Loss Equation Factors				
Amorphous				
Material	Thickness mils	Coefficient k	Coefficient (m)	Coefficient (n)
2605SC	0.80	$8.79(10^{-6})$	1.730	2.230
2714A	0.80	$10.1(10^{-6})$	1.550	1.670
Vitroperm 500	0.80	$0.864(10^{-6})$	1.834	2.112

Table 2-14. Core Loss Coefficients for Magnetics Ferrites Materials

Core Loss Equation Factors				
Magnetic's Ferrite Core Materials				
Material	Frequency Range	Coefficient k	Coefficient (m)	Coefficient (n)
L	The loss coefficients for the L material was not available at this time.			
L				
L				
R	f < 100kHz	5.597(10 ⁻⁴)	1.43	2.85
R	100kHz <= f < 500kHz	4.316(10 ⁻⁵)	1.64	2.68
R	f => 500kHz	1.678(10 ⁻⁶)	1.84	2.28
P	f < 100kHz	1.983(10 ⁻³)	1.36	2.86
P	100kHz <= f < 500kHz	4.855(10 ⁻⁵)	1.63	2.62
P	f => 500kHz	2.068(10 ⁻¹⁵)	3.47	2.54
F	f <= 10kHz	7.698(10 ⁻²)	1.06	2.85
F	10kHz < f < 100kHz	4.724(10 ⁻⁵)	1.72	2.66
F	100kHz <= f < 500kHz	5.983(10 ⁻⁵)	1.66	2.68
F	f => 500kHz	1.173(10 ⁻⁶)	1.88	2.29
J	f <= 20kHz	1.091(10 ⁻³)	1.39	2.50
J	f > 20kHz	1.658(10 ⁻⁸)	2.42	2.50
W	f <= 20kHz	4.194(10 ⁻³)	1.26	2.60
W	f > 20kHz	3.638(10 ⁻⁸)	2.32	2.62

Table 2-15. Core Loss Coefficients for Iron Powder Cores

Core Loss Equation Factors					
Micrometals Iron Powder Cores					
Material	Permeability μ	Coefficient (a)	Coefficient (b)	Coefficient (c)	Coefficient (d)
Mix-08	35	0.01235	0.8202	1.4694	3.85(10 ⁻⁷)
Mix-18	55	0.00528	0.7079	1.4921	4.70(10 ⁻⁷)
Mix-26	75	0.00700	0.4858	3.3408	2.71(10 ⁻⁶)
Mix-52	75	0.00700	0.4858	3.6925	9.86(10 ⁻⁷)

Selection of Magnetic Materials

Transformers used in static inverters, converters, and transformer-rectifier, (T-R), supplies, intended for aerospace and electronics industry power applications, are usually square loop tape, toroidal design. The design of reliable, efficient, and lightweight devices for this use has been seriously hampered by the lack of engineering data, describing the behavior of both the commonly used and more exotic core materials, with higher-frequency square wave excitation.

A program was carried out at the Jet Propulsion Laboratory, JPL, to develop this data from measurements of the dynamic B-H loop characteristics of the tape core materials presently available from various industry sources. Cores were produced in both toroidal and C forms, and were tested in both ungapped (uncut) and gapped (cut) configurations. The following section describes the results of that investigation.

Typical Operation

A transformer used for inverters, converters, and transformer-rectifier suppliers operates from a power bus, which could be dc or ac. In some power applications, a commonly used circuit is a driven transistor switch arrangement, such as that shown in Figure 2.25.

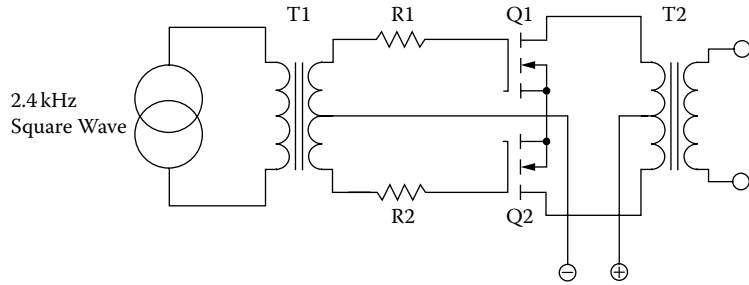


Figure 2-25. Typical Driven Power MOSFET Inverter.

One important consideration affecting the design of suitable transformers is that care must be taken to ensure that operation involves a balanced drive to the transformer primary. In the absence of a balanced drive, a net dc current will flow in the transformer primary, which causes the core to saturate easily during alternate half-cycles. A saturated core cannot support the applied voltage, limited mainly by its on resistance. The resulting high current, in conjunction with the transformer leakage inductance, results in a high-voltage spike during the switching sequence, which could be destructive to the power MOSFET. To provide a balanced drive, it is necessary to exactly match the MOSFETs for, $R_{DS(on)}$. But, this is not always sufficiently effective. Also, exact matching of the MOSFETs is a major problem in a practical sense.

Material Characteristics

Many available core materials approximate the ideal square loop characteristic, illustrated by the B-H curve, as shown in Figure 2-26. Representative, dc B-H loops for commonly available core materials, are shown in [Figure 2-27](#). Other characteristics are tabulated in [Table 2-16](#).

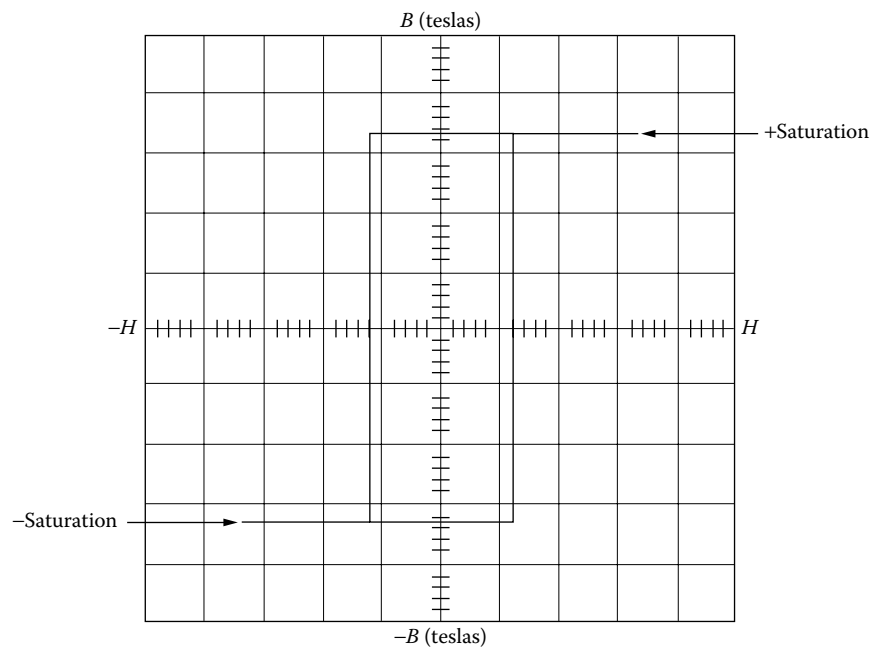


Figure 2-26. Ideal Square B-H Loop.

Many articles have been written about inverter and converter transformer design. Usually, authors' recommendations represent a compromise among material characteristics, such as those tabulated in Table 2-16, and displayed in [Figure 2-27](#). These data are typical of commercially available core materials that are suitable for the particular application.

As can be seen, the material that provides the highest flux density (supermendur) would result in the smallest component size, and this would influence the choice if size were the most important consideration. The ferrite material, (See the ferrite curve in Figure 2-27), has the lowest flux density. This results in the largest transformer. Magnetic materials selected for transformers or inductors cannot be chosen by flux alone. There are other parameters, such as frequency and core configuration that must be taken into consideration.

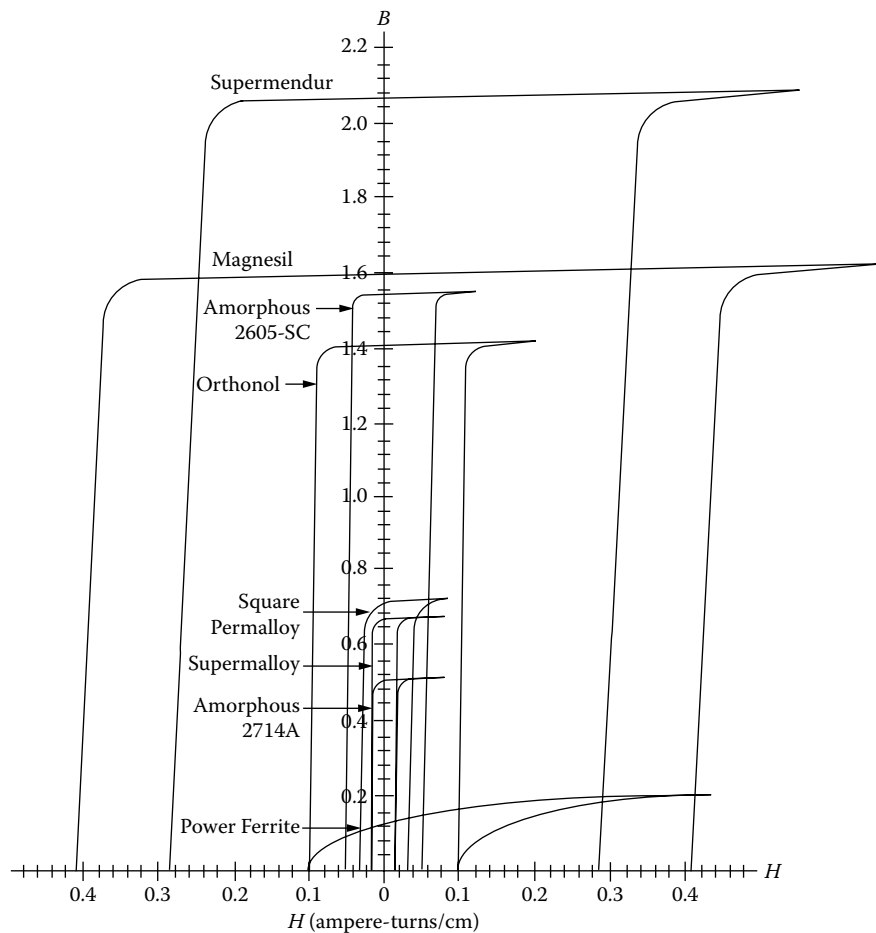


Figure 2-27. Typical dc B-H Loops of Magnetic Materials.

Usually, inverter transformer design is aimed at the smallest size, the highest efficiency and adequate performance under the widest range of environmental conditions. Unfortunately, the core material that can produce the smallest size has the lowest efficiency, and the highest efficiency materials result in the largest size. Thus, the transformer designer must make trade-offs between allowable transformer size and the minimum efficiency that can be tolerated. Then, the choice of core material will be based upon achieving the best characteristic on the most critical or important design parameter, and upon acceptable compromises on the other parameters.

After analysis of a number of designs, most engineers choose size rather than efficiency as the most important criterion, and select an intermediate loss factor on core material for their transformers. Consequently, as the frequency is increased, ferrites have become the most popular material.

Table 2-16. Magnetic Core Material Characteristics

Magnetic Core Material Characteristics						
Material Name	Composition	Initial Permeability μ_i	Flux Density Teslas B_s	Curie Temperature °C	dc. Coercive Force, H_c Oersteds	Density grams/cm³ δ
Magnesil	3% Si 97% Fe	1.5K	1.5-1.8	750	0.4-0.6	7.3
Supermendur*	49% Co 49% Fe 2% V	0.8K	1.9-2.2	940	0.15-0.35	8.15
Orthonol	50% Ni 50% Fe	2K	1.42-1.58	500	0.1-0.2	8.24
Sq. Permalloy	79% Ni 17% Fe 4% Mo	12K-100K	0.66-0.82	460	0.02-0.04	8.73
Supermalloy	78% Ni 17% Fe 5% Mo	10K-50K	0.65-0.82	460	0.003-0.008	8.76
Amorphous 2605-SC	81% Fe 13.5% B 3.5% Fe	3K	1.5-1.6	370	0.03-0.08	7.32
Amorphous 2714A	66% Co 15% Si 4% Fe	20K	0.5-0.58	205	0.008-0.02	7.59
Amorphous nano-crystal	73.5% Fe 1% Cu 15.5% Si	30K-80K	1.0-1.2	460	0.02-0.04	7.73
Ferrite	MnZn	0.75-15K	0.3-0.5	100-300	0.04-0.25	4.8

* Field Anneal.

Magnetic Material Saturation Defined

To standardize the definition of saturation, several unique points on the B-H loop are defined, as shown in Figure 2-28.

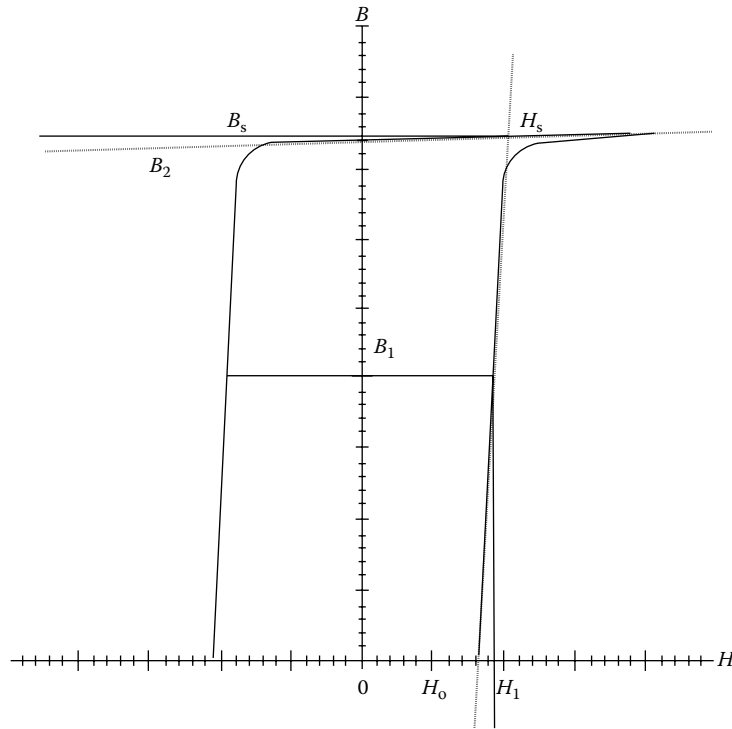


Figure 2-28. Defining the B-H Loop.

The straight line through $(H_o, 0)$ and (H_s, B_s) may be written as:

$$B = \left(\frac{\Delta B}{\Delta H} \right) (H - H_o) \quad [2-4]$$

The line through $(0, B_2)$ and (H_s, B_s) has essentially zero slope and may be written as:

$$B = B_2 \approx B_s \quad [2-5]$$

Equations [2-4] and [2-5] together define saturation conditions as follows:

$$B_s = \left(\frac{\Delta B}{\Delta H} \right) (H_s - H_o) \quad [2-6]$$

Solving Equation [2-6] for H_s yields:

$$H_s = H_o + \frac{B_s}{\mu_o} \quad [2-7]$$

Where by definition:

$$\mu_o = \frac{\Delta B}{\Delta H} \quad [2-8]$$

By definition, saturation occurs when the peak exciting current (B) is twice the average exciting current (A), as shown in Figure 2-29. Analytically, this means that:

$$H_{pk} = 2H_s \quad [2-9]$$

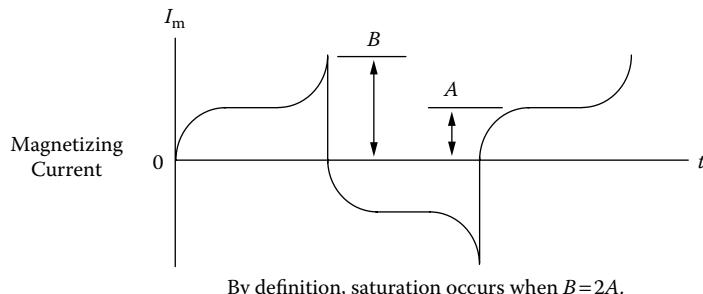


Figure 2-29. Defining the Excitation Current.

Solving Equation [2-1] for H_1 , we obtain:

$$H_1 = H_o + \frac{B_1}{\mu_o} \quad [2-10]$$

To obtain the pre-saturation dc margin (ΔH), Equation [2-4] is subtracted from Equation [2-6]:

$$\Delta H = H_s - H_1 = \left(\frac{B_s - B_1}{\mu_o} \right) \quad [2-11]$$

The actual unbalanced dc current must be limited to:

$$I_{dc} \leq \left(\frac{\Delta H(\text{MPL})}{N} \right), \quad [\text{amperes}] \quad [2-12]$$

Where, N is the number of turns

MPL is the mean magnetic path length.

Combining Equations [2-7] and [2-8] gives:

$$I_{dc} \leq \left(\frac{(B_s - B_1)(\text{MPL})}{\mu_o N} \right), \quad [\text{amperes}] \quad [2-13]$$

As mentioned earlier, in an effort to prevent core saturation, the drive to the switching power MosFet must be symmetrical and the power MosFet on resistance $R_{DS(on)}$ must be matched. The effect of core saturation, using an uncut or ungapped core, is shown in Figure 2-30, which illustrates the effect on the B-H loop transversed with a dc bias. Figure 2-31 shows typical B-H loops of 50-50 nickel-iron material excited from an ac source, with progressively reduced excitation; the vertical scale is 0.4 T/cm. It can be noted that the minor loop remains at one extreme position within the B-H major loop after reduction of excitation. The unfortunate effect of this random minor loop positioning is that, when conduction begins again in the transformer winding after shutdown, the flux swing could begin from the extreme ends rather than from the normal zero axis. The effect of this is to drive the core into saturation, with the production of spikes that can destroy transistors.

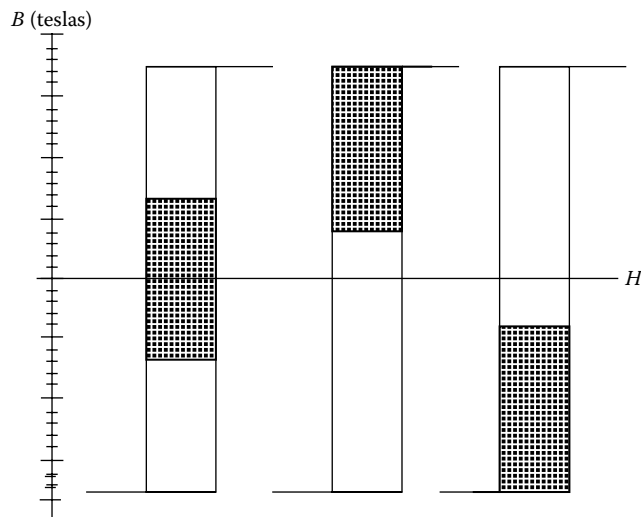


Figure 2-30. B-H Loop with dc Bias.

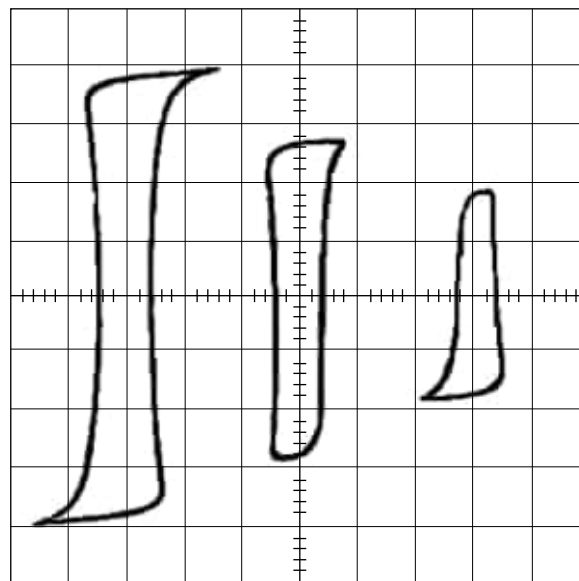


Figure 2-31. Typical Square Loop Material with dc Bias.

Test Conditions

The test fixture, schematically illustrated in Figure 2-32, was built to affect comparison of dynamic B-H loop characteristics of various core materials. Cores were fabricated from various core materials in the basic core configuration, designated No. 52029 for toroidal cores, manufactured by Magnetics Inc. The materials used were those most likely to be of interest to designers of inverter or converter transformers. Test conditions are listed in Table 2-17.

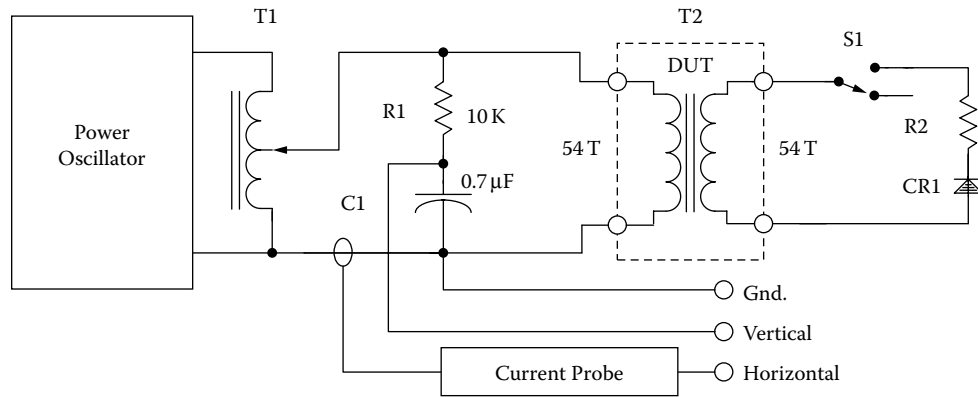


Figure 2-32. B-H Loop with dc Bias.

Winding Data were derived from the following:

$$N = \frac{V(10^4)}{4.0B_m f A_c}, \quad [\text{turns}] \quad [2-14]$$

Table 2-17. Materials and Test Conditions

Test Conditions					
Core Number*	Trade Name	B _s Teslas	Turns N	Frequency kHz	MPL cm
52029-2A	Orthonol	1.45	54	2.4	9.47
52029-2D	Sq. Permalloy	0.75	54	2.4	9.47
52029-2F	Supermalloy	0.75	54	2.4	9.47
52029-2H	48 Alloy	1.15	54	2.4	9.47
52029-2K	Magnesil	1.6	54	2.4	9.47

* Magnetics toroidal cores.

The test transformer, represented in Figure 2-32, consists of 54-turn primary and secondary windings, with square wave excitation on the primary. Normally, switch S1 is open. With switch S1 closed, the secondary current is rectified by the diode to produce a dc bias in the secondary winding.

Cores were fabricated from each of the materials by winding a ribbon of the same thickness on a mandrel of a given diameter. Ribbon termination was affected by welding in the conventional manner. The cores were vacuum impregnated, baked, and finished as usual.

Figures 2-33 through 2-36 show the dynamic B-H loops obtained for various core materials. In each of these Figures, switch S1 was in the open position, so there was no dc bias applied to the core and windings.

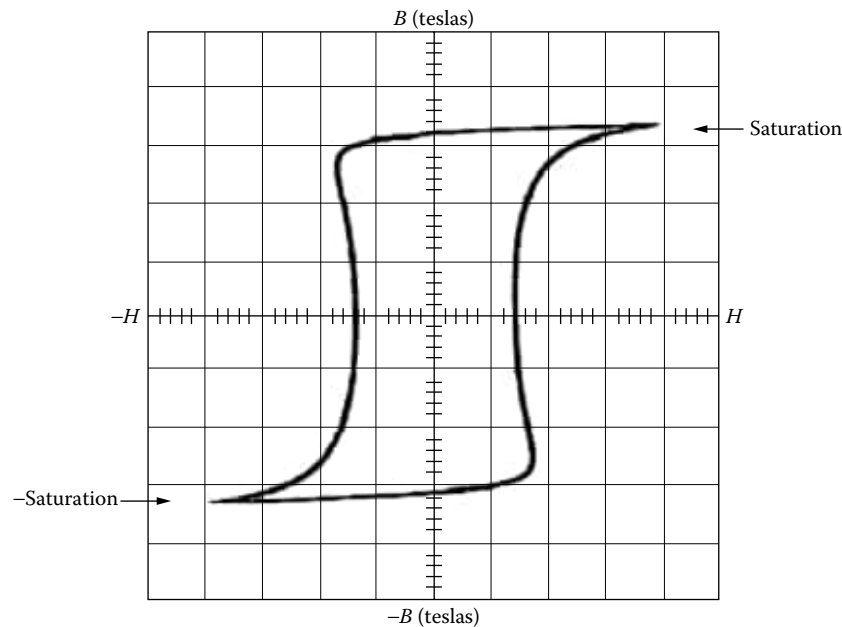


Figure 2-33. Magnesil (K) B-H Loop, $B = 0.5$ T/cm, $H = 100$ ma/cm.

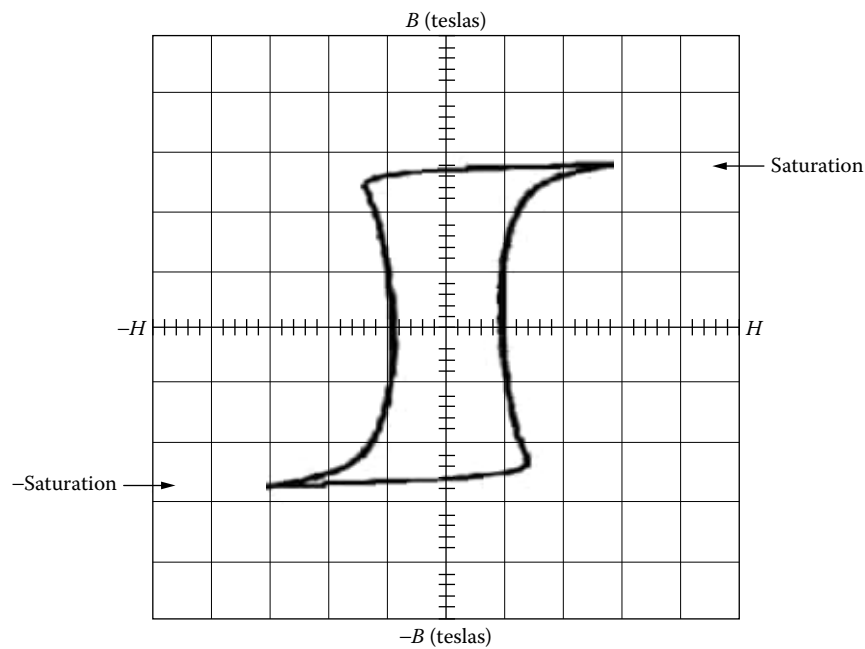


Figure 2-34. Orthonol (2A) B-H Loop, $B = 0.5$ T/cm, $H = 50$ ma/cm.

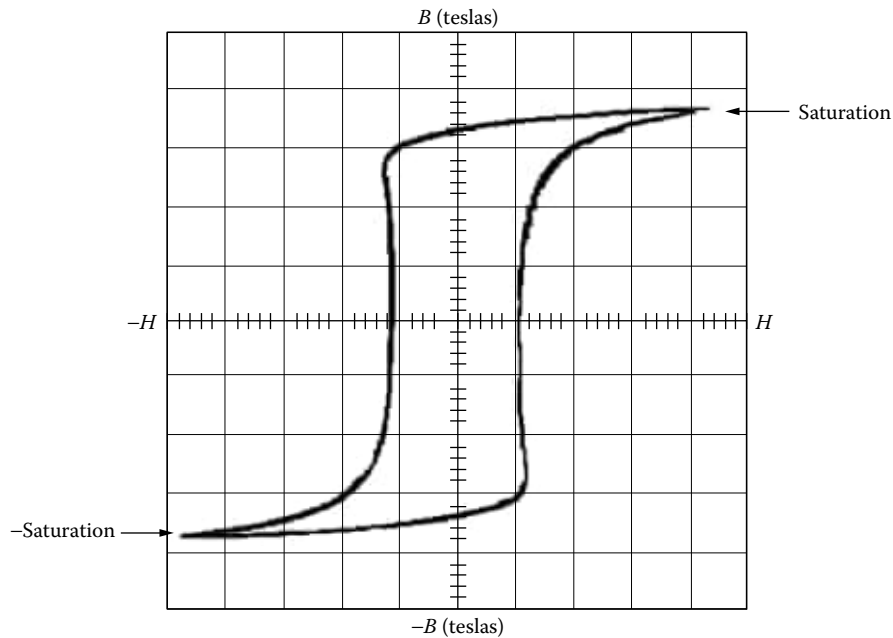


Figure 2-35. Square Permalloy (2D) B-H Loop, $B = 0.2$ T/cm, $H = 20$ ma/cm.

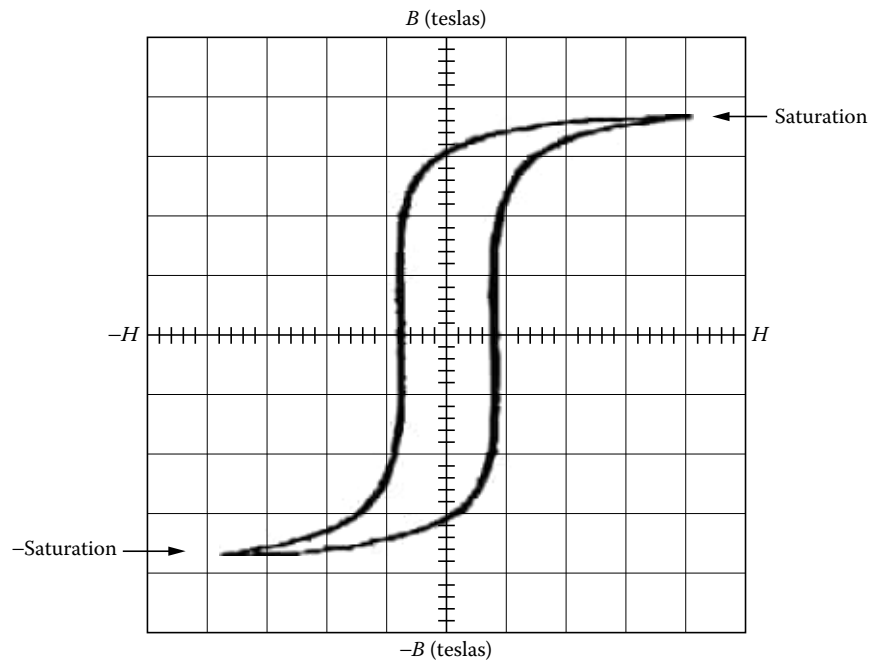


Figure 2-36. Supermalloy (2F) B-H Loop, $B = 0.2$ T/cm, $H = 10$ ma/cm.

Figures 2-37 to 2-40 show the dynamic B-H loop patterns obtained for various core materials when the test conditions are included in a sequence, in which S1 was in open condition (A), then in closed condition (B), and then, opened again, in condition (C). It is apparent from this data that, with a small amount of dc bias, the minor dynamic B-H loop can traverse the major B-H loop from saturation to saturation. Note that after the dc

bias has been removed, the minor B-H loops remained shifted to one side or the other. Because of the ac coupling of the integrator to the oscilloscope, the photographs in these figures do not present a complete picture of what really happens during the flux swing.

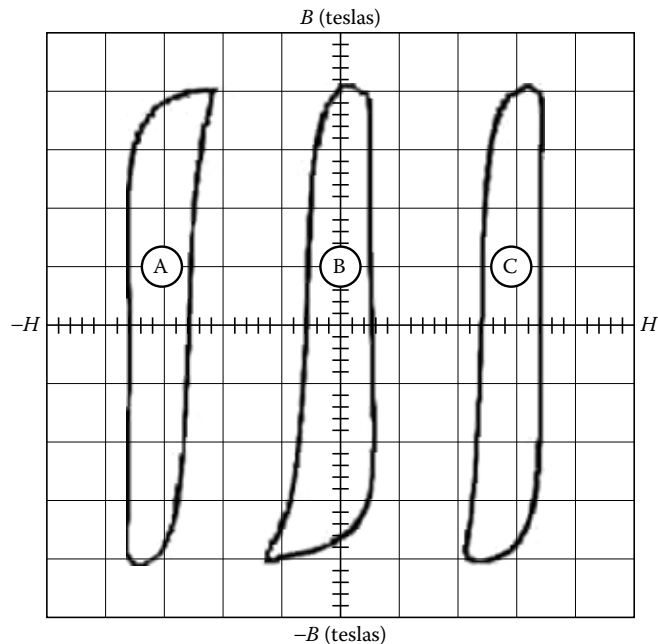


Figure 2-37. Magnesil (2K) B-H Loop, $B = 0.3$ T/cm, $H = 200$ ma/cm.

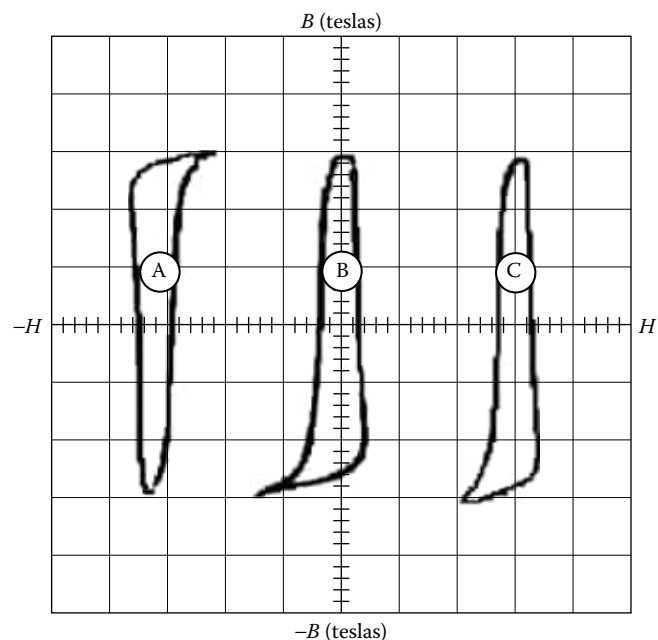


Figure 2-38. Orthonol (2A) B-H Loop, $B = 0.2$ T/cm, $H = 100$ ma/cm.

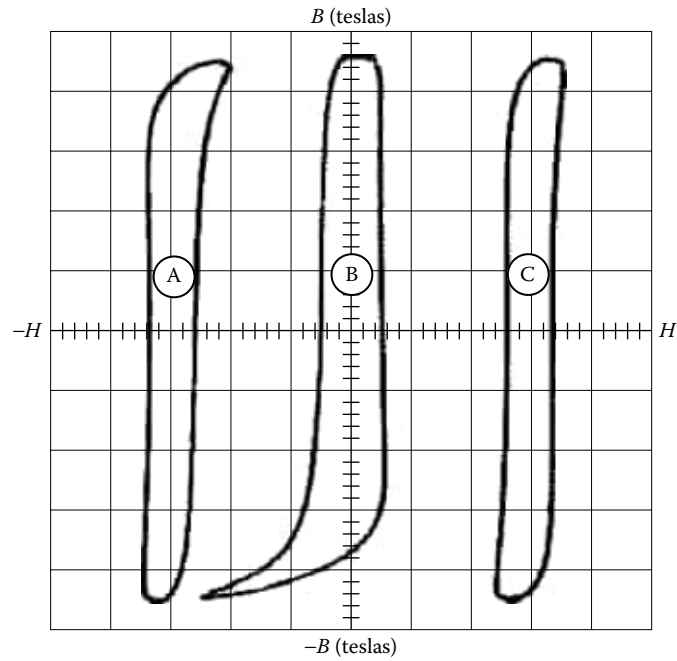


Figure 2-39. Sq. Permalloy (2D) B-H Loop, $B = 0.1$ T/cm, $H = 20$ ma/cm.

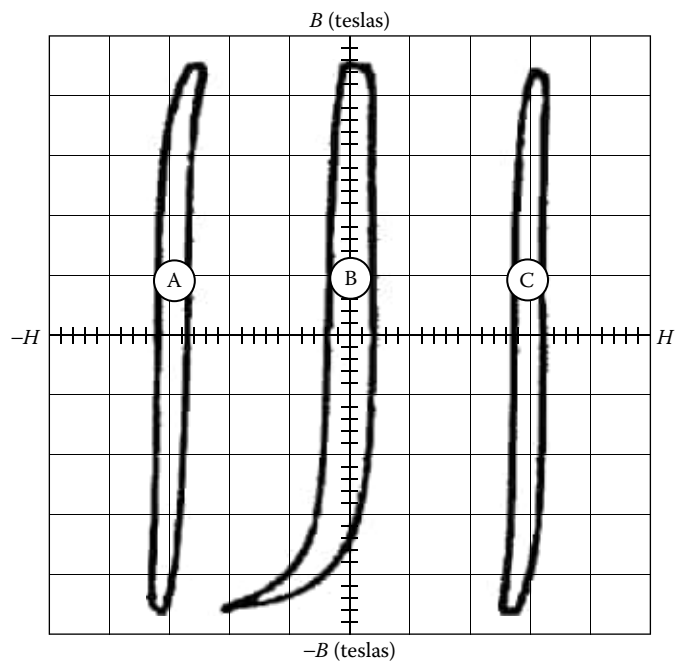


Figure 2-40. Supermalloy (2F) B-H Loop, $B = 0.1$ T/cm, $H = 10$ ma/cm.

Magnetic Material Saturation Theory

The domain theory of the nature of magnetism is based on the assumption that all magnetic materials consist of individual molecular magnets. These minute magnets are capable of movement within the material. When a magnetic material is in its unmagnetized state, the individual magnetic particles are arranged at random, and effectively neutralize each other. An example of this is shown in Figure 2-41, where the tiny magnetic particles are arranged in a disorganized manner. (The north poles are represented by the darkened ends of the magnetic particles.) When a material is magnetized, the individual particles are aligned or oriented in a definite direction, as shown in Figure 2-42.

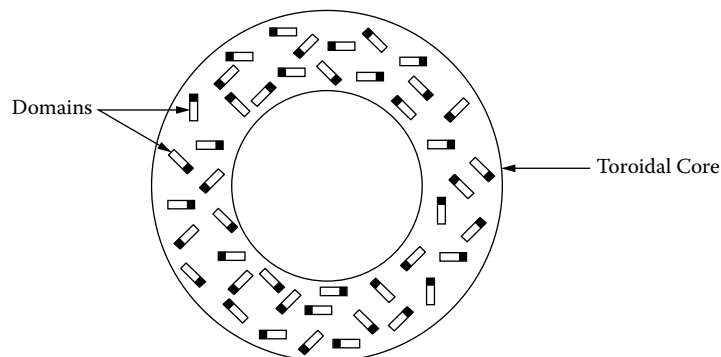


Figure 2-41. Magnetic Domains, Arranged in a Random Manner.

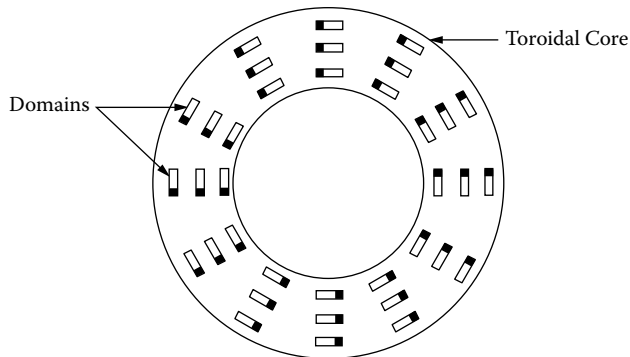


Figure 2-42. Magnetic Domains, Aligned in a Definite Direction.

The degree of magnetization of a material depends on the degree of alignment of the particles. The external magnetizing force can continue to affect the material up to the point of saturation, the point at which essentially all of the domains are lined up in the same direction.

In a typical toroidal core, the effective air gap is less than 10^{-6} cm. Such a gap is negligible in comparison to the ratio of mean length to permeability. If the toroid was subjected to a strong magnetic field (enough to saturate), essentially all of the domains would line up in the same direction. If suddenly the field were

removed at B_m , the domains would remain lined up, and be magnetized along that axis. The amount of flux density that remains is called the residual flux, B_r . The result of this effect was shown earlier in Figures 2-37 through 2-40.

Air Gap Effect

An air gap introduced into the core has a powerful demagnetizing effect, resulting in a “shearing over” of the hysteresis loop, and a considerable decrease in permeability of high-permeability materials. Direct current excitation follows the same pattern. However, the core bias is considerably less affected than the magnetization characteristics by the introduction of a small air gap. The magnitude of the air gap effect also depends on the length of the mean magnetic path and on the characteristics of the uncut core. For the same air gap, the decrease in permeability will be less with a greater magnetic flux path, but more pronounced in a high-permeability core with a low coercive force.

Effect of Gapping

Figure 2-43 shows a comparison of a typical toroidal core B-H loop, without and with a gap. The gap increases the effective length of the magnetic path. When voltage E is impressed across primary winding, N_p , of a transformer, the resulting current, I_m , will be small because of the highly inductive circuit, as shown in Figure 2-44. For a particular core size, maximum inductance occurs when the air gap is minimum.

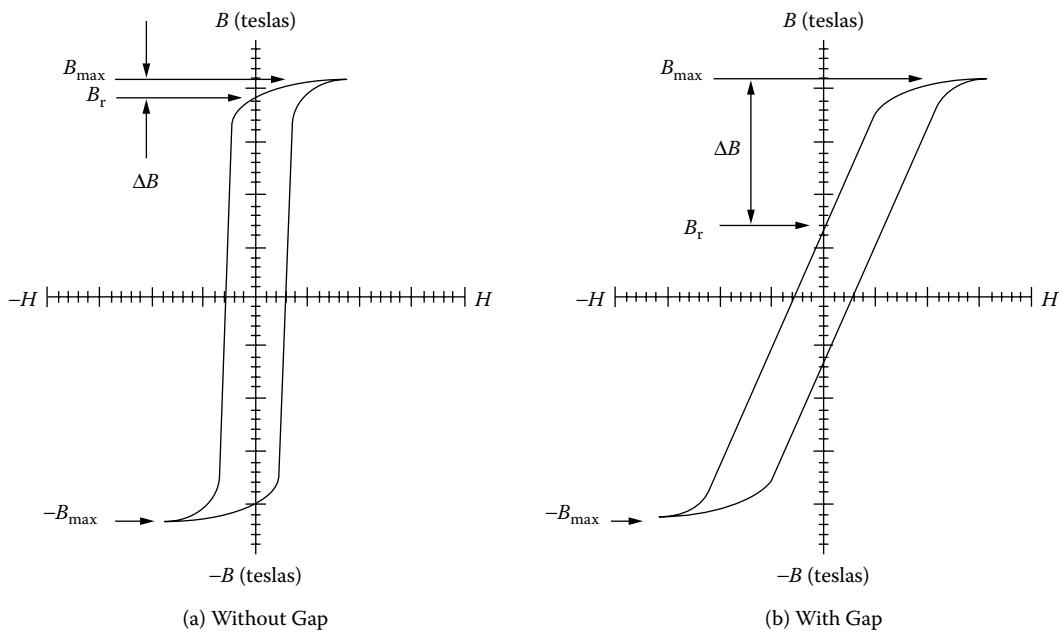


Figure 2-43. Comparing Magnetic Materials With and Without a Gap.

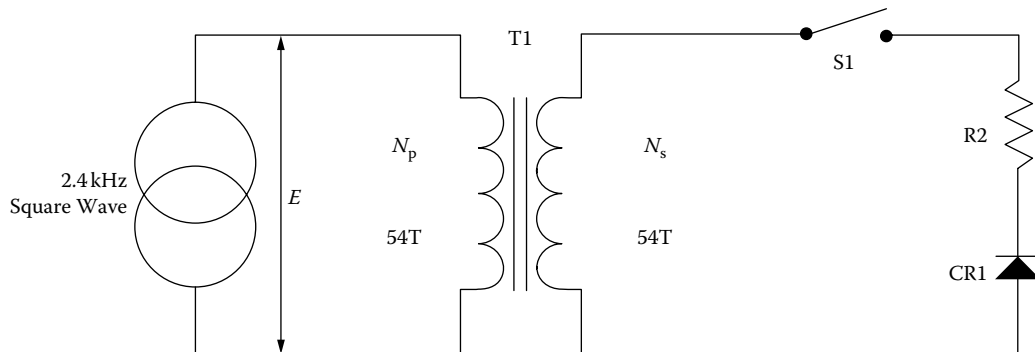


Figure 2-44. Implementing dc Unbalance.

When \$S_1\$ is closed, an unbalanced dc current flows in the secondary, \$N_s\$ turns, and the core is subjected to a dc magnetizing force, resulting in a flux density that may be expressed as:

$$B_{dc} = \frac{0.4\pi N_s I_{dc} (10^{-4})}{l_g + \frac{MPL}{\mu_r}}, \quad [\text{teslas}] \quad [2-15]$$

In converter and inverter design, this dc flux is augmented by the ac flux swing, which is:

$$B_{ac} = \frac{E (10^4)}{K_f f A_c N}, \quad [\text{teslas}] \quad [2-16]$$

If the sum of \$B_{dc}\$ and \$B_{ac}\$ shifts operations above the maximum operating flux density of the core material, the incremental permeability, \$(\mu_{ac})\$, is reduced. This condition lowers the impedance and increases the flow of magnetizing current, \$I_m\$. This condition can be remedied by introducing into the core assembly an air gap which causes a decrease in dc magnetization in the core. However, the size of the air gap that can be incorporated has a practical limitation. Since the air gap lowers impedance, it results in increased magnetizing current, \$I_m\$, which is inductive. The resultant voltage spikes produced by such currents apply a high stress to the switching transistors, and may cause failure. This stress can be minimized by tight control of lapping and etching of the gap to keep the gap to a minimum.

From Figure 2-43, it can be seen that the B-H curves depict maximum flux density, \$B_m\$, and residual flux, \$B_r\$, for ungapped and gapped cores, and that the useful flux swing is designated, \$\Delta B\$, which is the difference between, \$B_m\$ and \$B_r\$. It is noted, in Figure 2-43(a), that, \$B_r\$ approaches, \$B_m\$, but, in Figure 2-43(b), there is a much greater, \$\Delta B\$, between them. In either case, when excitation voltage is removed at the peak of the excursion of the B-H loop, flux falls to the, \$B_r\$, point. It is apparent that introducing an air gap reduces, \$B_r\$, to a lower level, and increases the useful flux density. Thus, insertion of an air gap in the core eliminates, or markedly reduces, the voltage spikes produced by the leakage inductance, due to the transformer saturation.

Two types of core configurations were investigated in the ungapped and gapped states. Figure 2-45 shows the type of toroidal core that was cut, and Figure 2-46 shows the type of C core that was cut. Toroidal cores are virtually gapless, when conventionally fabricated. To increase the gap, the cores were physically cut in half, and the cut edges were lapped, acid-etched to remove cut debris, and banded to form the cores. A minimum air gap, on the order of less than 25 μm , was established.

As is noted from [Figures 2-47 through 2-50](#), which show the B-H loops of the uncut and cut cores, the results obtained indicated that the effect of gapping was the same for both the C cores and the toroidal cores subjected to testing. It is noted, however, that gapping of the toroidal cores produced a lowered square characteristic for the B-H loop, as shown in [Table 2-18](#). This data was obtained from Figures 2-47 through 2-50. ΔH values extracted from the same figures, as shown in [Figure 2-51](#), are tabulated in [Table 2-19](#).

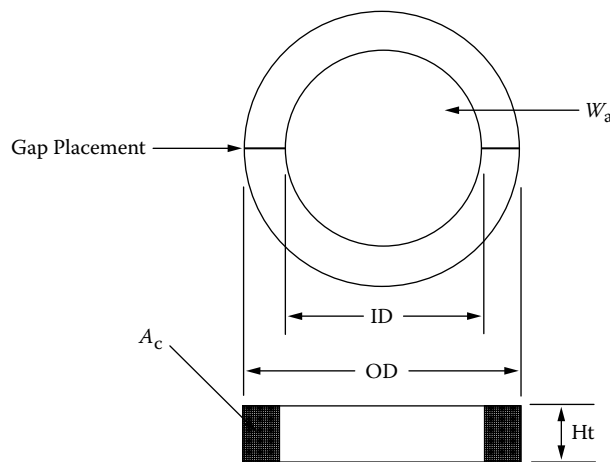


Figure 2-45. Typical Cut Toroidal Core.

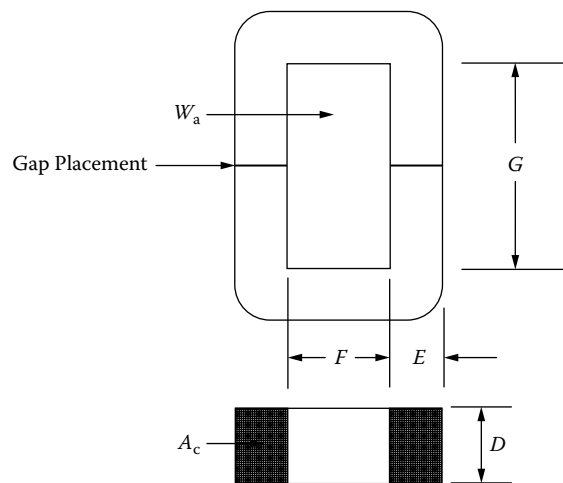


Figure 2-46. Typical Middle Cut C Core.

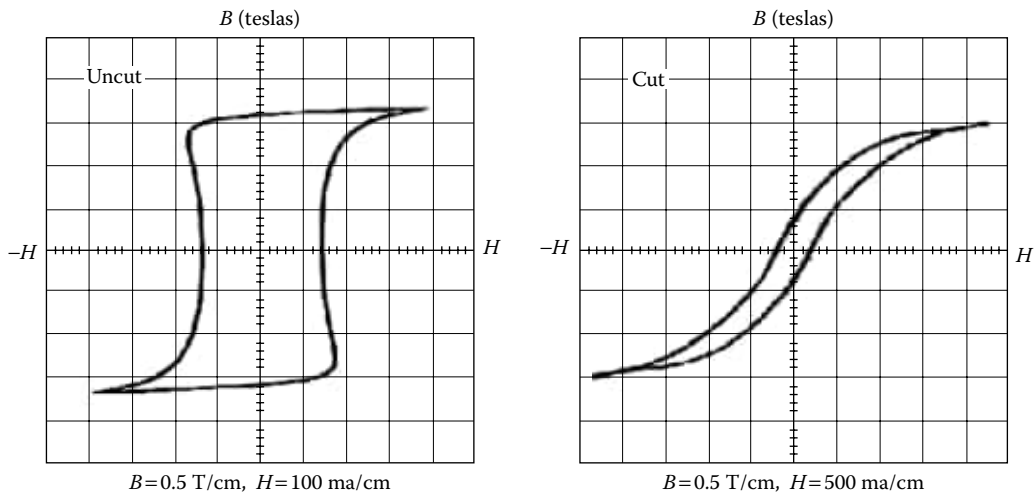


Figure 2-47. Magnesil (K) B-H Loop, Uncut and Cut with Minimum Gap.

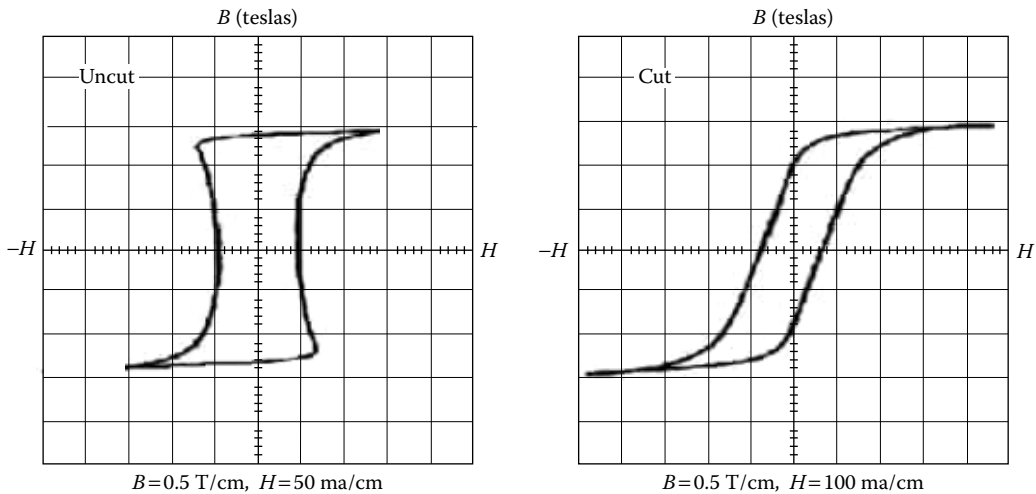


Figure 2-48. Orthonal (A) B-H Loop, Uncut and Cut with Minimum Gap.

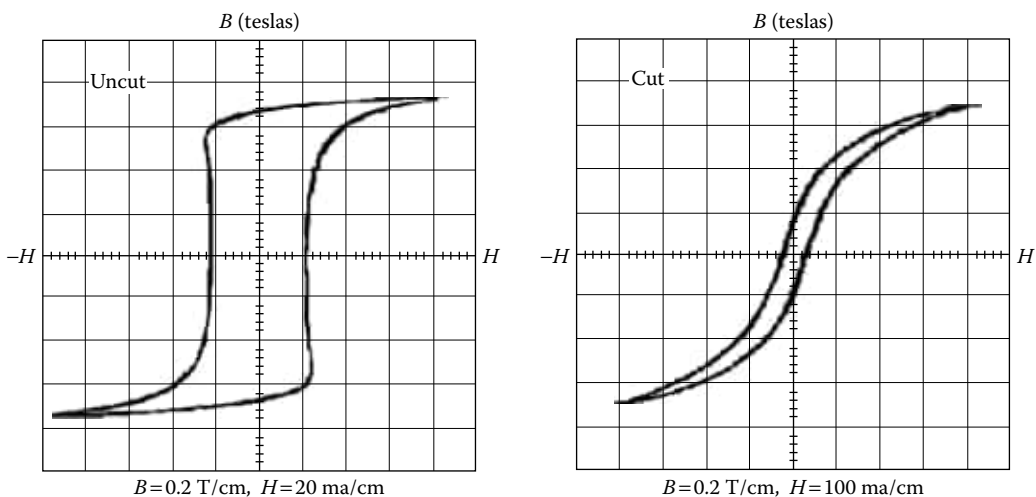


Figure 2-49. Square Permalloy (D) B-H Loop, Uncut and Cut with Minimum Gap.

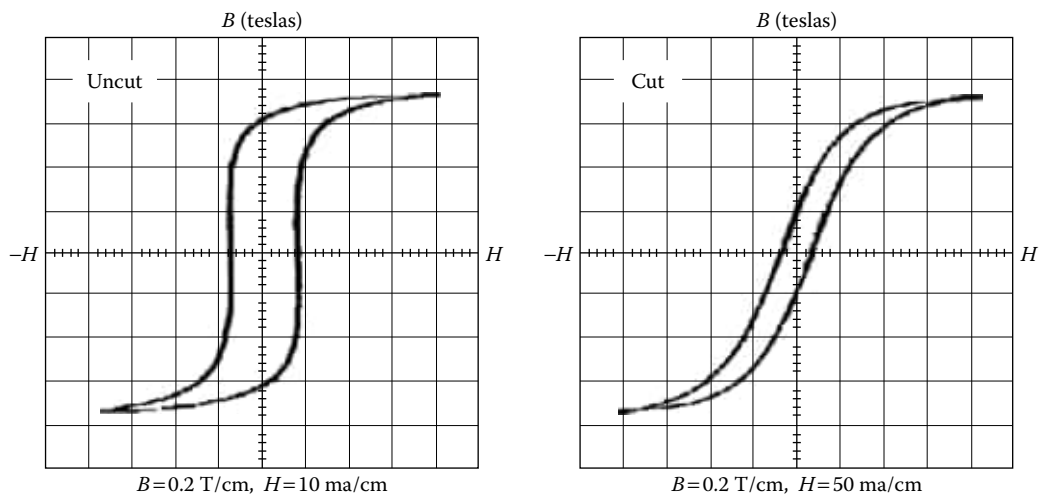


Figure 2-50. Supermalloy (F) B-H Loop, Uncut and Cut with Minimum Gap.

Table 2-18.

Comparing B_r/B_m on Uncut and Cut Cores					
Core Number*	Trade Name	Teslas B_s	Turns N	Uncut B_r/B_m	Cut B_r/B_m
52029-2A	Orthonol	1.45	54	0.96	0.62
52029-2D	Sq. Permalloy	0.75	54	0.86	0.21
52029-2F	Superpermalloy	0.75	54	0.81	0.24
52029-2K	Magnesil	1.60	54	0.93	0.22

* Magnetics toroidal cores.

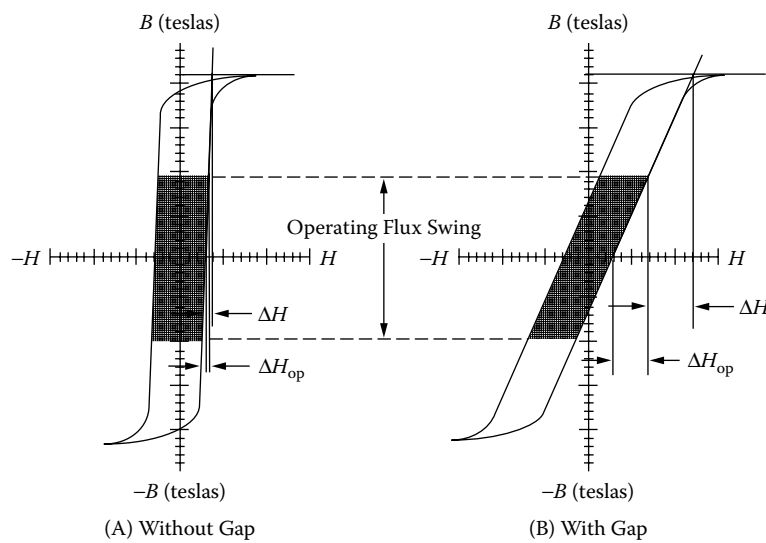


Figure 2-51. Defining ΔH_{op} and ΔH .

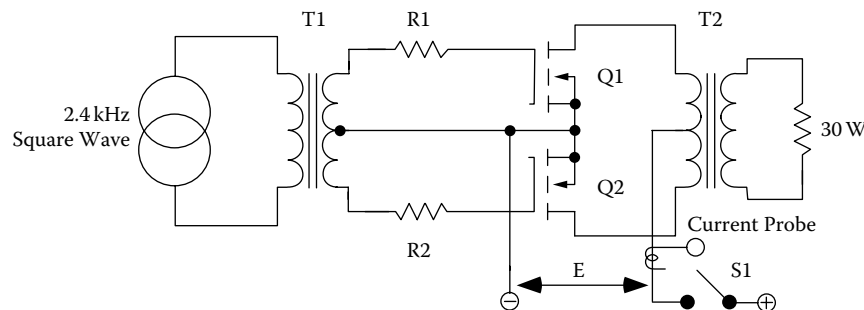
Table 2-19. Comparing ΔH and ΔH_{op} on Uncut and Cut Cores

Comparing ΔH and ΔH_{op} on Uncut and Cut Cores							
Material *Trade Name	Teslas B_m	Teslas B_{ac}	Teslas B_{dc}	Ampere-turns/cm			
				Uncut		Cut	
				ΔH_{op}	ΔH	ΔH_{op}	ΔH
Orthonol	1.44	1.15	0.288	0.0125	0	0.895	0.178
Sq permalloy	0.73	0.58	0.146	0.0100	0.005	0.983	0.178
Supermalloy	0.63	0.58	0.136	0.0175	0.005	0.491	0.224
Magnesil	1.54	1.23	0.310	0.0750	0.025	7.150	1.780

* Magnetics cores.

A direct comparison of cut and uncut cores was made electrically by means of two different test circuits. The magnetic material used in this branch of the test was Orthonol. The frequency was 2.4 kHz, and the flux density was 0.6 T. The first test circuit, shown in Figure 2-52, was a driven inverter operating into a 30-W load, with the power MOSFETs, operating into and out of saturation. Drive was applied continuously. S1 controls the supply voltage to Q1 and Q2.

With switch, S1, closed, transistor, Q1, was turned on and allowed to saturate. This applied voltage, $E - V_{DS(on)}$, across the transformer winding. Switch, S1, was then opened. Then, the flux in transformer, T2, dropped to the residual flux density, B_r . Switch, S1, was closed again. This was done several times in succession to catch the flux in an additive direction. Figures 2-53 and 2-54 show the inrush current measured at the center tap of T2.

**Figure 2-52.** Inverter Inrush Current Test Fixture.

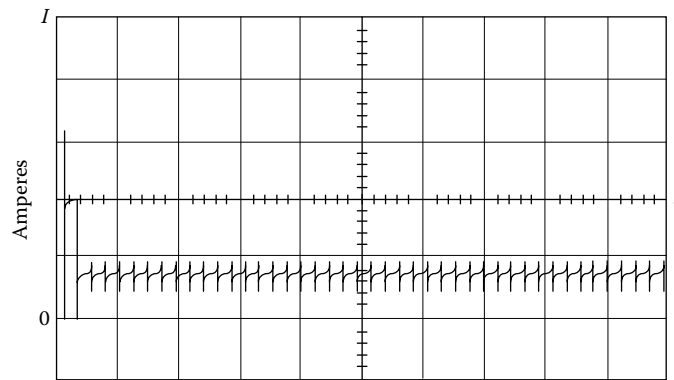


Figure 2-53. Typical Inrush Current of a Uncut Core in a Driven Inverter.

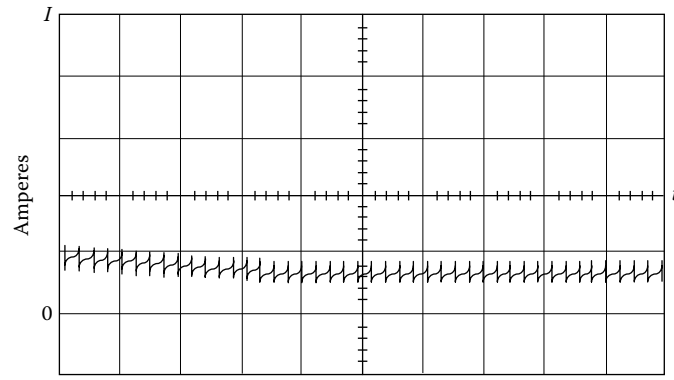


Figure 2-54. Resulting Inrush Current using a Cut Core.

It will be noted, in Figure 2-53, that the uncut core saturated, and the inrush current was limited only by circuit resistance and power, MOSFETs $R_{DS(on)}$. Figure 2-54 shows that saturation did not occur in the case of the cut core. Thus, the high inrush current and transistor stress were virtually eliminated.

The second test circuit arrangement is shown in [Figure 2-55](#). The purpose of this test was to excite a transformer and measure the inrush current, using a current probe. A square wave power oscillator was used to excite transformer, T2. Switch, S1, was opened and closed several times to catch the flux in an additive direction. [Figures 2-56](#) and [2-57](#) show inrush current for an uncut and cut core, respectively.

A small amount of air gap, less than $25 \mu\text{m}$, has a powerful effect on the demagnetizing force, but little effect on the core loss. This small air gap decreases the residual magnetism by “shearing over” the hysteresis loop, which eliminates the problem of the core tending to remain saturated.

A typical example of the merits of the cut core occurred in the checkout of a Mariner spacecraft. During the checkout of a prototype science package, a large (8 A, 200 us) turn-on transient was observed. The normal running current was 0.06 A, fused with a parallel-redundant 1/8-A fuse, as required by the Mariner Mars design philosophy. With the 8-A inrush current, the 1/8-A fuses were easily blown. This did not happen, on

every turn-on, but only when the core would “latch up” in the wrong direction for turn-on. Upon inspection, the transformer turned out to be a 50-50 nickel-iron toroid. The design was changed from a toroidal core to a cut core, with a 25 μm , air gap. The new design was completely successful in eliminating the 8-A turn-on transient.

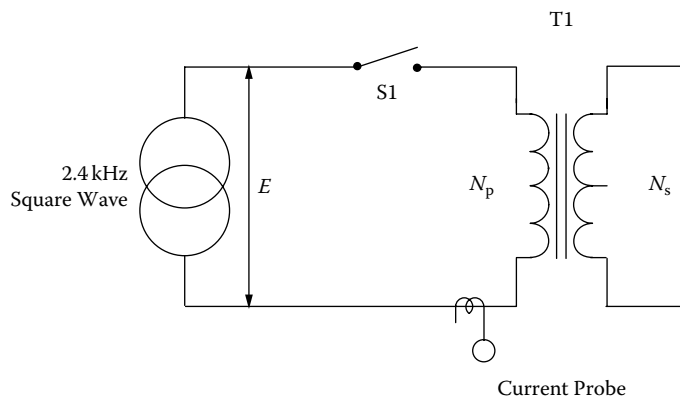


Figure 2-55. Transformer Rectifier Inrush Current Measurement.

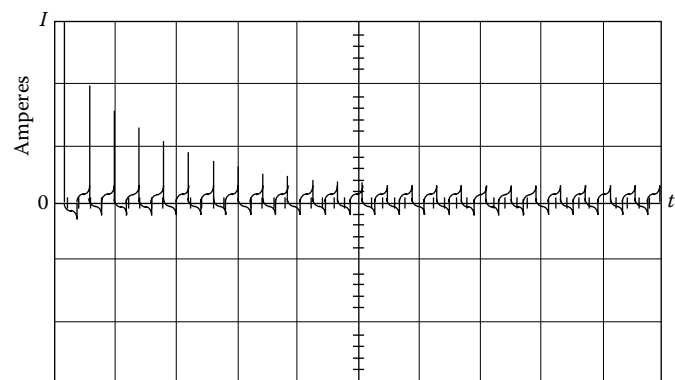


Figure 2-56. Inrush Current of a Transformer using a Uncut Core.

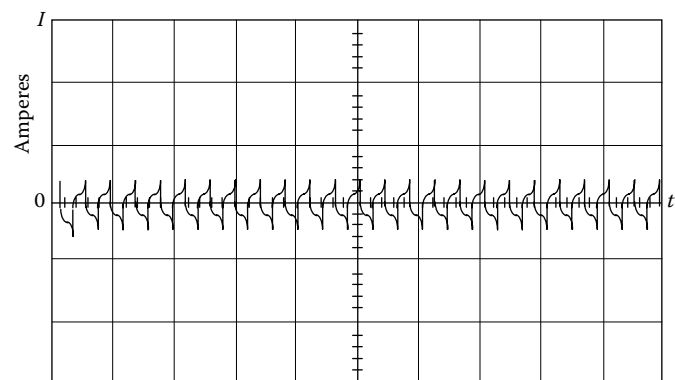


Figure 2-57. Inrush Current of a Transformer using a Cut Core.

Composite Core Configuration

A composite core configuration has been developed for transformers that combine the protective feature of a gapped core with the much lower magnetizing current requirement of an uncut core. The uncut core functions, under normal operating conditions, and the cut core takes over during abnormal conditions to prevent high switching transients and their potentially destructive effect on the transistors.

This configuration is a composite of cut and uncut cores assembled together concentrically, with the uncut core nested within the cut core. The uncut core has high permeability, and thus requires a very small magnetizing current. On the other hand, the cut core has a low permeability and thus requires a much higher magnetization current. The uncut core is designed to operate at a flux density that is sufficient for normal operation of the converter. The uncut core may saturate under the abnormal conditions previously described. The cut core then takes over and supports the applied voltage so that excessive current does not flow. In a sense, it acts like a ballast resistor in some circuits to limit current flow to a safe level.

Figures 2-58 and 2-59 show the magnetization curves for an uncut core and a composite core of the same material at the same flux density. The much lower, B_r characteristic of the composite compared to the uncut core is readily apparent.

The desired features of the composite core can be obtained more economically by using different materials for the cut and uncut portions of the core. It was found that when the design required high nickel (4/79), the cut portion could be low nickel, (50/50), and because low nickel has twice as high a flux density as high nickel, the core was made of 66% high nickel, and 33% low nickel.

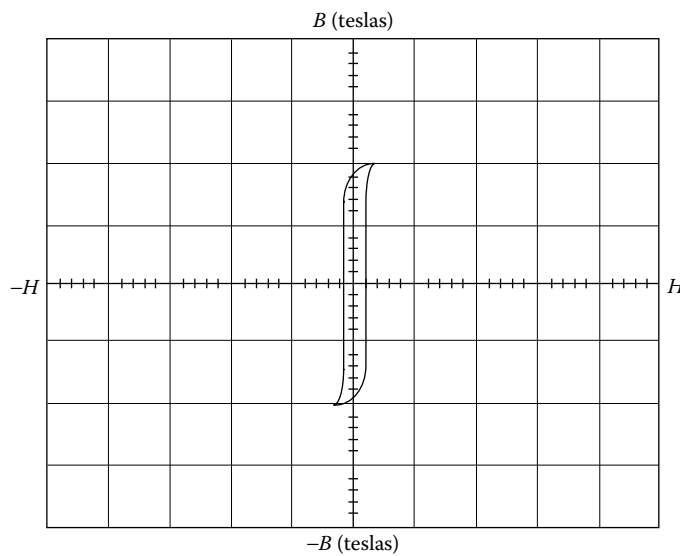


Figure 2-58. Uncut Core Excited at 0.2 T/cm.

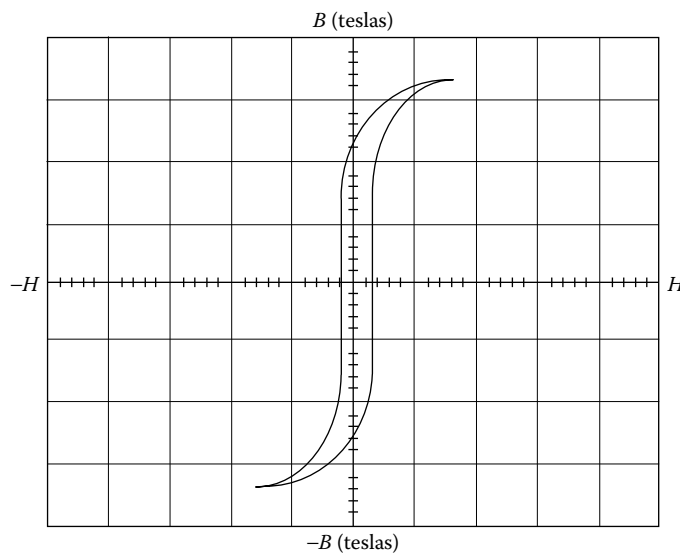


Figure 2-59. Both Cut and Uncut Cores Excited at 0.2 T/cm.

Figure 2-60 shows cut and uncut cores that have been impregnated to bond the ribbon layers together. The uncut core was first trimmed to fit within the inner diameter of the cut core by peeling off a wrap or two of the ribbon steel. The two cores are assembled into a composite core (Figure 2-61, on the right).

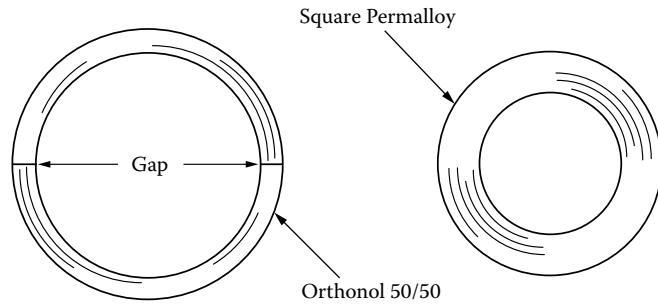


Figure 2-60. Composite Cores Ready for Final Assembly.

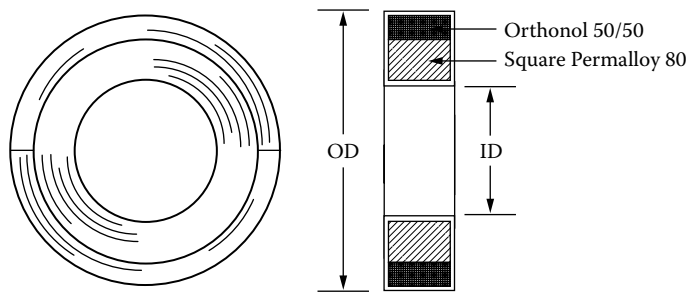


Figure 2-61. Composite Cores Assembled in Final Form.

To ensure uniform characteristics for gapped cores, a gap dimension of 50 μm is recommended, because variations produced by thermal cycling will not affect this gap greatly. In the composite core, the gap is obtained by inserting a sheet of paper Mylar or Kapton film material between the core ends during banding. The same protective feature can be accomplished in transformers with laminated cores. When laminations are stacked by interleaving them one-by-one, the result will be a minimum air gap, as shown in Figure 2-62 by the squareness of the B-H loop. Shearing over of the B-H loop, or decreasing the residual flux, as shown in Figure 2-63, is accomplished by butt joining half the laminations in the core-cross section, which introduces a small, additional air gap.

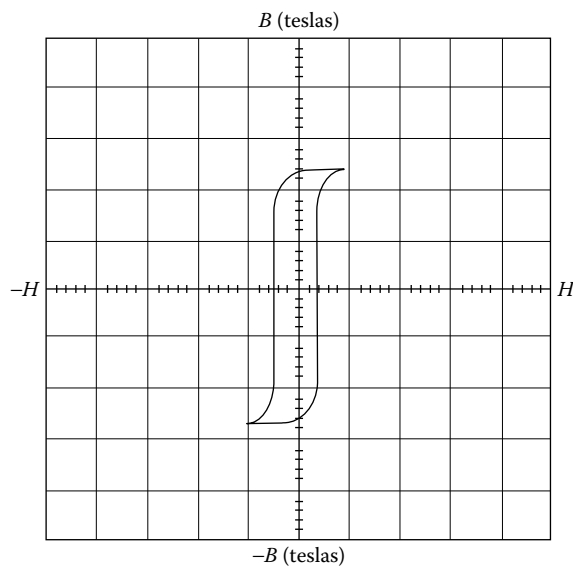


Figure 2-62. B-H Loop with Laminations Stacked 1×1 Interleaved.

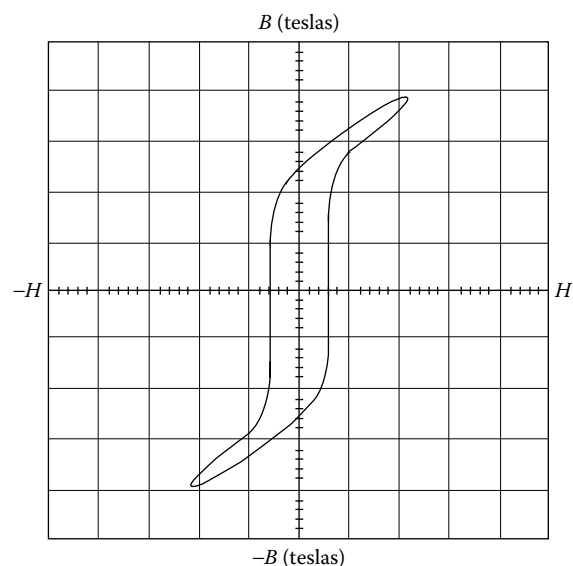


Figure 2-63. B-H Loop with Laminations Stack Half 1×1 and Half Butt Stack.

Table 2-20 is a compiling of composite cores manufactured by Magnetics Inc., alongside their standard dimensional equivalent cores. Also, included in Table 2-20, is the cores' area product, A_p , and the core geometry K_g , which is discussed in Chapter 7.

Table 2-20. Composite Core Listing Along with the Area Product and Core Geometry

Magnetics Inc. Composite Cores			
Composite Number	Standard Core Number	A_p (cm ⁴)	K_g (cm ⁵)
01605-2D	52000	0.0728	0.00105
01754-2D	52002	0.1440	0.00171
01755-2D	52076	0.2850	0.00661
01609-D2	52061	0.3890	0.00744
01756-2D	52106	0.4390	0.00948
01606-2D	52094	0.6030	0.02210
01761-2D	52318	0.7790	0.02600
01757-2D	52029	1.0900	0.02560
01760-2D	52188	1.1520	0.05120
02153-2D	52181	1.2200	0.04070
01758-2D	52032	1.4550	0.04310
01607-2D	52026	2.1800	0.08740
01966-2D	52030	2.3370	0.06350
01759-2D	52038	2.9100	0.14000
01608-2D	52035	4.6760	0.20600
01623-2D	52425	5.2550	0.26200
01624-2D	52169	7.1300	0.41800

$A_c = 66\%$ Square Permalloy 4/79.
 $A_c = 33\%$ Orthonol 50/50.
 $l_g = 2$ mil Kapton.

Summary

Low-loss tape-wound toroidal core materials, that have a very square hysteresis characteristic, (B-H loop), have been used extensively in the design of spacecraft transformers. Due to the squareness of the B-H loops of these materials, transformers designed with them tend to saturate quite easily. As a result, large voltage and current spikes, which cause undue stress on the electronic circuitry, can occur. Saturation occurs when there is any unbalance in the ac drive to the transformer, or when any dc excitation exists. Also, due to the square characteristic, a high residual flux state, (high, B_r), may remain when excitation is removed. Reapplication of excitation in the same direction may cause deep saturation, and an extremely large current spike. Limited by source impedance and transformer winding resistance can result. This can produce catastrophic failure.

With the introduction of a small, (less than 25 μm), air gap into the core, the problems described above can be avoided while retaining the low-loss properties of the materials. The air gap has the effect of “shearing over” the B-H loop of the material so that the residual flux state is low. The margin between operating flux density and saturation flux density is high. The air gap thus has a powerful demagnetizing effect upon the square loop materials. Properly designed transformers, using cut toroid or C core square-loop materials, will not saturate upon turn-on, and can tolerate a certain amount of unbalanced drive or dc excitation.

It must be emphasized, however, that because of the nature of the material and the small size of the gap, extreme care and control must be taken in performing the gapping operation. Otherwise, the desired shearing effect will not be achieved, and the low-loss properties will be lost. The cores must be very carefully cut, lapped, and etched to provide smooth, residue-free surfaces. Reassembly must be performed with equal care.

A conversion, Table 2-21, has been added by popular request.

Table 2-21. Conversion Table

Conversion Table			
Item	Multiply	By	To Obtain
1	oersteds	79.5	amp-turn/m
2	oersteds	0.795	amp-turn/cm
3	amp-turn/m	0.0126	oersteds
4	amp-turn/cm	1.26	oersteds
5	gausses	0.0001	teslas
6	gausses	0.1	millitesla
7	teslas	10000	gausses
8	millitesla	10	gausses
9	inch	2.54	cm
10	cm	0.3937	inch
11	inch ²	6.452	cm ²
12	cm ²	0.155	inch ²
13	circular mils	5.07×10^{-6}	cm ²
14	cm ²	0.197×10^6	circular mils
15	ounces	28.35	grams
16	grams	0.0353	ounces
17	pounds	453.6	grams
18	grams	0.002205	pounds

Chapter 3

Magnetic Cores

Table of Contents

1. Introduction.....	3-4
2. Core Type and Shell Type Construction.....	3-5
3. Types of Core Materials	3-5
4. Eddy Currents and Insulation.....	3-6
5. Laminations.....	3-7
6. Annealing and Stress-Relief	3-8
7. Stacking Laminations and Polarity	3-9
8. Flux Crowding	3-10
9. Exciting Current	3-11
10. Tape Wound C, EE, and Toroidal Cores.....	3-12
11. Tape Toroidal Cores	3-14
12. Toroidal, Powder Core	3-15
13. Stacking Factors.....	3-15
14. Introduction to the Magnetic Cores.....	3-16
15. Design and Dimensional Data for EI Laminations	3-17
16. Design and Dimensional Data for UI Laminations	3-18
17. Design and Dimensional Data for LL Laminations	3-19
18. Design and Dimensional Data for DU Laminations	3-20
19. Design and Dimensional Data for Three-Phase Laminations.....	3-21
20. Design and Dimensional Data for Tape Wound C Cores	3-22
21. Dimensional Outline for Tape Wound EE Cores.....	3-23
22. Design and Dimensional Data for Tape Wound Toroidal Cores.....	3-24
23. Design and Dimensional Data for EE Ferrite Cores	3-25
24. Design and Dimensional Data for EE and EI Planar, Ferrite Cores	3-26
25. Design and Dimensional Data for EC, Ferrite Cores	3-27
26. Design and Dimensional Data for ETD, Ferrite Cores	3-28
27. Design and Dimensional Data for ETD/(low profile), Ferrite Cores.....	3-29
28. Design and Dimensional Data for ER, Ferrite Cores.....	3-30
29. Design and Dimensional Data for EFD, Ferrite Cores	3-31
30. Design and Dimensional Data for EPC, Ferrite Cores	3-32
31. Design and Dimensional Data for PC, Ferrite Cores	3-33
32. Design and Dimensional Data for EP, Ferrite Cores.....	3-34
33. Design and Dimensional Data for PQ, Ferrite Cores.....	3-35

Table of Contents**3-3**

34. Design and Dimensional Data for PQ/(low profile), Ferrite Cores	3-36
35. Design and Dimensional Data for RM, Ferrite Cores.....	3-37
36. Design and Dimensional Data for RM/(low profile), Ferrite Cores	3-38
37. Design and Dimensional Data for DS, Ferrite Cores	3-39
38. Design and Dimensional Data for UUR, Ferrite Cores.....	3-40
39. Design and Dimensional Data for UUS, Ferrite Cores	3-41
40. Design and Dimensional Data for Toroidal, Ferrite Cores.....	3-42
41. Design and Dimensional Data for Toroidal, MPP Powder Cores	3-43
42. Design and Dimensional Data for Toroidal, Iron Powder Cores	3-44
43. Design and Dimensional Data for Toroidal, Sendust Powder Cores	3-45
44. Design and Dimensional Data for Toroidal, High Flux Powder Cores	3-46
45. Design and Dimensional Data for EE, Iron Powder Cores.....	3-47
46. Design and Dimensional Data for EE, Sendust Powder Cores.....	3-48
47. Manufacturers' Material Product List.....	3-49
48. References.....	3-50

Introduction

The key ingredient in a magnetic device is the magnetic field (flux) created when current is passed through a coiled wire. The ability to control (channel, predict, conduct), the magnetic field (flux) is critical to controlling the operation of the magnetic device.

The ability of a material to conduct magnetic flux is defined as permeability. A vacuum is defined as having a permeability of 1.0 and the permeability of all other materials is measured against this baseline. Most materials, such as air, paper, and wood are poor conductors of magnetic flux, in that they have low permeability. If wire is wound on a dowel, it exhibits an exact magnetic field, as shown in Figure 3-1. There are a few materials, such as iron, nickel, cobalt, and their alloys that have high permeabilities, sometimes ranging into the hundreds of thousands. These materials and their alloys are used as the base materials for all core materials.

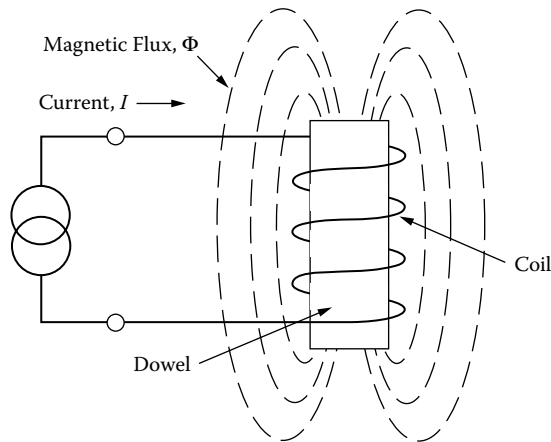


Figure 3-1. Air Core with an Intensified Magnetic Field.

The main purpose of the core is to contain the magnetic flux and create a well-defined, predictable path for the flux. This flux path, and the mean distance covered by the flux within the magnetic material, is defined as the Magnetic Path Length (MPL) (see Figure 3-2). The Magnetic Path Length and permeability are vital keys

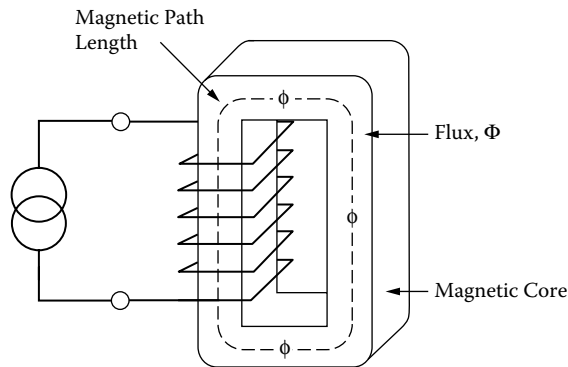


Figure 3-2. Magnetic Core Confines the Magnetic Field.

in predicting the operation characteristic of a magnetic device. Selection of a core material and geometry are usually based on a compromise between conflicting requirements, such as size, weight, temperature rise, flux density, core loss, and operating frequency.

Core Type and Shell Type Construction

There are two types of construction for magnetic cores, core type and shell type. The shell type construction is shown in Figure 3-3, and the core type construction is shown in Figure 3-4. In the shell type, shown in Figure 3-3, the core surrounds the coil. Here, the magnetic fields are around the outside of the coil. The advantage of this configuration is that it requires only one coil. In the core type of construction, shown in Figure 3-4, the coils are outside of the core. A good example of this is a toroid, where the coil is wound on the outside of a core.

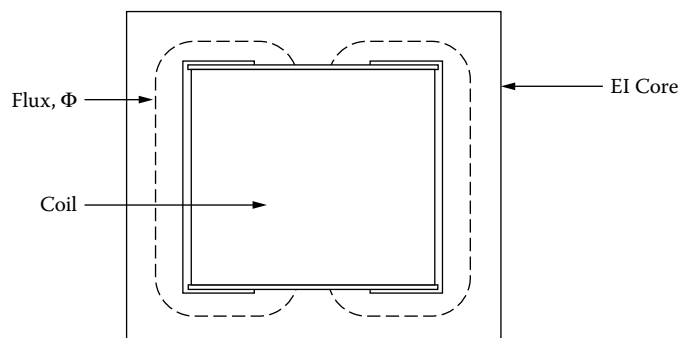


Figure 3-3. Shell Type Construction: the Core Surrounds the Coil.

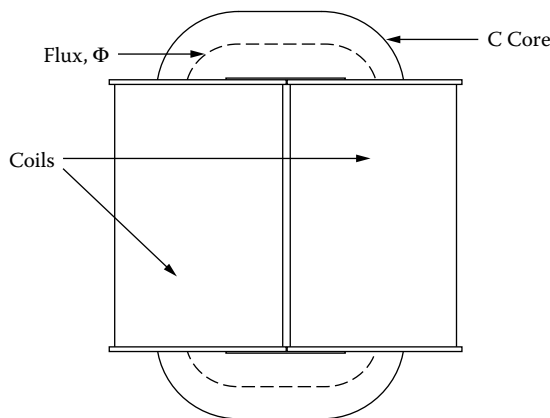


Figure 3-4. Core Type Construction the Coil Surrounds the Core.

Types of Core Materials

Magnetic cores are made of three basic materials. The first is bulk metal, the second is powdered materials, and the third is ferrite material.

The bulk metals are processed from the furnace into ingots. Then, the material is put into a process of hot and cold rolling. The rolling process produces a sheet of material with a thickness ranging from 0.004 to 0.031 inches that can be punched into laminations. It can be further rolled into thicknesses ranging from 0.002 to 0.000125 inches, then slit and wound into tape cores, such as C cores, E cores and toroids.

The powder cores, such as powder molypermalloy and powdered iron materials, are die-pressed into toroids, EE cores and slugs. Powder core processing starts at the ingot, then goes through various steps of grinding until the powder is the right consistency for the required performance. Normally, powder cores are not machined after processing.

Ferrites are ceramic materials of iron oxide, alloyed with oxides or carbonate of manganese, zinc, nickel, magnesium, or cobalt. Alloys are selected and mixed, based on the required permeability of the core. Then, these mixtures are molded into the desired shape with pressure of approximately 150-200 tons per square inch and fired at temperatures above 2000 degrees F. After the parts are made, they are usually tumbled to remove burrs and sharp edges, which are characteristic of this process. Ferrites can be machined to almost any shape to meet the engineer's needs.

Eddy Currents and Insulation

Transformers, operating at moderate frequency, require the reduction of eddy current losses in the magnetic material. To reduce the eddy current losses to a reasonable value requires electrical steel to have adequate resistivity. Also, it needs to be rolled to a specific thickness, and it needs effective electrical insulation or coating of the magnetic material.

If an alternating voltage is applied to the primary winding, as shown in Figure 3-5, it will induce an alternating flux in the core. The alternating flux will, in turn, induce a voltage on the secondary winding. This alternating

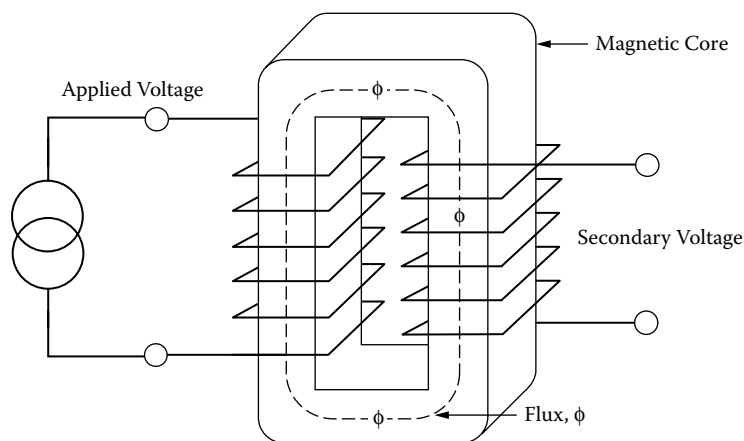


Figure 3-5. Applied Alternating Voltage Induces an Alternating Flux.

flux also induces a small alternating voltage in the core material. These voltages produce currents called eddy currents, which are proportional to the voltage. The magnitude of these eddy currents is also limited by the resistivity of the material. The alternating flux is proportional to the applied voltage. Doubling the applied voltage will double the eddy currents. This will raise the core loss by a factor of four. Eddy currents not only flow in the lamination itself, but could flow within the core as a unit, if the lamination is not properly stamped, and if the lamination is not adequately insulated, as shown in Figure 3-6.

There are two eddy currents, as shown in Figure 3-6, i_a and i_b . The intralaminar eddy current, i_a , is governed by flux, per lamination and resistance of the lamination. It is, therefore, dependent on lamination width, thickness, and volume resistivity.

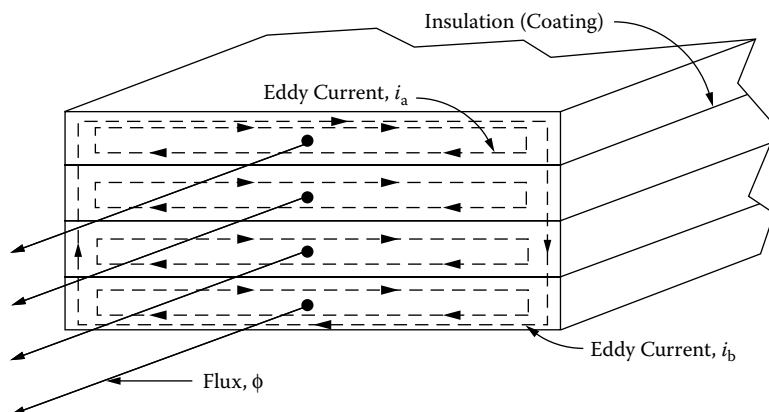


Figure 3-6. Insulation is Required between Laminations to Reduce Eddy Currents.

The interlaminar eddy current, i_b , is governed by total flux and resistance of the core stack. It is primarily dependent upon stack width and height, the number of laminations, and the surface insulation resistance, per lamination.

The magnetic materials used for tape cores and laminations are coated with an insulating material. The insulating coating is applied to reduce eddy currents. The American Iron and Steel Institute (AISI) has set up insulation standards for transformer steels used in different applications. High permeability, nickel-iron cores are very strain sensitive. Manufacturers of these cores normally have their own proprietary, insulating material.

Laminations

Laminations are available in scores of different shapes and sizes. The punch press technology for fabricating laminations has been well-developed. Most lamination sizes have been around forever. The most commonly used laminations are the EI, EE, FF, UI, LL, and the DU, as shown in [Figure 3-7](#). The laminations differ from each other by the location of the cut in the Magnetic Path Length. This cut introduces an air gap, which results

in the loss of permeability. To minimize the resulting air gap, the laminations are generally stacked in such a way that the air gaps in each layer are staggered.

There are bobbins and brackets for almost all standard stacking dimensions. Most of the EI lamination is the scrapless. The name, scrapless, is derived from shapes that are punched with minimum waste, as shown in Figure 3-8.

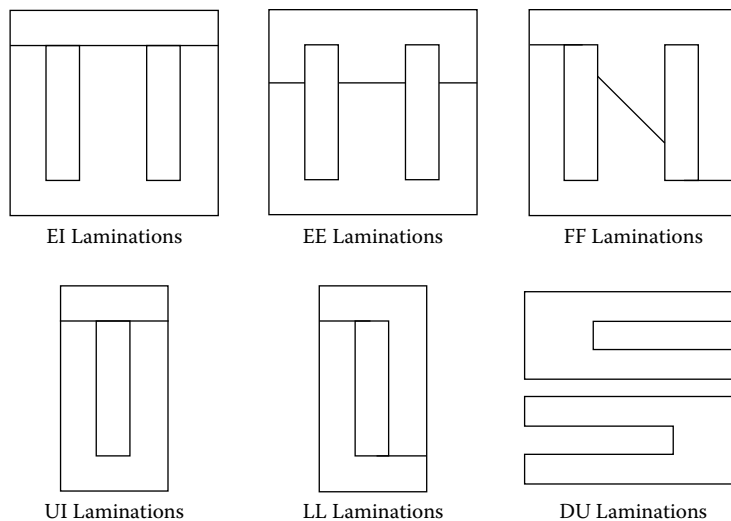


Figure 3-7. Commonly Used Lamination Shapes.

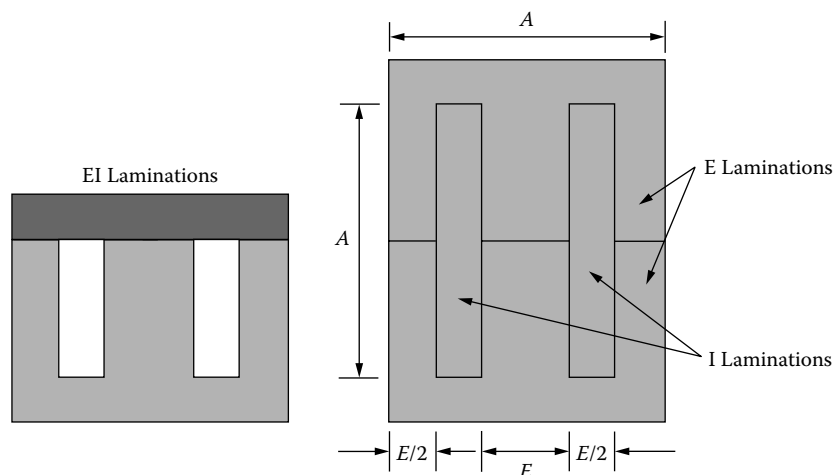


Figure 3-8. Typical, Scrapless EI Lamination.

Annealing and Stress-Relief

One of the most important parameters in transformer steels is permeability. Any stress or strain of the magnetic materials will have an impact on the permeability. The resulting stress could cause higher magnetizing current, or a lower inductance. When the transformer is being assembled (in the stacking process), and

a lamination is bent, (does not return to its original shape), that lamination has been stressed and should be replaced.

Some of the important magnetic properties are lost due to stress and strain after stamping, shearing and slitting. These properties, that have been lost or seriously reduced, can be restored to the magnetic materials by annealing. Basically, stress relief is accomplished by heating (annealing) the magnetic material to prescribed temperature, (depending on the material), followed by cooling to room temperature. The entire annealing process is a delicate operation. The annealing must be done under controlled conditions of time, temperature and the ambient atmosphere that will avoid, even minute, adverse changes in the chemistry of the steel.

Stacking Laminations and Polarity

The edges of the magnetic material that have been stamped, sheared, or slit, will have a burr, as shown in Figure 3-9. The quality of the equipment will keep the burr to a minimum. This burr now gives the lamination a polarity. When a transformer is being stacked, the lamination build is normally sized by dimensions, or it just fills the bobbin.

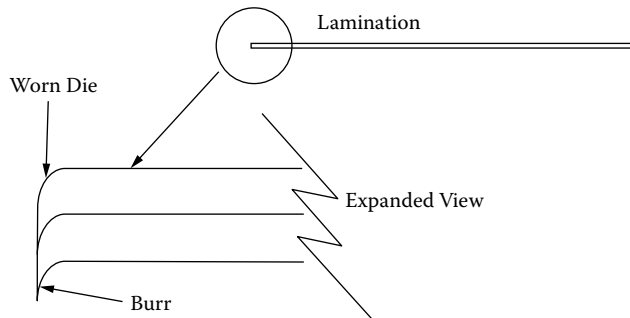


Figure 3-9. Expanded View, Showing Lamination Burr.

If the laminations are stacked correctly, all of the burred ends will be aligned. If the laminations are stacked randomly, such as the burr ends facing each other, then, the stacking factor would be affected. The stacking factor has a direct impact on the cross-section of the core. The end result would be less iron. This could lead to premature saturation, as an increase in the magnetizing current, or a loss of inductance.

There are several methods used in stacking transformer laminations. The most common technique used in stacking laminations is the alternate method. The alternate method is where one set of laminations, such as an E and an I, are assembled. Then, the laminations are reversed, as shown in [Figure 3-10](#). This technique, used in stacking, provides the lowest air gap and the highest permeability. Another method for stacking laminations is to interleave two-by-two, also shown in Figure 3-10. The second method of stacking would be in groups of two

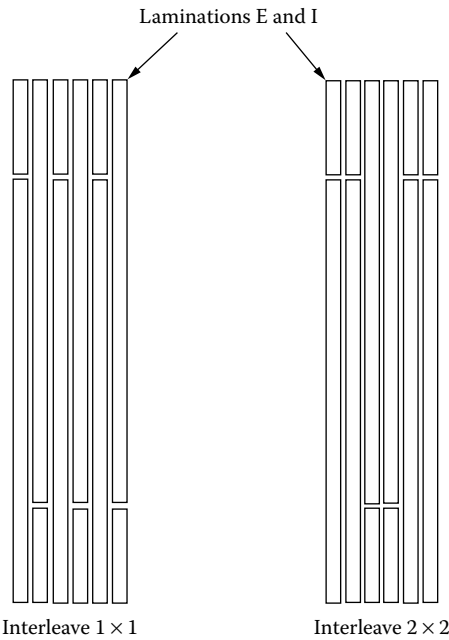


Figure 3-10. Methods for Stacking Laminations.

or more. This is done to cut the assembly time. The loss in performance in stacking, other than one-by-one, is the increase in magnetizing current and a loss of permeability.

Flux Crowding

When laminations are stacked, as shown in Figure 3-11, there is flux crowding. This flux crowding is caused by the difference in spacing between the E, I, and the adjacent lamination. The adjacent lamination has a minimum air gap, which translates into a higher permeability.

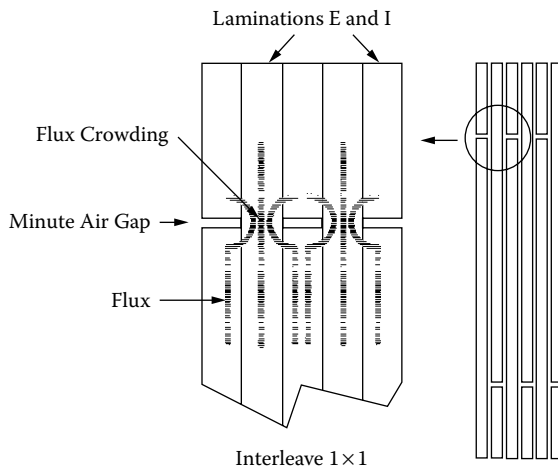


Figure 3-11. Flux Crowding, when Laminations are Interleaved.

Exciting Current

The flux will skirt the low permeability air gap and migrate into the adjacent lamination, causing flux crowding in that lamination. Eventually, this crowding will cause saturation in that portion of the lamination, and the excitation current will rise. After that portion of the lamination has saturated, the flux will migrate back to the lower permeability segment of the lamination from where it left. This effect can be easily viewed by observing the B-H loops at low and high flux densities, and comparing them with a toroidal core of the same material, with a minimum air gap, as shown in Figure 3-12. The B-H loop, along with the magnetizing current, I_m , of a toroidal core, is shown in Figure 3-12A. The toroidal core, with its inherent minimum air gap, will have almost a square of current. Using the same material in lamination form will exhibit a B-H loop, and a magnetizing current, I_m , similar to Figure 3-12B operating at low flux densities. Increasing the excitation will cause premature saturation of the lamination, as seen by the non-linear, exciting current, as shown in Figure 3-12C.

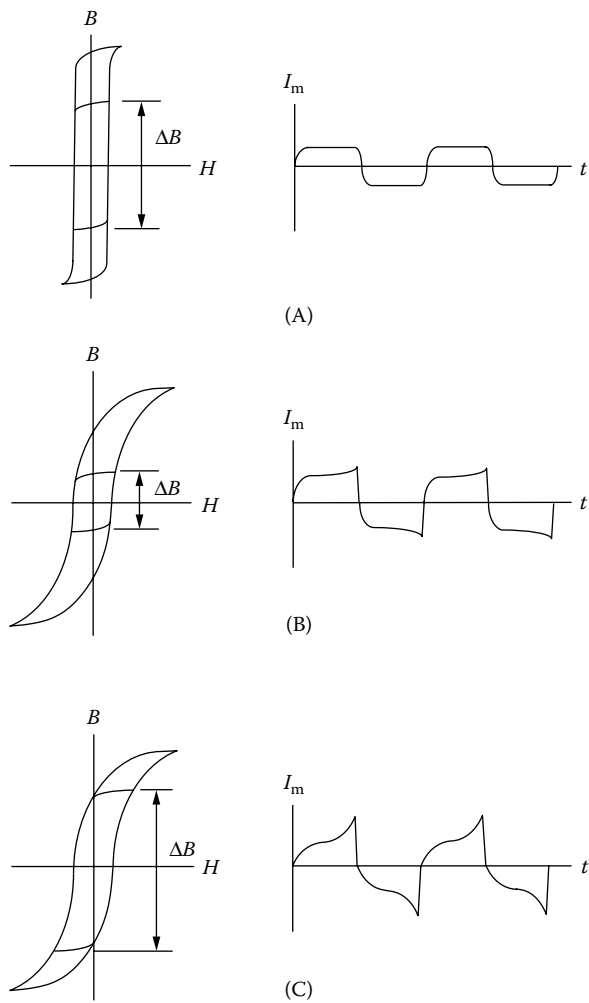


Figure 3-12. Comparing the Exciting Currents and Three B-H Loops.

Most finished transformers or inductors will have some sort of bracket, such as an L bracket, end bells, a channel bracket or maybe a bolt through the mounting holes to the chassis. When transformers are being assembled, there is a certain amount of attention that has to be used to get proper performance. The insulation material used to coat the lamination is normally very durable, but it can be scratched off and degrade the performance. When brackets are used in the transformer assembly, as shown in Figure 3-13, care must be taken on how the bolts and brackets are put together. The transformer assembly bolts, shown in Figure 3-13, should be the recommended size for the mounting hole and use all of the required hardware. This hardware should include the correct bolt size and length, and correct surface washer, lock washer and nut. Also, included in this hardware, should be fiber shoulder washers and proper sleeving to cover the bolt threads. If insulating hardware is not used, there is a good chance of a partial, shorted turn. The continuity for this partial turn can be created through the bolts and bracket, or the bolts, bracket, and the chassis. This partial shorted turn will downgrade the performance of the transformer.

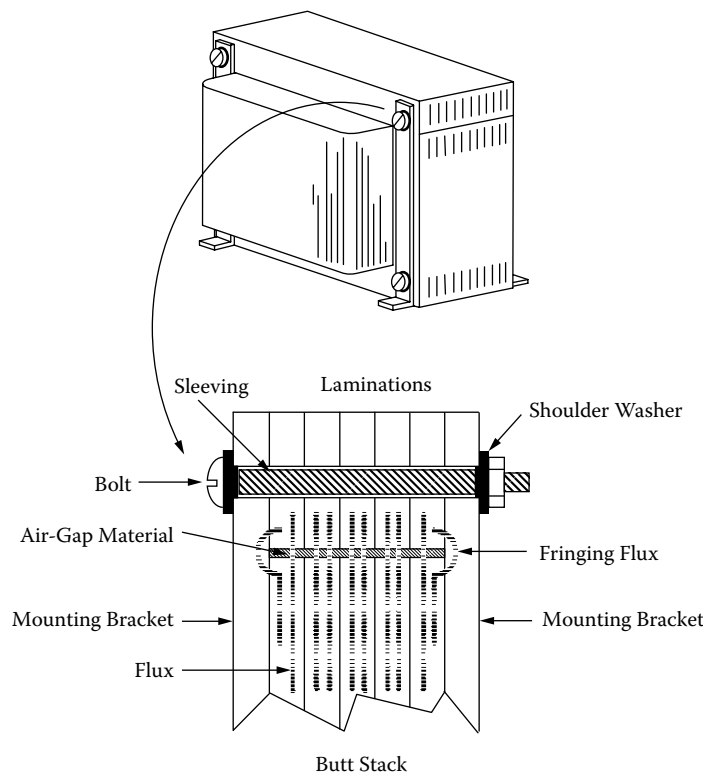


Figure 3-13. Lamination Mounting Hardware.

Tape Wound C, EE, and Toroidal Cores

Tape wound cores are constructed by winding around a mandrel, a magnetic material in the form of a preslit tape, as shown in [Figure 3-14](#). This tape material comes in all of the iron alloys, plus the amorphous materials. The tape thickness varies from 0.0005 inch (0.0127 mm) to 0.012 inch (0.305 mm). The advantage of this type

of construction is that the flux is parallel with the direction of rolling of the magnetic material. This provides the maximum utilization of flux with the minimum of magnetizing force. There are two disadvantages in this type of construction. When the core is cut in half, as shown in Figure 3-15, the mating surface has to be ground, lapped, and then, acid-etched. This is done to provide a smooth mating surface with the minimum of air gap and the maximum of permeability. The other disadvantage is when the cores are reassembled, the method used is normally done with a band and buckle, and this procedure requires a little skill to provide the right alignment and correct tension, as shown in Figure 3-16. The C cores are impregnated for strength, prior to being cut. The cut C core can be used in many configurations in the design of a magnetic component, as

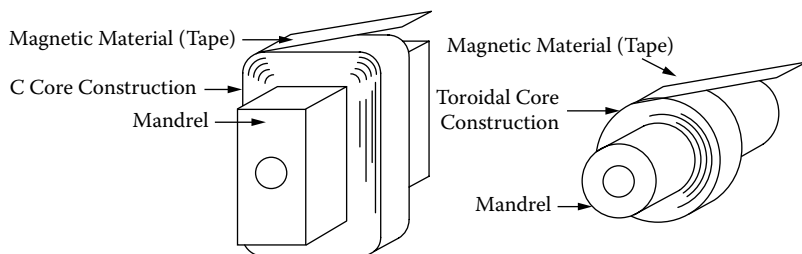


Figure 3-14. Tape Cores Being Wound on a Mandrel.

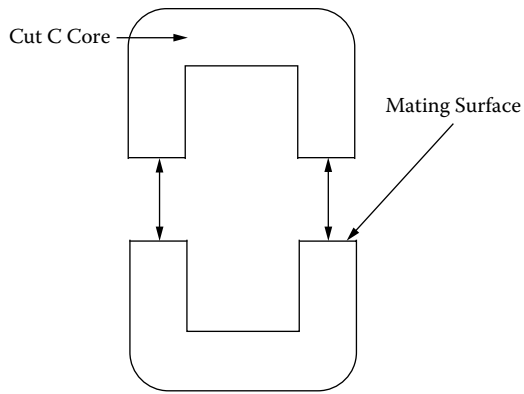


Figure 3-15. Two Halves of a Cut C Core.

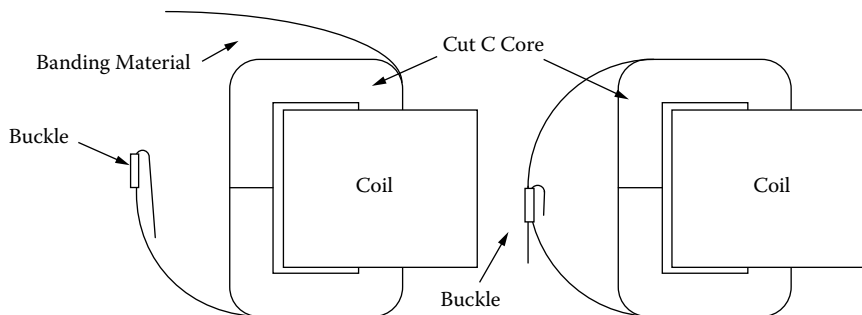


Figure 3-16. Banding the Cut C Core.

shown in Figure 3-17. The EE cores are constructed in the same way as C cores, but they have an additional overwind, as shown in Figure 3-18. The assembled three-phase transformer is shown in Figure 3-19.

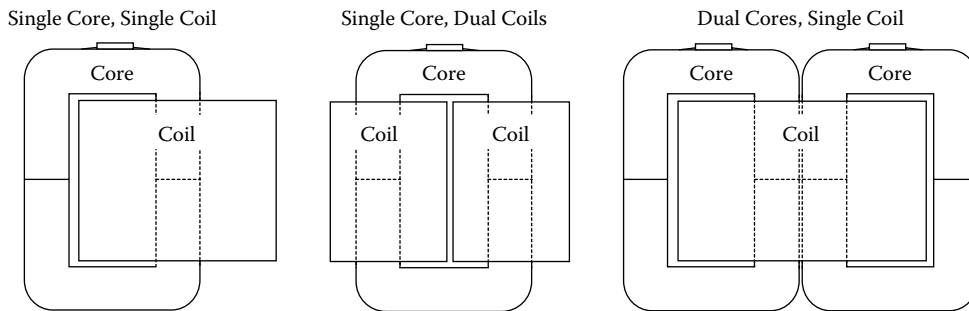


Figure 3-17. Three Different C Core Configurations.

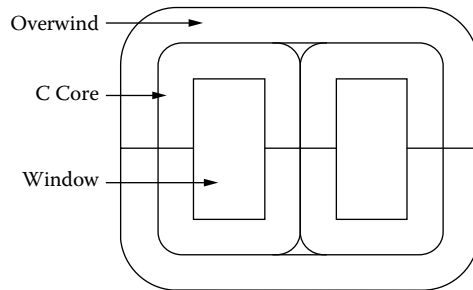


Figure 3-18. Three-Phase, Cut EE Core.

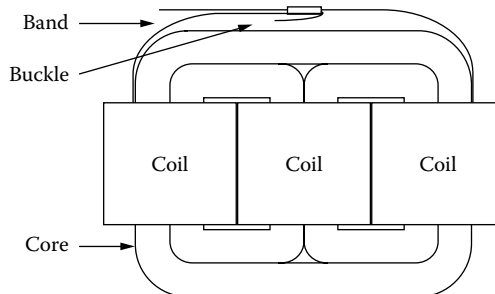


Figure 3-19. Typical, Assembled EE Cut Core.

Tape Toroidal Cores

Tape toroidal cores are constructed in the same way as tape C cores, by winding the magnetic material around a mandrel, in the form of a preslit tape. This tape material comes in all of the iron alloys, plus the amorphous materials. The tape thickness varies from 0.000125 inch (0.00318 mm) to 0.012 inch (0.305 mm). The tape toroid is normally offered in two configurations, cased and encapsulated, as shown in [Figure 3-20](#). The cased toroid offers superior electrical properties and stress protection against winding. The encapsulated cores are used when not all of the fine magnetic properties are important to the design, as in power transformers.

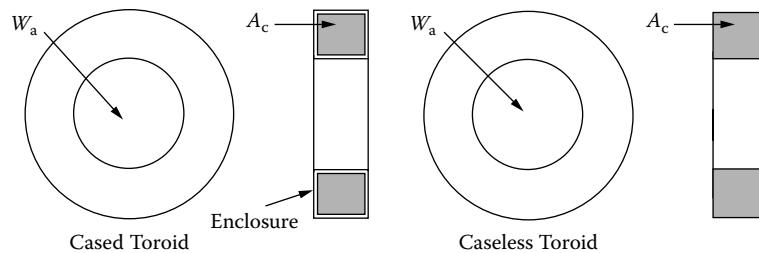


Figure 3-20. Outline of a Cased and a Caseless Toroidal Core.

Toroidal, Powder Core

Powder cores, as shown in Figure 3-21, are very unique. They give the engineer another tool to speed the initial design. Powder cores have a built-in air gap. They come in a variety of materials and are very stable with time and temperature. The cores are manufactured with good engineering aids. Manufacturers provide catalogs for their cores, listing not only the size, but also permeability and Millihenrys per 1000 turns. The data is presented to the engineer in such a way that it takes the minimum amount of time to have a design such that will function.

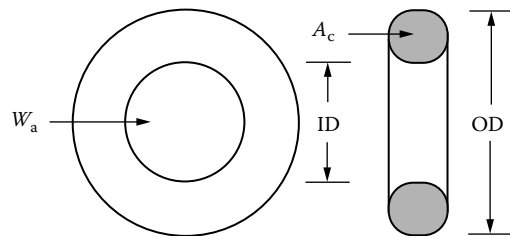


Figure 3-21. Outline of a Powder Toroidal Core.

Stacking Factors

The standard stacking factors for tape cores, wound cut cores and laminations are shown in Table 3-1.

Table 3-1. Standard Stacking Factors

Thickness mils	Standard Stacking Factors			(S.F.) ²	
	Tape Cores	Wound Cut Cores	Laminations		
			Butt Stack		
0.125	0.250			0.062	
0.250	0.375			0.141	
0.500	0.500			0.250	
1.000	0.750	0.830		0.562	
2.000	0.850	0.890		0.722	
4.000	0.900	0.900	0.900	0.810	
6.000		0.900	0.900	0.810	
12.000	0.940	0.950		0.884	
14.000	0.940	0.950	0.950	0.902	
18.000			0.950	0.900	
25.000			0.950	0.920	
				0.846	

Introduction to the Magnetic Core

The magnetic core data for this chapter has been taken from the catalogs of the leading manufacturers in the magnetics industry. The author has compiled dimensional data for over 200 magnetic cores. This compiled data has been placed into 32 tables. The 200 magnetic cores include:

1. Lamination, EI, UI, LL, DU and 3 phase EE cores.
2. Tape cores, C cores, Toroidal cores and 3 phase EE cores.
3. Ferrite cores, EE, UU, EC, ETD, Pot cores, PQ cores, RM cores, EFD cores, EPC cores.
4. Ferrite low profile core, EE, PQ cores, RM cores.
5. Molypermalloy powder cores, MPP cores.
6. High Flux powder cores, HF cores.
7. Sendust powder cores, Toroidal and EE cores.
8. Iron Powder cores, Toroidal and EE cores.

Following each dimensional table there is another table with design variables for each magnetic core. The list of variables are listed below:

1. The Weight of the copper, W_{tcu} .
2. The Weight of the core, W_{tf} , is supplied by the manufacturer.
3. The Mean Length Turn, MLT, See Chapter 4.
4. The Magnetic Path Length, MPL, is supplied by the manufacturer.
5. The ratio of the Window Area, W_a , over the Iron Area, A_c . Magnetic cores that have small ratio are considered low frequency line transformers. For high frequency transformers the ratio should be three and above.
6. The Iron area, A_c , this is supplied by the manufacturer.
7. The Window area, W_a , is calculated from the dimensional table.
8. The Area Product, A_p , is a power handling equation. See Chapter 21.

$$A_p = W_a A_c, \quad [\text{cm}^4] \quad [3-1]$$

9. The Core Geometry, K_g , is a power handling equation. See Chapter 21.

$$K_g = \frac{W_a A_c^2 K_u}{MLT}, \quad [\text{cm}^5] \quad [3-2]$$

The window utilization, K_u , has been calculated with 0.4 for all cores. When designing with ferrites or at high frequency, the window utilization, K_u , changes. See Chapter 4.

10. The Surface area, A_s , is calculated from the dimensional table. See Chapter 5.
11. The Millihenrys per 1000 turns, A_L , have been normalized for a permeability of 1000. For a close approximation, multiply this, A_L , value by the new permeability in kilo-perm. The permeability would change when using a 2500 perm by multiplying by 2.5.

Design and Dimensional Data for EI Laminations

Laminations are still one of the most widely-used cores in power conversion. The dimensional outline for EI laminations and an assembled transformer is shown in Figure 3-22. Dimensional data for EI laminations is given in Table 3-2; design data is given in Table 3-3.

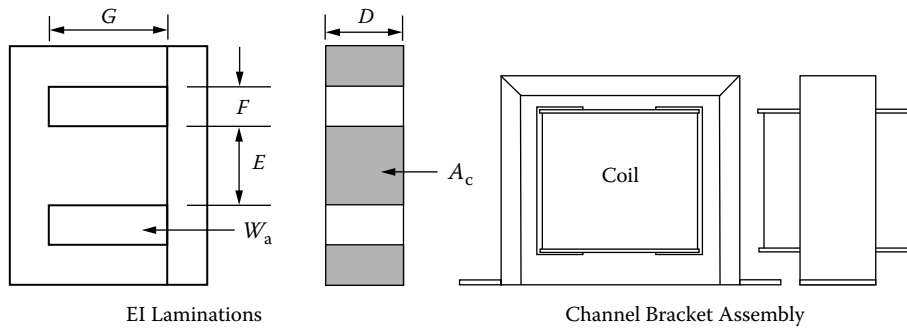


Figure 3-22. EI Lamination Outline.

Table 3-2. Dimensional Data for EI Laminations

EI, Laminations, (Tempel) 14 mil									
Part No.	D cm	E cm	F cm	G cm	Part No.	D cm	E cm	F cm	G cm
EI-375	0.953	0.953	0.794	1.905	EI-112	2.857	2.857	1.429	4.286
EI-021	1.270	1.270	0.794	2.064	EI-125	3.175	3.175	1.588	4.763
EI-625	1.588	1.588	0.794	2.381	EI-138	3.493	3.493	1.746	5.239
EI-750	1.905	1.905	0.953	2.857	EI-150	3.810	3.810	1.905	5.715
EI-875	2.223	2.223	1.111	3.333	EI-175	4.445	4.445	2.223	6.668
EI-100	2.540	2.540	1.270	3.810	EI-225	5.715	5.715	2.858	8.573

Table 3-3. Design Data for 14 mil EI Laminations

EI, Laminations, (Tempel) 14 mil										
Part No.	W _{tcu} grams	W _{tfe} grams	MLT cm	MPL cm	W _a	A _c cm ²	W _a cm ²	A _p cm ⁴	K _g cm ⁵	A _t cm ²
					A _c					
EI-375	36.1	47.2	6.7	7.3	1.754	0.862	1.512	1.303	0.067	46.2
EI-021	47.6	94.3	8.2	8.3	1.075	1.523	1.638	2.510	0.188	62.1
EI-625	63.5	170.0	9.5	9.5	0.418	2.394	1.890	4.525	0.459	83.2
EI-750	108.8	296.0	11.2	11.4	0.790	3.448	2.723	9.384	1.153	120.0
EI-875	171.0	457.0	13.0	13.3	0.789	4.693	3.705	17.384	2.513	163.0
EI-100	254.0	676.0	14.8	15.2	0.790	6.129	4.839	29.656	4.927	212.9
EI-112	360.0	976.0	16.5	17.2	0.789	7.757	6.124	47.504	8.920	269.4
EI-125	492.0	1343.0	18.3	19.1	0.789	9.577	7.560	72.404	15.162	333.0
EI-138	653.0	1786.0	20.1	21.0	0.789	11.588	9.148	106.006	24.492	403.0
EI-150	853.0	2334.0	22.0	22.9	0.789	13.790	10.887	150.136	37.579	479.0
EI-175	1348.0	3711.0	25.6	26.7	0.789	18.770	14.818	278.145	81.656	652.0
EI-225	2844.0	7976.0	32.7	34.3	0.789	31.028	24.496	760.064	288.936	1078.0

Design and Dimensional Data for UI Laminations

The dimensional outline for UI laminations and an assembled transformer is shown in Figure 3-23. Dimensional data for UI laminations is given in Table 3-4; design data is given in Table 3-5.

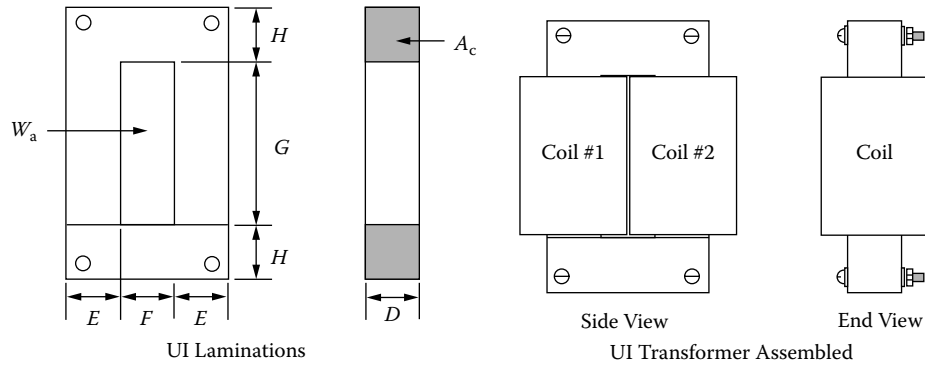


Figure 3-23. UI Lamination Outline.

Table 3-4. Dimensional Data for UI Laminations

UI, Standard Laminations 14 mil											
Part No.	D cm	E cm	F cm	G cm	H cm	Part No.	D cm	E cm	F cm	G cm	H cm
50UI	1.270	1.270	1.270	3.810	1.270	125UI	3.175	3.175	3.175	9.525	3.175
60UI	1.429	1.429	2.223	5.398	1.429	150UI	3.810	3.810	3.810	11.430	3.810
75UI	1.905	1.905	1.905	5.715	1.905	180UI	4.572	4.572	4.572	11.430	4.572
100UI	2.540	2.540	2.540	7.620	2.540	240UI	6.096	6.096	6.096	15.240	6.096

Table 3-5. Design Data for 14 mil UI Laminations

UI, Standard Laminations 14 mil										
Part No.	W _{tcu} grams	W _{tfe} grams	MLT cm	MPL cm	W _a	A _c	W _a	A _p	K _g	A _t
					A _c	cm ²	cm ²	cm ⁴	cm ⁵	cm ²
50UI	132	173	7.68	15.24	3.159	1.532	4.839	7.414	0.592	110
60UI	418	300	9.81	18.10	6.187	1.939	11.996	23.263	1.839	209
75UI	434	585	11.22	22.86	3.157	3.448	10.887	37.534	4.614	247
100UI	1016	1384	14.76	30.48	3.158	6.129	19.355	118.626	19.709	439
125UI	1967	2725	18.29	38.10	3.158	9.577	30.242	289.614	60.647	685
150UI	3413	4702	22.04	45.72	3.158	13.790	43.548	600.544	150.318	987
180UI	4884	7491	26.28	50.29	2.632	19.858	52.258	1037.740	313.636	1296
240UI	11487	17692	34.77	67.06	2.632	35.303	92.903	3279.770	1331.997	2304

Design and Dimensional Data for LL Laminations

The dimensional outline for LL laminations and an assembled transformer is shown in Figure 3-24. Dimensional data for LL laminations is given in Table 3-6; design data is given in Table 3-7.

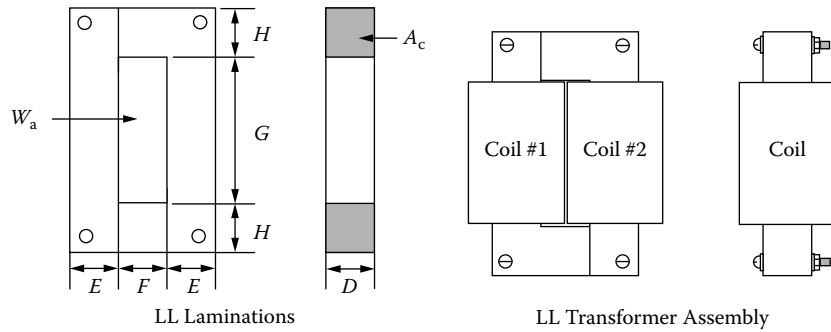


Figure 3-24. LL Lamination Outline.

Table 3-6. Dimensional Data for 14 mil LL Laminations

LL, Standard Laminations 14 mil											
Part No.	D cm	E cm	F cm	G cm	H cm	Part No.	D cm	E cm	F cm	G cm	H cm
141L	0.635	0.635	1.270	2.858	0.635	104L	1.270	1.270	1.984	5.555	1.270
108L	1.031	1.031	0.874	3.334	1.111	105L	1.270	1.270	1.905	6.826	1.270
250L	1.031	1.031	0.874	5.239	1.111	102L	1.429	1.429	1.588	5.398	1.429
101L	1.111	1.111	1.588	2.858	1.111	106L	1.429	1.429	2.223	5.398	1.429
7L	1.270	1.270	1.270	3.810	1.270	107L	1.588	1.588	2.064	6.350	1.588
4L	1.270	1.270	1.905	3.810	1.270						

Table 3-7. Design Data for 14 mil LL Laminations

LL, Standard Laminations 14 mil											
Part No.	W _{tcu} grams	W _{tfe} grams	MLT cm	MPL cm	W _a A _c cm ²			W _a cm ²	A _p cm ⁴	K _g cm ⁵	A _t cm ²
						A _c cm ²	cm ²				
141L	63.8	31.3	4.9	10.8	9.473	0.383	3.629	1.390	0.043	55.2	
108L	61.2	97.9	5.9	12.7	2.884	1.010	2.913	2.943	0.201	70.3	
250L	96.1	127.1	5.9	16.5	4.532	1.010	4.577	4.624	0.316	92.0	
101L	118.5	115.9	7.3	13.3	3.867	1.173	4.536	5.322	0.340	97.3	
7L	132.2	173.9	7.7	15.2	3.159	1.532	4.839	7.414	0.592	109.7	
4L	224.0	185.2	8.7	16.5	4.737	1.532	7.258	11.121	0.785	141.9	
104L	344.9	228.0	8.8	20.2	7.193	1.532	11.020	16.885	1.176	180.2	
105L	401.3	256.5	8.7	22.5	8.488	1.532	13.004	19.925	1.407	199.4	
102L	268.6	284.1	8.8	19.7	4.419	1.939	8.569	16.617	1.462	167.6	
106L	418.6	302.1	9.8	21.0	6.187	1.939	11.996	23.263	1.839	208.8	
107L	475.2	409.5	10.2	23.2	5.474	2.394	13.105	31.375	2.946	235.8	

Design and Dimensional Data for DU Laminations

The dimensional outline for DU laminations and an assembled transformer is shown in Figure 3-25. Dimensional data for DU laminations is given in Table 3-8; design data is given in Table 3-9.

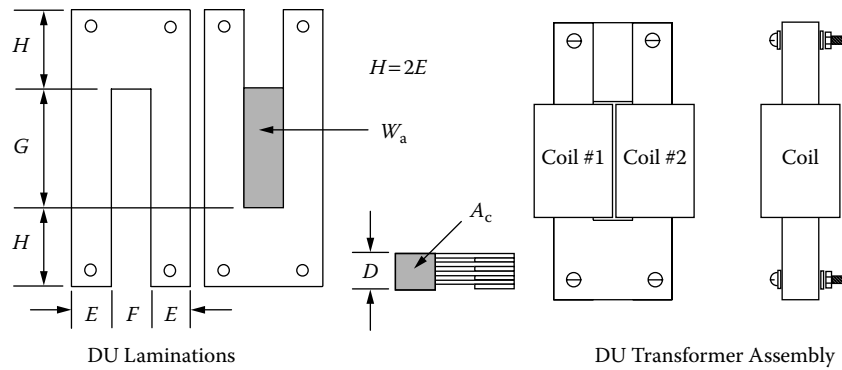


Figure 3-25. DU Lamination Outline.

Table 3-8. Dimensional Data for 14 mil DU Laminations

DU, Standard Laminations 14 mil											
Part No.	D cm	E cm	F cm	G cm	H cm	Part No.	D cm	E cm	F cm	G cm	H cm
DU-63	0.159	0.159	0.318	0.794	0.318	DU-39	0.953	0.953	0.953	2.858	1.905
DU-124	0.318	0.318	0.476	1.191	0.635	DU-37	0.953	0.953	1.905	3.810	1.905
DU-18	0.476	0.476	0.635	1.588	0.953	DU-50	1.270	1.270	2.540	5.080	2.540
DU-26	0.635	0.635	0.635	1.905	1.270	DU-75	1.905	1.905	3.810	7.620	3.810
DU-25	0.635	0.635	0.953	2.064	1.270	DU-1125	2.858	2.858	5.715	11.430	5.715
DU-1	0.635	0.635	0.953	3.810	1.270	DU-125	3.175	3.175	5.080	10.160	6.350

Table 3-9. Design Data for 14 mil DU Laminations

DU, Standard Laminations 14 mil										
Part No.	W _{tcu} grams	W _{tfe} grams	MLT cm	MPL cm	W _a	A _c	W _a	A _p	K _g	A _t
					A _c	cm ²	cm ²	cm ⁴	cm ⁵	cm ²
DU-63	1.4	0.6	1.5	3.2	10.500	0.024	0.252	0.006	0.00003	4.2
DU-124	4.9	4.3	2.4	5.2	5.906	0.096	0.567	0.054	0.0009	11.8
DU-18	11.9	13.5	3.3	7.3	4.688	0.215	1.008	0.217	0.0057	23.4
DU-26	17.0	28.9	3.9	8.9	3.159	0.383	1.210	0.463	0.0180	33.9
DU-25	31.1	30.4	4.4	9.9	5.133	0.383	1.966	0.753	0.0260	44.3
DU-1	57.3	42.4	4.4	13.3	9.634	0.383	3.630	1.390	0.0479	60.9
DU-39	55.3	104.5	5.7	13.3	3.158	0.862	2.722	2.346	0.1416	76.2
DU-37	186.0	124.5	7.2	17.2	8.420	0.862	7.258	6.256	0.2992	134.3
DU-50	443.9	287.8	9.7	22.8	8.422	1.532	12.903	19.771	1.2524	238.0
DU-75	1467.0	985.2	14.2	34.3	8.420	3.448	29.032	100.091	9.7136	537.1
DU-1125	4880.0	3246.0	21.0	51.4	8.421	7.757	65.322	506.709	74.8302	1208.0
DU-125	3906.0	3966.0	21.3	41.4	5.389	9.577	51.610	494.275	88.9599	1147.0

Design and Dimensional Data for Three-Phase Laminations

The dimensional outline for 3Phase EI laminations and an assembled transformer is shown in Figure 3-26. Dimensional data for 3Phase EI laminations is given in Table 3-10; design data is given in Table 3-11.

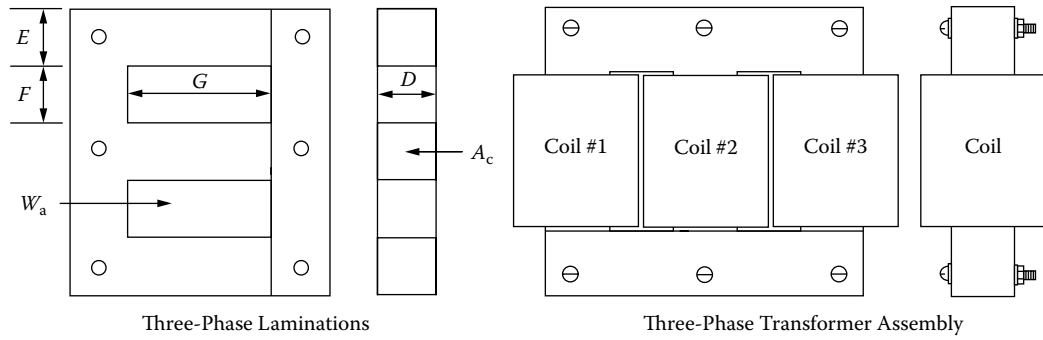


Figure 3-26. EI Three Phase Laminations Outline.

Table 3-10. Dimensional Data for 14 mil EI Three-Phase Laminations

3Phase, Standard Laminations, Thomas & Skinner 14 mil									
Part No.	D cm	E cm	F cm	G cm	Part No.	D cm	E cm	F cm	G cm
0.250EI	0.635	0.635	0.871	2.858	1.000EI	2.540	2.540	3.810	7.620
0.375EI	0.953	0.953	1.270	3.175	1.200EI	3.048	3.048	3.048	7.620
0.500EI	1.270	1.270	1.588	3.493	1.500EI	3.810	3.810	3.810	9.525
0.562EI	1.427	1.427	1.588	5.398	1.800EI	4.572	4.572	4.572	11.430
0.625EI	1.588	1.588	1.984	5.634	2.400EI	6.096	6.096	6.096	15.240
0.875EI	2.223	2.223	2.779	6.111	3.600EI	9.144	9.144	9.144	22.860

Table 3-11. Design Data for 14 mil EI Three Phase Laminations

3Phase, Standard Laminations, Thomas & Skinner 14 mil									
Part No.	W _{teu} grams	W _{te} grams	MLT cm	W _a 2A _c	A _c cm ²	W _a cm ²	A _p cm ⁴	K _g cm ⁵	A _t cm ²
0.250EI	57	54	4.3	3.251	0.383	2.49	1.43	0.051	53
0.375EI	134	154	6.2	2.339	0.862	4.03	5.21	0.289	102
0.500EI	242	324	8.2	1.810	1.532	5.54	12.74	0.955	159
0.562EI	403	421	8.8	2.213	1.936	8.57	24.88	2.187	207
0.625EI	600	706	10.1	2.334	2.394	11.18	40.13	3.816	275
0.875EI	1255	1743	13.9	1.809	4.693	16.98	119.53	16.187	487
1.000EI	2594	2751	16.7	2.368	6.129	29.03	266.91	39.067	730
1.200EI	2178	3546	17.6	1.316	8.826	23.23	307.48	61.727	725
1.500EI	4266	6957	22.0	1.316	13.790	36.29	750.68	187.898	1132
1.800EI	7326	12017	26.3	1.316	19.858	52.26	1556.61	470.453	1630
2.400EI	17230	28634	34.8	1.316	35.303	92.90	4919.66	1997.995	2899
3.600EI	58144	96805	52.2	1.316	79.432	209.03	24905.75	15174.600	6522

Design and Dimensional Data for Tape Wound C Cores

The dimensional outline for C cores is shown in Figure 3-27. Dimensional data for C cores is given in Table 3-12; design data is given in Table 3-13.

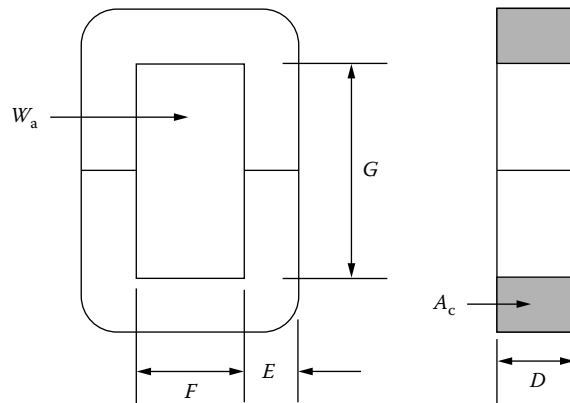


Figure 3-27. Tape C Core Dimensional Outline.

Table 3-12. Dimensional Data for Tape C Cores

C Cores, Magnetic Metals, 2 mil									
Part No.	D cm	E cm	F cm	G cm	Part No.	D cm	E cm	F cm	G cm
ML-002	0.635	0.476	0.635	1.588	ML-014	1.270	1.270	1.270	3.969
ML-004	0.635	0.635	0.635	2.223	ML-016	1.905	1.270	1.270	3.969
ML-006	1.270	0.635	0.635	2.223	ML-018	1.270	1.111	1.588	3.969
ML-008	0.953	0.953	0.953	3.016	ML-020	2.540	1.588	1.588	3.969
ML-010	1.588	0.953	0.953	3.016	ML-022	2.540	1.588	1.588	4.921
ML-012	1.270	1.111	1.270	2.858	ML-024	2.450	1.588	1.905	5.874

Table 3-13. Design Data for Tape C Cores

C Cores, Magnetic Metals, 2 mil										
Part No.	W _{tcu} grams	W _{tfe} grams	MLT cm	MPL cm	W _a	A _c	W _a	A _p	K _g	A _t
					A _c	cm ²	cm ²	cm ⁴	cm ⁵	cm ²
ML-002	13.0	13.0	3.6	6.4	3.747	0.269	1.008	0.271	0.0080	21.0
ML-004	19.8	22.6	3.9	8.3	3.933	0.359	1.412	0.507	0.0184	29.8
ML-006	27.2	45.2	5.4	8.3	1.967	0.718	1.412	1.013	0.0537	37.5
ML-008	58.4	72.5	5.7	11.8	3.556	0.808	2.874	2.323	0.1314	63.6
ML-010	73.5	120.8	7.2	11.8	2.134	1.347	2.874	3.871	0.2902	74.7
ML-012	95.1	121.7	7.4	12.7	2.891	1.256	3.630	4.558	0.3109	87.1
ML-014	137.7	170.4	7.7	15.6	3.513	1.435	5.041	7.236	0.5408	112.1
ML-016	160.5	255.6	9.0	15.6	2.341	2.153	5.041	10.854	1.0443	126.8
ML-018	176.2	149.1	7.9	15.6	5.019	1.256	6.303	7.915	0.5056	118.9
ML-020	254.5	478.4	11.4	17.5	1.756	3.590	6.303	22.626	2.8607	182.0
ML-022	315.6	530.5	11.4	19.4	2.177	3.590	7.815	28.053	3.5469	202.0
ML-024	471.7	600.1	11.9	21.9	3.117	3.590	11.190	40.170	4.8656	244.8

Dimensional Outline for Tape Wound EE Cores

The dimensional outline for EE cores is shown in Figure 3-28. Dimensional data for EE cores is given in Table 3-14; design data is given in Table 3-15.

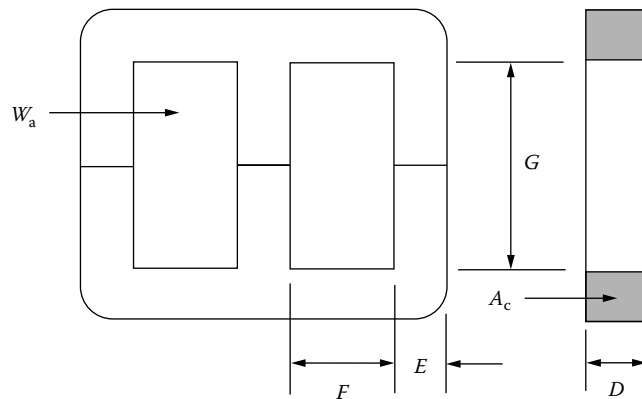


Figure 3-28. Tape EE Core Dimensional Outline.

Table 3-14. Dimensional Data for Tape EE Cores

3Phase E Cores, Magnetic Metals, 12 mil									
Part No.	D cm	E cm	F cm	G cm	Part No.	D cm	E cm	F cm	G cm
MTA-25	1.905	1.905	1.905	2.858	MTA-12	3.810	2.540	2.381	6.350
MTA-22	3.175	1.429	1.905	5.239	MTA-20	5.715	2.540	2.540	6.350
MTA-17	3.175	1.746	1.905	6.350	MTA-03	4.445	2.540	3.493	9.843
MTA-14	3.175	2.223	2.381	4.763	MTA-15	5.080	3.493	2.540	7.620

Table 3-15. Design Data for Tape EE Cores

3Phase E Cores, Magnetic Metals, 12 mil									
Part No.	W _{teu} grams	W _{tfe} grams	MLT cm	W _a	A _c cm ²	W _a cm ²	A _p cm ⁴	K _g cm ⁵	A _t cm ²
				2A _c					
MTA-25	326	686	11.2	0.789	3.448	5.44	28.16	3.461	261
MTA-22	682	1073	12.8	1.158	4.310	9.98	64.53	8.686	324
MTA-17	867	1422	13.4	1.148	5.266	12.10	95.56	14.977	400
MTA-14	916	1803	15.1	0.846	6.705	11.34	114.06	20.203	468
MTA-12	1391	2899	17.3	0.822	9.194	15.12	208.50	44.438	613
MTA-20	1834	4420	21.3	0.585	13.790	16.13	333.64	86.347	737
MTA-03	3717	4597	20.3	1.602	10.730	34.38	553.15	117.079	993
MTA-15	2266	6544	22.0	0.574	16.860	19.35	489.40	150.340	956

Design and Dimensional Data for Tape Wound Toroidal Cores

The dimensional outline for tape wound Toroidal cores is shown in Figure 3-29. Dimensional data for cased tape wound Toroidal cores is given in Table 3-16; design data is given in Table 3-17.

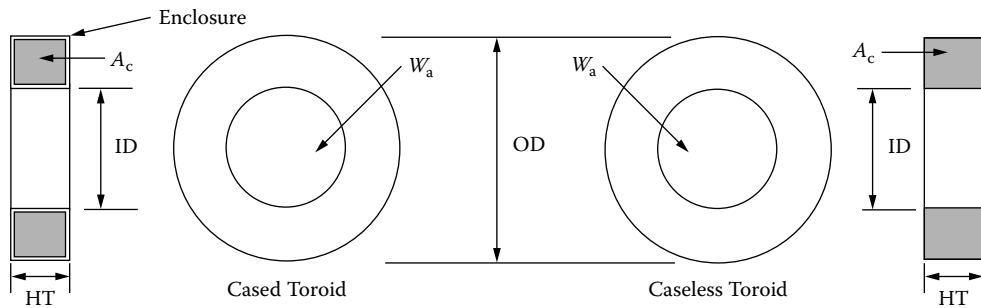


Figure 3-29. Tape Toroidal Core Dimensional Outline.

Table 3-16. Dimensional Data for Tape Toroidal Cores

Toroidal Tape Cores, Magnetics 2 mil Iron Alloy (cased and coated)											
Part No.	OD cm	ID cm	HT cm	Part No.	OD cm	ID cm	HT cm	Part No.	OD cm	ID cm	HT cm
52402	1.346	0.724	0.610	52057	2.134	1.359	0.610	52061	2.781	1.664	0.927
52107	1.651	1.041	0.610	52000	2.134	1.041	0.610	52004	3.429	2.286	0.927
52153	1.499	0.724	0.610	52155	1.659	0.884	0.927	52076	2.794	1.334	0.762
52056	1.816	1.041	0.610	52176	2.134	1.041	0.927	52007	2.794	1.334	0.927

Table 3-17. Design Data for Tape Toroidal Cores

Toroidal Tape Cores, Magnetics 2 mil Iron Alloy (cased)										
Part No.	W _{tcu} grams	W _{tfe} grams	MLT cm	MPL cm	W _a A _c	A _c cm ²	W _a cm ²	A _p cm ⁴	K _g cm ⁵	A _t cm ²
52402	2.84	0.50	2.16	3.25	18.727	0.022	0.412	0.00906	0.0000369	9.80
52107	6.76	0.70	2.30	4.24	38.682	0.022	0.851	0.01872	0.0000716	15.50
52153	3.20	1.10	2.20	3.49	9.581	0.043	0.412	0.01772	0.0001385	11.20
52056	7.40	1.50	2.40	4.49	19.791	0.043	0.851	0.03659	0.0002622	16.80
52057	13.80	1.80	2.70	5.48	33.744	0.043	1.451	0.06239	0.0003975	23.70
52000	8.10	3.30	2.70	4.99	9.895	0.086	0.851	0.07319	0.0009324	20.60
52155	6.10	2.60	2.80	3.99	7.140	0.086	0.614	0.05280	0.0006487	16.00
52176	9.70	6.50	3.20	4.99	4.977	0.171	0.851	0.14552	0.0031105	23.30
52061	28.70	9.10	3.70	6.98	12.719	0.171	2.175	0.37193	0.0068756	40.30
52004	61.70	11.70	4.20	8.97	24.000	0.171	4.104	0.70178	0.0114291	62.20
52076	17.20	9.50	3.50	6.48	7.244	0.193	1.398	0.26981	0.0059513	34.60
52007	18.50	12.70	3.70	6.48	5.440	0.257	1.398	0.35929	0.0099823	36.40

Design and Dimensional Data for EE Ferrite Cores

The dimensional outline for EE ferrite cores is shown in Figure 3-30. Dimensional data for EE ferrite cores is given in Table 3-18; design data is given in Table 3-19.

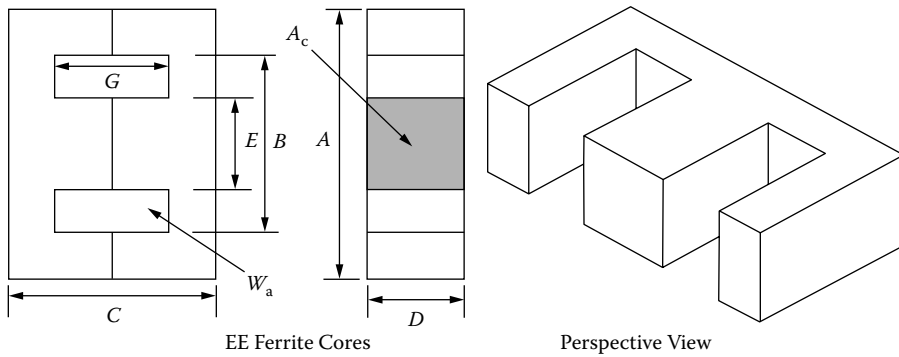


Figure 3-30. Dimension Outline for EE Ferrite Cores.

Table 3-18. Dimensional Data for EE Ferrite Cores

EE, Ferrite Cores (Magnetics)													
Part No.	A cm	B cm	C cm	D cm	E cm	G cm	Part No.	A cm	B cm	C cm	D cm	E cm	G cm
EE-187	1.910	1.433	1.620	0.475	0.475	1.140	EE-21	4.060	2.860	3.320	1.245	1.245	2.080
EE-2425	2.540	1.880	1.930	0.635	0.635	1.280	EE-625	4.690	3.920	3.920	1.560	1.560	2.420
EE-375	3.420	2.550	2.820	0.930	0.930	1.960	EE-75	5.610	3.810	4.720	1.880	1.880	2.920

Table 3-19. Design Data for EE Ferrite Cores

EE, Ferrite Cores (Magnetics)											
Part No.	W _{tcu} grams	W _{tfe} grams	MLT cm	MPL cm	W _a A _c	A _c cm ²	W _a cm ²	A _p cm ⁴	K _g cm ⁵	A _t cm ²	*AL mh/1K
EE-187	6.8	4.4	3.8	4.01	2.239	0.226	0.506	0.114	0.0027	14.4	501
EE-2425	13.9	9.5	4.9	4.85	2.010	0.395	0.794	0.314	0.0101	23.5	768
EE-375	36.4	33.0	6.6	6.94	1.769	0.870	1.539	1.339	0.0706	45.3	1160
EE-21	47.3	57.0	8.1	7.75	1.103	1.490	1.643	2.448	0.1801	60.9	1696
EE-625	64.4	103.0	9.4	8.90	0.825	2.340	1.930	4.516	0.4497	81.8	2330
EE-75	111.1	179.0	11.2	10.70	0.831	3.370	2.799	9.433	1.1353	118.0	3519

* This AL value has been normalized for a permeability of 1K. For a close approximation of AL for other values of permeability, multiply this AL value by the new permeability in kilo-perm. If the new permeability is 2500, then use 2.5.

Design and Dimensional Data for EE and EI Planar, Ferrite Cores

The dimensional outline for EE and EI planar ferrite cores is shown in Figure 3-31. Dimensional data for EE and EI planar ferrite cores is given in Table 3-20; design data is given in Table 3-21.

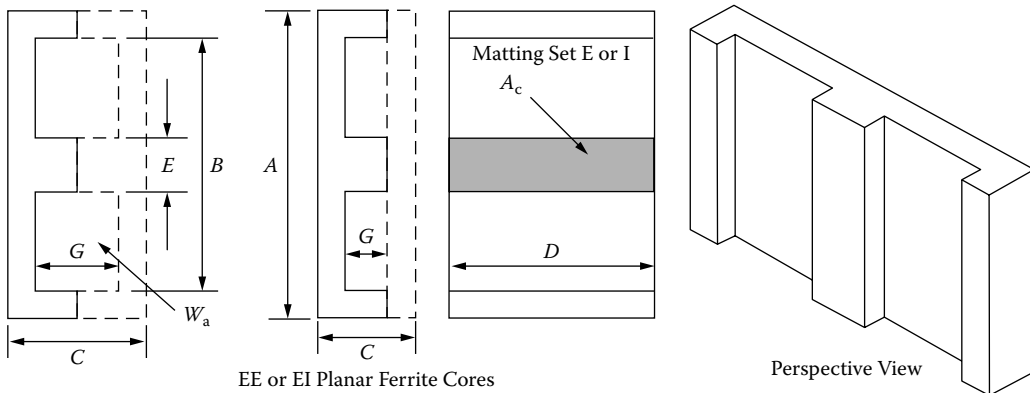


Figure 3-31. Dimension Outline for EE, EI Planar Ferrite Cores.

Table 3-20. Dimensional Data for EE, EI Planar Ferrite Cores

EE&EI/LP, Ferrite Cores (Magnetics)													
Part No.	A cm	B cm	C cm	D cm	E cm	G cm	Part No.	A cm	B cm	C cm	D cm	E cm	G cm
EI-41805	1.800	1.370	0.639	1.000	0.400	0.200	EI-43208	3.175	2.490	0.953	2.032	0.635	0.318
EE-41805	1.800	1.370	0.800	1.000	0.400	0.400	EE-43208	3.175	2.490	1.270	2.032	0.635	0.636
EI-42216	2.180	1.610	0.865	1.580	0.500	0.305	EI-44310	4.320	3.470	1.360	2.790	0.810	0.540
EE-42216	2.180	1.610	1.140	1.580	0.500	0.610	EE-44310	4.320	3.470	1.900	2.790	0.810	1.080

Table 3-21. Design Data for EE, EI Planar Ferrite Cores

EE&EI/LP, Ferrite Cores (Magnetics)											
Part No.	W _{tcu} grams	W _{tfe} grams	MLT cm	MPL cm	W _a A _c	A _c cm ²	W _a cm ²	A _p cm ⁴	K _g cm ⁵	A _t cm ²	*AL mh/1K
						cm ²					
EI-41805	1.5	4.1	4.7	2.03	0.2269	0.401	0.091	0.0365	0.00125	10.4	1410
EE-41805	3.1	4.9	4.7	2.42	0.4564	0.401	0.183	0.0734	0.00250	11.6	1460
EI-42216	3.8	10.4	6.5	2.58	0.2035	0.806	0.164	0.1322	0.00656	17.8	2699
EE-42216	7.8	13.0	6.5	3.21	0.4169	0.806	0.336	0.2708	0.01343	20.5	2203
EI-43208	8.9	22.0	8.9	3.54	0.2223	1.300	0.289	0.3757	0.02195	33.4	3183
EE-43208	17.8	26.0	8.9	4.17	0.4354	1.300	0.566	0.7358	0.04299	37.9	2913
EI-44310	29.7	58.0	11.9	5.06	0.3057	2.290	0.700	1.6030	0.12339	65.4	4622
EE-44310	59.4	70.8	11.9	6.15	0.6114	2.290	1.400	3.2060	0.24678	75.3	3944

* This AL value has been normalized for a permeability of 1K. For a close approximation of AL for other values of permeability, multiply this AL value by the new permeability in kilo-perm. If the new permeability is 2500, then use 2.5.

Design and Dimensional Data for EC, Ferrite Cores

The dimensional outline for EC ferrite cores is shown in Figure 3-32. Dimensional data for EC ferrite cores is given in Table 3-22; design data is given in Table 3-23.

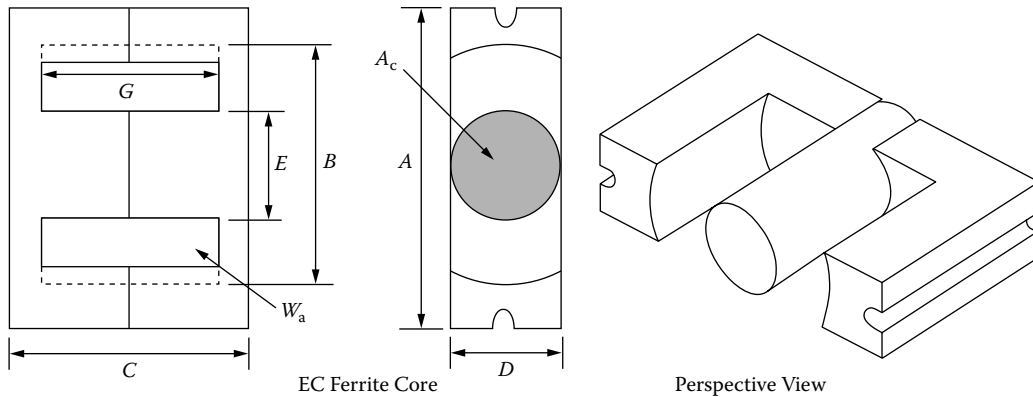


Figure 3-32. Dimension Outline for EC Ferrite Cores.

Table 3-22. Dimensional Data for EC Ferrite Cores

EC, Ferrite Cores (Magnetics)						
Part No.	A cm	B cm	C cm	D cm	E cm	G cm
EC-35	3.450	2.275	3.460	0.950	0.950	2.460
EC-41	4.060	2.700	3.900	1.160	1.160	2.780
EC-52	5.220	3.300	4.840	1.340	1.340	3.180
EC-70	7.000	4.450	6.900	1.640	1.640	4.450

Table 3-23. Design Data for EC Ferrite Cores

EC, Ferrite Cores (Magnetics)											
Part No.	W_{tcu} grams	W_{tfe} grams	MLT cm	MPL cm	W_a	A_c cm^2	W_a cm^2	A_p cm^4	K_g cm^5	A_t cm^2	*AL mh/1K
					A_c						
EC-35	35.1	36.0	6.3	7.59	1.864	0.843	1.571	1.324	0.071	50.2	962
EC-41	55.4	52.0	7.5	8.76	1.721	1.210	2.082	2.519	0.163	67.6	1510
EC-52	97.8	111.0	9.0	10.30	1.689	1.800	3.040	5.472	0.438	106.5	1681
EC-70	256.7	253.0	11.7	14.10	2.214	2.790	6.177	17.234	1.644	201.7	1917

* This AL value has been normalized for a permeability of 1K. For a close approximation of AL for other values of permeability, multiply this AL value by the new permeability in kilo-perm. If the new permeability is 2500, then use 2.5.

Design and Dimensional Data for ETD, Ferrite Cores

The dimensional outline for ETD ferrite cores is shown in Figure 3-33. Dimensional data for ETD ferrite cores is given in Table 3-24; design data is given in Table 3-25.

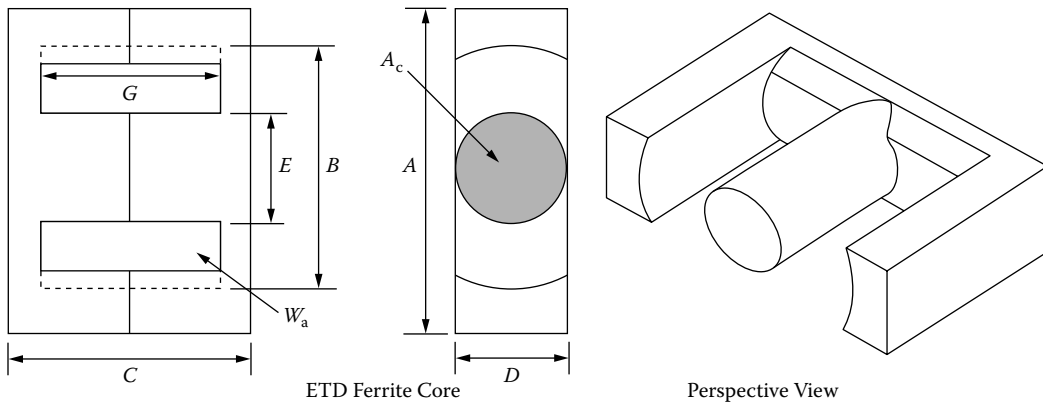


Figure 3-33. Dimension Outline for ETD Ferrite Cores.

Table 3-24. Dimensional Data for ETD Ferrite Cores

ETD, Ferrite Cores (Ferroxcube)													
Part No.	A cm	B cm	C cm	D cm	E cm	G cm	Part No.	A cm	B cm	C cm	D cm	E cm	G cm
ETD-29	3.060	2.270	3.160	0.980	0.980	2.200	ETD-49	4.980	3.610	4.940	1.670	1.670	3.540
ETD-34	3.500	2.560	3.460	1.110	1.110	2.360	ETD-54	5.450	4.120	5.520	1.890	1.890	4.040
ETD-39	4.000	2.930	3.960	1.280	1.280	2.840	ETD-59	5.980	4.470	6.200	2.165	2.165	4.500
ETD-44	4.500	3.250	4.460	1.520	1.520	3.220							

Table 3-25. Design Data for ETD Ferrite Cores

ETD, Ferrite Cores (Ferroxcube)											
Part No.	W _{teu} grams	W _{fe} grams	MLT cm	MPL cm	W _a A _c	A _c cm ²	W _a cm ²	A _p cm ⁴	K _g cm ⁵	A _t cm ²	*AL mh/1K
ETD-29	32.1	28.0	6.4	7.20	1.865	0.761	1.419	1.0799	0.0514	42.5	1000
ETD-34	43.4	40.0	7.1	7.87	1.757	0.974	1.711	1.6665	0.0914	53.4	1182
ETD-39	69.3	60.0	8.3	9.22	1.871	1.252	2.343	2.9334	0.1770	69.9	1318
ETD-44	93.2	94.0	9.4	10.30	1.599	1.742	2.785	4.8515	0.3596	87.9	1682
ETD-49	126.2	124.0	10.3	11.40	1.627	2.110	3.434	7.2457	0.5937	107.9	1909
ETD-54	186.9	180.0	11.7	12.70	1.609	2.800	4.505	12.6140	1.2075	133.7	2273
ETD-59	237.7	260.0	12.9	13.90	1.410	3.677	5.186	19.0689	2.1742	163.1	2727

* This AL value has been normalized for a permeability of 1K. For a close approximation of AL for other values of permeability, multiply this AL value by the new permeability in kilo-perm. If the new permeability is 2500, then use 2.5.

Design and Dimensional Data for ETD/(low profile), Ferrite Cores

The dimensional outline for ETD/lp low profile ferrite cores is shown in Figure 3-34. Dimensional data for ETD/lp low profile ferrite cores is given in Table 3-26; design data is given in Table 3-27.

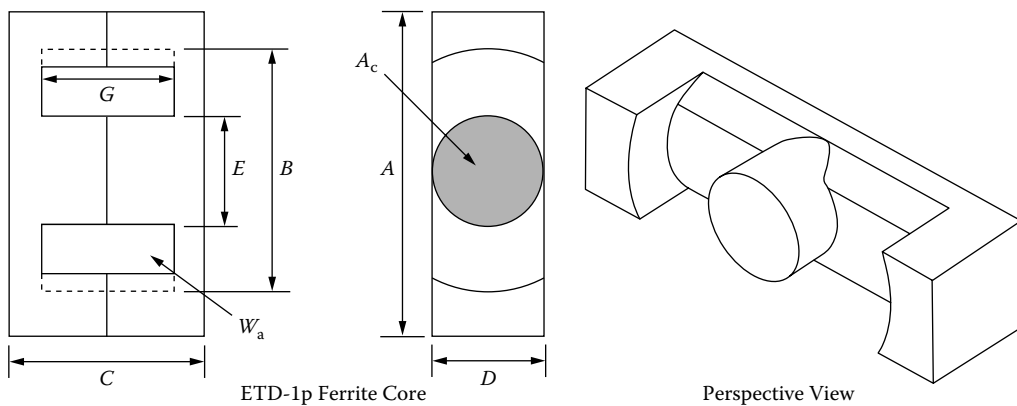


Figure 3-34. Dimension Outline for ETD/lp Ferrite Cores.

Table 3-26. Dimensional Data for ETD/lp Ferrite Cores

ETD/lp, Ferrite Cores (TSC Ferrite International)						
Part No.	A cm	B cm	C cm	D cm	E cm	G cm
ETD34(lp)	3.421	2.631	1.804	1.080	1.080	0.762
ETD39(lp)	3.909	3.010	1.798	1.250	1.250	0.762
ETD44(lp)	4.399	3.330	1.920	1.481	1.481	0.762
ETD49(lp)	4.869	3.701	2.082	1.631	1.631	0.762

Table 3-27. Design Data for ETD/lp Ferrite Cores

ETD/lp, Ferrite Cores (TSC Ferrite International)											
Part No.	W _{tcu} grams	W _{tfe} grams	MLT cm	MPL cm	W _a	A _c cm ²	W _a cm ²	A _p cm ⁴	K _g cm ⁵	A _t cm ²	*AL mh/1K
					A _c						
ETD34(lp)	15.1	32.7	7.2	4.65	0.609	0.970	0.591	0.5733	0.0309	33.1	2382
ETD39(lp)	20.0	46.3	8.4	5.03	0.559	1.200	0.671	0.8052	0.0460	39.6	2838
ETD44(lp)	24.6	72.1	9.5	5.40	0.420	1.730	0.727	1.2577	0.0916	48.4	3659
ETD49(lp)	29.1	95.0	10.4	5.85	0.374	2.110	0.789	1.6648	0.1351	58.2	4120

* This AL value has been normalized for a permeability of 1K. For a close approximation of AL for other values of permeability, multiply this AL value by the new permeability in kilo-perm. If the new permeability is 2500, then use 2.5.

Design and Dimensional Data for ER, Ferrite Cores

Surface Mount Device, SMD

The dimensional outline for ER ferrite cores is shown in Figure 3-35. Dimensional data for ER ferrite cores is given in Table 3-28; design data is given in Table 3-29.

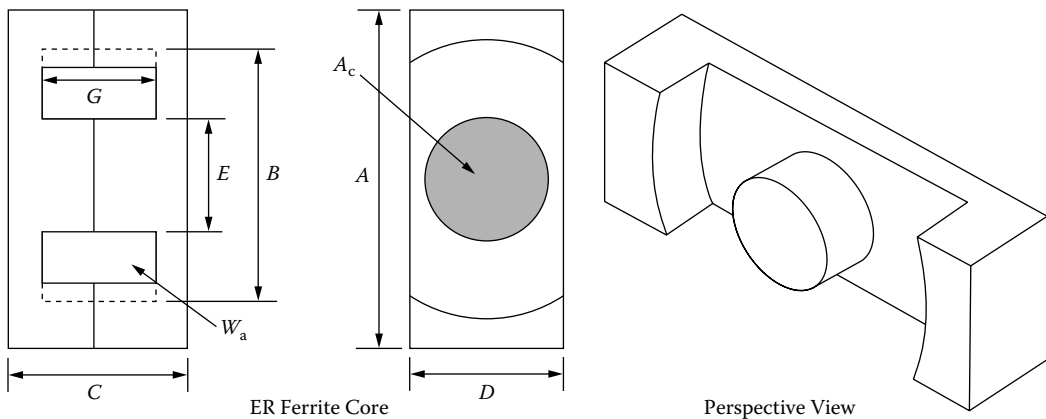


Figure 3-35. Dimension Outline for ER Ferrite Cores.

Table 3-28. Dimensional Data for ER Ferrite Cores

ER, Ferrite Cores (Ferroxcube)													
Part No.	A cm	B cm	C cm	D cm	E cm	G cm	Part No.	A cm	B cm	C cm	D cm	E cm	G cm
ER 9.5	0.950	0.750	0.490	0.500	0.350	0.320	ER 42	4.200	3.005	4.480	1.560	1.550	3.090
ER 11	1.100	0.870	0.490	0.600	0.425	0.300	ER 48	4.800	3.800	4.220	2.100	1.800	2.940
ER 35	3.500	2.615	4.140	1.140	1.130	2.950	ER 54	5.350	4.065	3.660	1.795	1.790	2.220

Table 3-29. Design Data for ER Ferrite Cores

ER, Ferrite Cores (Ferroxcube)												
Part No.	W _{tcu} grams	W _{tfe} grams	MLT cm	MPL cm	W _a A _c	A _c cm ²	W _a cm ²	A _p cm ⁴	K _g cm ⁵	A _t cm ²	*AL mh/1K	
ER 9.5	0.6	0.7	2.700	1.42	0.842	0.076	0.0640	0.00486	0.000055	3.0	435	
ER 11	0.7	1.0	3.200	1.47	0.650	0.103	0.0670	0.00690	0.000089	3.7	609	
ER 35	56.7	46.0	7.300	9.08	2.190	1.000	2.1900	2.19000	0.120000	62.4	1217	
ER 42	72.9	96.0	9.100	9.88	1.189	1.890	2.2480	4.24872	0.352971	81.0	2000	
ER 48	120.7	128.0	11.500	10.00	1.185	2.480	2.9400	7.29120	0.628945	100.1	2478	
ER 54	101.9	122.0	11.400	9.18	1.052	2.400	2.5250	6.06000	0.510316	96.2	2652	

* This AL value has been normalized for a permeability of 1K. For a close approximation of AL for other values of permeability, multiply this AL value by the new permeability in kilo-perm. If the new permeability is 2500, then use 2.5.

Design and Dimensional Data for EFD, Ferrite Cores

Surface Mount Device, SMD

The EFD cores, (Economic Flat Design), offer a significant advance in power transformer circuit miniaturization. The dimensional outline for EFD ferrite cores is shown in Figure 3-36. Dimensional data for EFD ferrite cores is given in Table 3-30; design data is given in Table 3-31.

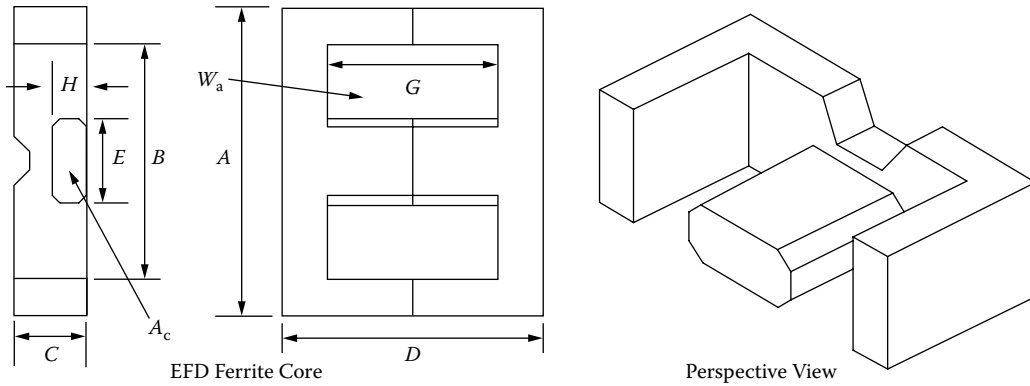


Figure 3-36. Dimension Outline for EFD Ferrite Cores.

Table 3-30. Dimensional Data for EFD Ferrite Cores

EFD, Ferrite Cores (Ferroxcube)							
Part No.	A cm	B cm	C cm	D cm	E cm	G cm	H cm
EFD-10	1.050	0.765	0.270	1.040	0.455	0.750	0.145
EFD-15	1.500	1.100	0.465	1.500	0.530	1.100	0.240
EFD-20	2.000	1.540	0.665	2.000	0.890	1.540	0.360
EFD-25	2.500	1.870	0.910	2.500	1.140	1.860	0.520
EFD-30	3.000	2.240	0.910	3.000	1.460	2.240	0.490

Table 3-31. Design Data for EFD Ferrite Cores

EFD, Ferrite Cores (Ferroxcube)											
Part No.	W _{tcu} grams	W _{tfe} grams	MLT cm	MPL cm	W _a A _c	A _c cm ²	W _a cm ²	A _p cm ⁴	K _g cm ⁵	A _t cm ²	*AL mh/1K
EFD-10	0.8	0.90	1.8	2.37	1.611	0.072	0.116	0.00835	0.00013	3.3	254
EFD-15	3.0	2.80	2.7	3.40	2.093	0.150	0.314	0.04710	0.00105	7.3	413
EFD-20	6.8	7.00	3.8	4.70	1.616	0.310	0.501	0.15531	0.00507	13.3	565
EFD-25	11.5	16.00	4.8	5.70	1.171	0.580	0.679	0.39382	0.01903	21.6	957
EFD-30	17.0	24.00	5.5	6.80	1.267	0.690	0.874	0.60306	0.03026	28.9	913

* This AL value has been normalized for a permeability of 1K. For a close approximation of AL for other values of permeability, multiply this AL value by the new permeability in kilo-perm. If the new permeability is 2500, then use 2.5.

Design and Dimensional Data for EPC, Ferrite Cores

Surface Mount Device, SMD

The dimensional outline for EPC ferrite cores is shown in Figure 3-37. Dimensional data for EPC ferrite cores is given in Table 3-32; design data is given in Table 3-33.

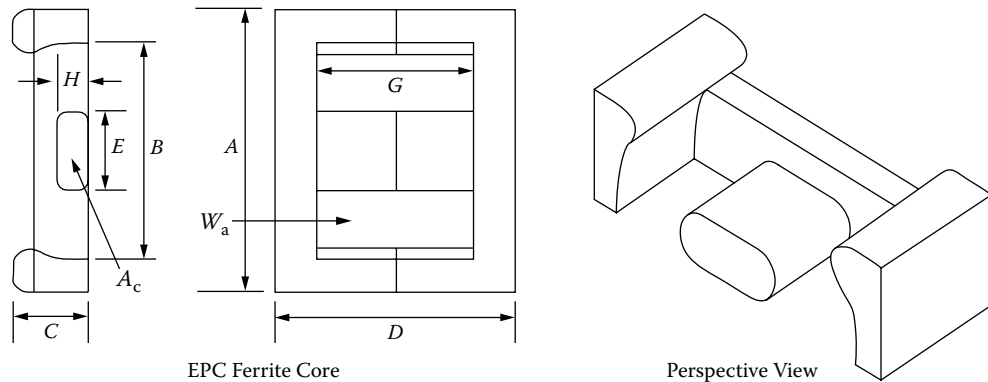


Figure 3-37. Dimension Outline for EPC Ferrite Cores.

Table 3-32. Dimensional Data for EPC Ferrite Cores

EPC, Ferrite Cores (TDK)							
Part No.	A cm	B cm	C cm	D cm	E cm	G cm	H cm
EPC-10	1.020	0.760	0.340	0.810	0.500	0.530	0.190
EPC-13	1.325	1.050	0.460	1.320	0.560	0.900	0.205
EPC-17	1.760	1.430	0.600	1.710	0.770	1.210	0.280
EPC-19	1.910	1.580	0.600	1.950	0.850	1.450	0.250
EPC-25	2.510	2.040	0.800	2.500	1.150	1.800	0.400
EPC-27	2.710	2.160	0.800	3.200	1.300	2.400	0.400
EPC-30	3.010	2.360	0.800	3.500	1.500	2.600	0.400

Table 3-33. Design Data for EPC Ferrite Cores

EPC, Ferrite Cores (TDK)											
Part No.	W _{tcu} grams	W _{tfe} grams	MLT cm	MPL cm	W _a A _c	A _c cm ²	W _a cm ²	A _p cm ⁴	K _g cm ⁵	A _t cm ²	*AL mh/1K
EPC-10	0.5	1.1	1.9	1.78	0.735	0.094	0.069	0.00648	0.000128	2.9	416
EPC-13	2.0	2.1	2.5	3.06	1.768	0.125	0.221	0.02763	0.000553	5.9	363
EPC-17	4.9	4.5	3.4	4.02	1.750	0.228	0.399	0.09097	0.002440	10.2	479
EPC-19	6.9	5.3	3.7	4.61	2.330	0.227	0.529	0.12008	0.002947	12.1	392
EPC-25	14.8	13.0	5.0	5.92	1.804	0.464	0.837	0.38837	0.014416	20.6	650
EPC-27	18.8	18.0	5.1	7.31	1.890	0.546	1.032	0.56347	0.024130	26.8	642
EPC-30	21.9	23.0	5.5	8.16	1.833	0.610	1.118	0.68198	0.030255	31.5	654

* This AL value has been normalized for a permeability of 1K. For a close approximation of AL for other values of permeability, multiply this AL value by the new permeability in kilo-perm. If the new permeability is 2500, then use 2.5.

Design and Dimensional Data for PC, Ferrite Cores

The dimensional outline for PC ferrite pot cores is shown in Figure 3-38. Dimensional data for PC ferrite pot cores is given in Table 3-34; design data is given in Table 3-35.

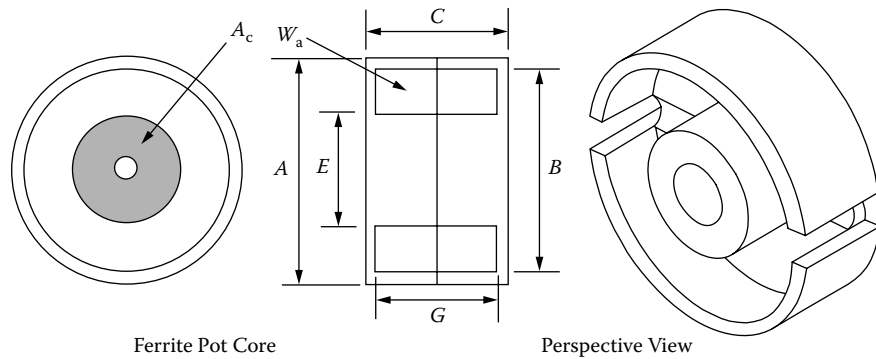


Figure 3-38. Dimension Outline for PC Ferrite Cores.

Table 3-34. Dimensional Data for PC Ferrite Cores

PC, Ferrite Cores (Magnetics)											
Part No.	A cm	B cm	C cm	E cm	G cm	Part No.	A cm	B cm	C cm	E cm	G cm
PC-40905	0.915	0.763	0.526	0.380	0.345	PC-42616	2.550	2.160	1.610	1.130	1.102
PC-41408	1.405	1.160	0.840	0.580	0.580	PC-43019	3.000	2.540	1.890	1.330	1.300
PC-41811	1.800	1.515	1.060	0.740	0.740	PC-43622	3.560	3.040	2.190	1.590	1.460
PC-42213	2.160	1.820	1.340	0.940	0.940	PC-44229	4.240	3.630	2.940	1.740	2.040

Table 3-35. Design Data for PC Ferrite Cores

PC, Ferrite Cores (Magnetics)											
Part No.	W _{tcu} grams	W _{tfe} grams	MLT cm	MPL cm	W _a / A _c	A _c cm ²	W _a cm ²	A _p cm ⁴	K _g cm ⁵	A _t cm ²	*AL mh/1K
PC-40905	0.5	1.0	1.9	1.25	0.654	0.101	0.066	0.00668	0.000142	2.8	440
PC-41408	1.6	3.2	2.9	1.97	0.670	0.251	0.168	0.04222	0.001462	6.8	893
PC-41811	3.5	7.3	3.7	2.59	0.662	0.433	0.287	0.12418	0.005813	11.1	1333
PC-42213	6.2	13.0	4.4	3.12	0.652	0.634	0.414	0.26222	0.015114	16.4	1757
PC-42616	10.1	20.0	5.3	3.76	0.604	0.939	0.568	0.53288	0.037764	23.1	2267
PC-43019	16.7	34.0	6.3	4.50	0.574	1.370	0.787	1.07751	0.093726	31.9	2904
PC-43622	26.7	57.0	7.5	5.29	0.524	2.020	1.059	2.13817	0.230352	44.5	3783
PC-44229	55.9	104.0	8.6	6.85	0.718	2.686	1.928	5.17807	0.646898	67.7	4000

* This AL value has been normalized for a permeability of 1K. For a close approximation of AL for other values of permeability, multiply this AL value by the new permeability in kilo-perm. If the new permeability is 2500, then use 2.5.

Design and Dimensional Data for EP, Ferrite Cores

The EP ferrite cores are typically used in transformer applications. The shape of the assembly is almost cubical, allowing high package densities on the PCB. The dimensional outline for EP ferrite cores is shown in Figure 3-39. Dimensional data for EP ferrite cores is given in Table 3-36; design data is given in Table 3-37.

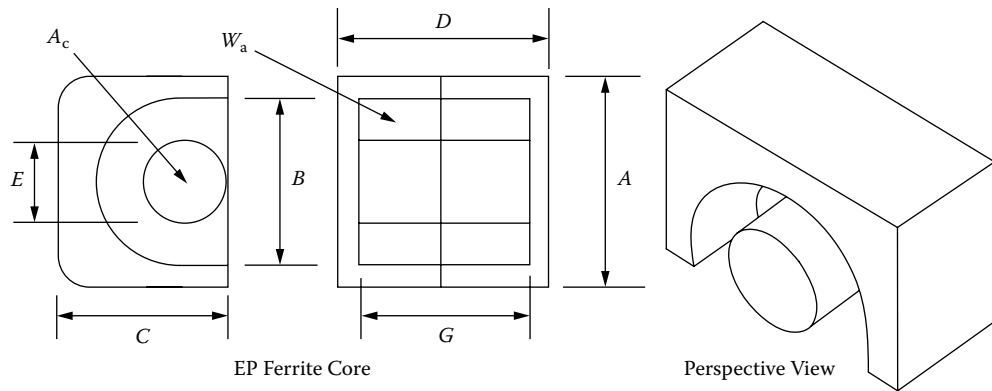


Figure 3-39. Dimension Outline for EP Ferrite Cores.

Table 3-36. Dimensional Data for EP Ferrite Cores

EP, Ferrite Cores (Magnetics)						
Part No.	A cm	B cm	C cm	D cm	E cm	G cm
EP-07	0.920	0.720	0.635	0.740	0.340	0.500
EP-10	1.150	0.920	0.760	1.030	0.345	0.720
EP-13	1.250	1.000	0.880	1.290	0.435	0.920
EP-17	1.800	1.200	1.100	1.680	0.570	1.140
EP-20	2.400	1.650	1.500	2.140	0.880	1.440

Table 3-37. Design Data for EP Ferrite Cores

EP, Ferrite Cores (Magnetics)											
Part No.	W _{tcu} grams	W _{tfe} grams	MLT cm	MPL cm	W _a A _c	A _c cm ²	W _a cm ²	A _p cm ⁴	K _g cm ⁵	A _t cm ²	*AL mh/1K
EP-07	1.4	1.4	1.8	1.55	0.888	0.107	0.095	0.01017	0.00024	3.5	414
EP-10	1.6	2.8	2.1	1.93	1.832	0.113	0.207	0.02339	0.00050	5.7	400
EP-13	2.0	5.1	2.4	2.42	1.200	0.195	0.234	0.04563	0.00148	7.7	667
EP-17	11.6	11.6	2.9	2.95	0.955	0.337	0.322	0.10851	0.00504	13.7	1034
EP-20	7.4	27.6	4.2	4.11	0.632	0.787	0.497	0.39114	0.02932	23.8	1667

* This AL value has been normalized for a permeability of 1K. For a close approximation of AL for other values of permeability, multiply this AL value by the new permeability in kilo-perm. If the new permeability is 2500, then use 2.5.

Design and Dimensional Data for PQ, Ferrite Cores

The PQ ferrite cores, (Power Quality), feature round center legs with rather small cross-sections. The dimensional outline for PQ ferrite cores is shown in Figure 3-40. Dimensional data for PQ ferrite cores is given in Table 3-38; design data is given in Table 3-39.

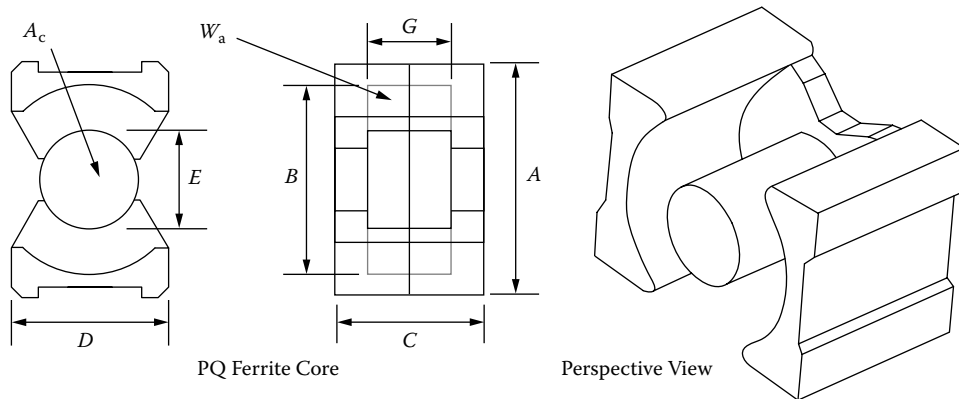


Figure 3-40. Dimension Outline for PQ Ferrite Cores.

Table 3-38. Dimensional Data for PQ Ferrite Cores

PQ, Ferrite Cores (TDK)													
Part No.	A cm	B cm	C cm	D cm	E cm	G cm	Part No.	A cm	B cm	C cm	D cm	E cm	G cm
PQ20/16	2.050	1.800	1.620	1.400	0.880	1.030	PQ32/30	3.200	2.750	3.035	2.200	1.345	2.130
PQ20/20	2.050	1.800	2.020	1.400	0.880	1.430	PQ35/35	3.510	3.200	3.475	2.600	1.435	2.500
PQ26/20	2.650	2.250	2.015	1.900	1.200	1.150	PQ40/40	4.050	3.700	3.975	2.800	1.490	2.950
PQ26/25	2.650	2.250	2.475	1.900	1.200	1.610	PQ50/50	5.000	4.400	4.995	3.200	2.000	3.610
PQ32/20	3.200	2.750	2.055	2.200	1.345	1.150							

Table 3-39. Design Data for PQ Ferrite Cores

PQ, Ferrite Cores (TDK)											
Part No.	W _{tcu} grams	W _{tfe} grams	MLT cm	MPL cm	W _a / A _c	A _c cm ²	W _a cm ²	A _p cm ⁴	K _g cm ⁵	A _t cm ²	*AL mh/1K
PQ20/16	7.4	13.0	4.4	3.74	0.765	0.620	0.474	0.294	0.0166	16.9	1617
PQ20/20	10.4	15.0	4.4	4.54	1.061	0.620	0.658	0.408	0.0230	19.7	1313
PQ26/20	31.0	31.0	5.6	4.63	0.508	1.190	0.604	0.719	0.0611	28.4	2571
PQ26/25	17.0	36.0	5.7	5.55	0.716	1.180	0.845	0.997	0.0826	32.6	2187
PQ32/20	18.9	42.0	6.6	5.55	0.475	1.700	0.808	1.374	0.1415	36.3	3046
PQ32/30	35.5	55.0	6.7	7.46	0.929	1.610	1.496	2.409	0.2315	46.9	2142
PQ35/35	59.0	73.0	7.5	8.79	1.126	1.960	2.206	4.324	0.4520	60.7	2025
PQ40/40	97.2	95.0	8.4	10.20	1.622	2.010	3.260	6.553	0.6272	77.1	1792
PQ50/50	158.5	195.0	10.3	11.30	1.321	3.280	4.332	14.209	1.8099	113.9	2800

* This AL value has been normalized for a permeability of 1K. For a close approximation of AL for other values of permeability, multiply this AL value by the new permeability in kilo-perm. If the new permeability is 2500, then use 2.5.

Design and Dimensional Data for PQ/(low profile), Ferrite Cores

The PQ/lp cores are a cut-down version of the standard PQ cores. The PQ/lp cores have a substantially reduced total height. The dimensional outline for PQ ferrite cores is shown in Figure 3-41. Dimensional data for PQ ferrite cores is given in Table 3-40; design data is given in Table 3-41.

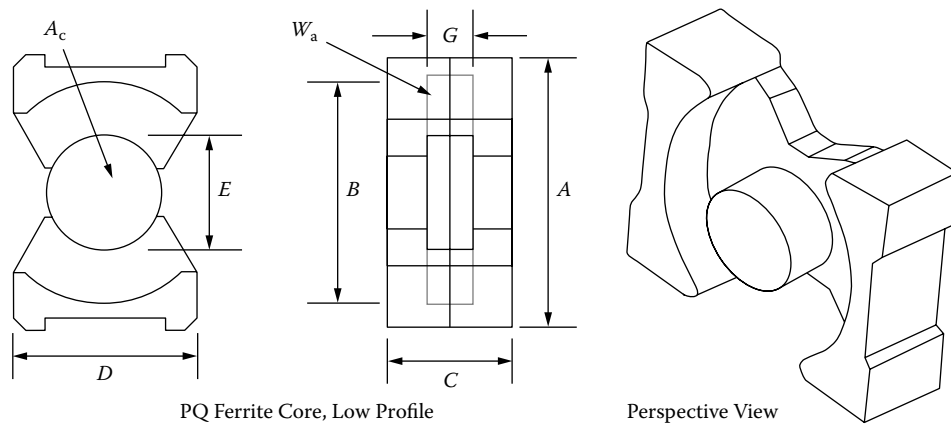


Figure 3-41. Dimension Outline for PQ/lp Ferrite Cores.

Table 3-40. Dimensional Data for PQ/lp Ferrite Cores

PQ/lp, Ferrite Cores (Ferrite International)						
Part No.	A cm	B cm	C cm	D cm	E cm	G cm
PQ20-14-14lp	2.125	1.801	1.352	1.400	0.884	0.762
PQ26-16-14lp	2.724	2.250	1.630	1.900	1.199	0.762
PQ32-17-22lp	3.302	2.751	1.670	2.200	1.348	0.762
PQ35-17-26lp	3.612	3.200	1.738	2.601	1.435	0.762
PQ40-18-28lp	4.148	3.701	1.784	2.799	1.491	0.762

Table 3-41. Design Data for PQ/lp Ferrite Cores

PQ/lp, Ferrite Cores (TSC Ferrite International)											
Part No.	W _{tcu} grams	W _{tfe} grams	MLT cm	MPL cm	W _a A _c	A _c cm ²	W _a cm ²	A _p cm ⁴	K _g cm ⁵	A _t cm ²	*AL mh/1K
PQ20-14-14lp	5.4	12.5	4.4	3.2	0.563	0.620	0.349	0.216	0.0122	15.4	1948
PQ26-16-19lp	7.9	28.0	5.6	3.9	0.336	1.190	0.400	0.476	0.0405	25.4	3170
PQ32-17-22lp	12.5	39.4	6.6	4.8	0.315	1.700	0.535	0.910	0.0937	32.9	3659
PQ35-17-26lp	17.8	44.9	7.4	5.3	0.343	1.960	0.672	1.317	0.1395	40.4	3893
PQ40-18-28lp	24.9	63.5	8.3	5.8	0.419	2.010	0.842	1.692	0.1639	48.0	3850

* This AL value has been normalized for a permeability of 1K. For a close approximation of AL for other values of permeability, multiply this AL value by the new permeability in kilo-perm. If the new permeability is 2500, then use 2.5.

Design and Dimensional Data for RM, Ferrite Cores

The RM cores, (Rectangular Modular), were developed for high Printed Circuit Board, (PCB), packing densities. The dimensional outline for RM ferrite cores is shown in Figure 3-42. Dimensional data for RM ferrite cores is given in Table 3-42; design data is given in Table 3-43.

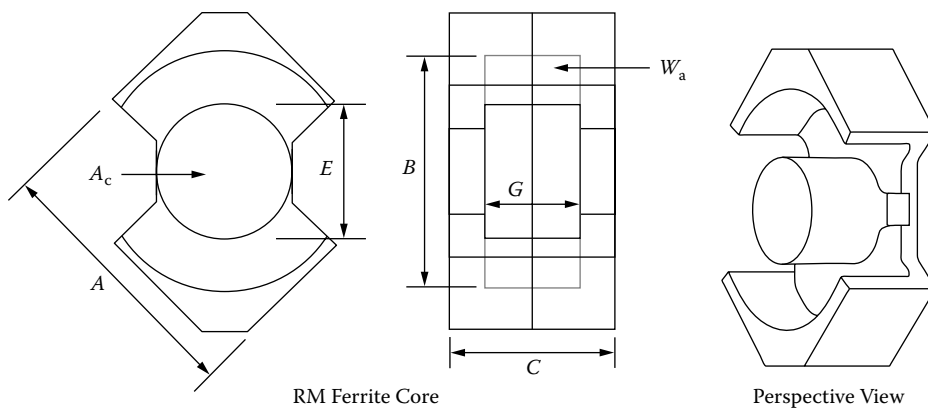


Figure 3-42. Dimension Outline for RM Ferrite Cores.

Table 3-42. Dimensional Data for RM Ferrite Cores

RM, Ferrite Cores (TDK)											
Part No.	A cm	B cm	C cm	E cm	G cm	Part No.	A cm	B cm	C cm	E cm	G cm
RM-4	0.963	0.815	1.04	0.38	0.72	RM-10	2.415	2.165	1.86	1.07	1.27
RM-5	1.205	1.04	1.04	0.48	0.65	RM-12	2.925	2.55	2.35	1.26	1.71
RM-6	1.44	1.265	1.24	0.63	0.82	RM-14	3.42	2.95	2.88	1.47	2.11
RM-8	1.935	1.73	1.64	0.84	1.1						

Table 3-43. Design Data for RM Ferrite Cores

RM, Ferrite Cores (TDK)											
Part No.	W_{tcu} grams	W_{tfe} grams	MLT cm	MPL cm	W_a	A_c cm ²	W_a cm ²	A_p cm ⁴	K_g cm ⁵	A_t cm ²	*AL mh/1K
					A_c						
RM-4	1.1	1.7	2.0	2.27	1.121	0.140	0.157	0.0220	0.0006	5.9	489
RM-5	1.6	3.0	2.5	2.24	0.768	0.237	0.182	0.0431	0.0016	7.9	869
RM-6	2.9	5.5	3.1	2.86	0.710	0.366	0.260	0.0952	0.0045	11.3	1130
RM-8	7.3	13.0	4.2	3.80	0.766	0.640	0.490	0.3136	0.0191	20.2	1233
RM-10	13.2	23.0	5.3	4.40	0.709	0.980	0.695	0.6811	0.0504	29.6	1833
RM-12	24.4	42.0	6.2	5.69	0.788	1.400	1.103	1.5442	0.1395	44.6	2434
RM-14	39.9	70.0	7.2	6.90	0.830	1.880	1.561	2.9347	0.3065	62.8	2869

* This AL value has been normalized for a permeability of 1K. For a close approximation of AL for other values of permeability, multiply this AL value by the new permeability in kilo-perm. If the new permeability is 2500, then use 2.5.

Design and Dimensional Data for RM/(low profile), Ferrite Cores

Surface Mount Device, SMD

The RM/lp ferrite cores are a cut down version of the standard RM cores. The dimensional outline for RM/lp ferrite cores is shown in Figure 3-43. Dimensional data for RM/lp ferrite cores is given in Table 3-44; design data is given in Table 3-45.

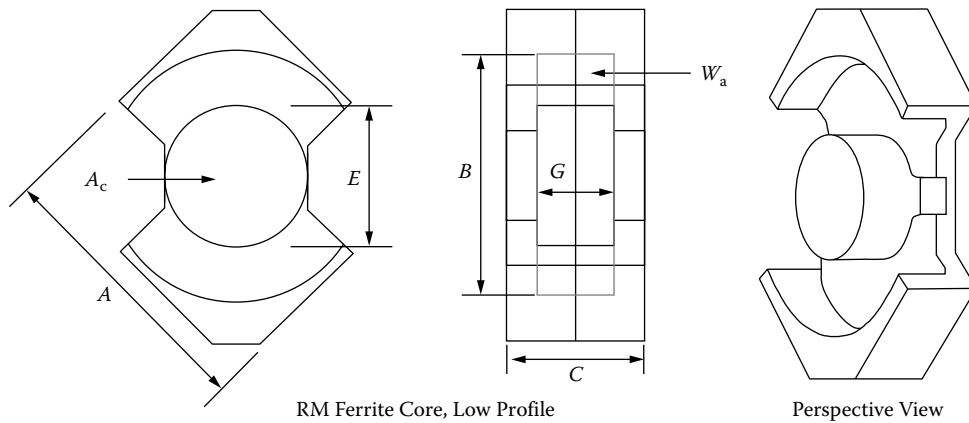


Figure 3-43. Dimension Outline for RM/lp Ferrite Cores.

Table 3-44. Dimensional Data for RM/lp Ferrite Cores

RM/lp, Ferrite Cores (Ferroxcube)											
Part No.	A cm	B cm	C cm	E cm	G cm	Part No.	A cm	B cm	C cm	E cm	G cm
RM4/ILP	0.980	0.795	0.780	0.390	0.430	RM8/ILP	1.970	1.700	1.160	0.855	0.590
RM5/ILP	1.230	1.020	0.780	0.490	0.360	RM10/ILP	2.470	2.120	1.300	1.090	0.670
RM6S/LP	1.470	1.240	0.900	0.640	0.450	RM12/ILP	2.980	2.500	1.680	1.280	0.900
RM7/ILP	1.720	1.475	0.980	0.725	0.470	RM14/ILP	3.470	2.900	2.050	1.500	1.110

Table 3-45. Design Data for RM/lp Ferrite Cores

RM/lp, Ferrite Cores (Ferroxcube)											
Part No.	W _{tcu} grams	W _{tfe} grams	MLT cm	MPL cm	W _a A _c	A _c cm ²	W _a cm ²	A _p cm ⁴	K _g cm ⁵	A _t cm ²	*AL mh/1K
						cm ²					
RM4/ILP	0.6	1.5	2.0	1.73	0.770	0.113	0.087	0.00983	0.00022	5.0	609
RM5/ILP	0.9	2.2	2.5	1.75	0.525	0.181	0.095	0.01720	0.00050	6.9	1022
RM6S/LP	1.5	4.2	3.1	2.18	0.433	0.312	0.135	0.04212	0.00170	9.6	1380
RM7/ILP	2.3	6.0	3.6	2.35	0.444	0.396	0.176	0.06970	0.00307	12.7	1587
RM8/ILP	3.7	10.0	4.2	2.87	0.449	0.554	0.249	0.13795	0.00728	16.9	1783
RM10/ILP	6.4	17.0	5.2	3.39	0.426	0.809	0.345	0.27911	0.01737	25.0	2435
RM12/ILP	11.9	34.0	6.1	4.20	0.439	1.250	0.549	0.68625	0.05625	37.8	3087
RM14/ILP	19.5	55.0	7.1	5.09	0.463	1.680	0.777	1.30536	0.12355	52.5	3652

* This AL value has been normalized for a permeability of 1K. For a close approximation of AL for other values of permeability, multiply this AL value by the new permeability in kilo-perm. If the new permeability is 2500, then use 2.5.

Design and Dimensional Data for DS, Ferrite Cores

The DS ferrite cores are similar to standard Pot Cores. These cores have a large opening to bring out many strands of wire, which is convenient for high power and multiple outputs. The dimensional outline for DS ferrite cores is shown in Figure 3-44. Dimensional data for DS ferrite cores is given in Table 3-46; design data is given in Table 3-47.

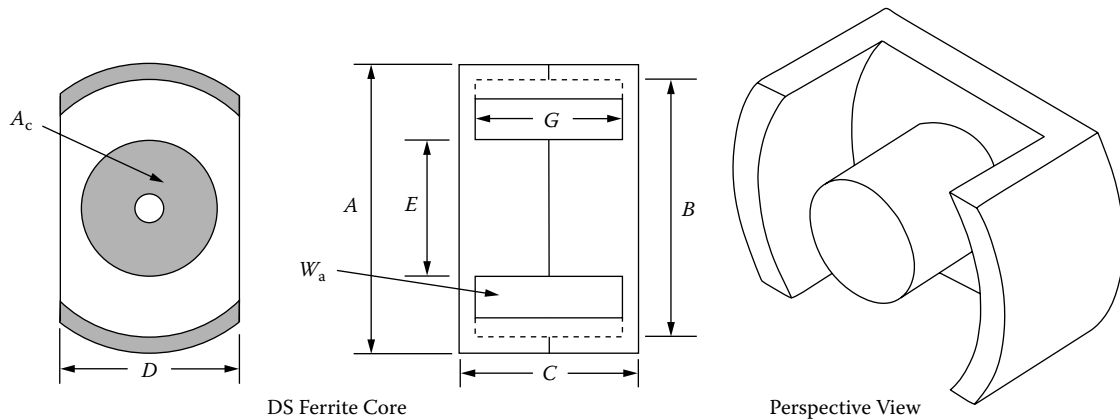


Figure 3-44. Dimension Outline for DS Ferrite Cores.

Table 3-46. Dimensional Data for DS Ferrite Cores

DS, Ferrite Cores (Magnetics)						
Part No.	A cm	B cm	C cm	D cm	E cm	G cm
DS-42311	2.286	1.793	1.108	1.524	0.990	0.726
DS-42318	2.286	1.793	1.800	1.524	0.990	1.386
DS-42616	2.550	2.121	1.610	1.709	1.148	1.102
DS-43019	3.000	2.500	1.880	2.032	1.351	1.300
DS-43622	3.561	2.990	2.170	2.385	1.610	1.458
DS-44229	4.240	3.561	2.960	2.840	1.770	2.042

Table 3-47. Design Data for DS Ferrite Cores

DS, Ferrite Cores (Magnetics)											
Part No.	W _{tcu} grams	W _{tf} grams	MLT cm	MPL cm	W _a A _c	A _c cm ²	W _a cm ²	A _p cm ⁴	K _g cm ⁵	A _t cm ²	*AL mh/1K
DS-42311	4.7	10.0	4.5	2.68	0.568	0.512	0.291	0.149	0.00678	16.2	1496
DS-42318	9.1	13.0	4.6	3.99	0.959	0.580	0.556	0.322	0.01626	21.1	1264
DS-42616	10.1	15.0	5.3	3.89	0.696	0.770	0.536	0.413	0.02398	23.1	1664
DS-43019	16.7	22.0	6.3	4.62	0.638	1.170	0.747	0.874	0.06492	31.9	1930
DS-43622	26.6	37.0	7.5	5.69	0.619	1.620	1.002	1.623	0.14025	44.2	2348
DS-44229	56.0	78.0	8.6	7.60	0.788	2.320	1.829	4.243	0.45788	67.7	2827

* This AL value has been normalized for a permeability of 1K. For a close approximation of AL for other values of permeability, multiply this AL value by the new permeability in kilo-perm. If the new permeability is 2500, then use 2.5.

Design and Dimensional Data for UUR, Ferrite Cores

The UUR ferrite cores feature round legs with rather small cross sections. The round legs allow easy winding with either wire or foil. U cores are used for power, pulse and high-voltage transformers. The dimensional outline for UUR ferrite cores is shown in Figure 3-45. Dimensional data for UUR ferrite cores is given in Table 3-48; design data is given in Table 3-49.

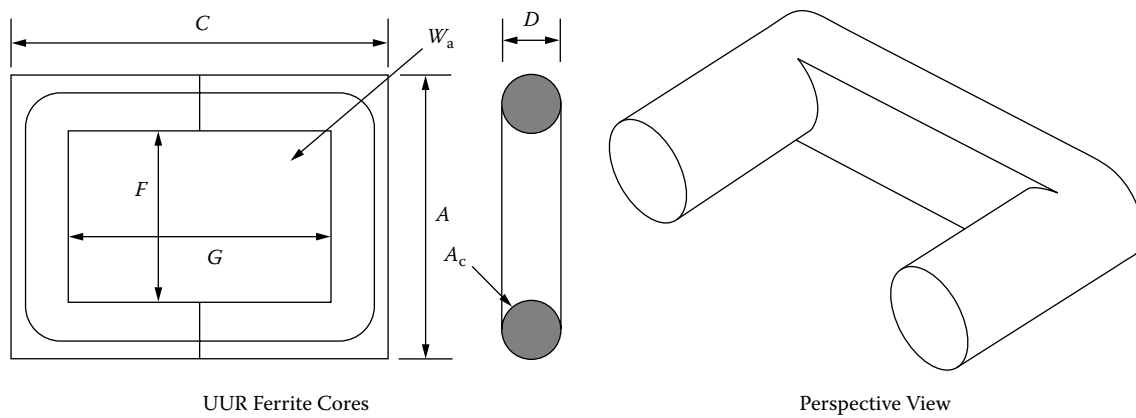


Figure 3-45. Dimension Outline for UUR Ferrite Cores.

Table 3-48. Dimensional Data for UUR Ferrite Cores

UUR, Ferrite Cores (Magnetics)					
Part No.	A cm	C cm	D cm	F cm	G cm
UUR-44121	4.178	5.080	1.194	1.880	3.180
UUR-44119	4.178	4.120	1.194	1.880	2.200
UUR-44125	4.178	5.080	1.194	1.880	3.180
UUR-44130	4.178	6.100	1.194	1.880	4.160

Table 3-49. Design Data for UUR Ferrite Cores

Part No.	W _{tcu} grams	W _{tfe} grams	MLT cm	MPL cm	W _a	A _c cm ²	W _a cm ²	A _p cm ⁴	K _g cm ⁵	A _t cm ²	*AL mh/1K
					A _c						
UUR-44121	119.0	55.0	8.0	11.5	3.643	1.143	4.164	4.759	0.272	98.5	817
UUR-44119	146.2	54.0	8.0	12.1	5.619	0.911	5.119	4.663	0.212	102.9	707
UUR-44125	171.3	64.0	8.0	13.4	5.302	1.131	5.997	6.783	0.384	116.1	606
UUR-44130	227.0	75.0	8.0	15.5	7.095	1.120	7.946	8.900	0.498	134.9	609

* This AL value has been normalized for a permeability of 1K. For a close approximation of AL for other values of permeability, multiply this AL value by the new permeability in kilo-perm. If the new permeability is 2500, then use 2.5.

Design and Dimensional Data for UUS, Ferrite Cores

The UUS ferrite cores feature square or rectangular legs. U cores are used for power, pulse and high-voltage transformers. The dimensional outline for UUS ferrite cores is shown in Figure 3-46. Dimensional data for UUS ferrite cores is given in Table 3-50; design data is given in Table 3-51.

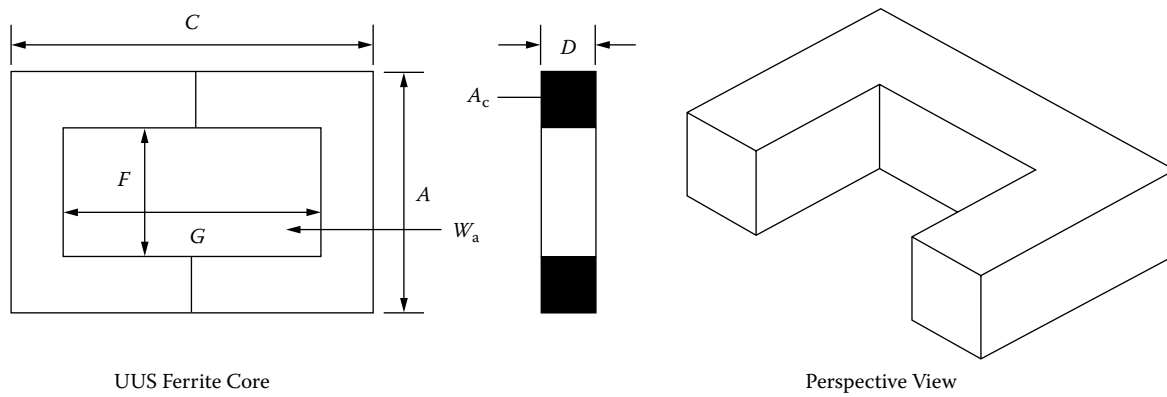


Figure 3-46. Dimension Outline for UUS Ferrite Cores.

Table 3-50. Dimensional Data for UUS Ferrite Cores

UUS, Ferrite Cores (Ferroxcube)					
Part No.	A cm	C cm	D cm	F cm	G cm
U10-08-03	1.000	1.640	0.290	0.435	1.000
U20-16-07	2.080	3.120	0.750	0.640	1.660
U25-20-13	2.480	3.920	1.270	0.840	2.280
U30-25-16	3.130	5.060	1.600	1.050	2.980
U67-27-14	6.730	5.400	1.430	3.880	2.540
U93-76-16	9.300	15.200	1.600	3.620	9.600

Table 3-51. Design Data for UUS Ferrite Cores

UUS, Ferrite Cores (Ferroxcube)											
Part No.	W _{tcu} grams	W _{tf} grams	MLT cm	MPL cm	W _a A _c	A _c cm ²	W _a cm ²	A _p cm ⁴	K _g cm ⁵	A _t cm ²	*AL mh/1K
U10-08-03	3.5	1.8	2.2	3.8	5.370	0.081	0.435	0.0352	0.000519	8.1	213
U20-16-07	16.4	19.0	4.4	6.8	1.896	0.560	1.062	0.5947	0.030277	29.5	826
U25-20-13	41.6	47.0	6.1	8.8	1.841	1.040	1.915	1.9916	0.135821	51.1	1261
U30-25-16	83.9	86.0	7.5	11.1	1.943	1.610	3.129	5.0377	0.432570	82.5	1609
U67-27-14	435.0	170.0	12.4	17.3	4.831	2.040	9.855	20.1042	1.322986	240.2	1652
U93-76-16	1875.2	800.0	15.2	35.4	7.757	4.480	34.752	155.6890	18.354909	605.3	1478

* This AL value has been normalized for a permeability of 1K. For a close approximation of AL for other values of permeability, multiply this AL value by the new permeability in kilo-perm. If the new permeability is 2500, then use 2.5.

Design and Dimensional Data for Toroidal, Ferrite Cores

The toroidal ferrite core has the best possible shape from the magnetic point of view. The magnetic flux path is completely enclosed within the magnetic structure. The toroidal structure fully exploits the capabilities of a ferrite material. The dimensional outline for toroidal ferrite cores is shown in Figure 3-47. Dimensional data for toroidal ferrite cores is given in Table 3-52; design data is given in Table 3-53.

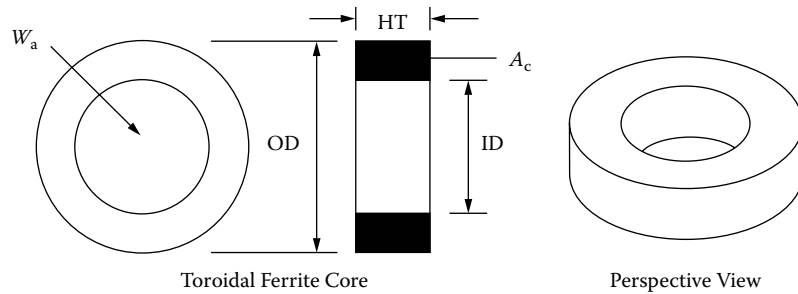


Figure 3-47. Dimension Outline for Toroidal Ferrite Cores.

Table 3-52. Dimensional Data for Toroidal Ferrite Cores

Toroidal, Ferrite Z Coated Cores (Magnetics)							
Part No.	OD cm	ID cm	HT cm	Part No.	OD cm	ID cm	HT cm
TC-40907	1.017	0.504	0.766	TC-42206	2.286	1.295	0.691
TC-41005	1.017	0.420	0.533	TC-42908	2.990	1.811	0.806
TC-41206	1.334	0.452	0.691	TC-43806	3.925	1.790	0.691
TC-41306	1.334	0.729	0.691	TC-43610	3.715	2.205	1.065
TC-41605	1.664	0.812	0.521	TC-43813	3.925	1.790	1.334
TC-42106	2.134	1.193	0.691	TC-48613	8.738	5.389	1.334

Table 3-53. Design Data for Toroidal Ferrite Cores

Toroidal, Ferrite Cores (Magnetics)											
Part No.	W _{tcu} grams	W _{tfe} grams	MLT cm	MPL cm	W _a A _c	A _c cm ²	W _a cm ²	A _p cm ⁴	K _g cm ⁵	A _t cm ²	*AL mh/1K
TC-41005	0.8	1.2	1.7	2.07	1.220	0.109	0.133	0.014497	0.000372	5.3	661
TC-40907	1.4	1.6	2.0	2.27	1.401	0.137	0.192	0.026304	0.000721	6.6	754
TC-41206	1.2	3.3	2.2	2.50	0.727	0.220	0.160	0.035200	0.001408	8.6	1130
TC-41306	3.2	2.4	2.2	3.17	2.937	0.142	0.417	0.059214	0.001529	10.2	591
TC-41605	4.0	2.8	2.2	3.72	3.321	0.156	0.518	0.080808	0.002292	12.8	530
TC-42106	11.2	5.4	2.8	5.03	4.819	0.232	1.118	0.259376	0.008596	22.7	600
TC-42206	13.7	6.4	2.9	5.41	5.105	0.258	1.317	0.339786	0.012092	25.8	604
TC-42908	33.7	12.9	3.7	7.32	7.000	0.368	2.576	0.947968	0.037714	44.6	634
TC-43806	38.0	29.4	4.2	8.28	4.323	0.582	2.516	1.464312	0.081165	61.2	878
TC-43610	63.6	26.4	4.7	8.96	6.139	0.626	3.843	2.405718	0.128168	68.5	883
TC-43813	47.2	51.7	5.3	8.29	2.203	1.142	2.516	2.873272	0.247644	71.0	1674
TC-48613	740.1	203.0	9.1	21.50	12.068	1.890	22.809	43.109010	3.581364	348.0	1091

* This AL value has been normalized for a permeability of 1K. For a close approximation of AL for other values of permeability, multiply this AL value by the new permeability in kilo-perm. If the new permeability is 2500, then use 2.5.

Design and Dimensional Data for Toroidal, MPP Powder Cores

The dimensional outline for MPP powder cores is shown in Figure 3-48. Dimensional data for MPP powder cores is given in Table 3-54; design data is given in Table 3-55. See Chapter 2 for more information.

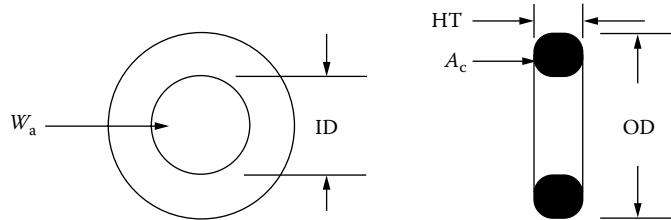


Figure 3-48. Dimension Outline for Toroidal MPP Powder Cores.

Table 3-54. Dimensional Data for Toroidal MPP Powder Cores

MPP Powder Cores, Magnetics 60 mu (coated)											
Part No.	OD cm	ID cm	HT cm	Part No.	OD cm	ID cm	HT cm	Part No.	OD cm	ID cm	HT cm
55021	0.699	0.229	0.343	55381	1.803	0.902	0.711	55076	3.670	2.150	1.135
55281	1.029	0.427	0.381	55848	2.110	1.207	0.711	55083	4.080	2.330	1.537
55291	1.029	0.427	0.460	55059	2.360	1.334	0.838	55439	4.760	2.330	1.892
55041	1.080	0.457	0.460	55351	2.430	1.377	0.965	55090	4.760	2.790	1.613
55131	1.181	0.584	0.460	55894	2.770	1.410	1.194	55716	5.170	3.090	1.435
55051	1.346	0.699	0.551	55071	3.380	1.930	1.143	55110	5.800	3.470	1.486
55121	1.740	0.953	0.711	55586	3.520	2.260	0.978				

Table 3-55. Design Data for Toroidal MPP Powder Cores

MPP Powder Cores, Magnetics 60 mu (coated)											
Part No.	W _{tcu} grams	W _{tfe} grams	MLT cm	MPL cm	W _a	A _c cm ²	W _a cm ²	A _p cm ⁴	K _g cm ⁵	A _t cm ²	AL mh/1K
					A _c						
55021	0.10	0.553	1.10	1.36	0.723	0.047	0.034	0.001598	0.000027	2.30	24
55281	0.70	1.307	1.40	2.18	1.729	0.075	0.130	0.009776	0.000210	4.80	25
55291	0.70	1.645	1.60	2.18	1.376	0.095	0.130	0.012285	0.000290	5.10	32
55041	0.90	1.795	1.60	2.38	1.500	0.100	0.150	0.015000	0.000375	5.60	32
55131	1.50	1.993	1.70	2.69	2.759	0.091	0.250	0.022650	0.000483	6.90	26
55051	2.50	2.886	2.00	3.12	3.175	0.114	0.362	0.041268	0.000941	9.30	27
55121	6.10	6.373	2.50	4.11	3.563	0.192	0.684	0.131328	0.004034	16.00	35
55381	5.60	7.670	2.60	4.14	2.634	0.232	0.611	0.141752	0.005059	16.30	43
55848	11.10	8.836	2.80	5.09	4.898	0.226	1.107	0.250182	0.008077	22.70	32
55059	15.20	14.993	3.20	5.67	4.097	0.331	1.356	0.448836	0.018571	28.60	43
55351	17.90	18.706	3.50	5.88	3.727	0.388	1.446	0.561048	0.024878	31.40	51
55894	22.30	33.652	4.10	6.35	2.320	0.654	1.517	0.992118	0.063302	39.80	75
55071	46.20	44.086	4.50	8.15	4.263	0.672	2.865	1.925280	0.115003	58.30	61
55586	61.40	34.900	4.40	8.95	8.681	0.454	3.941	1.789214	0.073846	64.40	38
55076	60.20	48.692	4.80	8.98	5.255	0.678	3.563	2.415714	0.136488	68.00	56
55083	85.30	86.198	5.70	9.84	3.910	1.072	4.191	4.492752	0.337981	87.50	81
55439	101.90	170.140	6.80	10.74	2.106	1.990	4.191	8.340090	0.976281	112.60	135
55090	136.90	122.576	6.40	11.63	4.497	1.340	6.026	8.074840	0.676268	117.20	86
55716	169.30	132.540	6.40	12.73	5.917	1.251	7.402	9.259902	0.724009	133.10	73
55110	233.30	164.500	7.00	14.300	6.474	1.444	9.348	13.498512	1.113820	164.70	75

Design and Dimensional Data for Toroidal, Iron Powder Cores

The dimensional outline for Iron powder cores is shown in Figure 3-49. Dimensional data for Iron powder cores is given in Table 3-56; design data is given in Table 3-57. See Chapter 2 for more information.

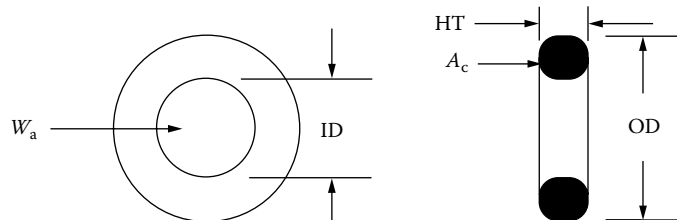


Figure 3-49. Dimension Outline for Toroidal Iron Powder Cores.

Table 3-56. Dimensional Data for Toroidal Iron Powder Cores

Iron Powder Cores, Micrometals 75 mu (coated)											
Part No.	OD cm	ID cm	HT cm	Part No.	OD cm	ID cm	HT cm	Part No.	OD cm	ID cm	HT cm
T20-26	0.508	0.224	0.178	T50-26	1.270	0.770	0.483	T130-26	3.300	1.980	1.110
T25-26	0.648	0.305	0.244	T60-26	1.520	0.853	0.594	T132-26	3.300	1.780	1.110
T26-26	0.673	0.267	0.483	T68-26	1.750	0.940	0.483	T131-26	3.300	1.630	1.110
T30-26	0.780	0.384	0.325	T80-26	2.020	1.260	0.635	T141-26	3.590	2.240	1.050
T37-26	0.953	0.521	0.325	T94-26	2.390	1.420	0.792	T150-26	3.840	2.150	1.110
T38-26	0.953	0.445	0.483	T90-26	2.290	1.400	0.953	T175-26	4.450	2.720	1.650
T44-26	1.120	0.582	0.404	T106-26	2.690	1.450	1.110				

Table 3-57. Design Data for Toroidal Iron Powder Cores

Iron Powder Cores, Micrometals 75 mu (coated)											
Part No.	W _{tcu} grams	W _{tfe} grams	MLT cm	MPL cm	W _a	A _c	W _a	A _p	K _g	A _t	AL mh/1K
					A _c	cm ²	cm ²	cm ⁴	cm ⁵	cm ²	
T20-26	0.10	0.19	0.70	1.15	1.713	0.023	0.039	0.000906	0.000012	1.2	18.5
T25-26	0.24	0.39	0.90	1.50	1.973	0.037	0.073	0.002701	0.000044	2.0	24.5
T26-26	0.26	0.93	1.30	1.47	0.644	0.090	0.058	0.005220	0.000145	2.6	57
T30-26	0.47	0.77	1.14	1.84	1.933	0.060	0.116	0.006960	0.000147	3.1	33.5
T37-26	0.97	1.04	1.28	2.31	3.328	0.064	0.213	0.013632	0.000273	4.5	28.5
T38-26	0.85	1.74	1.50	2.18	1.360	0.114	0.155	0.017670	0.000537	4.8	49
T44-26	1.46	1.86	1.50	2.68	2.687	0.099	0.266	0.026334	0.000695	6.2	37
T50-26	2.96	2.50	1.80	3.19	4.071	0.112	0.456	0.051072	0.001271	8.8	33
T60-26	4.40	4.89	2.20	3.74	3.053	0.187	0.571	0.106777	0.003630	12.2	50
T68-26	5.36	5.30	2.17	4.23	3.877	0.179	0.694	0.124226	0.004099	14.4	43.5
T80-26	11.66	8.31	2.63	5.14	5.394	0.231	1.246	0.287826	0.010112	21.4	46
T94-26	17.44	15.13	3.10	5.97	4.373	0.362	1.583	0.573046	0.026767	29.6	60
T90-26	18.37	15.98	3.40	5.78	3.894	0.395	1.538	0.607510	0.028231	29.4	70
T106-26	23.05	29.94	3.93	6.49	2.504	0.659	1.650	1.087350	0.072970	38.0	93
T130-26	48.33	40.46	4.40	8.28	4.408	0.698	3.077	2.147746	0.136284	56.9	81
T132-26	39.05	44.85	4.40	7.96	3.089	0.805	2.487	2.002035	0.146513	53.9	103
T131-26	32.75	47.83	4.40	7.72	2.357	0.885	2.086	1.845818	0.148504	51.7	116
T141-26	62.70	45.70	4.60	9.14	5.743	0.674	3.871	2.609054	0.152913	66.6	75
T150-26	62.55	58.24	4.85	9.38	4.091	0.887	3.629	3.218923	0.235479	71.6	96
T175-26	128.04	105.05	6.20	11.20	4.334	1.340	5.808	7.782318	0.672794	107.4	105

Design and Dimensional Data for Toroidal, Sendust Powder Cores

The dimensional outline for Sendust powder cores is shown in Figure 3-50. Dimensional data for Sendust powder cores is given in Table 3-58; design data is given in Table 3-59. See Chapter 2 for more information.

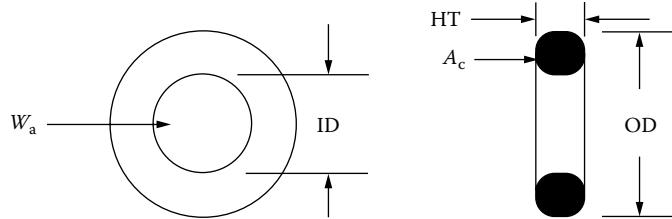


Figure 3-50. Dimension Outline for Toroidal Sendust Powder Cores.

Table 3-58. Dimensional Data for Toroidal Sendust Powder Cores

Sendust Powder Cores, Magnetics 60 mu (coated)											
Part No.	OD cm	ID cm	HT cm	Part No.	OD cm	ID cm	HT cm	Part No.	OD cm	ID cm	HT cm
77021	0.699	0.229	0.343	77381	1.803	0.902	0.711	77076	3.670	2.150	1.135
77281	1.029	0.427	0.381	77848	2.110	1.207	0.711	77083	4.080	2.330	1.537
77291	1.029	0.427	0.460	77059	2.360	1.334	0.838	77439	4.760	2.330	1.892
77041	1.080	0.457	0.460	77351	2.430	1.377	0.965	77090	4.760	2.790	1.613
77131	1.181	0.584	0.460	77894	2.770	1.410	1.194	77716	5.170	3.090	1.435
77051	1.346	0.699	0.551	77071	3.380	1.930	1.143	77110	5.800	3.470	1.486
77121	1.740	0.953	0.711	77586	3.520	2.260	0.978				

Table 3-59. Design Data for Toroidal Sendust Powder Cores

Sendust Powder Cores, Magnetics 60 mu (coated)											
Part No.	W _{tcu} grams	W _{tfe} grams	MLT cm	MPL cm	W _a	A _c cm ²	W _a cm ²	A _p cm ⁴	K _g cm ⁵	A _t cm ²	AL mh/1K
77021	0.10	0.448	1.10	1.36	0.723	0.047	0.034	0.001598	0.000027	2.30	24
77281	0.70	1.148	1.40	2.18	1.729	0.075	0.130	0.009776	0.000210	4.80	25
77291	0.70	1.442	1.60	2.18	1.376	0.095	0.130	0.012285	0.000290	5.10	32
77041	0.90	1.666	1.60	2.38	1.500	0.100	0.150	0.015000	0.000375	5.60	32
77131	1.50	1.706	1.70	2.69	2.759	0.091	0.250	0.022650	0.000483	6.90	26
77051	2.50	2.490	2.00	3.12	3.175	0.114	0.362	0.041268	0.000941	9.30	27
77121	6.10	5.524	2.50	4.11	3.563	0.192	0.684	0.131328	0.004034	16.00	35
77381	5.60	6.723	2.60	4.14	2.634	0.232	0.611	0.141752	0.005059	16.30	43
77848	11.10	8.052	2.80	5.09	4.898	0.226	1.107	0.250182	0.008077	22.70	32
77059	15.20	13.137	3.20	5.67	4.097	0.331	1.356	0.448836	0.018571	28.60	43
77351	17.90	15.970	3.50	5.88	3.727	0.388	1.446	0.561048	0.024878	31.40	51
77894	22.30	29.070	4.10	6.35	2.320	0.654	1.517	0.992118	0.063302	39.80	75
77071	46.20	38.338	4.50	8.15	4.263	0.672	2.865	1.925280	0.115003	58.30	61
77586	61.40	28.443	4.40	8.95	8.681	0.454	3.941	1.789214	0.073846	64.40	38
77076	60.20	42.619	4.80	8.98	5.255	0.678	3.563	2.415714	0.136488	68.00	56
77083	85.30	73.839	5.70	9.84	3.910	1.072	4.191	4.492752	0.337981	87.50	81
77439	101.90	149.608	6.80	10.74	2.106	1.990	4.191	8.340090	0.976281	112.60	135
77090	136.90	109.089	6.40	11.63	4.497	1.340	6.026	8.074840	0.676268	117.20	86
77716	169.30	111.477	6.40	12.73	5.917	1.251	7.402	9.259902	0.724009	133.10	73
77110	233.30	144.544	7.00	14.300	6.474	1.444	9.348	13.498512	1.113820	164.70	75

Design and Dimensional Data for Toroidal, High Flux Powder Cores

The dimensional outline for High Flux powder cores is shown in Figure 3-51. Dimensional data for High Flux powder cores is given in Table 3-60; design data is given in Table 3-61. See Chapter 2 for more information.

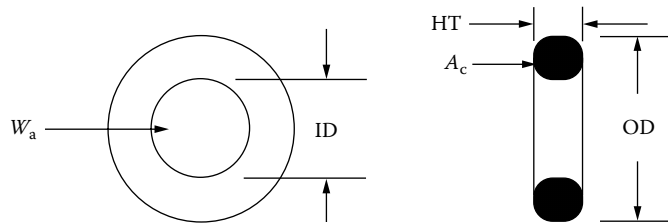


Figure 3-51. Dimension Outline for Toroidal High Flux Powder Cores.

Table 3-60. Dimensional Data for Toroidal High Flux Powder Cores

High Flux Powder Cores, Magnetics 60 mu (coated)											
Part No.	OD cm	ID cm	HT cm	Part No.	OD cm	ID cm	HT cm	Part No.	OD cm	ID cm	HT cm
58021	0.699	0.229	0.343	58381	1.803	0.902	0.711	58076	3.670	2.150	1.135
58281	1.029	0.427	0.381	58848	2.110	1.207	0.711	58083	4.080	2.330	1.537
58291	1.029	0.427	0.460	58059	2.360	1.334	0.838	58439	4.760	2.330	1.892
58041	1.080	0.457	0.460	58351	2.430	1.377	0.965	58090	4.760	2.790	1.613
58131	1.181	0.584	0.460	58894	2.770	1.410	1.194	58716	5.170	3.090	1.435
58051	1.346	0.699	0.551	58071	3.380	1.930	1.143	58110	5.800	3.470	1.486
58121	1.740	0.953	0.711	58586	3.520	2.260	0.978				

Table 3-61. Design Data for Toroidal High Flux Powder Cores

High Flux Powder Cores, Magnetics 60 mu (coated)											
Part No.	W _{tcu} grams	W _{tfe} grams	MLT cm	MPL cm	W _a A _c	A _c cm ²	W _a cm ²	A _p cm ⁴	K _g cm ⁵	A _t cm ²	AL mh/1K
58021	0.10	0.519	1.10	1.36	0.723	0.047	0.034	0.001598	0.000027	2.30	24
58281	0.70	1.222	1.40	2.18	1.729	0.075	0.130	0.009776	0.000210	4.80	25
58291	0.70	1.598	1.60	2.18	1.376	0.095	0.130	0.012285	0.000290	5.10	32
58041	0.90	1.692	1.60	2.38	1.500	0.100	0.150	0.015000	0.000375	5.60	32
58131	1.50	1.870	1.70	2.69	2.759	0.091	0.250	0.022650	0.000483	6.90	26
58051	2.50	2.726	2.00	3.12	3.175	0.114	0.362	0.041268	0.000941	9.30	27
58121	6.10	5.960	2.50	4.11	3.563	0.192	0.684	0.131328	0.004034	16.00	35
58381	5.60	7.238	2.60	4.14	2.634	0.232	0.611	0.141752	0.005059	16.30	43
58848	11.10	8.366	2.80	5.09	4.898	0.226	1.107	0.250182	0.008077	22.70	32
58059	15.20	14.100	3.20	5.67	4.097	0.331	1.356	0.448836	0.018571	28.60	43
58351	17.90	17.672	3.50	5.88	3.727	0.388	1.446	0.561048	0.024878	31.40	51
58894	22.30	31.772	4.10	6.35	2.320	0.654	1.517	0.992118	0.063302	39.80	75
58071	46.20	41.548	4.50	8.15	4.263	0.672	2.865	1.925280	0.115003	58.30	61
58586	61.40	30.926	4.40	8.95	8.681	0.454	3.941	1.789214	0.073846	64.40	38
58076	60.20	45.966	4.80	8.98	5.255	0.678	3.563	2.415714	0.136488	68.00	56
58083	85.30	81.310	5.70	9.84	3.910	1.072	4.191	4.492752	0.337981	87.50	81
58439	101.90	160.740	6.80	10.74	2.106	1.990	4.191	8.340090	0.976281	112.60	135
58090	136.90	115.620	6.40	11.63	4.497	1.340	6.026	8.074840	0.676268	117.20	86
58716	169.30	125.020	6.40	12.73	5.917	1.251	7.402	9.259902	0.724009	133.10	73
58110	233.30	155.100	7.00	14.300	6.474	1.444	9.348	13.498512	1.113820	164.70	75

Design and Dimensional Data for EE, Iron Powder Cores

The dimensional outline for EE iron powder cores is shown in Figure 3-52. Dimensional data for EE iron powder cores is given in Table 3-62; design data is given in Table 3-63. See Chapter 2 for more information.

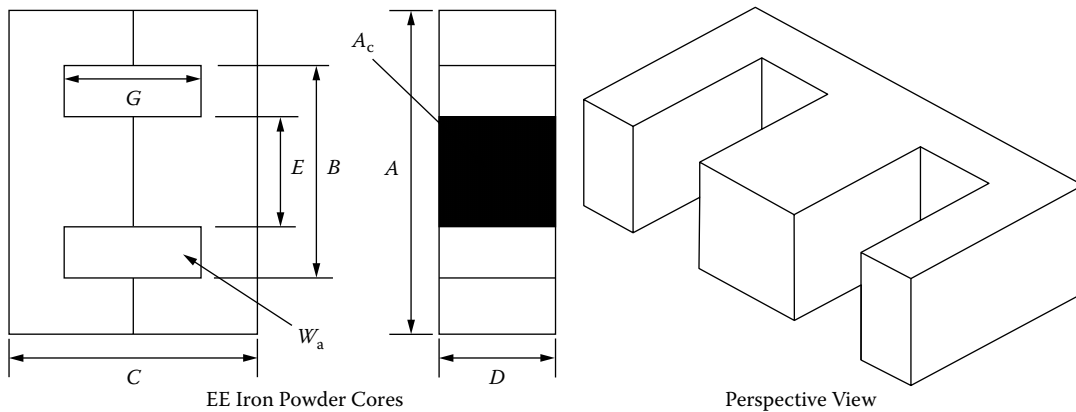


Figure 3-52. Dimension Outline for EE Iron Powder Cores.

Table 3-62. Dimensional Data for EE Iron Powder Cores

EE, Iron Powder Cores (Micrometals) 75 mu Mix-26													
Part No.	A cm	B cm	C cm	D cm	E cm	G cm	Part No.	A cm	B cm	C cm	D cm	E cm	G cm
DIN-16-5	1.640	1.130	1.630	0.462	0.462	1.200	DIN-42-15	4.280	3.070	4.220	1.500	1.200	3.070
EI-187	1.910	1.430	1.610	0.475	0.475	1.160	DIN-42-20	4.280	3.070	4.220	2.000	1.200	3.070
EE-24-25	2.540	1.910	1.910	0.635	0.635	1.270	EI-625	4.740	3.180	3.940	1.570	1.570	2.420
EI-375	3.490	2.540	2.910	0.953	0.953	1.960	DIN-55-21	5.610	3.860	5.540	2.080	1.730	3.830
EI-21	4.130	2.860	3.410	1.270	1.270	2.140	EI-75	5.690	3.810	4.760	1.890	1.890	2.900

Table 3-63. Design Data for EE Iron Powder Cores

EE, Iron Powder Cores (Micrometals) 75 mu Mix-26											
Part No.	W _{tcu} grams	W _{tfe} grams	MLT cm	MPL cm	W _a A _c	A _c cm ²	W _a cm ²	A _p cm ⁴	K _g cm ⁵	A _t cm ²	AL mh/1K
DIN-16-5	4.7	5.3	3.3	3.98	1.790	0.224	0.401	0.090	0.00243	11.5	58
EI-187	7.5	5.5	3.8	4.10	2.451	0.226	0.554	0.125	0.00298	14.4	64
EI-24-25	14.3	12.2	5.0	5.10	2.010	0.403	0.810	0.326	0.01052	23.5	92
EI-375	37.1	40.1	6.7	7.40	1.714	0.907	1.555	1.410	0.07637	46.8	134
EI-21	50.2	80.8	8.2	8.40	1.071	1.610	1.725	2.777	0.21812	63.3	210
DIN-42-15	91.3	112.4	8.9	10.40	1.586	1.810	2.870	5.195	0.42258	84.4	195
DIN-42-20	101.5	149.6	9.9	10.40	1.191	2.410	2.870	6.917	0.67350	92.9	232
EI-625	65.2	141.1	9.4	9.5	0.785	2.480	1.948	4.831	0.50983	82.4	265
DIN-55-21	167.9	283.7	11.6	13.2	1.133	3.600	4.079	14.684	1.82289	141.3	275
EI-75	110.7	245.8	11.2	11.5	0.778	3.580	2.784	9.967	1.27432	119.3	325

Design and Dimensional Data for EE, Sendust Powder Cores

The dimensional outline for EE Sendust cores is shown in Figure 3-53. Dimensional data for EE Sendust powder cores is given in Table 3-64; design data is given in Table 3-65. See Chapter 2 for more information.

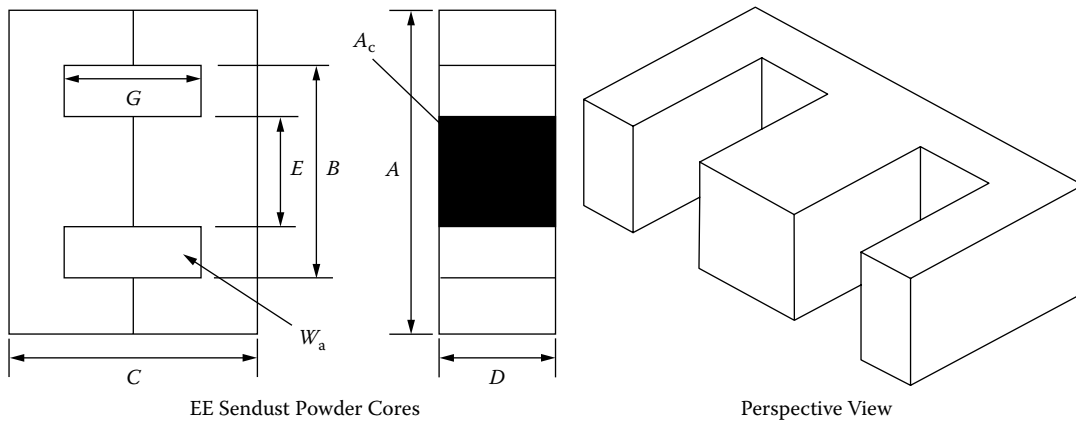


Figure 3-53. Dimension Outline for EE Sendust Powder Cores.

Table 3-64. Dimensional Data for EE Sendust Powder Cores

EE, Sendust Powder Cores (Magnetics) 60 mu													
Part No.	A cm	B cm	C cm	D cm	E cm	G cm	Part No.	A cm	B cm	C cm	D cm	E cm	G cm
EI-187	1.910	1.430	1.610	0.475	0.475	1.160	DIN-42-15	4.280	3.070	4.220	1.500	1.200	3.070
EE-24-25	2.540	1.910	1.910	0.635	0.635	1.270	DIN-42-20	4.280	3.070	4.220	2.000	1.200	3.070
EI-375	3.490	2.540	2.910	0.953	0.953	1.960	DIN-55-21	5.610	3.860	5.540	2.080	1.730	3.830
EI-21	4.130	2.860	3.410	1.270	1.270	2.140							

Table 3-65. Design Data for EE Sendust Powder Cores

EE, Sendust Powder Cores (Magnetics) 60 mu											
Part No.	W _{tcu} grams	W _{tfe} grams	MLT cm	MPL cm	W _a A _c	A _c cm ²	W _a cm ²	A _p cm ⁴	K _g cm ⁵	A _t cm ²	AL mh/1K
EI-187	7.5	6.4	3.8	4.01	2.451	0.226	0.554	0.125	0.00298	14.4	48
EI-24-25	14.3	13.1	5.0	4.85	2.010	0.403	0.810	0.326	0.01052	23.5	70
EI-375	37.1	40.8	6.7	6.94	1.714	0.907	1.555	1.410	0.07637	46.8	102
EI-21	50.2	82.6	8.2	7.75	1.071	1.610	1.725	2.777	0.21812	63.3	163
DIN-42-15	91.3	126.0	8.9	9.84	1.586	1.810	2.870	5.195	0.42258	84.4	150
DIN-42-20	101.5	163.0	9.9	9.84	1.191	2.410	2.870	6.917	0.67350	92.9	194
DIN-55-21	167.9	302.0	11.6	12.3	1.133	3.600	4.079	14.684	1.82289	141.3	219

Manufacturers' Material Product List

Table 3-66 has been put together to show a product list of the leading manufacturers for ferrites, powder cores, nickel-iron tape cores, amorphous tape cores, and laminations. Listed in the references are the manufacturers and their web-page address.

Table 3-66

Manufacturers Material Product List				
Ferrites Cores				
Manufacturers	Mn-Zn	Ni-Zn	Special Machining	
Ferroxcube	X			
TDK	X			
Magnetics	X			X
EPCOS, Inc.	X			
TSC Ferrite Int.	X			
Fair-Rite	X	X		X
MMG	X	X		
Ceramic Magnetics, Inc.	X	X		X
Powder Cores				
Manufacturers	MPP	Hi-Flux	Sendust	Iron Powder
Magnetics	X	X	X	X
Micrometals	X	X	X	X
MMG	X	X	X	X
Tape Toroids and C Cores				
Manufacturers	Silicon	Supermendur	50-50 NiFe	80-20 NiFe
Magnetics	X	X	X	X
Magnetic Metals	X	X	X	X
Electro-Core, Inc.	X			
Amorphous Tape Toroids and C Cores				
Manufacturers	2605SC	2714A	Nanocrystalline	Special
Magnetic Metals	X	X	X	
Metglas	X	X		
VAC	X	X	X	
MK Magnetics, Inc.	X	X	X	Only
Laminations				
Manufacturers	Silicon	Supermendur	50-50 NiFe	80-20 NiFe
Thomas & Skinner, Inc.	X			
Magnetic Metals	X	X	X	X
Tempel Steel Co.	X			

References

Ceramic Magnetics, Inc. www.cmi-ferrite.com

Electro-Core Inc. www.electro-core.com

EPCOS www.usa.epcos.com

Fair Rite www.fair-rite.com

Ferroxcube www.ferroxcube.com

Magnetics www.mag-inc.com

Magnetic Metals Corp. www.magmet.com

Metglas www.metglas.com

Micrometals www.micrometals.com

MK Magnetics www.mkmagnetics.com

MMG www.mmgca.com

TDK www.tdk.com

Tempel Steel Co. www.tempel.com

Thomas and Skinner, Inc. www.thomas-skinner.com

TSC Ferrite International www.tscinternational.com

VAC www.vaccorp.com

Chapter 4

Window Utilization, Magnet Wire and Insulation

Table of Contents

1.	Window Utilization Factor, K_u	4-4
2.	S_1 , Wire Insulation.....	4-5
3.	S_2 , Fill Factor.....	4-6
4.	S_3 , Effective Window	4-9
5.	S_4 , Insulation Factor	4-12
6.	Summary	4-12
7.	Window Utilization Factor, K_u for Bobbin Ferrites.....	4-13
8.	Circular mil and Square mil	4-14
9.	Magnet Wire	4-15
10.	Magnet Wire, Film Insulation.....	4-16
11.	Wire Table	4-16
12.	Solderable Insulation.....	4-19
13.	Bondable Magnet Wire	4-20
14.	Base Film Insulation.....	4-20
15.	Bonding Methods.....	4-21
16.	Miniature Square Magnet Wire.....	4-21
17.	Multistrand Wire and Skin Effect	4-22
18.	Reduce Skin Effect in Transformers	4-23
19.	Calculating Skin Effect in Inductors	4-24
20.	Multistrand Litz Wire	4-27
21.	Proximity Effect.....	4-28
22.	Proximity Effect in Transformers.....	4-29
23.	Multiple Layer High Frequency Transformers and High Loss	4-29
24.	Proximity Effect Using Dowell Curves	4-31
25.	Specialty Wire	4-33
26.	Triple Insulated Wire.....	4-33
27.	Triple Insulated Litz.....	4-34
28.	Polyfilar Magnetic Wire.....	4-35
29.	Standard Foils	4-36
30.	The Use of Foils	4-37
31.	Calculating, MLT	4-40
32.	Calculating, MLT (toroid).....	4-40

Table of Contents	4-3
33. Copper Resistance	4-41
34. Copper Weight	4-41
35. Electrical Insulating Materials.....	4-41
36. References.....	4-42

Window Utilization Factor, K_u

The window utilization factor is the amount of copper that appears in the window area of the transformer or inductor. The window utilization factor is influenced by five main factors:

1. Wire insulation, S_1 .
2. Wire lay fill factor, layer or random wound, S_2 .
3. Effective window area (or when using a toroid, the clearance hole for passage of the shuttle), S_3 .
4. Insulation required for multiplayer windings, or between windings, S_4 .
5. Workmanship, (quality).

These factors, multiplied together, will give a normalized window utilization of $K_u = 0.4$, as shown in Figure 4-1.

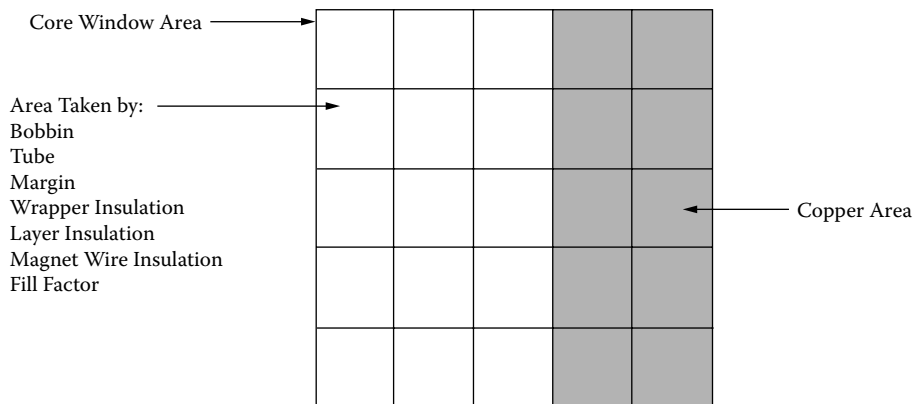


Figure 4-1. Window Area Occupied by Copper.

The window utilization factor, K_u , of the available core window is that space occupied by the winding (copper), and is calculated from areas S_1 , S_2 , S_3 , and S_4 :

$$K_u = S_1 S_2 S_3 S_4 \quad [4-1]$$

Where:

S_1 = conductor area/wire area

S_2 = wound area/usable window area

S_3 = usable window area/window area

S_4 = usable window area/usable window area + insulation

In which:

Conductor area, $A_{w(B)}$ = copper area.

Wire area, A_w = copper area + insulation area.

Wound area = number of turns \times wire area of one turn.

Usable window area = available window area – residual area, that results from the particular winding technique used.

Window area = available window area.

Insulation area = area used for winding insulation.

S₁, Wire Insulation

In the design of high-current or low-current transformers, the ratio of the conductor area to the total wire area can vary from 0.941 to 0.673, depending on the wire size. In Figure 4-2, the thickness of the insulation has been exaggerated to show how the insulation impacts the overall area of the wire.

It can be seen, in Figure 4-2, that, by using multi-strands of fine wire to reduce the skin effect, it will have a significant impact on the window utilization factor, K_u . S_1 is not only dependent upon wire size, but it is also dependent upon insulation coating. [Table 4-1](#) shows the ratio of bare magnet wire to the magnet wire with insulation for single, heavy, triple, and quad insulation. When designing low-current transformers, it is advisable to re-evaluate, S_1 , because of the increased amount of insulating material.

$$S_1 = \frac{A_{w(B)}}{A_w} \quad [4-2]$$

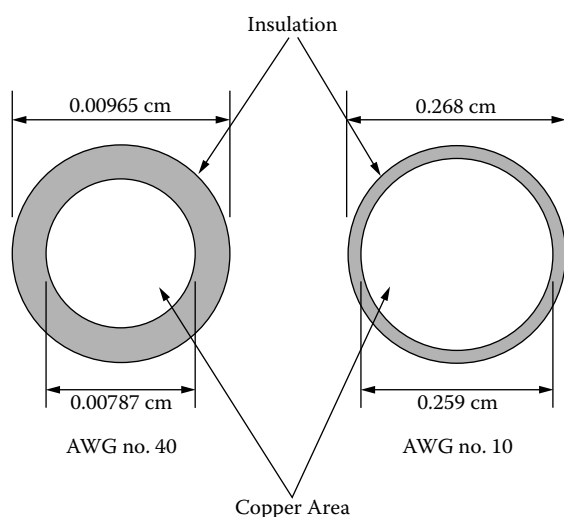


Figure 4-2. Comparing Insulation with Different Wire Gauges.

Table 4-1. Magnetic Wire Data (Nominal)

Magnetic Wire Data (Nominal)					
Size AWG	Bare Area (cm ²)	Ratio Bare/Single	Ratio Bare/Heavy	Ratio Bare/Triple	Ratio Bare/Quad
10	0.1019	0.961	0.930	0.910	0.880
15	0.0571	0.939	0.899	0.867	0.826
20	0.0320	0.917	0.855	0.812	0.756
25	0.0179	0.878	0.793	0.733	0.662
30	0.0100	0.842	0.743	0.661	0.574
35	0.0056	0.815	0.698	0.588	0.502
40	0.0031	0.784	0.665	0.544	0.474

S₂, Fill Factor

S₂ is the fill factor, or the wire lay, for the usable window area. When winding a large number of turns tightly on a smooth surface, the winding length exceeds the calculated value from the wire diameter by 10 to 15%, depending on the wire gauge. See [Figure 4-3](#). The wire lay is subjected to wire tension, and wire quality, such as continuous wire diameter and the winding technique depending on the skill of the operator. The wire lay factor relationship for various wire sizes for layer wound coils is shown in Table 4-2, and for random wound coils in Table 4-3. These two Tables list the outside diameter for heavy film magnetic wire, 10–44 AWG.

Table 4-2. Wire Lay Factors For Layer Wound Coils

Wire Lay Factors For Layer Wound Coils			
AWG	Insulated Wire OD (inch)	Insulated Wire OD (cm)	Wire Lay Factor
10 to 25	0.1051-0.0199	0.2670-0.0505	0.90
26 to 30	0.0178-0.0116	0.0452-0.0294	0.89
31 to 35	0.0105-0.0067	0.0267-0.0170	0.88
36 to 38	0.0060-0.0049	0.0152-0.0124	0.87
39 to 40	0.0043-0.0038	0.0109-0.0096	0.86
41 to 44	0.0034-0.0025	0.00863-0.00635	0.85
Heavy film magnetic wire.			

Table 4-3. Wire Lay Factor For Random Wound Coils

Wire Lay Factor For Random Wound Coils			
AWG	Insulated Wire OD (inch)	Insulated Wire OD (cm)	Wire Lay Factor
10 to 22	0.1051-0.0276	0.267-0.0701	0.90
23 to 39	0.0623-0.0109	0.0249-0.0043	0.85
40 to 44	0.0038-0.0025	0.0096-0.00635	0.75
Heavy film magnet wire.			

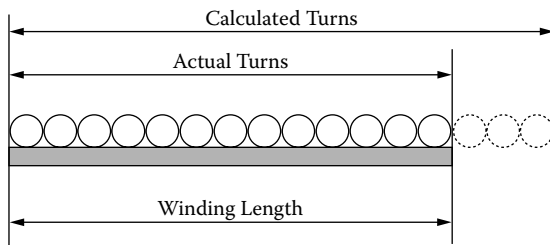


Figure 4-3. Capable Turns per Unit Length.

There are two ideal winding arrangements shown in Figure 4-4 and Figure 4-5. The square winding is shown in Figure 4-4 and the hexagonal winding is shown in Figure 4-5. The simplest form of winding is done by a coil being wound, turn-by-turn and layer-upon-layer, as shown in Figure 4-4. The square winding pattern has a theoretical, fill factor of 0.785.

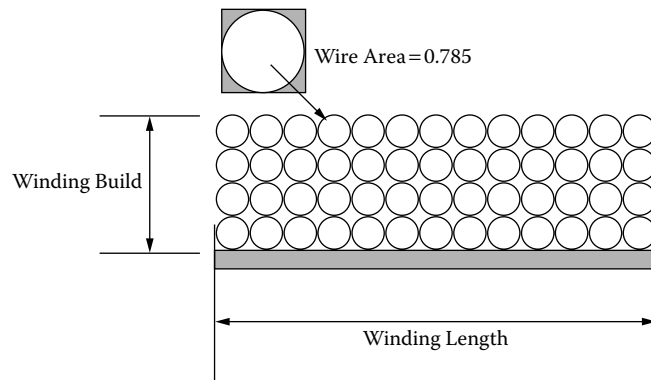


Figure 4-4. Theoretically, the Square Winding Pattern Fill Factor 0.785.

A seemingly, better fill factor can be achieved by using the hexagonal winding in Figure 4-5, compared to the square winding in Figure 4-4. In this type of winding, the individual wires do not lie exactly above each other, as in the square winding pattern. Instead, the wires lie in the grooves of the lower layer, as shown in Figure 4-5.

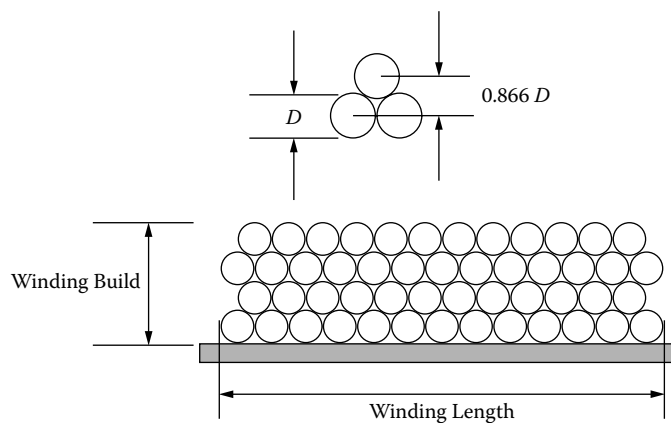


Figure 4-5. Theoretically, the Hexagonal Winding Pattern Fill Factor 0.907.

This style of winding produces the tightest possible packing of the wire. The hexagonal style of winding will yield a theoretical, fill factor of 0.907.

The fill factor, using the square-winding pattern of 0.785, would be nearly impossible to achieve by hand winding without some layer insulation. Any layer insulation will reduce the fill factor even further. The fill factor, using the hexagonal winding pattern of 0.907, is just as hard to get. Hand-winding, using the hexagonal technique, will result in the following: The first layer goes down with almost complete order. In the second layer, some disordering has occurred. With the third and fourth layer, disordering really sets in and the winding goes completely awry. This type of winding performs well with a small number of turns, but, with a large number of turns, it becomes randomly wound.

The ideal winding on a rectangular bobbin is shown in Figure 4-6. Then, when winding rectangular bobbins or tubes, the actual winding height in the region covered by the core will be greater than the calculated winding height or build, due to the bowing of the windings. See [Figure 4-7](#). The amount of bowing depends on the proportions of the winding and the height of the winding. Usually, the available winding build should be reduced by 15 to 20%, or 0.85 times the winding build. When winding on a round bobbin or tube, this bowing effect is negligible.

The conclusion is, when comparing the square winding pattern used in the layer wound coil with its insulation with the hexagonal winding pattern and its awry winding pattern, both seem to have a fill factor of about 0.61. But there is always the hundred to one exception, such as, when a design happens to have the right bobbin, the right number of turns, and the right wire size. This normally only happens when the design is not critical.

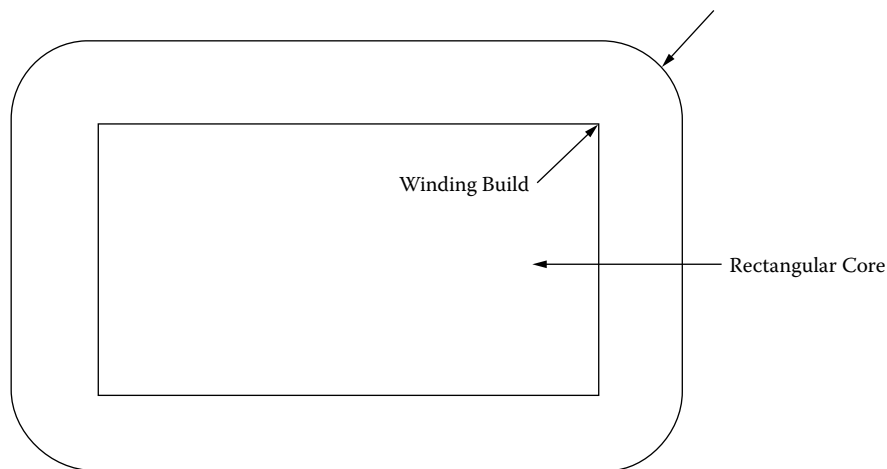
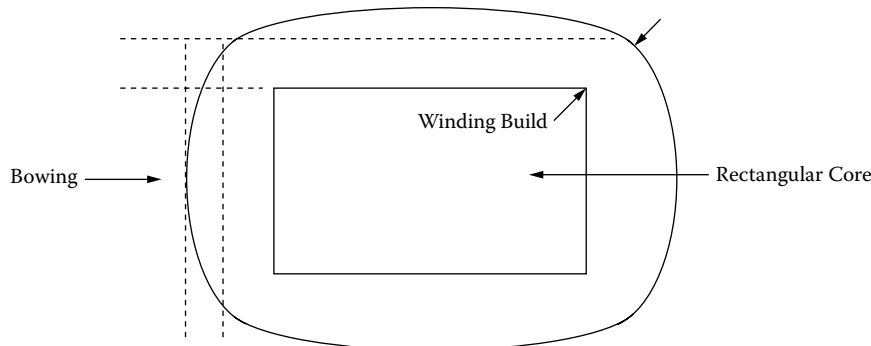
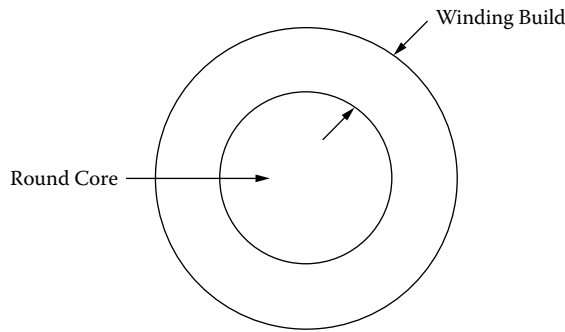


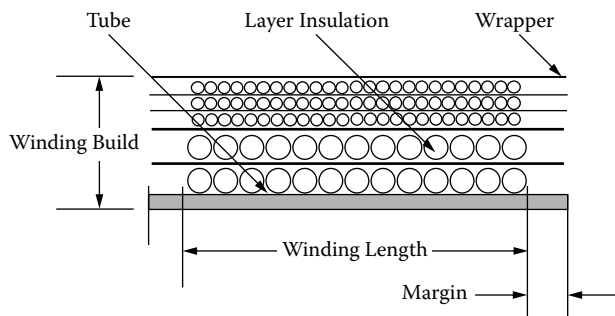
Figure 4-6. Ideal Winding on a Rectangular Bobbin.

**Figure 4-7.** Bowing in Transformer Windings.

To minimize this bowing effect and to insure a minimum build for either random or layer winding, the round bobbin, shown in Figure 4-8, will provide the most compact design. It can be seen, in Figure 4-8, that the round bobbin provides a uniform tension, all 360 degrees around the bobbin, for both layer and random windings. The other benefit, in using a round bobbin, is the reduction and minimizing of the leakage inductance caused from the bowing.

**Figure 4-8.** A Round Bobbin Insures Minimum Bowing.**S₃, Effective Window**

The effective window, S₃, defines how much of the available window space may actually be used for the winding. The winding area available to the designer depends on the bobbin or tube configuration. Designing a layer winding that uses a tube will require a margin, as shown in [Figure 4-9](#). The margin dimensions will vary with wire size. See [Table 4-4](#). It can be seen, in Figure 4-9 and Table 4-4, how the margin reduces the effective window area. When transformers are constructed, using the layer winding technique, there is an industry standard for layer insulation thickness. This thickness is based on the diameter of the wire, as shown in [Table 4-5](#).

**Figure 4-9.** Transformer Windings with Margins.**Table 4-4.** Winding Margins Versus AWG

Winding Margins Versus AWG		
AWG	Margin	
	cm	inch
10-15	0.635	0.25
16-18	0.475	0.187
19-21	0.396	0.156
22-31	0.318	0.125
32-37	0.236	0.093
38-up	0.157	0.062

Table 4-5. Layer Insulation Thickness

Layer Insulation Thickness		
AWG	Insulation Thickness	
	cm	inch
10 - 16	0.02540	0.01000
17 - 19	0.01780	0.00700
20 - 21	0.01270	0.00500
22 - 23	0.00760	0.00300
24 - 27	0.00510	0.00200
28 - 33	0.00381	0.00150
34 - 41	0.00254	0.00100
42 - 46	0.00127	0.00050

A single bobbin design, as shown in [Figure 4-10](#), offers an effective area, W_a , between 0.835 to 0.929 for laminations, and 0.55 to 0.75 for ferrites; a two bobbin configuration, as shown in [Figure 4-11](#), offers an effective area, W_a , between 0.687 to 0.873 for the tape C cores.

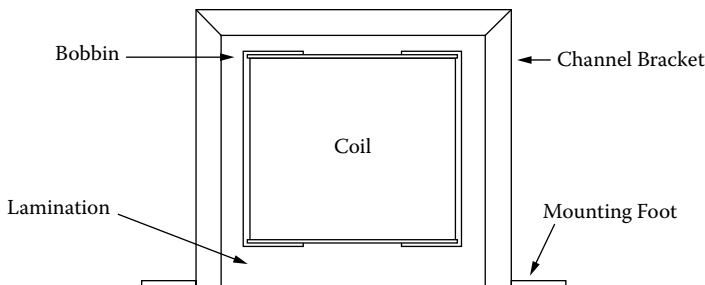


Figure 4-10. Transformer Construction with Single Bobbin.

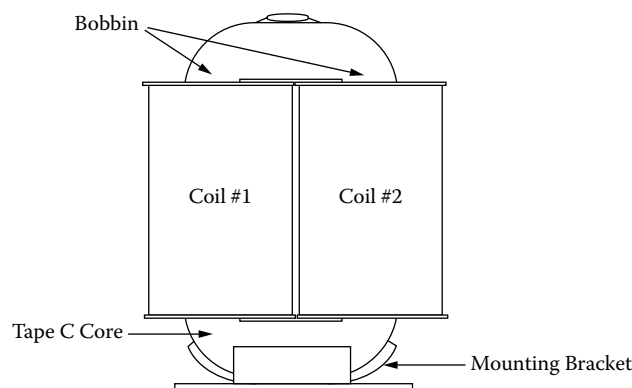


Figure 4-11. Transformer Construction with Dual Bobbins.

The toroid is a little different. The term, S₃, defines how much of the available window space can actually be used for the winding. In order to wind the toroidal core, there has to be room to allow free passage of the shuttle. If half of the inside diameter is set aside for the shuttle, then, there will be 75% of the window area, (W_a), left for the design which is a good value for the effective window area factor, S₃ = 0.75, as shown in Figure 4-12. The toroid would fall within its limits, into all of the above categories.

$$\text{Effective Window area } W_{a(\text{eff})} = (0.75)(\pi)(ID)^2/4$$

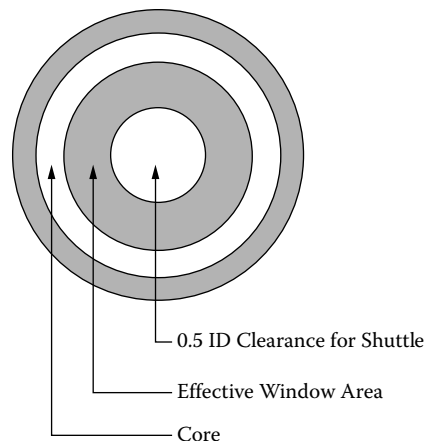


Figure 4-12. Effective Winding Area of a Toroidal Core.

S₄, Insulation Factor

The insulation factor, S₄, defines how much of the usable window space is actually being used for insulation. If the transformer has multiple secondaries with significant amounts of insulation, S₄, should be reduced by 5 to 10% for each additional secondary winding, partly because of the added space occupied by insulation and partly because of the poorer space factor.

The insulation factor, S₄, is not taken into account in [Figure 4-12](#). The insulation factor, S₄, is to be 1.0. The window utilization factor, K_u, is highly influenced by insulation factor, S₄, because of the rapid buildup of insulation in the toroid, as shown in Figure 4-13.

In Figure 4-13, it can be seen that the insulation buildup is greater on the inside, than on the outside. For example, in Figure 4-13, if 1.27 cm (1/2") wide tape was used with an overlap of 0.32 cm (1/8") on the outside diameter, the overlap thickness would be four times the thickness of the tape. It should be noted that the amount of overlap depends greatly on the size of the toroid and the required tape. In the design of toroidal components, and using the 0.5 ID remaining for passage of the shuttle, there is normally enough room for the wrapper.

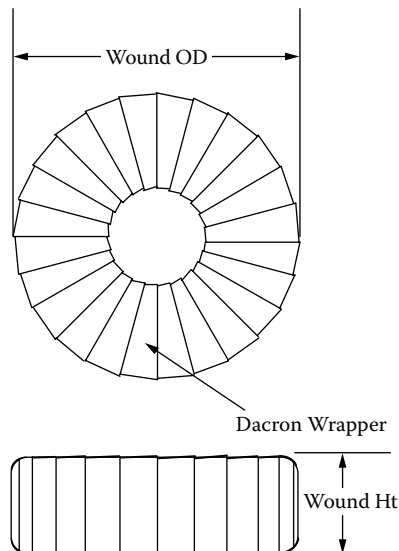


Figure 4-13. Wrapped Toroid.

Summary

The author hopes to have cleared up some of the mystery of how the window utilization factor, K_u, was derived and that the magic of 0.4 is now clear. All the different parts making up window utilization, have been explained, hopefully eliminating confusion and simplifying the complexity of the subject.

As stated at the beginning of this chapter, a good approximation for the window utilization factor is $K_u = 0.4$.

S_1 = conductor area/wire area = 0.855, #20 AWG

S_2 = wound area/usable window area = 0.61

S_3 = usable window area/window area = 0.75

S_4 = usable window area/usable window area + insulation = 1

$$K_u = S_1 S_2 S_3 S_4 \quad [4-3]$$

$$K_u = (0.855)(0.61)(0.75)(1.0) = 0.391 \approx 0.4$$

Being a very conservative number, it can be used in most designs. It is an important factor in all designs of magnetic components.

Window Utilization Factor, K_u for Bobbin Ferrites

In high frequency power electronics, the majority of the designs will use some kind of bobbin ferrite. The main reasons for using ferrites is its high frequency performance and cost. The window utilization factor, K_u , for bobbin ferrites is not as high as it is for iron alloy materials, such as laminations and C cores. Design engineers, who have been using bobbin ferrite materials, know the drawback in the window utilization factor, K_u . Once this problem is understood, then, the problem should go away.

Ferrite materials are fired in kilns like ceramic pottery. There is a certain amount of shrinkage after firing, and the amount varies from one manufacturer's process to another. The amount of shrinkage could vary as much as 15 to 30%, as shown in Figure 4-14. The ferrite manufacturers try to keep a tight control on the amount of shrinkage, because these cores must meet a dimensional tolerance after firing. Even though the shrinkage is under tight control, the tolerances on the end product are much larger than the iron alloy, stamped laminations. The end result is the bobbin has to slip on and meet all of the minimum and maximum dimensional tolerances.

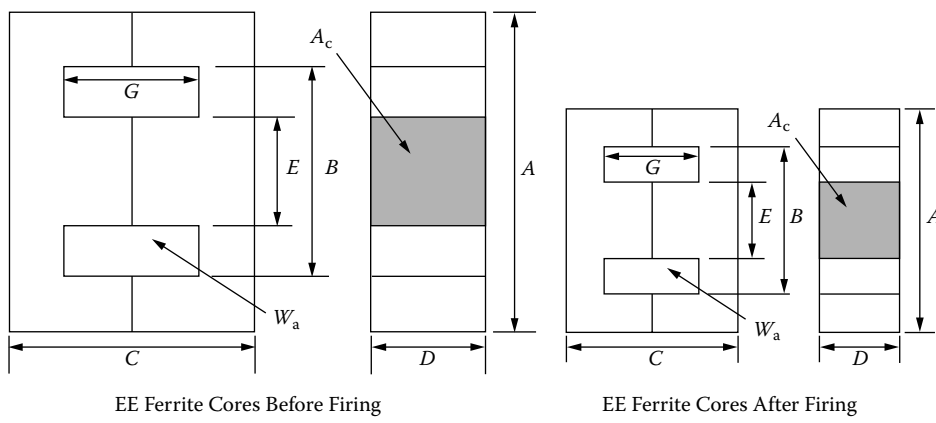


Figure 4-14. Ferrite EE Core Before and After Firing.

This dimensional tolerance has an impact on the winding area of the bobbin, clearly shown in Table 4-6. This smaller winding area reduces the power handling capability of the core. Operating at high frequency will also reduce the power handling capability of the core because of the skin effect. The skin effect requires the use of multistrands of fine wire in place of a large single strand. The selection of the correct wire size to minimize the skin effect at a given frequency is shown in Equations [4-5] through [4-9]. Also shown is an example of the largest wire size that should be used when operating at 100kHz. Reevaluate the, K_u , Equation [4-3] so that it can operate at 100kHz, using a #26 wire, and using a cut ferrite core.

$$S_1 = \text{conductor area/wire area} = 0.79, \#26 \text{ AWG (Transformers)}$$

$$S_1 = \text{conductor area/wire area} = 0.855, \#20 \text{ AWG (DC Inductors)}$$

$$S_2 = \text{wound area/usable window area} = 0.61$$

$$S_3 = \text{usable window area/window area} = 0.6$$

$$S_4 = \text{usable window area/usable window area + insulation} = 1$$

$$K_u = S_1 S_2 S_3 S_4$$

$$K_u = (0.79)(0.61)(0.6)(1.0) = 0.289, [\text{Transformers}] \quad [4-4]$$

$$K_u = (0.855)(0.61)(0.6)(1.0) = 0.313, [\text{DC Inductors}]$$

Table 4-6. Effective Window Area

Effective Window Area			
Core	Window cm ²	Bobbin cm ²	Ratio B/W
RM-6	0.260	0.150	0.577
RM-8	0.449	0.303	0.675
RM-12	1.103	0.730	0.662
PQ-20/16	0.474	0.256	0.540
PQ-26/25	0.845	0.502	0.594
PQ-35/35	2.206	1.590	0.721
EFD-10	0.116	0.042	0.362
EFD-15	0.314	0.148	0.471
EFD-25	0.679	0.402	0.592
EC-35	1.571	0.971	0.618
EC-41	2.082	1.375	0.660
EC-70	6.177	4.650	0.753
Laminations			
EI-187	0.529	0.368	0.696
EI-375	1.512	1.170	0.774
EI-21	1.638	1.240	0.757

Circular mil and Square mil

There are engineers that use Circular mils (CM)/amp or square mils/amp. This is the reciprocal current density. The norm is to use amps/cm², which is a true current density. There have been some requests to define circular mils and square mils. First, let's define a mil, which is .001 inch. [Figure 4-15](#) shows the area of a square mil, and the area of a circular mil.

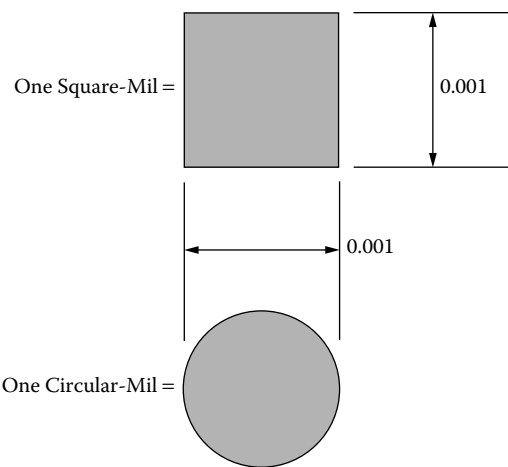


Figure 4-15. Comparing Circular-Mils and Square-Mils.

To convert Square mils to Circular mils, multiply by 1.2732.

To convert Circular mils to Square mils, multiply by 0.7854.

To convert Circular mils to Square centimeters, multiply by 5.066×10^{-6} .

To convert Square mils to Square centimeters, multiply by 6.45×10^{-6} .

Note: Designers have used this rule of thumb for many years:

$$500\text{CM/Amp} \approx 400 \text{Amps/cm}^2$$

$$1000\text{CM/Amp} \approx 200 \text{Amps/cm}^2$$

Magnet Wire

Standard magnet wire is available in three different materials, shown in Table 4-7. The most common material is copper, but aluminum and silver are available. Aluminum magnet wire is one-third the weight of copper for the same size conductor and one-half the weight for the same conductivity. Aluminum magnet wire is a little more difficult to terminate, but it can be done. Silver magnet wire has the highest conductivity, is easy to solder to, and weighs 20% more than copper.

Table 4-7. Magnet Wire Material Properties

Magnet Wire Material Properties						
Material	Symbol	Density grams/cm ³	Resistivity $\mu\Omega/\text{cm}$	Weight Factor	Resistance Factor	Temperature Coefficient
Copper	Cu	8.89	1.72	1	1	0.00393
Silver	Ag	10.49	1.59	1.18	0.95	0.00380
Aluminum	Al	2.703	2.83	0.3	1.64	0.00410

Magnet Wire, Film Insulation

It is the design engineer's responsibility to ensure that the selected magnet wire used in the design is compatible with the environmental and design specification. The environmental specification will set the ambient temperature. The maximum operating temperature of the magnet wire is obtained by summing the maximum ambient temperature, plus the temperature rise of the magnetic component. After the maximum temperature has been obtained, see Table 4-8 for the Temperature Class. The magnet wire insulation guide listing in [Table 4-7](#), is only a partial list from NEMA, Standard MW 1000.

The maximum operating temperature is the "Achilles Heel" to the magnet wire. Standard magnet wire is rated by temperature. The range is from 105°C to 220°C, as shown in Table 4-8. The insulation film of the magnet wire is on the surface of the copper wire. This insulation film is the most vulnerable to thermal overloads, so the selection of the insulation film is very critical for long life. When magnet wire is subjected to thermal overloads, or a high ambient temperature above its rated temperature, the life of the magnet wire is greatly reduced, as shown in [Figures 4-16](#) and [4-17](#). The engineer must be very careful of hot spots so as not to degrade the service life of the magnetic component.

Table 4-8. Magnet Wire Insulation Guide

Magnet Wire Insulation Guide			
Temperature Class	Insulation Type	Dielectric Constant	NEMA Standard MW 1000
105°C	Polyurethane*	6.20	MW-2-C
105°C	Formvar	3.71	MW-15-C
130°C	Polyurethane-Nylon*	6.20	MW-28-C
155°C	Polyurethane-155	6.20	MW-79-C
180°C	Polyester Solderable*	3.95	MW-77-C
200°C	Polyester-amid-imide	4.55	MW-35-C
220°C	Polyimide (ML)	3.90	MW-16-C

* Solderable insulations.

Wire Table

[Table 4-9](#) is the Wire Table for AWG, 10 to 44, heavy film wire. The bare wire areas are given in cm² in column 2, and the circular mils are given in column 3 for each wire size. The equivalent resistance in micro-ohms per centimeter ($\mu\Omega/cm$ or $10^{-6} \Omega/cm$) is given in column 4 for each wire size. Columns 5 through 13 relate to the heavy, insulated film coating. The weight of the magnet wire is found in column 13, in grams, per centimeter.

[Table 4-10](#) provides the maximum outside diameter for magnet wire with single, heavy, triple, and quad film insulation. The dimensional data is in centimeters and inches, for AWG 10 through 44.

Table 4-9. Wire Table

Wire Table												
AWG	Bare Area		Resistance $\mu\Omega/cm$ 20°C	Heavy Synthetics								
				Area		Diameter		Turns-Per		Turns-Per		Weight
	cm ² (10 ⁻³)	cir-mil		cm ² (10 ⁻³)	cir-mil	cm	Inch	cm	Inch	cm ²	Inch ²	gm/cm
1	2	3	4	5	6	7	8	9	10	11	12	13
10	52.6100	10384.00	32.7	55.9000	11046.00	0.2670	0.105	3.9	10	11	69	0.46800
11	41.6800	8226.00	41.4	44.5000	8798.00	0.2380	0.094	4.4	11	13	90	0.37500
12	33.0800	6529.00	52.1	35.6400	7022.00	0.2130	0.084	4.9	12	17	108	0.29770
13	26.2600	5184.00	65.6	28.3600	5610.00	0.1900	0.075	5.5	13	21	136	0.23670
14	20.8200	4109.00	82.8	22.9500	4556.00	0.1710	0.068	6.0	45	26	169	0.18790
15	16.5100	3260.00	104.3	18.3700	3624.00	0.1530	0.060	6.8	17	33	211	0.14920
16	13.0700	2581.00	131.8	14.7300	2905.00	0.1370	0.054	7.3	19	41	263	0.11840
17	10.3900	2052.00	165.8	11.6800	2323.00	0.1220	0.048	8.2	21	51	331	0.09430
18	8.2280	1624.00	209.5	9.3260	1857.00	0.1090	0.043	9.1	23	64	415	0.07474
19	6.5310	1289.00	263.9	7.5390	1490.00	0.0980	0.039	10.2	26	80	515	0.05940
20	5.1880	1024.00	332.3	6.0650	1197.00	0.0879	0.035	11.4	29	99	638	0.04726
21	4.1160	812.30	418.9	4.8370	954.80	0.0785	0.031	12.8	32	124	800	0.03757
22	3.2430	640.10	531.4	3.8570	761.70	0.0701	0.028	14.3	36	156	1003	0.02965
23	2.5880	510.80	666.0	3.1350	620.00	0.0632	0.025	15.8	40	191	1234	0.02372
24	2.0470	404.00	842.1	2.5140	497.30	0.0566	0.022	17.6	45	239	1539	0.01884
25	1.6230	320.40	1062.0	2.0020	396.00	0.0505	0.020	19.8	50	300	1933	0.01498
26	1.2800	252.80	1345.0	1.6030	316.80	0.0452	0.018	22.1	56	374	2414	0.01185
27	1.0210	201.60	1687.0	1.3130	259.20	0.0409	0.016	24.4	62	457	2947	0.00945
28	0.8046	158.80	2142.0	1.0515	207.30	0.0366	0.014	27.3	69	571	3680	0.00747
29	0.6470	127.70	2664.0	0.8548	169.00	0.0330	0.013	30.3	77	702	4527	0.00602
30	0.5067	100.00	3402.0	0.6785	134.50	0.0294	0.012	33.9	86	884	5703	0.00472
31	0.4013	79.21	4294.0	0.5596	110.20	0.0267	0.011	37.5	95	1072	6914	0.00372
32	0.3242	64.00	5315.0	0.4559	90.25	0.0241	0.010	41.5	105	1316	8488	0.00305
33	0.2554	50.41	6748.0	0.3662	72.25	0.0216	0.009	46.3	118	1638	10565	0.00241
34	0.2011	39.69	8572.0	0.2863	56.25	0.0191	0.008	52.5	133	2095	13512	0.00189
35	0.1589	31.36	10849.0	0.2268	44.89	0.0170	0.007	58.8	149	2645	17060	0.00150
36	0.1266	25.00	13608.0	0.1813	36.00	0.0152	0.006	62.5	167	3309	21343	0.00119
37	0.1026	20.25	16801.0	0.1538	30.25	0.0140	0.006	71.6	182	3901	25161	0.00098
38	0.0811	16.00	21266.0	0.1207	24.01	0.0124	0.005	80.4	204	4971	32062	0.00077
39	0.0621	12.25	27775.0	0.0932	18.49	0.0109	0.004	91.6	233	6437	41518	0.00059
40	0.0487	9.61	35400.0	0.0723	14.44	0.0096	0.004	103.6	263	8298	53522	0.00046
41	0.0397	7.84	43405.0	0.0584	11.56	0.0086	0.003	115.7	294	10273	66260	0.00038
42	0.0317	6.25	54429.0	0.0456	9.00	0.0076	0.003	131.2	333	13163	84901	0.00030
43	0.0245	4.84	70308.0	0.0368	7.29	0.0069	0.003	145.8	370	16291	105076	0.00023
44	0.0202	4.00	85072.0	0.0316	6.25	0.0064	0.003	157.4	400	18957	122272	0.00020

Table 4-10. Dimensional Data for Film Insulated Magnetic Wire

Dimensional Data for Film Insulated Magnetic Wire								
Wire Size AWG	Maximum Diameter							
	Single-Insulation		Heavy-Insulation		Triple-Insulation		Quad-Insulation	
	Inches	Centimeters	Inches	Centimeters	Inches	Centimeters	Inches	Centimeters
10	0.1054	0.2677	0.1071	0.2720	0.1084	0.2753	0.1106	0.2809
11	0.9410	2.3901	0.0957	0.2431	0.0969	0.2461	0.0991	0.2517
12	0.0840	0.2134	0.0855	0.2172	0.0867	0.2202	0.0888	0.2256
13	0.0750	0.1905	0.0765	0.1943	0.0776	0.1971	0.0796	0.2022
14	0.0670	0.1702	0.0684	0.1737	0.0695	0.1765	0.0715	0.1816
15	0.0599	0.1521	0.0613	0.1557	0.0624	0.1585	0.0644	0.1636
16	0.0534	0.1356	0.0548	0.1392	0.0558	0.1417	0.0577	0.1466
17	0.0478	0.1214	0.0492	0.1250	0.0502	0.1275	0.0520	0.1321
18	0.0426	0.1082	0.0440	0.1118	0.0450	0.1143	0.0468	0.1189
19	0.0382	0.0970	0.0395	0.1003	0.0404	0.1026	0.0422	0.1072
20	0.0341	0.0866	0.0353	0.0897	0.0362	0.0919	0.0379	0.0963
21	0.0306	0.0777	0.0317	0.0805	0.0326	0.0828	0.0342	0.0869
22	0.0273	0.0693	0.0284	0.0721	0.0292	0.0742	0.0308	0.0782
23	0.0244	0.0620	0.0255	0.0648	0.0263	0.0668	0.0279	0.0709
24	0.0218	0.0554	0.0229	0.0582	0.0237	0.0602	0.02520	0.06401
25	0.0195	0.0495	0.0206	0.0523	0.0214	0.0544	0.0228	0.0579
26	0.0174	0.0442	0.0185	0.0470	0.0192	0.0488	0.0206	0.0523
27	0.0156	0.0396	0.0165	0.0419	0.0172	0.0437	0.0185	0.0470
28	0.0139	0.0353	0.0148	0.0376	0.0155	0.0394	0.0166	0.0422
29	0.0126	0.0320	0.0134	0.0340	0.0141	0.0358	0.0152	0.0386
30	0.0112	0.0284	0.0120	0.0305	0.0127	0.0323	0.0137	0.0348
31	0.0100	0.0254	0.0108	0.0274	0.0115	0.0292	0.0124	0.0315
32	0.0091	0.0231	0.0098	0.0249	0.0105	0.0267	0.0113	0.0287
33	0.0081	0.0206	0.0088	0.0224	0.0095	0.0241	0.0102	0.0259
34	0.0072	0.0183	0.0078	0.0198	0.0084	0.0213	0.0091	0.0231
35	0.0064	0.0163	0.0070	0.0178	0.0076	0.0193	0.0082	0.0208
36	0.0058	0.0147	0.0063	0.0160	0.0069	0.0175	0.0074	0.0188
37	0.0052	0.0132	0.0057	0.0145	0.0062	0.0157	0.0067	0.0170
38	0.0047	0.0119	0.0051	0.0130	0.0056	0.0142	0.0060	0.0152
39	0.0041	0.0104	0.0045	0.0114	0.0050	0.0127	0.0053	0.0135
40	0.0037	0.0094	0.0040	0.0102	0.0044	0.0112	0.0047	0.0119
41	0.0033	0.0084	0.0036	0.0091	0.0040	0.0102	0.0043	0.0109
42	0.0030	0.0076	0.0032	0.0081	0.0037	0.0094	0.0038	0.0097
43	0.0026	0.0066	0.0029	0.0074	0.0033	0.0084	0.0035	0.0089
44	0.0024	0.0061	0.0027	0.0069	0.0030	0.0076	0.0032	0.0081

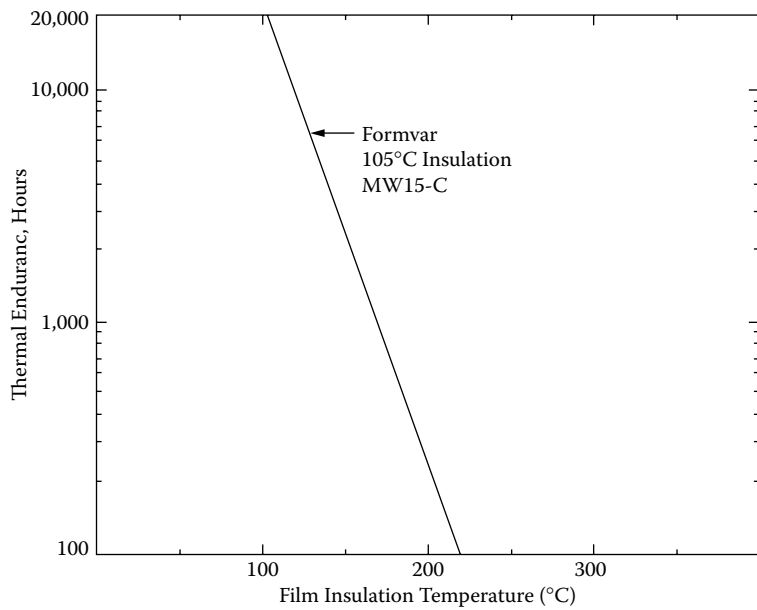


Figure 4-16. Thermal Endurance, for 105°C Formvar Insulation.

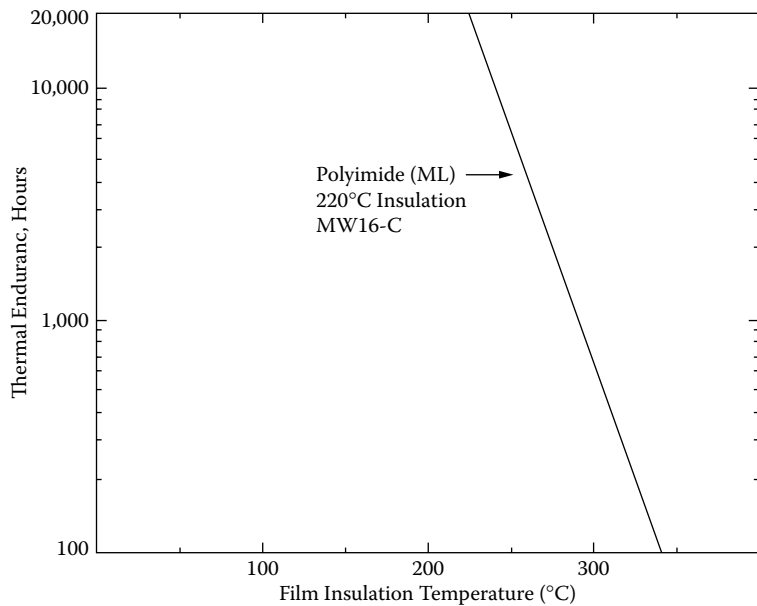


Figure 4-17. Thermal Endurance for 220°C Polyimide Insulation (ML).

Solderable Insulation

Solderable insulation is a special film insulation that is used on magnet wire in low cost, high volume applications. The magnet wire, with this solderable insulation, is wrapped around the terminal or pin, as shown in [Figure 4-18](#). Then the terminal can be dip-soldered at the prescribed temperature without prior stripping. The ambient temperature range for this type of film insulation is 105°C to 180°C.

There are drawbacks in using some of the solderable insulation magnet wire. Prior to using, check your application with the wire manufacturer. Some solderable film insulation is not recommended where severe overloads may occur. Some solderable film insulations are susceptible to softening, due to prolonged exposure to strong solvents, such as alcohol, acetone, and methylethylketone.

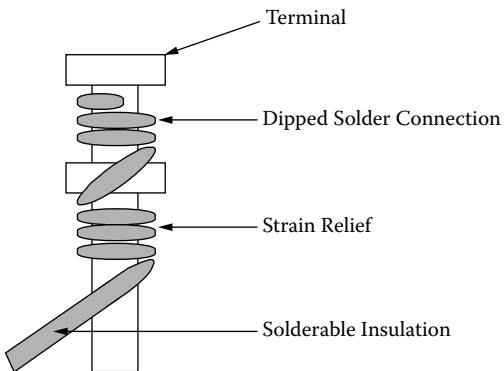


Figure 4-18. Solderable Insulation on a Dip Solder Terminal.

Bondable Magnet Wire

Bondable, magnet wires are a film-coated, copper or aluminum, with an additional coating of a thermoplastic adhesive. See Figure 4-19. They are used in applications where it is desirable to have the bonding agent, such as a solvent, which will hold the coil form until it is oven-baked. Most adhesive coatings can be softened with solvents or heat. If a coil is wound with an irregular shape, held in a form, and then raised to the appropriate temperature, the coil will retain its shape. Bondable magnet wires have applications such as armatures, field coils, and self-supporting coils.

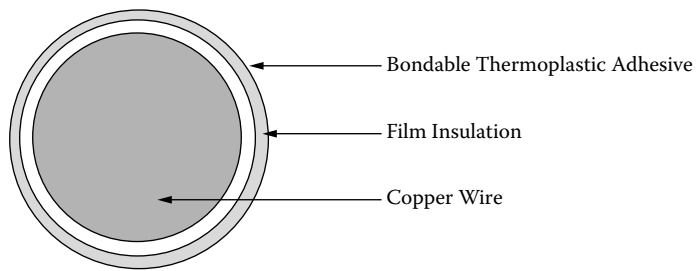


Figure 4-19. Typical Cross-Section of a Bondable Magnet Wire.

Base Film Insulation

All conventional film insulations may be adhesive-coated to achieve a bondable wire. However, care should be taken in selecting wires, which are insulated with high temperature films, since the adhesive coating may not withstand the equally high temperatures. See [Table 4-11](#). The temperatures, in Table 4-11, are for reference

only. It is wise to always check with the manufacturer for the latest in materials and application notes. The addition of the adhesive coating over the film insulation will result in an increase in the finished diameter, by the same magnitude, as if going from a single to a heavy insulation.

Table 4-11. Bondable Overcoats

Bondable Overcoats			
Type	Operating Temperature	Heat Activation Temperature	Solvents Activating Agents
Polyvinyl Butryal	105°C	120° - 140°C	Alcohol
Epoxy	130°C	130° - 150°C	Methylethylketone Acetone
Polyester	130°C	130° - 150°C	Methylethylketone
Nylon	155°C	180° - 220°C	None

Bonding Methods

Heat Bonding may be accomplished by the use of a temperature-controlled oven. Small components can use a controlled hot air blower to bond the wires. In either case, caution should be used when handling the coil while it is still hot, since deformation can take place.

Resistance Bonding is a method where a current is passed through the winding to achieve the desired bonding temperature. This method generates a very even, heat distribution resulting in a good bonding throughout the winding. Many coils can be resistance-bonded at the same time. The current required for one coil, will be the same current required when many are connected in series. Just solder the coils in series then adjust the applied voltage until the same current is reached.

Solvent Bonding is a method where the solvent activates the bonding material. This can be done, by passing the wire through a solvent-saturated felt pad or a light spray application. There are many activating solvents that can be used: denatured ethyl alcohol, isopropyl alcohol, methylethylketone and acetone. The solvents should always be checked on with the manufacturer for the latest in materials and for application notes.

Miniature Square Magnet Wire

When product miniaturization calls for more copper in a given area, MWS Microsquare film, insulated magnet wire allows the design of compact coils to deliver more power in less space. See [Table 4-12](#). Microsquare magnet wire is available in both copper and aluminum. It is also available in a range of solderable and high temperature film insulation. A cross-section of a Number 26, heavy-build, microsquare magnet wire is shown in [Figure 4-20](#).

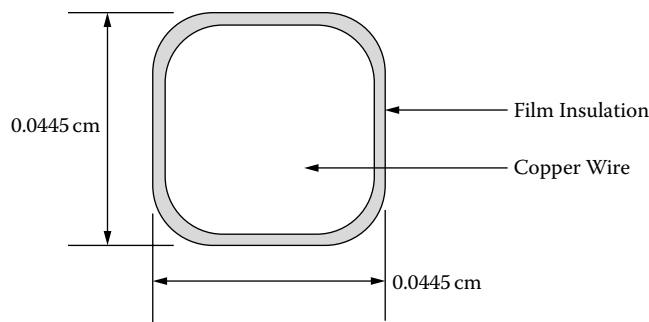


Figure 4-20. Cross-Section of a #26, Heavy-build, Microsquare Magnet Wire.

Table 4-12. Micro-Square Magnetic Wire (Nominal Dimension)

Micro-Square Magnetic Wire (Nominal Dimension)								
Wire Size AWG	Bare Width cm	Bare Width Inch	Wire Area cm ²	Wire Area sq-mils	Copper Resistance Ω/cm	Aluminum Resistance Ω/cm	Single Width cm	Heavy Width cm
15	0.1450	0.0571	0.019614	3041	0.0000879	0.000144	0.1483	0.1514
16	0.1290	0.0508	0.015228	2361	0.0001132	0.000186	0.1323	0.1354
17	0.1151	0.0453	0.011816	1832	0.0001459	0.000239	0.1184	0.1212
18	0.1024	0.0403	0.009675	1500	0.0001782	0.000293	0.1054	0.1080
19	0.0912	0.0359	0.007514	1165	0.0002294	0.000377	0.0940	0.0968
20	0.0813	0.0320	0.006153	954	0.0002802	0.000460	0.0841	0.0866
21	0.0724	0.0285	0.004786	742	0.0003602	0.000591	0.0749	0.0772
22	0.0643	0.0253	0.003935	610	0.0004382	0.000719	0.0668	0.0688
23	0.0574	0.0226	0.003096	480	0.0005568	0.000914	0.0599	0.0620
24	0.0511	0.0201	0.002412	374	0.0007147	0.001173	0.0536	0.0556
25	0.0455	0.0179	0.002038	316	0.0008458	0.001388	0.0480	0.0498
26	0.0404	0.0159	0.001496	232	0.0011521	0.001891	0.0427	0.0445
27	0.0361	0.0142	0.001271	197	0.0013568	0.002227	0.0389	0.0409
28	0.0320	0.0126	0.001006	156	0.0017134	0.002813	0.0348	0.0366
29	0.0287	0.0113	0.000787	122	0.0021909	0.003596	0.0312	0.0330
30	0.0254	0.0100	0.000587	91	0.0029372	0.004822	0.0277	0.0295

Multistrand Wire and Skin Effect

Electronic equipment now operates at higher frequencies. With direct current and low frequencies the efficiency can be predicted. The current carried by the conductor is distributed uniformly across the cross-section of the conductor. The flux generated by the magnet wire is shown in [Figure 4-21](#). There is a concentration of current near the wire surface at higher frequencies, which is termed the skin effect. This is the result of magnetic flux lines that generate eddy currents in the magnet wire, as shown in [Figure 4-22](#).

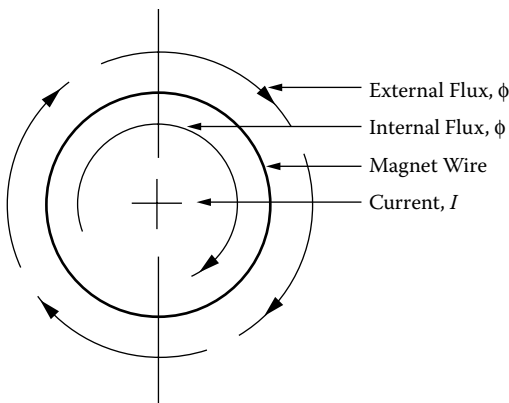


Figure 4-21. Flux Distribution in a Magnet Wire.

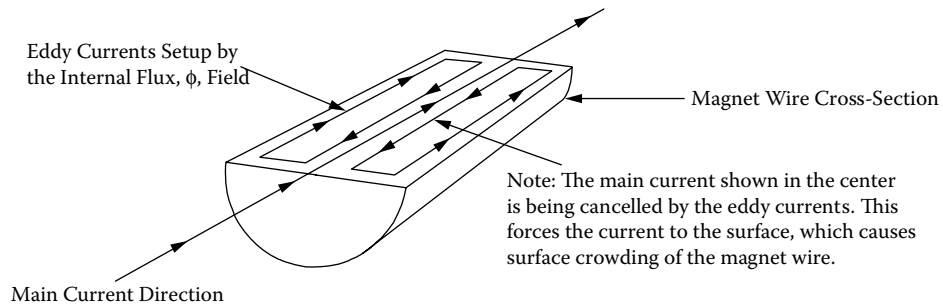


Figure 4-22. Eddy Currents Generated in a Magnet Wire.

Reduce Skin Effect in Transformers

Skin effect accounts for the fact that the ratio of effective alternating current resistance to direct current is greater than unity. The magnitude of this effect, at high frequency on conductivity, magnetic permeability, and inductance, is sufficient to require further evaluation of conductor size, during design. The skin depth is defined as the distance below the surface, where the current density has fallen to $1/\epsilon$ or 37 percent of its value at the surface.

$$\epsilon = \left(\frac{6.62}{\sqrt{f}} \right) K, \quad [\text{cm}] \quad [4-5]$$

ϵ , is the skin depth
 f , is frequency in hertz
 K , is equal to 1 for copper

When selecting the wire for high frequency, select a wire where the relationship between the ac resistance and the dc resistance is 1.

$$R_R = \frac{R_{ac}}{R_{dc}} = 1 \quad [4-6]$$

Using this approach, select the largest wire, operating at 100 kHz.

$$\begin{aligned}\varepsilon &= \left(\frac{6.62}{\sqrt{f}} \right) K, \quad [\text{cm}] \\ \varepsilon &= \left(\frac{6.62}{\sqrt{100,000}} \right) (1), \quad [\text{cm}] \\ \varepsilon &= 0.0209, \quad [\text{cm}]\end{aligned}\quad [4-7]$$

The wire diameter is:

$$\begin{aligned}D_{AWG} &= 2(\varepsilon), \quad [\text{cm}] \\ D_{AWG} &= 2(0.0209), \quad [\text{cm}] \\ D_{AWG} &= 0.0418, \quad [\text{cm}]\end{aligned}\quad [4-8]$$

The bare wire area $A_{w(B)}$ is:

$$\begin{aligned}A_{w(B)} &= \frac{\pi D_{AWG}^2}{4}, \quad [\text{cm}^2] \\ A_{w(B)} &= \frac{(3.14)(0.0418)}{4}, \quad [\text{cm}^2] \\ A_{w(B)} &= 0.00137, \quad [\text{cm}^2]\end{aligned}\quad [4-9]$$

The wire size closest to this area of 0.00137 is AWG #26 with 0.00128 cm². (See [Table 4-9](#).)

Calculating Skin Effect in Inductors

Inductors have skin effect problems just like transformers. The skin effect depends on the amount of ac current ΔI in the inductor. The high frequency inductor current has two components: the dc current, I_{dc} , and the ac current, ΔI . The dc current travels in the center of the conductor, and the ac travels on the surface of the conductor, as shown in Figure 4-23.

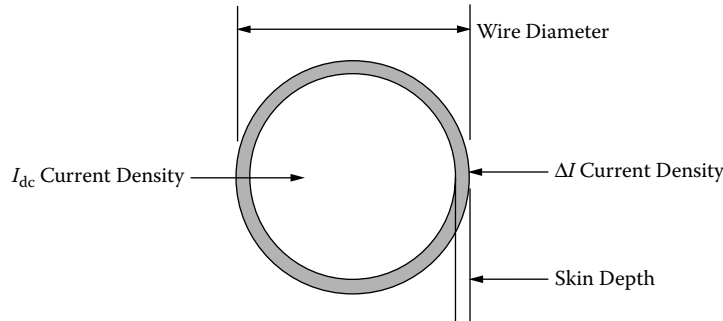


Figure 4-23. DC Inductor High Frequency Current Distribution.

The following procedure is used to calculate the high frequency current density, ΔI , while using Figure 4-23, as a reference.

Calculating Skin Effect in Inductors

4-25

The skin depth Equation is:

$$\epsilon = \left(\frac{6.62}{\sqrt{f}} \right) K, \quad [\text{cm}] \quad [4-10]$$

Calculate the diameter of the copper conductor:

$$D_{AWG} = \sqrt{\frac{4(A_{w(B)})}{\pi}}, \quad [\text{cm}] \quad [4-11]$$

Subtract two times the skin depth, ϵ , from the diameter, D_{AWG} .

$$D_n = D_{AWG} - 2\epsilon, \quad [\text{cm}] \quad [4-12]$$

Calculate the new wire area, A_n .

$$A_n = \frac{\pi(D_n)^2}{4}, \quad [\text{cm}^2] \quad [4-13]$$

The high frequency wire area, $A_{w(\Delta I)}$, is the difference between the wire area, $A_{w(B)}$, and the new area, A_n .

$$A_{w(\Delta I)} = A_{w(B)} - A_n, \quad [\text{cm}^2] \quad [4-14]$$

The ac current, ΔI , in an inductor is a triangular waveform. The, ΔI_{rms} , current is:

$$\Delta I_{rms} = I_{pk} \sqrt{\frac{1}{3}}, \quad [\text{amps}] \quad [4-15]$$

Calculate the current density for the delta rms current, ΔI_{rms} .

$$J = \frac{\Delta I_{rms}}{A_{w(\Delta I)}}, \quad [\text{amps-per-cm}^2] \quad [4-16]$$

The delta rms current, ΔI_{rms} , current density, J , should be:

$$\Delta I_{rms} \text{ current density} \leq I_{dc} \text{ current density}$$

A graph of Skin Depth, as a function of frequency, is shown in Figure 4-24. The relationship of Skin Depth to AWG radius is shown in Figure 4-25, where $R_{ac}/R_{dc} = 1$, is plotted on a graph of AWG versus frequency.

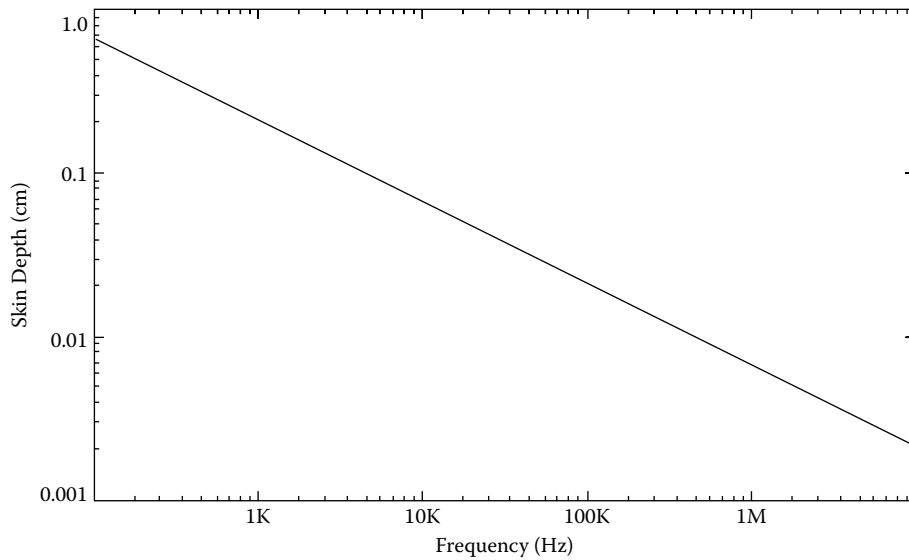


Figure 4-24. Skin Depth Versus Frequency.

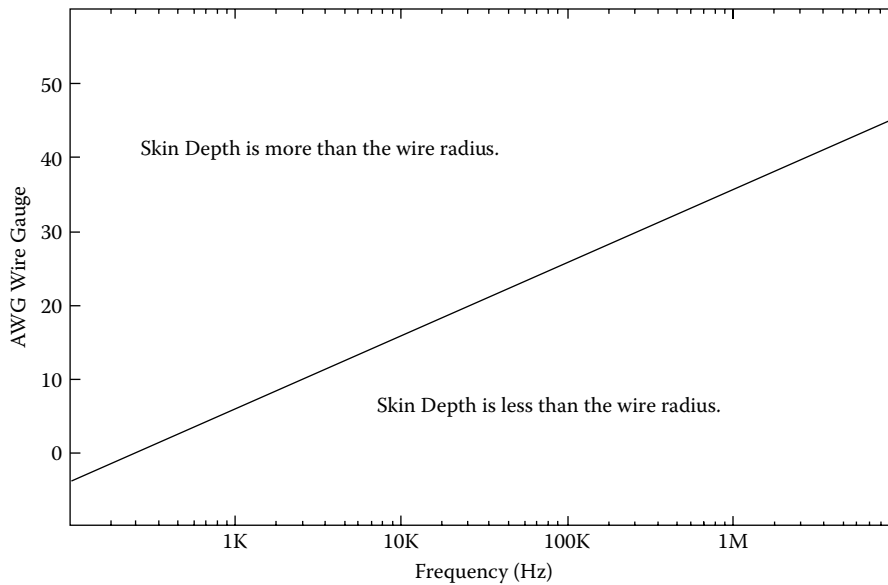


Figure 4-25. AWG Versus Frequency at Which Skin Depth Equals the Radius.

To illustrate how the AWG ac/dc resistance ratio changes with frequency, see [Table 4-13](#). In Table 4-13, it can be seen that when a converter operates at 100 kHz, the largest wire that should be used is a Number 26, with an ac/dc resistance ratio of 1.001.

Table 4-13. AWG ac/dc Resistance Ratio at Common Converter Frequencies

AWG	D _(AWG) cm	AWG ac/dc Resistance Ratio at Common Converter Frequencies							
		25 kHz		50 kHz		100 kHz		200 kHz	
		ε cm	R _{ac} R _{dc}	ε cm	R _{ac} R _{dc}	ε cm	R _{ac} R _{dc}	ε cm	R _{ac} R _{dc}
12	0.20309	0.041868	1.527	0.029606	2.007	0.020934	2.704	0.014802	3.699
14	0.16132	0.041868	1.300	0.029606	1.668	0.020934	2.214	0.014802	2.999
16	0.12814	0.041868	1.136	0.029606	1.407	0.020934	1.829	0.014802	2.447
18	0.10178	0.041868	1.032	0.029606	1.211	0.020934	1.530	0.014802	2.011
20	0.08085	0.041868	1.001	0.029606	1.077	0.020934	1.303	0.014802	1.672
22	0.06422	0.041868	1.000	0.029606	1.006	0.020934	1.137	0.014802	1.410
24	0.05101	0.041868	1.000	0.029606	1.000	0.020934	1.033	0.014802	1.214
26	0.04052	0.041868	1.000	0.029606	1.000	0.020934	1.001	0.014802	1.078
28	0.03219	0.041868	1.000	0.029606	1.000	0.020934	1.000	0.014802	1.006
30	0.02557	0.041868	1.000	0.029606	1.000	0.020934	1.000	0.014802	1.000
AWG Copper, skin depth is at 20°C.									

Multistrand Litz Wire

The term litz wire is extracted from the German word, meaning woven wire. Litz wire is generally defined, as a wire constructed of individually, film insulated wires, braided together in a uniform pattern of twists and length of lay. This multistrand configuration minimizes the power losses, otherwise encountered, in a solid conductor, due to the skin effect. The minimum and maximum number of strand for standard litz wire is shown in Table 4-14. Magnet wire suppliers will supply larger, twisted magnet wire, on request.

Table 4-14. Standard Litz Wire

Standard Litz Wire				
AWG	Minimum Strands	Approximate AWG	Maximum Strands	Approximate AWG
30	3	25	20	17.0
32	3	27	20	19.0
34	3	29	20	21.0
36	3	31	60	18.5
38	3	33	60	20.5
40	3	35	175	18.0
41	3	36	175	18.5
42	3	37	175	19.5
43	3	38	175	21.0
44	3	39	175	21.5
45	3	40	175	22.5
46	3	41	175	23.5
47	3	42	175	25.0
48	3	43	175	25.5

Proximity Effect

The operating frequency for power supplies is now in the range of 50 to 500 kHz. With it came along some new tasks for the engineer to address, skin effect and proximity effect. They are quite similar in that they both generate eddy currents in the magnet wire. The eddy currents produced by these effects have the same solution, keeping the ratio of the ac resistance, R_{ac} , to the dc resistance, R_{dc} down:

$$R_R = \frac{R_{ac}}{R_{dc}} \quad [4-17]$$

The information provided here on proximity effect is taken from the five References provided at the end of this Chapter. The references are excellent, providing an in-depth analysis of the losses due to proximity effect, which is beyond the intent of this effort.

Proximity effect is caused by eddy currents induced in a wire due to the alternating magnetic field of other conductors in the vicinity. The flux generated by the magnet wire is shown in Figure 4-26. The eddy currents cause a distortion of the current density. This distortion is the result of magnetic flux lines that generate eddy currents in the magnet wire, therefore enhancing the main current, I , on one side and subtracting from the main current on the other, as shown in Figure 4-27. A magnet wire with its distorted current density is shown in Figure 4-28.

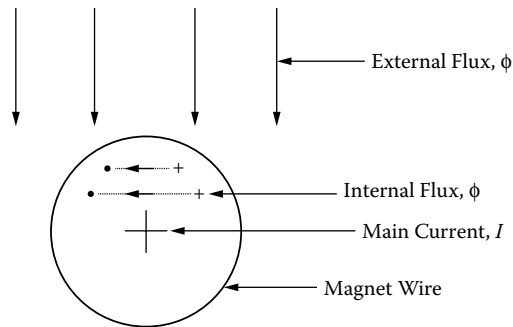


Figure 4-26. Flux Distribution in a Magnet Wire.

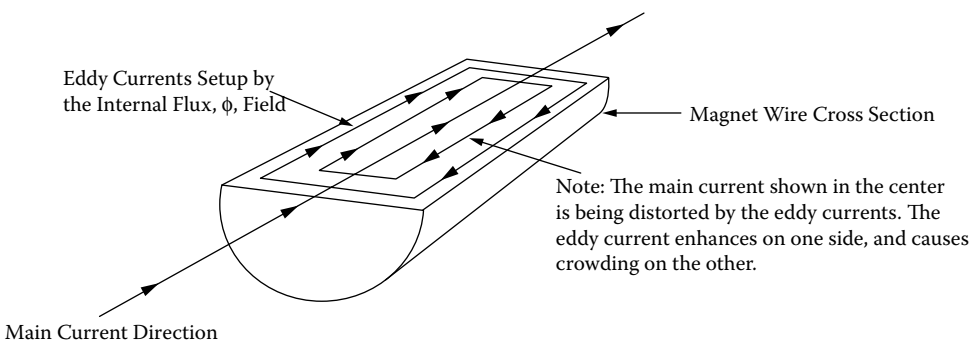


Figure 4-27. Eddy Currents Generated in a Magnet Wire.

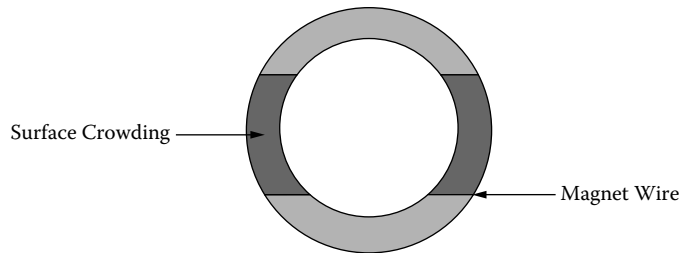


Figure 4-28. Magnet Wire, Showing Distorted Surface Crowding.

Proximity Effect in Transformers

Proximity effect has a minimum of impact on a transformer with a single layer secondary, as shown in Figure 4-29 along with its low frequency magneto-motive force (mmf) diagram. Keeping the proximity effect to a minimum requires the transformer to be designed with a minimum of layers. The selection of a core with a long narrow window will produce a design with a minimum of layers, in the same way as picking a core for a minimum of leakage inductance.

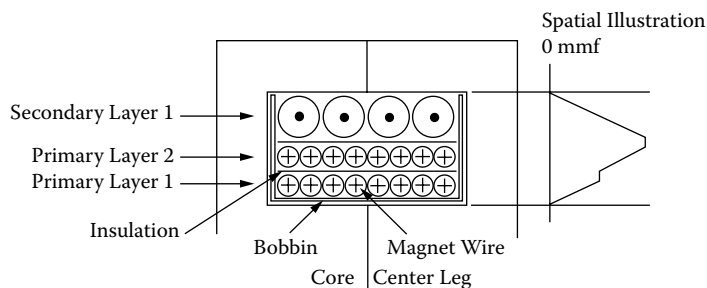


Figure 4-29. Simple Transformer Showing mmf.

Multiple Layer High Frequency Transformers and High Loss

The proximity effect is outlined for a transformer having a secondary with three layers, evenly spaced, as shown in Figure 4-30. A schematic diagram version of the transformer is shown in Figure 4-31, showing the different magneto-motive force (mmf = F_m) potentials. It is assumed that the high frequency penetration depth

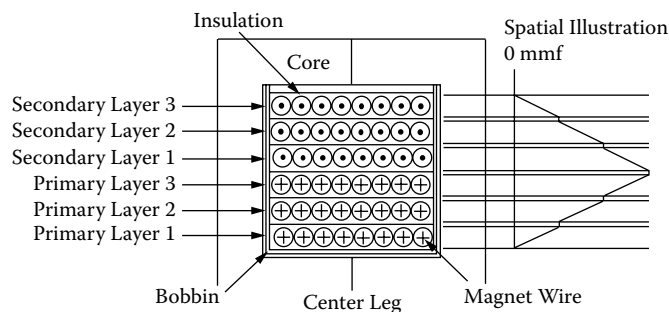


Figure 4-30. A Simple Transformer, Showing the Magneto-Motive Force, mmf.

is twenty-five percent. The transformer has a 24 turn primary and a 24 turn secondary at 1 ampere. The transformer, A-T or magneto-motive force, (mmf) or F_m , is equal to 24.

$$F_m = NI, \text{ [magneto-motive force, mmf]} \quad [4-18]$$

cgs, $F_m = 0.8NI, \text{ [magneto-motive force, mmf]}$

The schematic diagram as shown in Figure 4-31, is used as a guide to show how the proximity effect impacts the layer wound transformers. The load current, I_o , equals 1 amp, and the secondary will have three identical layers, with each layer having eight turns. Due to the skin effect or penetration depth, each wire uses only 25% of the available area. Therefore, the current will be crowded into 25% of the available copper wire.

To the right of S3, the mmf is 0. At the left of S3, $F_m = 8 \text{ A-T}$.

1. The magnet field, ϕ_3 , set up by the load current, I_o , of 1 amp in layer S3 will generate a current, I_{g3} , in the winding layer, S2. It is in the opposite direction to the normal current flow and cancels the load current, I_o . The magneto-motive force, F_m , will generate 16 A-T or $I_c = 2$ amps to preserve the original load current, I_o , of 1 amp.
2. The magnet field, ϕ_2 , set up by the load current, I_o , plus the difference between, I_c and I_g , in S2 will generate, $2I_g$, in the winding layer, S1. This is in the opposite direction to the normal current flow that cancels the load current, I_o , out. The magneto-motive force, F_m , will generate, 24 A-T or $I_c = 3$ amps, to preserve the original load current, I_o , equals 1 amp.

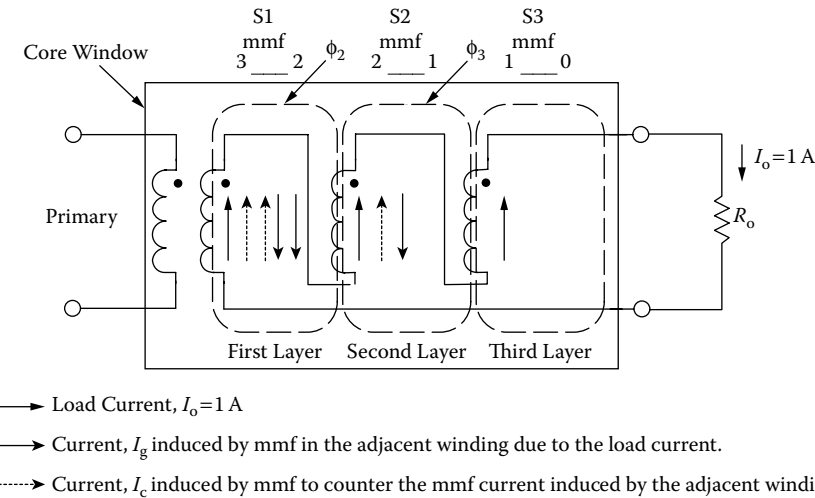


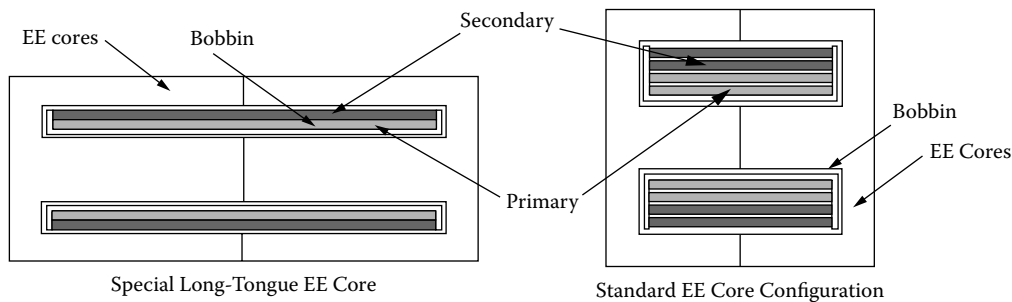
Figure 4-31. Transformer Schematic Diagram Showing mmf.

If the current in each layer is just the 1 amp, and limited in penetration, due to skin effect of only 25% of the conductor's thickness, the ac to dc resistance ratio, R_R , would be 4:1. The surface currents successive layers become much larger, as discussed above. The winding currents are tabulated in [Table 4-15](#). The summation of the currents is given in Table 4-15. The current, I_g , is the adjacent winding induced current. The current, I_c , is the counter-current induced by the magneto-motive force, mmf.

Table 4-15. Secondary Current Levels

Secondary Current Levels						
Winding	I_o	I_c	$I_o + I_c$	$I_o + I_c$	I_g	Total Wire Current
	amps	amps	amps	amps ²	amps	amps ²
S3	1	0	1	1	0	$(I_o + I_c)^2 = 1$
S2	1	1	2	4	1	$(I_o + I_c)^2 + (I_g)^2 = 5$
S1	1	2	3	9	2	$(I_o + I_c)^2 + (I_g)^2 = 13$

It can be seen, from the data in Table 4-15 that transformers with multiple layers operating at high frequency could be a real problem with proximity effect. The eddy current losses caused by the proximity effect go up exponentially as the number of layers. The selection of a core with a long winding length to a winding height ratio, will reduce the number of layers to a minimum, as shown in Figure 4-32.

**Figure 4-32.** Comparing the Standard and the Special Long Tongue EE Cores.

Proximity Effect Using Dowell Curves

Dowell curves on proximity effect are shown in Figure 4-33. The vertical scale is, R_R , the ratio of, R_{ac} , to R_{dc} . The horizontal scale, K, is the ratio of the effective conductor height, or layer thickness, to the penetration depth, ϵ . On the right side of the curve it is labeled Number of Layers. These are segmented layers. Segmented layers are when the secondary is interleaved with the primary, then, each separation is a segment. The equation for K is:

$$K = \frac{h\sqrt{F_l}}{\epsilon} \quad [4-19]$$

$$h = 0.866D_{AWG}$$

Where:

$$F_l = \frac{ND_{AWG}}{l_w} \quad [4-20]$$

The variables in Equation 4-20 are described in Figure 4-34. It can be seen that if the number of turns, N, times the wire diameter, D_{AWG} , are equal to the winding length, l_w , then, Equation 4-21 is simplified to:

$$K = \frac{h}{\varepsilon} \quad [4-21]$$

$$h = 0.866D_{AWG}$$

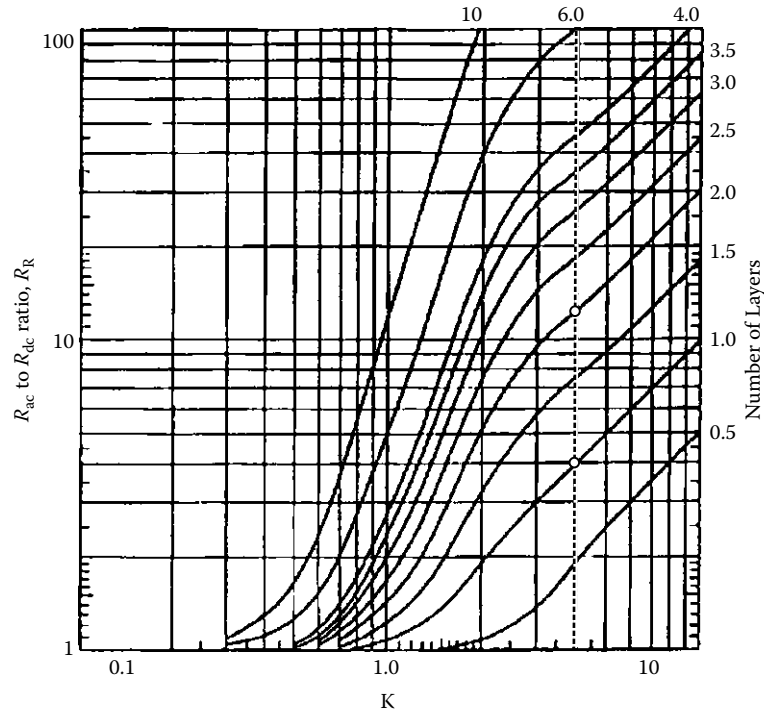


Figure 4-33. Ratio of ac/dc Resistance Due to Proximity Effect.

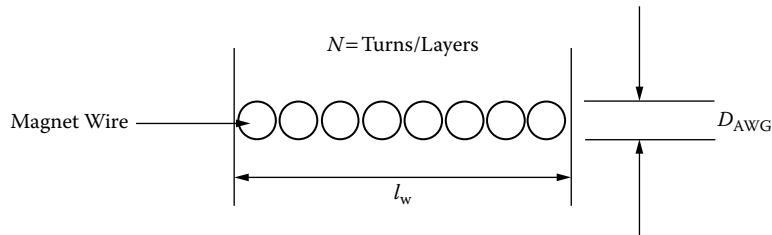


Figure 4-34. Winding Layer Parameters.

Use the Dowell curves, as shown in Figure 4-33. As shown in [Figure 4-35](#), compare the loss ratio between the transformer in configuration A with two layers and transformer B that has the secondary interleaved with the primary. With a skin effect penetration depth of 25%, it will yield a, K, factor of 4. Both transformers, A and B, have the same A-T, but since the windings on transformer B are interleaved. It has only half the low frequency magneto-motive force (mmf).

There is a vertical dotted line shown in [Figure 4-33](#), where $K = 4$. Follow the dotted line up to where it intersects 1 layer, then read the vertical column on the left, $R_R = 4$. Now, follow the dotted line up to where it intersects 2 layers, then read the vertical column on the left, $R_R = 13$. Transformer B, with its interleaved windings, has a lower ac to dc resistance ratio, R_R , by a factor 3.25.

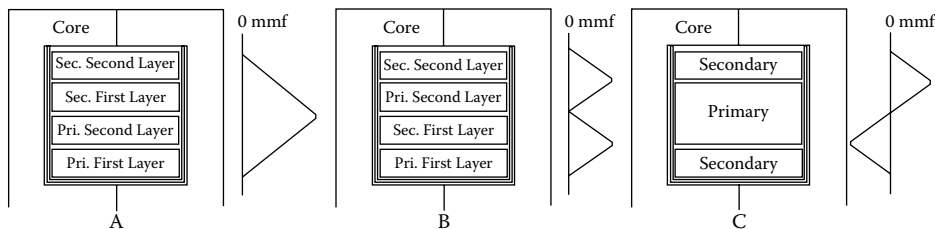


Figure 4-35. Transformers Wound with Different Primary and Secondary Configurations.

The proximity effect, with its exponentially losses tends to be the dominant conductor loss mechanism in high frequency magnetic components, particularly when windings are multi-layered.

Specialty Wire

There are a lot of new ideas out in the wire industry, if only the engineer had the time to evaluate these new concepts to build confidence and apply them.

Triple Insulated Wire

Transformers designed to meet the IEC/VDE safety specification requirements for creepage and clearance must adhere to one of the following specifications:

1. VDE0805
2. IEC950
3. EN60950
4. UL1950-3e
5. CSA 950-95

The engineer must be aware that one specification does not encompass all applications. For example, the IEC has specifications for office machines, data-processing equipment, electromedical equipment, appliances, and others.

Originally these IEC specifications were developed around linear 50 and 60 Hz transformers, and were not, always, conducive to optimal designs for high frequency, such as switching power transformers. The complexity of a standard, high frequency, switching type transformer, designed to the IEC/VDE safety specification, is shown in [Figure 4-36](#). In any switching transformer, coupling has the highest priority because of the leakage flux.

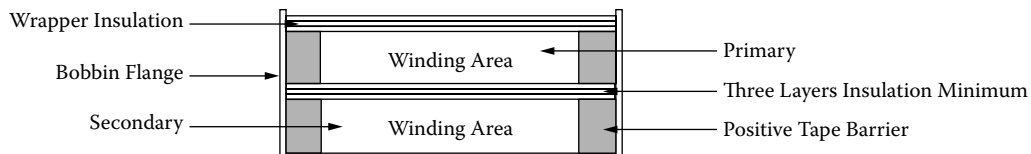


Figure 4-36. Bobbin Cross-Section Design to Meet IEC/VDE Specifications.

The triple, insulated wire was developed to meet the above specification and eliminate the need for three layers of insulating tape between primary and secondary. Also, the triple, insulated wire eliminates the need for the creepage margin, and now, the whole bobbin can be used for winding. This wire can also be used as hook-up wire, from the primary or secondary, to the circuits, without the use of sleeving or tubing.

The construction of the triple, insulated wire is shown in Figure 4-37. The temperature range for this type of wire is from 105°C to 180°C. The dimensions for triple, insulated wire are shown in [Table 4-16](#), using a 0.002 inch coat per layer. Other thicknesses are available. The manufacturer, Rubadue Wire Company, is listed in the Reference Section of this chapter.

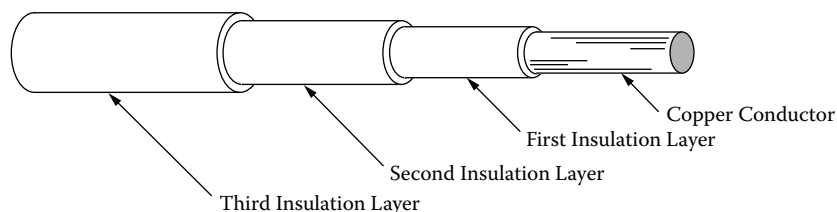


Figure 4-37. Triple, Insulated Wire Construction.

Triple Insulated Litz

High frequency litz wire, shown in Figure 4-38, is also available as a triple insulated wire from manufacturers. The insulation layers' thickness for litz wire comes in 0.002 and 0.003 inches.

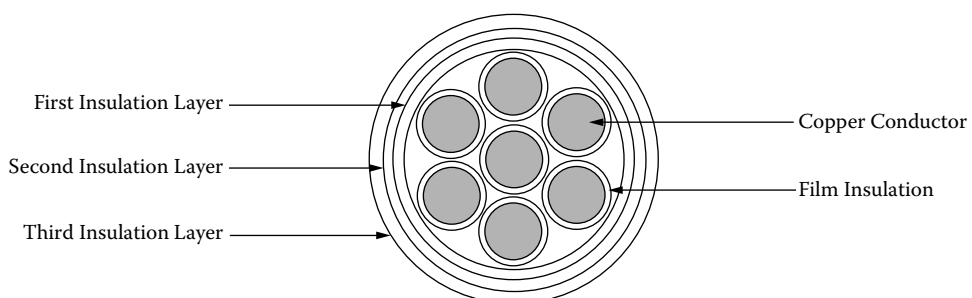


Figure 4-38. Triple, Insulated Litz Wire.

Table 4-16. Triple Insulated Wire (.002) Material

Triple Insulated Wire (.002) Material						
	Bare Wire				With Insulation	
AWG	Area cm ² (10 ⁻³)	Diameter inch	Diameter mm	Resistance μΩ/cm	Diameter inch	Diameter mm
16	13.0700	0.0508	1.2903	132	0.0628	1.5951
18	8.2280	0.0403	1.0236	166	0.0523	1.3284
19	6.5310	0.0359	0.9119	264	0.0479	1.2167
20	5.1880	0.0320	0.8128	332	0.0440	1.1176
21	4.1160	0.0285	0.7239	419	0.0405	1.0287
22	3.2430	0.0253	0.6426	531	0.0373	0.9474
23	2.5880	0.0226	0.5740	666	0.0346	0.8788
24	2.0470	0.0201	0.5105	842	0.0321	0.8153
25	1.6230	0.0179	0.4547	1062	0.0299	0.7595
26	1.2800	0.0159	0.4039	1345	0.0279	0.7087
27	1.0210	0.0142	0.3607	1687	0.0262	0.6655
28	0.8046	0.0126	0.3200	2142	0.0246	0.6248
29	0.6470	0.0113	0.2870	2664	0.0233	0.5918
30	0.5067	0.0100	0.2540	3402	0.0220	0.5588
32	0.3242	0.0080	0.2032	5315	0.0200	0.5080
34	0.2011	0.0063	0.1600	8572	0.0183	0.4648
36	0.1266	0.0050	0.1270	13608	0.0170	0.4318
38	0.0811	0.0040	0.1016	21266	0.0160	0.4064

Polyfilar Magnetic Wire

Poly or multiple strands of magnet wire, bonded together, can be used in many high frequency transformer and inductor applications. Round polyfilar magnet wire is shown in [Figure 4-39](#), and square polyfilar is shown in [Figure 4-40](#). Both can be used in place of foil in some applications. Polyfilar magnet wire can be used as a foil type winding, such as a low voltage, high current, or even a Faraday shield. The polyfilar, magnet wire strip width can be easily increased or decreased by adding or removing wires to provide the proper strip width to fit a bobbin. It is relatively easy to wind. Polyfilar wire has complete insulation, and it does not have the sharp edge problem that could cut insulation in the way foil does. It is not recommended to wind a transformer with polyfilar magnet wire in order to have an exact center tap, unless it is just a few turns, because of the penalty in capacitance. If the use of polyfilar is necessary, then use a magnet wire with a film insulation that has a low dielectric constant. See [Table 4-8](#).

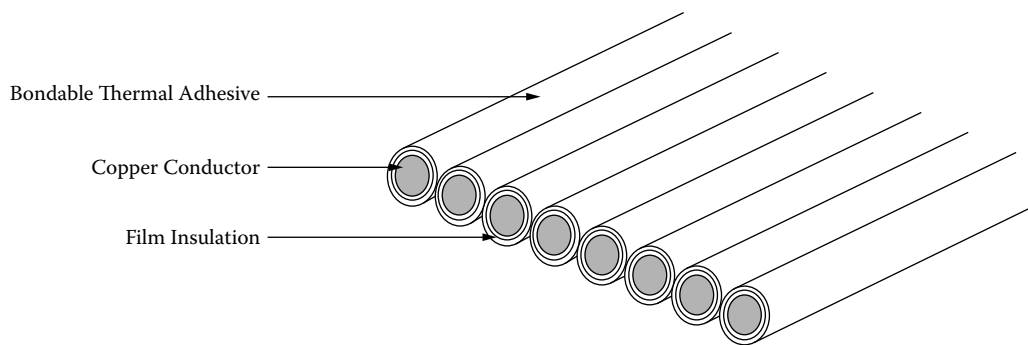


Figure 4-39. Polyfilar, Strip-Bonded, Round Magnet Wire.

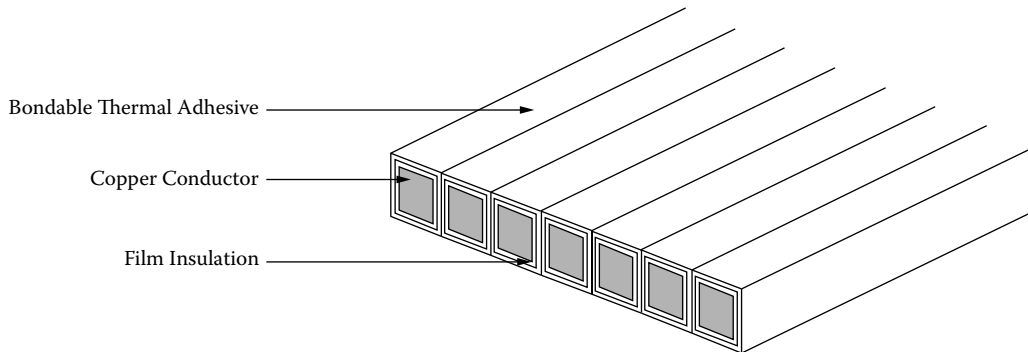


Figure 4-40. Polyfilar, Strip-Bonded, Square Magnet Wire.

Standard Foils

The biggest advantage for using foil over magnet wire is the fill factor. The design of a high current, high frequency, dc to dc converter is common place. The main reason for going to high frequency is the reduction in size. The power transformer is the largest component in the design. When designing high frequency transformers, the design equations relate to a very small transformer. When operating transformers at high frequencies, the skin effect becomes more and more dominate, and requires the use of smaller wire. If larger wire is required, because of the required current density, then, more parallel strands of wire will have to be used (litz wire). The use of small wire has a large effect on the fill factor.

When using foil, the gain in the fill factor is the biggest improvement over litz. To make a comparison, a litz design is shown in [Figure 4-41](#), and a foil design is shown in [Figure 4-42](#). In the litz design, there is a percentage of the winding area which cannot be used for the conductors. This lost area is made up of voids, space between the wires, and the insulation film on the wire. The foil wound coil, shown in [Figure 4-42](#), can be designed to make optimum use of the available winding area. Each turn of the foil can extend, within limits, edge-to-edge of the bobbin or tube. The insulation required between layers is at a minimum, as long as the foil has been rolled to remove the sharp burr, as shown in [Figure 4-46](#).

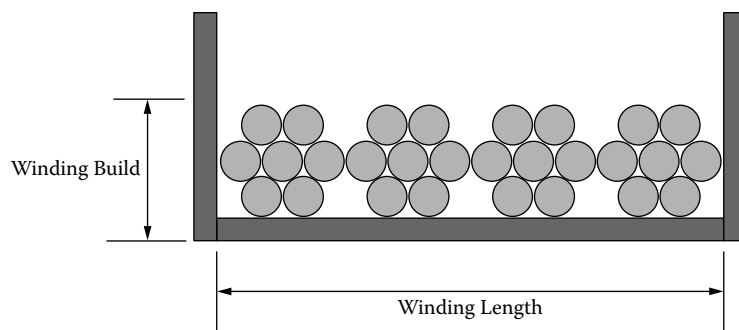


Figure 4-41. Layer Winding, Using Litz Magnet Wire.

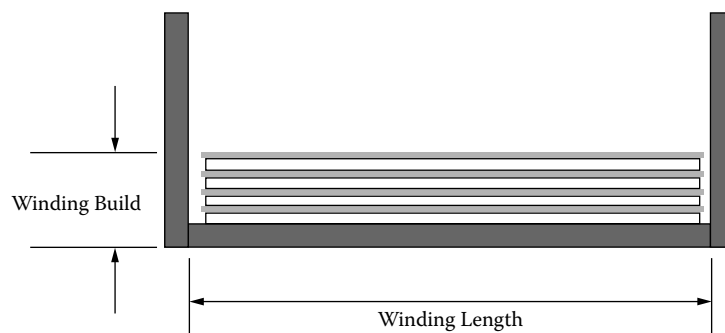


Figure 4-42. Layer Winding, Using Foil with Insulation.

The Use of Foils

Designing transformers and inductors, with foil, is a very laborious task, especially if the engineer only does it now and then. A monumental job, in itself, is finding out where to get the materials. Foil has its advantages, mainly, in high current, high frequency, and a high density environment.

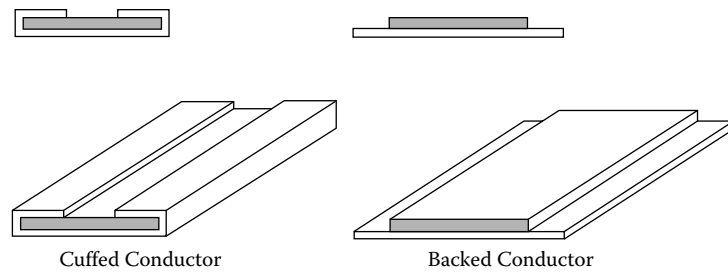
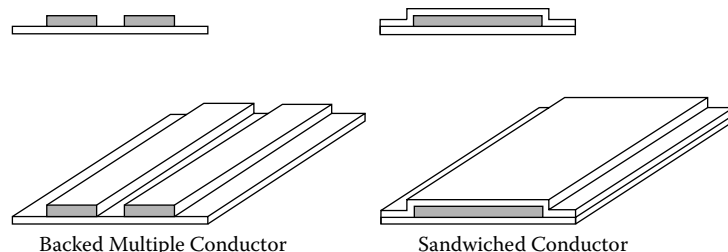
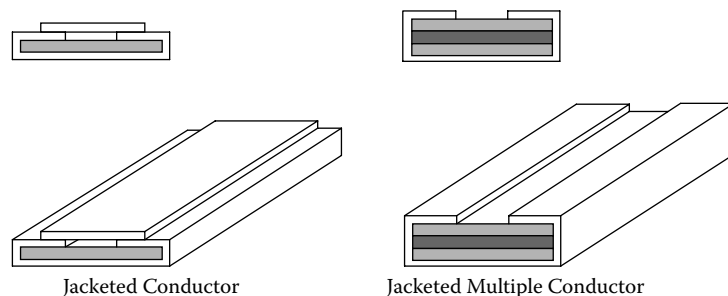
The window utilization factor, K_u , can be greater than 0.6, under the right conditions, without a lot of force. The standard foil materials used, by transformer engineers, are copper and aluminum. The engineer has a good selection of standard thicknesses as shown:

1.0 mil, 1.4 mil, 2.0 mil, 5.0 mil, and 10 mil

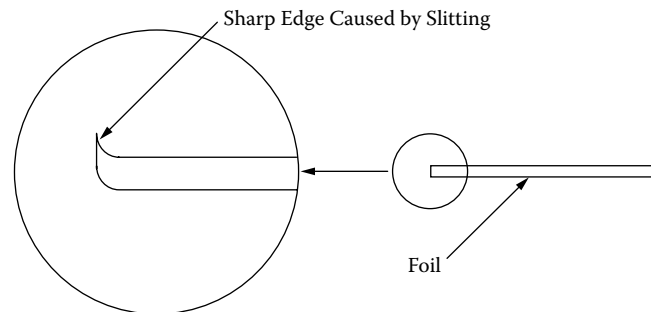
The engineer will find other thicknesses available, but standard thicknesses should be considered first. Be careful of using a nonstandard thickness. What the engineer might be using could be from an overrun, and definitely could create problems for him. Foil comes in standard widths, in inches, as shown:

0.25, 0.375, 0.50, 0.625, 0.75, 1.0, 1.25, 1.50, 2.00, 2.50, 3.00, 4.00 (inches)

Standard widths are the widths that are most readily available. There are also different styles of pre-fab foils, as shown in [Figures 4-43, 4-44, and 4-45](#).

**Figure 4-43.** Pre-fab Foils.**Figure 4-44.** Pre-fab Foils.**Figure 4-45.** Pre-fab Foils.

Although special slitting is done all the time, there is normally a minimum buy. When slitting is done, special care must be attended to, with the sharp edges, as shown in Figure 4-46. The cut edge should be rolled after slitting it, at least two times, to remove the sharp burrs that could cut through the insulation. Therefore, it is wise not to use insulation between layers of less than 1 mil.

**Figure 4-46.** Foil with Sharp Edge Burrs, after Slitting.

When winding transformers or inductors with foil, special care must be taken with lead finishing. One of the biggest problems about using foil is solder wicking. This wicking will puncture the insulation, resulting in a shorted turn. The normal insulation used for foil is very thin. Winding with foil, the coil is still subjected to bowing, only more so, as shown in Figure 4-7.

Foil used for winding transformers and inductors should be dead soft. There is another shortcoming about using foil, and that is, the inherit capacitance build-up, as shown in Figure 4-47.

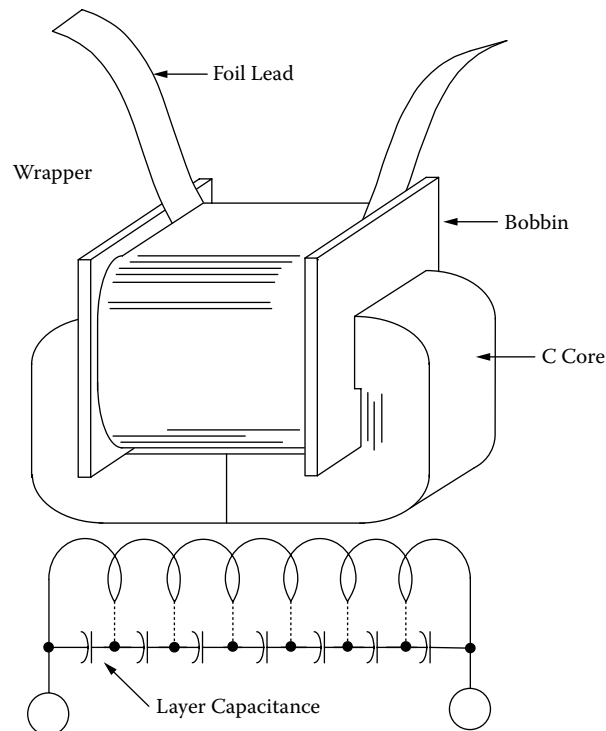


Figure 4-47. Foil Capacitance Equation.

The capacitance build-up is expressed:

$$C = 0.0885 \left(\frac{K(N-1)(MLT)(G)}{d} \right), \quad [pf/d] \quad [4-22]$$

K = Dielectric Constant

MLT = Mean Length Turn

N = Number of Turns

G = Foil Width, cm

d = Layer Insulation Thickness, cm

The dielectric constant K for different materials can be found in [Table 4-17](#).

Table 4-17. Dielectric Constants

Dielectric Constants	
Material	K
Kapton	3.2-3.5
Mylar	3-3.5
Kraft Paper	1.5-3.0
Fish Paper	1.5-3.0
Nomex	1.6-2.9

Calculating, MLT

The Mean Length Turn, (MLT), is required to calculate the winding resistance and weight for any given winding. The winding dimensions, relating to the Mean Length Turn, (MLT) for a tube or bobbin coil, are shown in Figure 4-48.

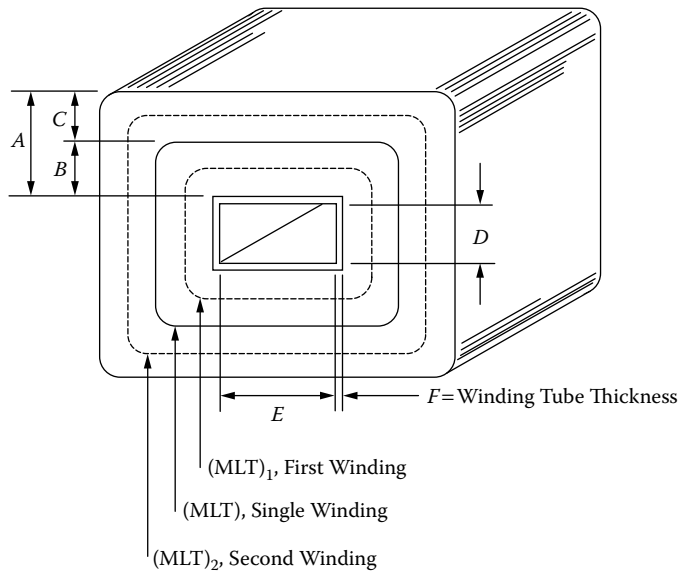


Figure 4-48. Dimensions, Relating to the Winding Mean Length Turn, (MLT).

$$MLT = 2(D + 2F) + 2(E + 2F) + \pi A, \text{ single winding}$$

$$MLT_1 = 2(D + 2F) + 2(E + 2F) + \pi B, \text{ first winding} \quad [4-23]$$

$$MLT_2 = 2(D + 2F) + 2(E + 2F) + \pi(2B + C), \text{ second winding}$$

Calculating, MLT (toroid)

It is very difficult to calculate the Mean Length Turn (MLT) for a toroidal core that would satisfy all conditions. There are just too many ways to wind a toroid. If the toroid was designed to be wound by machine, then that would require a special clearance for a wire shuttle. If the toroid was designed to be

hand-wound, the inside wound diameter would be different. The fabrication of a toroidal design depends heavily on the skill of the winder. A good approximation for a toroidal core, Mean Length Turn (MLT), is shown in Figure 4-49.

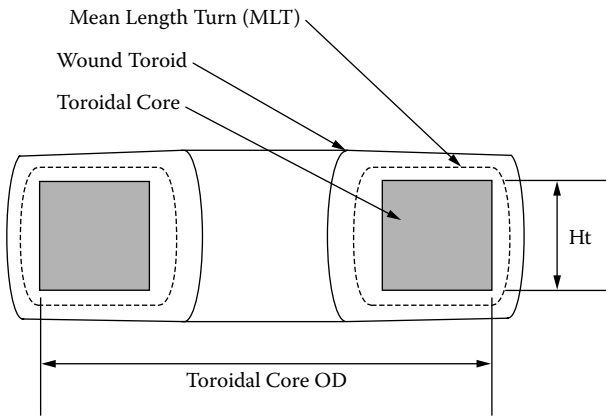


Figure 4-49. Toroidal Mean Length Turn (MLT), is an Approximation.

$$\text{MLT} = 0.8(OD + 2(Ht)), \text{ approximation}$$

[4-24]

Copper Resistance

The dc resistance calculation of a winding requires knowing the total length, l , of the conductor, the cross-sectional area, A_w , of the conductor, and the resistivity, ρ , of the conductor material. The value for the resistivity, ρ , in $\mu\Omega$ per cm for three different conductor materials can be found in [Table 4-7](#).

$$R_{dc} = \left(\frac{\rho l}{A_w} \right), \quad [\Omega] \quad [4-25]$$

Copper Weight

The weight calculation of a winding requires knowing the total length, l , of the conductor, the cross-sectional area, A_w , of the conductor, and the density, λ , of the conductor material. The value for the density, λ , in grams per cm^3 for three different conductor materials, can be found in [Table 4-7](#).

$$W_t = \lambda l A_w, \quad [\text{grams}] \quad [4-26]$$

Electrical Insulating Materials

The reliability and life span of a magnetic component depends on the stress level put upon the insulating materials. If the design or workmanship is not incorporated, then, insulation will not help the engineer.

References

1. P.L. Dowell, "Effects of Eddy Currents in Transformer Windings," *Proceedings IEE (UK)*, Vol. 113, No.8, August, 1966, pp. 1387–1394.
2. B. Carsten, "High Frequency Conductor Losses in Switch Mode Magnetics," High Frequency Power Converter Conference, 1986, pp. 155–176.
3. L. Dixon, Eddy Current Losses in Transformer Windings and Circuit Wiring, Unitrode Corp. Power Supply Seminar Handbook, Unitrode Corp., Watertown MA, 1988.
4. E. Snelling, *Soft Ferrites*, pp. 341–348, Iliffe, London, 1969.
5. A.I. Pressman, *Switching Power Supply Design*, pp. 298–317, McGraw-Hill, Inc., New York 1991.
6. E.C. Snelling, *Soft Ferrites*, CRC Press, Iliffe Books Ltd., 42 Russell Square, London, W.C.I, 1969.
7. Werner Osterland, "The Influence of Wire Characteristics on the Winding Factor and Winding Method," *WIRE*, Coburg, Germany. Issue 97, October, 1968.
8. H.A. George, "Orthocyclic Winding of Magnet Wire Without Interleaving Materials," *Insulation/Circuits*, August, 1976.
9. MWS Wire Industries, "Wire Catalog," Revised June, 1992, 31200 Cedar Valley Drive, Westlake Village, CA 91362.
10. Alpha-Core Inc. (Special Foils), 915 Pembroke Street, Bridgeport, CT 06608.
11. Industrial Dielectrics West, Inc., (Special Foils), 455 East 9th Street, San Bernardino, CA 92410.
12. Rubadue Wire Company, Inc., (Triple Insulated Wire), 5150 E. LaPalma Avenue, Suite 108, Anaheim Hills, CA 92807 Email: www.rubaduewire.com.

Chapter 5

Transformer Design Trade-Offs

Table of Contents

1. Introduction.....	5-3
2. The Design Problem Generally	5-3
3. Power Handling Ability.....	5-4
4. Relationship, A_p , to Transformer Power Handling Capability	5-4
5. Relationship, K_g , to Transformer Regulation and Power Handling Capability.....	5-5
6. Transformer Area Product, A_p	5-6
7. Transformer Volume and the Area Product, A_p	5-6
8. Transformer Weight and the Area Product, A_p	5-9
9. Transformer Surface Area and the Area Product, A_p	5-11
10. Transformer Current Density, J , and the Area Product, A_p	5-15
11. Transformer Core Geometry, K_g , and the Area Product, A_p	5-18
12. Weight Versus Transformer Regulation.....	5-20
13. References.....	5-21

Introduction

The conversion process in power electronics requires the use of transformer components that are frequently the heaviest and bulkiest item in the conversion circuit. They also have a significant effect upon the overall performance and efficiency of the system. Accordingly, the design of such transformers has an important influence on the overall system weight, power conversion efficiency, and cost. Because of the interdependence and interaction of these parameters, judicious trade-offs are necessary to achieve design optimization.

The Design Problem Generally

The designer is faced with a set of constraints that must be observed in the design on any transformer. One of these constraints is the output power, P_o , (operating voltage multiplied by maximum current demand) in that the secondary winding must be capable of delivering to the load within specified regulation limits. Another constraint relates to the minimum efficiency of the operation, which is dependent upon the maximum power loss that can be allowed in the transformer. Still another constraint defines the maximum permissible temperature rise for the transformer when it is used in a specified temperature environment.

One of the basic steps in transformer design is the selection of proper a core material. Magnetic materials used to design low and high frequency transformers are shown in [Table 5-1](#). Each one of these materials has its own optimum point in the cost, size, frequency and efficiency spectrum. The designer should be aware of the cost difference between silicon-iron, nickel-iron, amorphous and ferrite materials. Other constraints relate to volume occupied by the transformer and, particularly in aerospace applications, weight minimization is an important goal. Finally, cost effectiveness is always an important consideration.

Depending upon the application, some of these constraints will dominate. Parameters affecting others may then be traded-off, as necessary, to achieve the most desirable design. It is not possible to optimize all parameters in a single design because of their interaction and interdependence. For example, if volume and weight are of great significance, reductions in both can often be affected, by operating the transformer at a higher frequency, but with the penalty being in efficiency. When, the frequency cannot be increased, reduction in weight and volume may still be possible by selecting a more efficient core material, but there would be the penalty of increased cost. Thus, judicious trade-offs must be affected to achieve the design goals.

Transformer designers have used various approaches in arriving at suitable designs. For example, in many cases, a rule of thumb is used for dealing with current density. Typically, an assumption is made that a good working level is 200 amps-per-cm² (1000 circular mils-per-ampere). This rule of thumb will work in many instances, but the wire size needed to meet this requirement may produce a heavier and bulkier transformer than desired or required. The information presented in this Chapter makes it possible to develop a more economical design with great accuracy, therefore avoiding the above assumption and other rules of thumb.

Table 5-1. Magnetic Materials and Their Characteristics

Magnetic Core Material Characteristics					
Material Name	Initial Permeability μ_i	Flux Density Teslas B_s	Curie Temperature °C	dc, Coercive Force, H_c Oersteds	Operating Frequency f
Iron Alloys					
Magnesil	1.5K	1.5-1.8	750	0.4-0.6	<2 kHz
Supermendur*	0.8K	1.9-2.2	940	0.15-0.35	<1 kHz
Orthonol	2K	1.42-1.58	500	0.1-0.2	<2 kHz
Sq. permalloy	12K-100K	0.66-0.82	460	0.02-0.04	<25 kHz
Supermalloy	10K-50K	0.65-0.82	460	0.003-0.008	<25 kHz
Amorphous					
2605-SC	3K	1.5-1.6	370	0.03-0.08	<250 kHz
2714A	20K	0.5-0.58	>200	0.008-0.02	<250 kHz
Vitro perm 500	30K	1.0-1.2	>200	<0.05	<250 kHz
Ferrite					
MnZn	0.75-15K	0.3-0.5	100-300	0.04-0.25	<2 MHz
NiZn	15-1500	0.3-0.5	150-450	0.3-0.5	<100 MHz

*Field Anneal.

Power Handling Ability

For years, manufacturers have assigned numeric codes to their cores to indicate their power-handling ability. This method assigns to each core a number called the area product, A_p . That is the product of the window area, W_a , and the core cross-section, A_c . The core suppliers use these numbers to summarize dimensional and electrical properties in their catalogs. They are available for laminations, C cores, ferrite cores, powder cores, and toroidal tape wound cores.

Relationship, A_p , to Transformer Power Handling Capability

Transformers

According to the newly developed approach, the power handling capability of a core is related to its area product, A_p , by an Equation, which may be stated as:

$$A_p = \frac{P_t (10^4)}{K_f K_u B_m J_f}, \quad [\text{cm}^4] \quad [5-1]$$

Where:

K_f = waveform coefficient

4.0 square wave

4.44 sine wave

From the above, it can be seen that the factors, such as flux density, frequency of operation, and window utilization factor K_u, define the maximum space which may be occupied by the copper in the window.

Relationship, K_g, to Transformer Regulation and Power Handling Capability

Although most transformers are designed for a given temperature rise, they can also be designed for a given regulation. The regulation and power-handling ability of a core is related to two constants:

$$\alpha = \frac{P_t}{2K_g K_e}, \quad [\%] \quad [5-2]$$

$$\alpha = \text{Regulation (\%)} \quad [5-3]$$

The constant, K_g, (See Chapter 7) is determined by the core geometry, which may be related by the following equations:

$$K_g = \frac{W_a A_c^2 K_u}{MLT}, \quad [\text{cm}^5] \quad [5-4]$$

The constant, K_e, is determined by the magnetic and electric operating conditions, which may be related by the following Equation:

$$K_e = 0.145 K_f^2 f^2 B_m^2 (10^{-4}) \quad [5-5]$$

Where:

K_f = waveform coefficient

4.0 square wave

4.44 sine wave

From the above, it can be seen that the factors, such as flux density, frequency of operation, and waveform coefficient, have an influence on the transformer size. Because of their significance, the area product, A_p, and the core geometry, K_g, are treated extensively in this handbook. A great deal of other information is also presented for the convenience of the designer. Much of the information is in tabular form to assist designers in making the trade-offs best suited for the particular application, in a minimum amount of time.

Transformer Area Product, A_p

The author has developed additional relationships between, A_p , numbers and current density, J , for given regulation and temperature rise. The area product, A_p , is a length dimension to the fourth power, (l^4), as shown in Figure 5-1.

$$\begin{aligned} W_a &= FG, \quad [\text{cm}^2] \\ A_c &= DE, \quad [\text{cm}^2] \\ A_p &= W_a A_c, \quad [\text{cm}^4] \end{aligned} \quad [5-6]$$

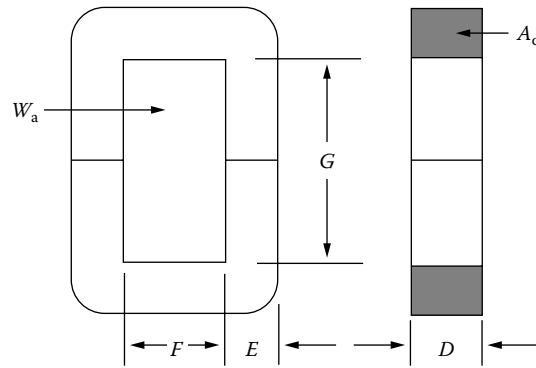


Figure 5-1. C Core Outline Showing the Window Area, W_a and Iron Area, A_c .

It should be noted that the constants for tape-wound cores, such as: K_{vol} , K_w , K_s , K_j and K_p will have a tendency to jump around and not be consistent. This inconsistency has to do with the core being in a housing, without true proportions.

Transformer Volume and the Area Product, A_p

The volume of a transformer can be related to the area product, A_p of a transformer, treating the volume, as shown in Figures 5-2 to 5-4, as a solid quantity without any subtraction for the core window. The relationship is derived according to the following reasoning: Volume varies in accordance with the cube of any linear dimension, (l), whereas area product, A_p , varies as the fourth power:

$$\text{Volume} = K_1 l^3, \quad [\text{cm}^3] \quad [5-7]$$

$$A_p = K_2 l^4, \quad [\text{cm}^4] \quad [5-8]$$

$$l^4 = \frac{A_p}{K_2} \quad [5-9]$$

$$l = \left(\frac{A_p}{K_2} \right)^{(0.25)} \quad [5-10]$$

$$l^3 = \left[\left(\frac{A_p}{K_2} \right)^{0.25} \right]^3 = \left(\frac{A_p}{K_2} \right)^{0.75} \quad [5-11]$$

$$\text{Volume} = K_1 \left(\frac{A_p}{K_2} \right)^{0.75} \quad [5-12]$$

$$K_{vol} = \frac{K_1}{K_2^{(0.75)}} \quad [5-13]$$

The volume-area product, A_p , relationship is therefore:

$$\text{Volume} = K_{vol} A_p^{(0.75)}, \quad [\text{cm}^3] \quad [5-14]$$

In which, K_{vol} , is a constant related to core configuration whose values are given in Table 5-2. These values were obtained by averaging the values from the data taken from Tables 3-1 through Tables 3-64 in Chapter 3.

Table 5-2. Volume-Area Product Relationship

Volume-Area Product Relationship	
Core Type	K_{vol}
Pot Core	14.5
Powder Core	13.1
Laminations	19.7
C Core	17.9
Single-coil C Core	25.6
Tape-wound Core	25.0

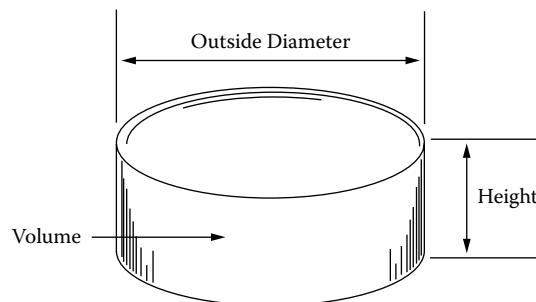


Figure 5-2. Toroidal Transformer Outline, Showing the Volume.

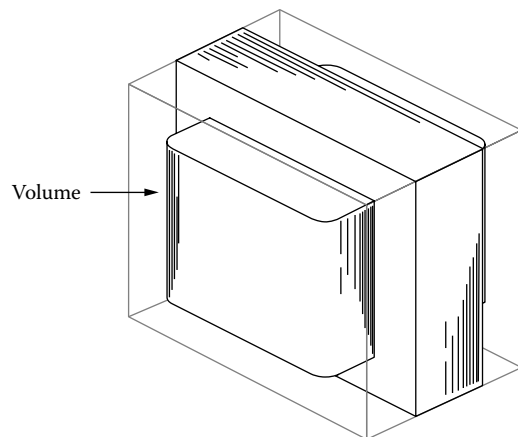


Figure 5-3. EI Core Transformer Outline, Showing the Volume.

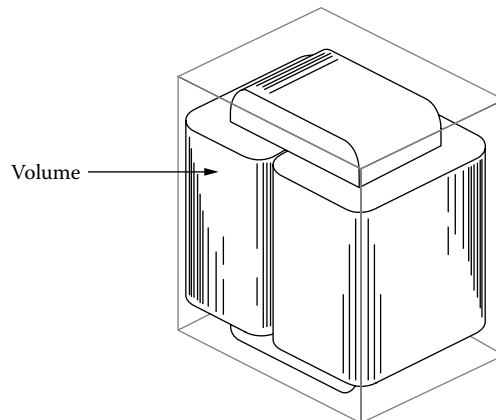


Figure 5-4. C Core Transformer Outline, Showing the Volume.

The relationship between volume and area product, A_p , for various core types is graphed in Figures 5-5 through 5-7. The data for these Figures has been taken from Tables in Chapter 3.

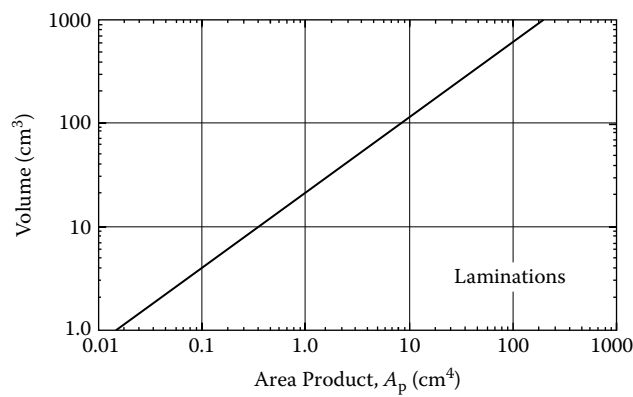


Figure 5-5. Volume Versus Area Product, A_p for EI Laminations.

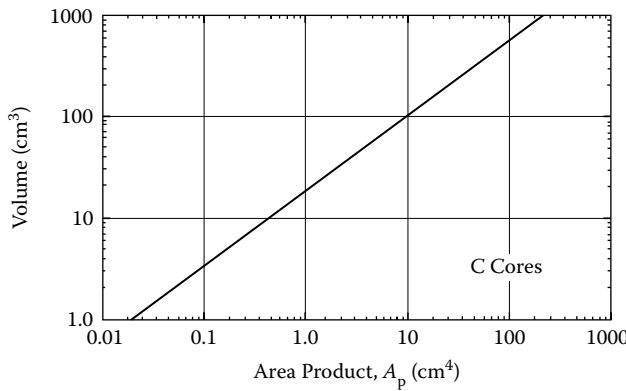


Figure 5-6. Volume Versus Area Product, A_p for C Cores.

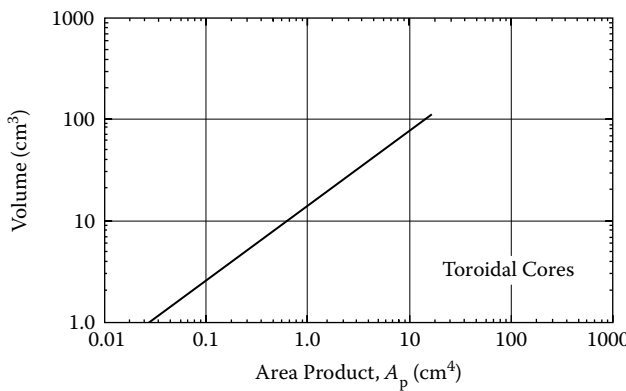


Figure 5-7. Volume Versus Area Product, A_p , for Toroidal MPP Cores.

Transformer Weight and the Area Product, A_p

The total weight of a transformer can also be related to the area product, A_p , of a transformer. The relationship is derived according to the following reasoning: weight, W_t , varies, in accordance with the cube of any linear dimension, (l), whereas area product, A_p , varies, as the fourth power:

$$W_t = K_3 l^3, \quad [\text{grams}] \quad [5-15]$$

$$A_p = K_2 l^4, \quad [\text{cm}^4] \quad [5-16]$$

$$l^4 = \frac{A_p}{K_2} \quad [5-17]$$

$$l^3 = \left[\left(\frac{A_p}{K_2} \right)^{0.25} \right]^3 = \left(\frac{A_p}{K_2} \right)^{0.75} \quad [5-18]$$

$$l^3 = \left[\left(\frac{A_p}{K_2} \right)^{0.25} \right]^3 = \left(\frac{A_p}{K_2} \right)^{0.75} \quad [5-19]$$